Structure of Nickel-Iron and Nickel-Zinc Electrodeposits

Volume II

Claudia Erdmuthe Lehmberg

A thesis submitted in partial fulfilment of the requirements of Sheffield Hallam University for the degree of Doctor of Philosophy

November 1998

8 Tables and Figures

8. 1 Tables

Table 2-1: Comparison of Investigative Techniques Used in Present Work.

	GDOES	XRD	TEM				SEM		
			electron diffraction SADP	imaging mode BF	imaging mode DF	STEM/ EDX	imaging mode SEI	imaging mode BSI	EDX
Parameters									
Excitation	ions	X-rays	e^-	e^-	e^-	e^-	e^-	e^-	e^-
Transmission	*hv* (optical)	X-rays	e^-	e^-	e^-	X-rays	secondary e^-	backscattered e^-	X-rays
Information									
Nucleation and Growth	no	no	cross-section only	cross-section only	cross-section only	cross-section only	no	no	no
Composition	yes	no	no	no	no	yes	no	no	yes
Texture	no	surf. texture	local texture	no	local texture	no	no	no	no
Overall Structure	no	no	no	local	local	no	surf. topography	atomic number contrast	no
Grain Size	no	no	no	yes	yes	no	no	no	no
Dislocation Density	no	no	no	yes	yes	no	no	no	no
Depth Profile									
Composition	yes	no	no	no	no	cross-section only	no	no	cross-section only
Texture	no	yes	cross-section only	no	cross-section only	no	no	no	no
Application	ex situ	ex situ, also in situ [65]	ex situ	ex situ	ex situ	ex situ	ex situ	ex situ	ex situ

Table 2-2: Comparison of Alternative Investigative Techniques not Used in Present Work.

	XRF	AES	STM	Voltammetry
Parameters				
Excitation	X-rays	e^-	voltage	(i) voltage (ii) current
Transmission	fluorescent radiation	e^-	tunnelling e^-	(i) current (ii) voltage
Information				
Nucleation and Growth	no	no	no	indirect
Composition	no	yes	no	no
Texture	no	no	no	no
Overall Structure	no	no	surf. topography	no
Grain Size	no	no	no	no
Dislocation Density	no	no	no	no
Depth Profile	no	no	no	no
Composition	no	no	no	no
Texture	no	no	no	no
Application	ex situ	ex situ	ex situ, also in situ [66, 67, 68].	in situ

Table 3-1: Composition and Working Parameters of Nickel-Iron Electrolytes.

Component		Solution 1 mol l^{-1}	2 mol l^{-1}	3 mol l^{-1}	4 mol l^{-1}
Nickel(II)-sulphate	$NiSO_4*6H_2O$	0.81	0.45	0.69	0.69
Nickel(II)-chloride	$NiCl_2*6H_2O$	0.21	0.21	0.21	0.21
Boric acid	H_3BO_3	0.48	0.48	0.48	0.48
Ferrous(II)-sulphate	$FeSO_4*7H_2O$	0.1	0.47	0.29	0.29
Citric acid	$C_3H_4(OH)(COOH)_3*H_2O$	0.003	0.003	0.003	0.003
Sodium lauryl sulphate	$NaC_{12}H_{25}SO_4$	-	0.002	0.002	-
Saccharine	$C_6H_4CONHSO_2$	-	-	0.003	0.003
Ascorbic acid	$C_6H_8O_6$	-	-	0.003	0.003

Working Condition	Solution 1	2	3	4
agitation	N_2-agitation 1. uncontrolled 2. 1 l min^{-1} 3. 3 l min^{-1} 4. 6 l min^{-1}	magnetic stirrer on hot plate; speed 7	submersible magnetic stirrer in water bath: speed: 7; reverse mode: 10	N_2-agitation: 1 l min^{-1}

Table 3-2: Composition and Working Parameters of Nickel-Zinc Electrolytes.

Component		Solution 1 mol l^{-1}	2 mol l^{-1}	3 mol l^{-1}	4 mol l^{-1}	5 mol l^{-1}	6 mol l^{-1}	7 mol l^{-1}	8 mol l^{-1}
Nickel(II)-sulphate	$NiSO_4*6H_2O$	0.57	0.57	0.57	0.57	0.57	0.57	1.11	1.2
Zinc(II)-sulphate	$ZnSO_4*7H_2O$	0.7	0.7	0.7	0.7	0.7	0.7	0.16	0.07
Boric acid	H_3BO_3	0.32	0.32	0.32	0.64	0.64	0.64	0.32	0.32
p-toluene sulfonic acid	$C_7H_8O_3S*H_2O$	0.01	0.01	-	-	0.01	0.01	0.01	0.01
Sodium lauryl sulphate	$NaC_{12}H_{25}SO_4$	-	0.002	-	-	-	0.002	-	-

Working Condition	Solution 1	2	3	4	5	6	7	8
Anodes	nickel	nickel	nickel	nickel	nickel	nickel	inert	inert
pH	3 (*/**)	3 (**)	3 (**)	~2 (***)	~2 (***)	~2 (***)	3 (**)	3 (**)
Volume	500 ml	500 ml	500 ml	500 ml	500 ml	500 ml	1500 ml	1500 ml
Agitation	a); b)	a); b)	a)	a); b)	a); b)	a)	b)	b)

*pH-value adjusted with ammonia solution
**pH-value adjusted with sodium hydroxide solution
***no pH-value adjusted; solution had ~2
agitation: a) submersible magnetic stirrer: speed 5, reverse mode 5
b) agitated with nitrogen gas; 1.5 l min^{-1}

Table 3-3: Description of Degreasing Agent for Copper and Brass.

Trade name	*KLEENAX*
Manufacturer	Canning (Birmingham, UK)
Remarks	Contains cyanide
Concentration	125 g l^{-1}
Operating parameters	i_c: 30 mA cm^{-2} T: 40 °C t: 1 - 2 min

Table 3-4: Description of Degreasing Agent for Steel.

Trade name	*Activax*
Manufacturer	Canning (Birmingham, UK)
Remarks	Cyanide-free
Concentration	50 g l^{-1}
Operating parameters	i_a: 30 mA cm^{-2} T: 70 °C t: 30 s

Table 3-5: Description of Activating Agent.

Trade name	*Activator No. 2*
Manufacturer	Lea Ronal (Buxton, UK)
Concentration	50 g l^{-1}
Operating parameters	T: room temperature t: 1 min

Table 3-6: Composition and Operating Parameters of the Cyanide Copper Electrolyte.

Constituents	Concentration [g l^{-1}]
CuCN	40
KCN	66
K_2CO_3	39
$NaKC_4H_4O_6$	60
T	40-60 °C
Anodes	Electrolytic Copper
Anode:Cathode	1:2
i_c	10 mA cm^{-2}

Table 3-7: Composition and Operating Parameters of the Acid Copper Electrolyte.

Constituents	Concentration [g l^{-1}]
$CuSO_4 \cdot 5H_2O$	200
H_2SO_4	50
T	40 °C
Anodes	Electrolytic Copper
Anode:Cathode	1:2
i_c	100 mA cm^{-2}

Table 3-8: *K* Emission Lines (Weighted Mean) [89] and Mass Absorption Coefficients K_{edge} [90].

Element	Atomic Number	K_α [nm]	K_β [nm]	K_{edge} [nm]
Cobalt	27	0.179026	0.162080	0.1608
Nickel	28	...	...	0.1488
Copper	29	0.154186	0.139222	0.1380
Molybdenum	42	0.071073	0.063229	0.061977

Table 3-9: Steps of Angular Ranges to Diffract Planes of fcc Nickel-Iron.

Angular range °2θ	**Reflection**
41.4 - 46.5	{111}
49 - 53	{200}
72 - 78	{220}
87 - 93	{311}
132 - 149	{331}

Table 3-10: Steps of Angular Ranges to Diffract Planes of bcc Nickel-Iron.

Angular range 2θ	**Reflection**
41.4 - 46.5	{110}
62 - 68	{200}
79 - 85	{211}
112 - 120	{310}
132 - 149	{222}

Table 4-1: Composition and Visual Evaluation of Quiescent Nickel-Iron Solution 1 Employing 1A Cell Current.

current density [mA cm^{-2}]	composition mass-% Ni	mass-% Fe	observation deposit appearance
4	73.1	26.9	dull; dark, brownish-grey; no pitting
10	69.7	30.3	dull; brownish-grey; slightly pitted
15	71.1	28.9	dull; brownish-grey; slightly pitted
20	71.0	29.0	dull; brownish-grey; pitted
30	76.3	23.7	dull; brownish-grey; pitted
40	78.3	21.7	dull; brownish-grey; pitted
50	83.1	16.9	dull; brownish-grey; pitted

Table 4-2: Composition and Visual Evaluation of Quiescent Nickel-Iron Solution 1 Employing 3A Cell Current.

current density [mA cm^{-2}]	composition mass-% Ni	mass-% Fe	observation deposit appearance
12	71.6	28.4	dull; brownish-grey; slightly pitted
30	76.3	23.7	dull; brownish-grey; slightly pitted
60	81.6	18.4	dull; brownish-grey; slightly pitted
90	84.2	15.8	dull; brownish-grey; slightly pitted
150	87.1	12.9	dull; brownish-grey; pitted

Table 4-3: Composition and Visual Evaluation of Quiescent Nickel-Iron Solution 1 Employing 7A Cell Current.

current density [mA cm^{-2}]	composition mass-% Ni	mass-% Fe	observation deposit appearance
52.5	83.6	16.4	dull; brownish-grey; slightly pitted
140	88.5	11.5	dull; brownish-grey; slightly pitted
210	87.7	12.3	dull; brownish-grey; pitted
350	90.2	9.8	dull; brownish-grey; pitted

Table 4-4: Composition and Visual Evaluation of Nitrogen Agitated Nickel-Iron Solution 1 Employing 1A Cell Current.

current density [mA cm^{-2}]	composition mass-% Ni	mass-% Fe	observation deposit appearance
4	67.7	30.3	dull; yellowish-grey; no pitting
10	64.5	35.5	dull; yellowish-grey; no pitting
15	64.6	35.4	dull; yellowish-grey; slightly pitted
20	65.4	34.6	dull; yellowish-grey; pitted
30	61.4	38.6	dull; yellowish-grey; pitted
40	57.5	42.5	dull; yellowish-grey; pitted
50	59.1	40.9	dull; brownish-grey; pitted

Table 4-5: Composition and Visual Evaluation of Nitrogen Agitated Nickel-Iron Solution 1 Employing 3A Cell Current.

current density [mA cm^{-2}]	composition mass-% Ni	mass-% Fe	observation deposit appearance
15	60.3	39.7	dull; yellowish-grey; slightly pitted
30	56.7	43.3	dull; yellowish-grey; slightly pitted
60	53.9	46.1	dull; grey; slightly pitted
90	56.6	43.4	dull; grey; slightly pitted
150	58.6	41.4	dull; grey; slightly pitted

Table 4-6: Composition and Visual Evaluation of Nitrogen Agitated Nickel-Iron Solution 1 Employing 7A Cell Current.

current density [mA cm^{-2}]	composition mass-% Ni	mass-% Fe	observation deposit appearance
52.5	65.7	34.3	dull; yellowish-grey; slightly pitted
140	62.8	37.2	dull; grey; slightly pitted
210	64.8	35.2	dull; grey; slightly pitted
350	71.9	28.1	dull; grey; slightly pitted

Table 4-7: Composition and Visual Evaluation of Quiescent Nickel-Iron Solution 4 Employing 1A Cell Current.

current density [mA cm^{-2}]	composition mass-% Ni	mass-% Fe	observation deposit appearance
4	53.2	46.8	shiny; silverish-grey; smooth
5	51.5	48.5	shiny; silverish-grey; smooth
7.5	48.1	51.9	shiny; silverish-grey; smooth
10	45.8	54.2	shiny; silverish-grey; smooth
12.5	45.8	54.2	shiny; silverish-grey; smooth
15	45.3	54.7	shiny; silverish-grey; smooth
20	45.8	54.2	shiny; silverish-grey; smooth
30	47.3	52.7	shiny; silverish-grey; slightly pitted
40	50.9	49.1	shiny; silverish-grey; slightly pitted
50	53.5	46.5	slightly dull; silverish-grey; slightly pitted

Table 4-8: Composition and Visual Evaluation of Quiescent Nickel-Iron Solution 4 Employing 3A Cell Current.

current density [mA cm^{-2}]	composition mass-% Ni	mass-% Fe	observation deposit appearance
12	49.9	50.1	shiny; silverish-grey; smooth
15	49.2	50.8	shiny; silverish-grey; smooth
22.5	48.6	51.4	shiny; silverish-grey; smooth
30	51.8	48.2	shiny; silverish-grey; slightly pitted
37.5	51.4	48.6	shiny; silverish-grey; slightly pitted
45	53.8	46.2	shiny; silverish-grey; slightly pitted
60	55.9	44.1	dull; silverish-grey; slightly pitted
90	60.6	39.4	dull; silverish-grey; slightly pitted
120	64.2	35.8	dull; silverish-grey; slightly pitted
150	68.3	31.7	dull; silverish-grey; slightly pitted

Table 4-9: Composition and Visual Evaluation of Quiescent Nickel-Iron Solution 4 Employing 7A Cell Current.

current density [mA cm^{-2}]	composition mass-% Ni	mass-% Fe	observation deposit appearance
28	54.1	45.9	shiny; silverish-grey; smooth
35	54.4	45.6	shiny; silverish-grey; smooth
52.5	58.9	41.1	shiny; silverish-grey; smooth
70	61.4	38.6	dull; silverish-grey; slightly pitted
87.5	64.4	35.6	dull; silverish-grey; slightly pitted
105	66.1	33.9	dull; silverish-grey; slightly pitted
140	68.9	31.1	dull; silverish-grey; slightly pitted
210	70.8	29.3	dull; silverish-grey; slightly pitted
280	61.1	38.9	burnt; non-adherent deposit
350	57.6	42.4	burnt; non-adherent deposit

Table 4-10: Composition and Visual Evaluation of Nitrogen Agitated Nickel-Iron Solution 4 Employing 1A Cell Current.

current density [mA cm^{-2}]	composition mass-% Ni	mass-% Fe	observation deposit appearance
4	55.0	45.0	shiny; silverish-grey; smooth
5	52.6	47.4	shiny; silverish-grey; smooth
7.5	47.8	52.2	shiny; silverish-grey; smooth
10	45.4	54.6	shiny; silverish-grey; smooth
12.5	43.1	56.9	shiny; silverish-grey; smooth
15	39.8	60.2	shiny; silverish-grey; smooth
20	36.5	63.5	shiny; silverish-grey; smooth
30	35.1	64.9	shiny; silverish-grey; smooth
40	34.0	66.0	shiny; silverish-grey; smooth
50	32.5	67.5	shiny; silverish-grey; smooth

Table 4-11: Composition and Visual Evaluation of Nitrogen Agitated Nickel-Iron Solution 4 Employing 3A Cell Current.

current density [mA cm^{-2}]	composition mass-% Ni	mass-% Fe	observation deposit appearance
12	43.3	56.7	shiny; silverish-grey; smooth
15	41.9	58.1	shiny; silverish-grey; smooth
22.5	39.3	60.7	shiny; silverish-grey; smooth
30	36.5	63.5	shiny; silverish-grey; smooth
37.5	36.0	64.0	shiny; silverish-grey; smooth
45	35.0	65.0	shiny; silverish-grey; smooth
60	34.1	65.9	shiny; silverish-grey; smooth
90	34.0	66.0	shiny; silverish-grey; smooth
120	34.0	66.0	shiny; silverish-grey; fine cracks
150	33.4	66.6	shiny; silverish-grey; pitted, fine cracks

Table 4-12: Composition and Visual Evaluation of Nitrogen Agitated Nickel-Iron Solution 4 Employing 7A Cell Current.

current density [mA cm^{-2}]	composition mass-% Ni	mass-% Fe	observation deposit appearance
28	48.1	51.9	shiny; silverish-grey; smooth
35	46.9	53.1	shiny; silverish-grey; smooth
52.5	46.5	53.5	shiny; silverish-grey; smooth
70	43.5	56.5	shiny; silverish-grey; smooth
87.5	43.9	56.1	shiny; silverish-grey; smooth
105	39.1	60.9	shiny; silverish-grey; smooth
140	40.7	59.3	shiny; silverish-grey; pitted, fine cracks
210	44.6	55.4	less shiny; silverish-grey; pitted, fine cracks
280	40.4	59.6	less shiny; silverish-grey; pitted, fine cracks
350	41.0	59.1	less shiny; silverish-grey; pitted, fine cracks

Table 4-13: Composition and Visual Evaluation of Nitrogen Agitated Nickel-Zinc Solution 7 Employing 1A Cell Current.

current density [mA cm^{-2}]	composition		observation
	mass-% Ni	mass-% Zn	deposit appearance
5	38.8	61.2	shiny; brownish-grey
10	29.5	70.5	dull; brownish-grey
20	19.4	80.6	dull; yellowish-grey
30	19.0	81.0	shiny; silverish-grey
40	18.9	81.1	shiny; silverish-grey
50	19.8	80.2	shiny; silverish-grey

Table 4-14: Composition and Visual Evaluation of Quiescent Nickel-Zinc Solution 8 Employing 1A Cell Current.

current density [mA cm^{-2}]	composition mass-% Ni	mass-% Zn	observation deposit appearance
4	64.2	35.8	shiny; brownish-grey
5	54.0	46.0	shiny; brownish-grey
15	37.5	62.5	dull; silver-grey
20	35.7	64.3	dull; silver-grey
30	34.4	65.6	dull; silverish-grey
50	41.3	58.7	dull; silverish-grey

Table 4-15: Composition and Visual Evaluation of Quiescent Nickel-Zinc Solution 8 Employing 3A Cell Current.

current density [mA cm^{-2}]	composition mass-% Ni	mass-% Zn	observation deposit appearance
12	88.2	11.8	dull; brownish-grey, silver-grey patches
15	56.1	43.9	dull; brownish-grey, silver-grey patches
30	63.3	36.7	dull; brownish-grey, silver-grey patches
60	74.5	25.5	dull; brownish-grey, silver-grey patches
120	81.2	18.8	burnt, black powdery deposit
150	95.4	4.6	burnt, black powdery deposit

Table 4-16: Composition and Visual Evaluation of Quiescent Nickel-Zinc Solution 8 Employing 5A Cell Current.

current density [mA cm^{-2}]	composition mass-% Ni	mass-% Zn	observation deposit appearance
20	71.7	28.3	dull; brownish-grey
25	86.8	13.2	dull; brownish-grey
50	89.4	10.6	dull, brownish-grey; deposit cracked
75	87.3	12.7	dull; brownish-grey; deposit cracked
100	93.1	6.9	dull; brownish-grey; deposit cracked
150	86.3	13.7	burnt, black powdery deposit
200	78.1	21.9	burnt, black powdery deposit
250	84.3	15.7	burnt, black powdery deposit

Table 4-17: Composition and Visual Evaluation of Nitrogen Agitated Nickel-Zinc Solution 8 Employing 1A Cell Current.

current density [mA cm^{-2}]	composition mass-% Ni	mass-% Zn	observation deposit appearance
4	63.0	36.9	shiny; brownish-grey
5	60.7	39.3	shiny; brownish-grey
15	45.9	54.1	shiny; brownish-grey
20	32.1	67.9	slightly dull; silverish-grey
30	26.4	73.6	dull; silverish-grey
40	25.9	74.1	dull; silverish-grey
50	44.9	55.1	dull; silverish-grey

Table 4-18: Composition and Visual Evaluation of Nitrogen Agitated Nickel-Zinc Solution 8 Employing 3A Cell Current.

current density [mA cm^{-2}]	composition mass-% Ni	mass-% Zn	observation deposit appearance
12	32.3	67.7	shiny; silverish-grey
15	30.4	69.6	shiny; silverish-grey
30	41.0	59.0	dull; silverish-grey
45	58.4	41.6	dull; silverish-grey
60	64.8	35.2	dull; silverish-grey
120	71.7	28.3	dull; silverish-grey
150	77.7	22.3	burnt, black, powdery deposit

Table 4-19: Composition and Visual Evaluation of Nitrogen Agitated Nickel-Zinc Solution 8 Employing 5A Cell Current.

current density [mA cm^{-2}]	composition mass-% Ni	mass-% Zn	observation deposit appearance
20	89.1	10.9	dull; brownish-grey with silver patches
25	89.1	10.9	dull; brownish-grey with silver patches
62.5	72.3	27.7	dull; silverish-grey
75	70.8	29.2	dull; silverish-grey
100	72.3	27.7	dull; silverish-grey
150	95.8	4.2	burnt, black, powdery deposit
200	95.5	4.5	burnt, black, powdery deposit
250	97.4	2.6	burnt, black, powdery deposit

Table 4-20: Elemental Compositions Determined by EDX and GDOES of Deposits Produced in Nickel-Iron Solution 1 at Individual Current Densities.

Current Density [mA cm^{-2}]	Composition (EDX)		Composition (GDOES)	
	mass-% Ni	mass-% Fe	mass-% Ni	mass-% Fe
10	66.5	33.5	68.1	31.9
20	62.2	37.8	65.7	34.3
30	60.8	39.2	64.5	35.5
40	60.2	39.8	62.3	37.7
60	60.7	39.3	59.7	40.3

Table 4-21: Elemental Compositions Determined by GDOES of Deposits Produced in Nickel-Iron Solution 3 at Individual Current Densities.

Current Density [mA cm^{-2}]	Composition (GDOES)	
	mass-% Ni	mass-% Fe
10	61.3	38.7
20	57.5	42.5
30	56.0	44.0
40	35.5	64.5
60	36.5	63.5

Table 4-22: Elemental Compositions Determined by GDOES of Deposits Produced in Nickel-Iron Solution 4 at Individual Current Densities.

Current Density [mA cm^{-2}]	Composition (GDOES)	
	mass-% Ni	mass-% Fe
10	41.4	58.6
20	33.2	66.8
30	32.9	67.1
40	31.6	68.4
60	30.3	69.7

Table 4-23: Elemental Compositions Determined by GDOES at Various Areas of Deposits Produced in Nickel-Zinc Solution 8 at Individual Current Densities.

Current Density [mA cm^{-2}]	Area on Sample (see fig. 4-5)	Composition	
		mass-% Ni	mass-% Zn
10	1	45.8	54.2
10	2	37.0	63.0
10	3	29.5	70.5
20	1	27.5	72.5
20	2	29.2	70.8
20	3	24.0	76.0
30	1	30.0	70.0
30	2	28.6	71.4
30	3	25.2	74.8
40	1	24.9	75.1
40	2	23.6	76.4
40	3	33.7	66.3
50	1	52.4	47.6
50	2	44.6	45.4
50	3	37.9	62.1
60	1	34.2	65.8
60	2	36.9	63.1
60	3	38.0	62.0

Table 4-24: Raw Data $R_{\{hkl\}}$, $I_{\{hkl\}}$ and Planar Distribution in per cent of the Copper Sheet Substrate.

	Planes: Copper Sheet Substrate									
	111		**200**		**220**		**311**		**331**	
Raw Data	$R_{\{hkl\}}$	$I_{\{hkl\}}$	$R_{\{hkl\}}$	$I_{\{hkl\}}$	$R_{\{hkl\}}$	$I_{\{hkl\}}$	$R_{\{hkl\}}$	$I_{\{hkl\}}$	$R_{\{hkl\}}$	$I_{\{hkl\}}$
	245.3	1335	112.9	2083	59.5	396	65.4	352	48.7	449
%	12.1		40.9		14.7		11.9		20.4	

Table 4-25: Raw Data: Measured 2θ Bragg Angles. Calculated Interplanar Spacings 'd' and Lattice Parameter 'a' of Copper Sheet Substrate.

	Reflections						
Copper	**111**	**200**	**220**	**311**	**222**	**400**	**331**
°2θ	43.3	50.4	74.1	89.9	95.1	116.9	136.4
d [nm]	0.20874	0.18091	0.12786	0.10905	0.10437	0.09041	0.08296
a [nm]	0.36155	0.36182	0.36164	0.36169	0.36154	0.36164	0.36160

Table 4-26: Raw Data $R_{\{hkl\}}$ and $I_{\{hkl\}}$ of fcc NiFe Electrodeposits on Copper Sheet Substrates Deposited in NiFe Solution 1.

Current Density	***Planes***							
	111		**200**		**220**		**311**	
[mA cm^{-2}]	$R_{\{hkl\}}$	$I_{\{hkl\}}$	$R_{\{hkl\}}$	$I_{\{hkl\}}$	$R_{\{hkl\}}$	$I_{\{hkl\}}$	$R_{\{hkl\}}$	$I_{\{hkl\}}$
10	89.9	1468	41.0	479	21.5	356	24.0	342
30	83.7	1742	38.0	305	20.1	184	22.4	553
60	76.7	1807	34.8	276	18.4	118	20.5	541

Table 4-27: Planar Distribution in per cent of fcc NiFe Electrodeposits on Copper Sheet Substrates Deposited in NiFe Solution 1.

i	*Planes* Distribution in per cent			
[mA cm^{-2}]	**111**	**200**	**220**	**311**
10	27.8	19.9	28.1	24.2
30	33.2	12.8	14.6	39.4
60	36.6	12.4	9.9	41.1

Table 4-28: Raw Data: Measured 2θ Bragg Angles of fcc NiFe Electrodeposits on Copper Sheet Substrates Deposited in NiFe Solution 1.

i	*Reflections:* 2θ° Bragg Angles			
[mA cm^{-2}]	**111**	**200**	**220**	**311**
10	44.04	51.32	75.55	91.81
30	43.97	51.32	75.44	91.78
60	43.85	51.22	75.31	91.60

Table 4-29: Calculated d-Spacings of fcc NiFe Electrodeposits on Copper Sheet Substrates Deposited in NiFe Solution 1.

i	*Reflections:* Calculated d-Spacings [nm]			
[mA cm^{-2}]	**111**	**200**	**220**	**311**
10	0.20543	0.17789	0.12575	0.10726
30	0.20578	0.17789	0.12591	0.10728
60	0.20628	0.17821	0.12609	0.10745

Table 4-30: Raw Data $R_{\{hkl\}}$ and $I_{\{hkl\}}$ of fcc NiFe Electrodeposits on Copper Sheet Substrates Deposited in NiFe Solution 3.

Current	*Planes*							
Density	**111**		**200**		**220**		**311**	
[mA cm^{-2}]	$R_{\{hkl\}}$	$I_{\{hkl\}}$	$R_{\{hkl\}}$	$I_{\{hkl\}}$	$R_{\{hkl\}}$	$I_{\{hkl\}}$	$R_{\{hkl\}}$	$I_{\{hkl\}}$
10	78.8	1346	35.8	244	18.9	126	21.0	414
30	72.1	1222	32.8	144	17.2	78	19.2	370

Table 4-31: Raw Data $R_{\{hkl\}}$ and $I_{\{hkl\}}$ of fcc/bcc NiFe Electrodeposits on Copper Sheet Substrates Deposited in NiFe Solution 3 (i = 60 mA cm^{-2}).

Planes (fcc)							
111		**200**		**220**		**311**	
$R_{\{hkl\}}$	$I_{\{hkl\}}$	$R_{\{hkl\}}$	$I_{\{hkl\}}$	$R_{\{hkl\}}$	$I_{\{hkl\}}$	$R_{\{hkl\}}$	$I_{\{hkl\}}$
55.9	788	25.7	90	13.6	72	15.3	65

Planes (bcc)									
110		**200**		**211**		**310**		**222**	
$R_{\{hkl\}}$	$I_{\{hkl\}}$	$R_{\{hkl\}}$	$I_{\{hkl\}}$	$R_{\{hkl\}}$	$I_{\{hkl\}}$	$R_{\{hkl\}}$	$I_{\{hkl\}}$	$R_{\{hkl\}}$	$I_{\{hkl\}}$
74.8	557	10.3	20	18.7	130	2.7	46	1.1	94.8

Table 4-32: Planar Distribution in per cent of fcc NiFe on Copper Sheet Substrates Deposited at 10 and 30 mA cm^{-2} in NiFe Solution 3.

i	*Planes: Distribution in per cent*			
[mA cm^{-2}]	**111**	**200**	**220**	**311**
10	34.0	13.6	13.2	39.2
30	37.5	9.7	10.1	42.7

Table 4-33: Planar Distribution in per cent of fcc/bcc NiFe on Copper Sheet Substrates Deposited at 60 mA cm^{-2} in NiFe Solution 3.

Planes (fcc): *Distribution in per cent*			
111	**200**	**220**	**311**
51.9	12.9	19.6	15.6
Planes (bcc): *Distribution in per cent*			
110	**200**	**211**	**310**	**222**
6.1	1.6	5.7	14.0	72.6

Table 4-34: Raw Data: Measured 2θ Bragg Angles of fcc NiFe Electrodeposits on Copper Sheet Substrates Deposited in NiFe Solution 3 at 10 and 30 mA cm^{-2}.

i	***Reflections:*** 2θ° Bragg Angles			
[mA cm^{-2}]	**111**	**200**	**220**	**311**
10	43.87	51.20	75.36	91.66
30	43.77	51.06	75.26	91.52

Table 4-35: Raw Data: Measured 2θ Bragg Angles of fcc/bcc NiFe Electrodeposits on Copper Sheet Substrates Deposited in NiFe Solution 3 at 60 mA cm^{-2}.

Reflections / 2θ° Bragg Angles ***(fcc)***			
111	**200**	**220**	**311**
43.70	50.85	74.95	90.97
Reflections / 2θ° Bragg Angles ***(bcc)***				
110	**200**	**211**	**310**	**222**
44.61	65.40	82.58	117.74	138.52

Table 4-36: Calculated d-Spacings of fcc NiFe Electrodeposits on Copper Sheet Substrates Deposited in NiFe Solution 3.

i [mA cm^{-2}]	***Reflections*** / calculated d-Spacings [nm]			
	111	**200**	**220**	**311**
10	0.20622	0.17826	0.12602	0.10739
30	0.20666	0.17874	0.12617	0.10752

Table 4-37: Calculated d-Spacings of fcc/bcc Electrodeposits on Copper Sheet Substrates Deposited in NiFe Solution 3.

Reflections / calculated d-Spacings [nm] ***(fcc)***			
111	**200**	**220**	**311**
0.20696	0.17942	0.12660	0.10803
Reflections / calculated d-Spacings [nm] ***(bcc)***				
110	**200**	**211**	**310**	**222**
0.20295	0.14259	0.11680	0.09076	0.82852

Table 4-38: Raw Data $R_{\{hkl\}}$ and $I_{\{hkl\}}$ of fcc NiFe Electrodeposit on Copper Sheet Substrate Deposited in NiFe Solution 4 (i = 10 mA cm^{-2}).

Planes							
111		**200**		**220**		**311**	
$R_{\{hkl\}}$	$I_{\{hkl\}}$	$R_{\{hkl\}}$	$I_{\{hkl\}}$	$R_{\{hkl\}}$	$I_{\{hkl\}}$	$R_{\{hkl\}}$	$I_{\{hkl\}}$
59.0	8331	26.8	128	14.5	52	16.1	88

Table 4-39: Raw Data $R_{\{hkl\}}$ and $I_{\{hkl\}}$ of bcc NiFe Electrodeposits on Copper Sheet Substrates Deposited in NiFe Solution 4 (i = 30 mA cm^{-2}), (i = 60 mA cm^{-2}).

Current	***Planes***									
Density	**110**		**200**		**211**		**310**		**222**	
[mA cm^{-2}]	$R_{\{hkl\}}$	$I_{\{hkl\}}$	$R_{\{hkl\}}$	$I_{\{hkl\}}$	$R_{\{hkl\}}$	$I_{\{hkl\}}$	$R_{\{hkl\}}$	$I_{\{hkl\}}$	$R_{\{hkl\}}$	$I_{\{hkl\}}$
30	72.2	77	10.0	*	18.3	58	9.7	*	3.8	1074
60	69.5	17	9.8	*	17.7	37	9.5	*	3.7	1473

* not detectable

Table 4-40: Planar Distribution in per cent of fcc NiFe Electrodeposit on Copper Sheet Substrate Deposited in NiFe Solution 4 (i = 10 mA cm^{-2}).

Planes: *Distribution in per cent*			
111	**200**	**220**	**311**
91.1	3.1	2.3	3.5

Table 4-41: Planar Distribution in per cent of bcc NiFe Electrodeposits on Copper Sheet Substrates deposited in NiFe Solution 4 (i = 30 mA cm^{-2}), (i = 60 mA cm^{-2}).

i	***Planes:*** *Distribution in per cent*				
[mA cm^{-2}]	**110**	**200**	**211**	**310**	**222**
30	0.4	*	1.1	*	98.5
60	0.1	*	0.5	*	99.4

* not detectable

Table 4-42: Raw Data: Measured 2θ Bragg Angles of fcc NiFe Electrodeposit on Copper Sheet Substrate Deposited in NiFe Solution 4 (i = 10 mA cm^{-2}).

Reflections / 2θ° Bragg Angles *(fcc)*			
111	**200**	**220**	**311**
43.71	51.02	74.63	90.87

Table 4-43: Raw Data: Measured 2θ Bragg Angles of bcc NiFe Electrodeposits on Copper Sheet Substrates Deposited in NiFe Solution 4 (i = 30 mA cm^{-2}), (i = 60 mA cm^{-2}).

i	***Reflections*** / 2θ° Bragg Angles *(bcc)*				
[mA cm^{-2}]	**110**	**200**	**211**	**310**	**222**
30	44.61	*	82.31	*	137.65
60	44.68	*	82.36	*	137.61

* not detectable

Table 4-44: Calculated d-Spacings of fcc NiFe Electrodeposit on Copper Sheet Substrate Deposited in NiFe Solution 4 (i = 10 mA cm^{-2}).

Reflections / calculated d-Spacings [nm]			
111	**200**	**220**	**311**
0.20694	0.17885	0.12707	0.10812

Table 4-45: Calculated d-Spacings of bcc NiFe Electrodeposits on Copper Sheet Substrates Deposited in NiFe Solution 4 (i = 30 mA cm^{-2}), (i = 60 mA cm^{-2}).

i [mA cm^{-2}]	***Reflections*** / calculated d-Spacings [nm]				
	110	**200**	**211**	**310**	**222**
30	0.20295	*	0.11705	*	0.08261
60	0.20266	*	0.11699	*	0.08262

Table 4-46: Structure of Nickel-Zinc Deposited at Various Current Densities in As-Deposited and Heat-Treated State.

Current Density [mA cm^{-2}]	**Structure As - Deposited**	**Structure Heat - Treated**
10	bcc γ-phase	Tetragonal β_1-phase + bcc γ-phase
20	bcc γ-phase	Tetragonal β_1-phase + bcc γ-phase
30	bcc γ-phase	bcc γ-phase
40	bcc γ-phase + fcc α-phase	Tetragonal β_1-phase + bcc γ-phase + fcc α-phase
50	bcc γ-phase + fcc α-phase	Tetragonal β_1-phase + bcc γ-phase + fcc α-phase
60	bcc γ-phase	Tetragonal β_1-phase + bcc γ-phase

Table 4-47: Comparison Between Lattice Parameters of Nickel-Zinc Alloys Crystallized under Equilibrium Conditions and Through Electrocrystallization at Current Densities from 10 to 60 mA cm^{-2}.

	Lattice Parameter [nm]		**Approximate Chemical Formula**
	γ-phase	**α-phase**	
JCPDS	0.892		Ni_5Zn_{21}
i [mA cm^{-2}]			
10	0.8704		NiZn
20	0.8801		Ni_3Zn_7
30	0.8903		Ni_6Zn_{19}
40	0.8850	0.3535	-
50	0.8850	0.3532	-
60	0.8865		$Ni_{13}Zn_{36}$

Table 4-48: Comparison between Lattice Parameters of γ-Phase Nickel-Zinc Alloy Deposits in As-Deposited and Heat-Treated State.

Current Density [mA cm^{-2}]	Lattice Parameter [nm]		
	γ-phase as-deposited	γ-phase heat treated	Δ a
10	0.8704	0.8840	0.0136
20	0.8801	0.8869	0.0068
30	0.8903	0.8878	0.0025
40	0.8850	0.8850	0
50	0.8850	0.8850	0
60	0.8865	0.8860	0.0005

Table 4-49: Elemental Composition of fcc Nickel-Iron Deposit at Different Distances from Copper Substrate/Deposit Interface.

Distance from Interface Substrate/Deposit [nm]	Composition Mass-%	
	Ni	Fe
5	37.54	62.46
10	36.38	63.62
15	37.54	62.46
20	37.93	62.07
25	37.02	62.98
30	37.25	62.75
35	36.58	63.42
40	37.59	62.41
45	38.32	61.68
50	36.25	63.75
55	36.56	63.44
60	35.96	64.04
65	36.03	63.97
70	36.50	63.50
75	36.70	63.30
80	36.84	63.15
85	35.98	64.02
90	35.96	64.04

Table 4-50: Elemental Composition of bcc Nickel-Iron Deposit at Different Distances from Copper Substrate/Deposit Interface.

Distance from Interface Substrate/Deposit [nm]	Composition Mass-%	
	Ni	Fe
5	29.48	70.52
10	29.39	70.61
15	29.43	70.57
20	29.05	70.95
25	28.84	71.16
30	28.88	71.12
35	28.93	71.07
40	28.95	71.05
45	29.00	71.00
50	29.37	70.63
55	29.15	70.85
60	29.09	70.91
65	29.08	70.92
70	29.01	70.99
75	28.95	71.05
80	28.83	71.17
85	28.57	71.43
90	28.64	71.36

Table 4-51: Elemental Composition of Double Layered fcc/bcc Nickel-Iron Deposit.

Structure	Composition [Mass-%]	
	Ni	Fe
fcc	41.07	58.93
fcc	40.74	59.26
fcc	39.56	60.44
bcc	26.01	73.99
bcc	26.10	73.90
bcc	26.05	73.95

Table 4-52: Elemental Composition of Double Layered bcc/fcc Nickel-Iron Deposit.

Structure	Composition [Mass-%]	
	Ni	Fe
bcc	26.06	73.94
fcc	37.12	62.88

Table 4-53: Elemental Composition of bcc Nickel-Zinc Deposit (i = 10 mA cm^{-2}) at Different Distances from Copper Substrate/Deposit Interface.

Distance from Interface Substrate/Deposit [nm]	Composition Mass-%	
	Ni	Zn
5	31.43	68.57
10	31.50	68.50
15	31.57	68.43
20	31.53	68.47
25	31.87	68.13
30	31.56	68.44
35	31.66	68.34
40	31.49	68.51
45	31.41	68.59
50	31.63	68.37
55	31.59	68.41
60	31.36	68.64
65	31.30	68.70
70	30.94	69.06
...		
...		
middle of deposit	31.02	68.98

Table 4-54: Elemental Composition of bcc Nickel-Zinc Deposit (i = 60 mA cm^{-2}) at Different Distances from Copper Substrate/Deposit Interface.

Distance from Interface Substrate/Deposit [nm]	Composition Mass-%	
	Ni	Zn
5	35.42	64.58
10	38.21	61.79
15	38.38	61.62
20	34.34	65.66
25	34.17	65.75
30	33.25	66.75
35	34.71	65.29
40	34.10	65.90
45	33.70	66.30
50	34.49	65.51
55	33.79	66.21

Table 4-55: Elemental Composition of bcc Nickel-Zinc Deposit (i = 60 mA cm^{-2}) at Similar Distance from Copper Substrate/Deposit Interface but in Different Grains.

Spot	Composition Mass-%	
	Ni	Zn
1	32.88	67.12
2	30.52	69.48
3	29.93	70.07

Table 4-56: Elemental Composition of bcc Nickel-Zinc Deposit (i = 10 mA cm^{-2}) at Different Distances from Steel Substrate/Deposit Interface.

Distance from Interface Substrate/Deposit [nm]	Composition Mass-%	
	Ni	Zn
5	59.13	40.87
10	51.92	48.08
15	42.34	57.66
20	34.31	65.69
25	34.16	65.84
30	31.64	68.36
35	33.01	66.99
40	34.89	65.11
45	30.56	69.44

Table 4-57: Raw Data $R_{\{hkl\}}$, $I_{\{hkl\}}$ and Planar Distribution in per cent of the Copper Disc Substrate.

	Planes: Copper Disc Substrate									
	111		**200**		**220**		**311**		**331**	
Raw	$R_{\{hkl\}}$	$I_{\{hkl\}}$	$R_{\{hkl\}}$	$I_{\{hkl\}}$	$R_{\{hkl\}}$	$I_{\{hkl\}}$	$R_{\{hkl\}}$	$I_{\{hkl\}}$	$R_{\{hkl\}}$	$I_{\{hkl\}}$
Data	245.5	9344	112.9	4711	59.6	170	65.5	698	48.7	103
%	39.9		43.7		3.0		11.2		2.2	

Table 4-58: Raw Data: Measured 2θ Bragg Angles. Calculated Interplanar Spacings 'd' and Lattice Parameter 'a' of Copper Disc Substrate.

	Reflections						
Copper	**111**	**200**	**220**	**311**	**222**	**400**	**331**
°2θ	43.31	50.41	74.09	89.86	95.10	116.76	136.35
d [nm]	0.20873	0.18089	0.12787	0.10907	0.10439	0.09046	0.08298
a [nm]	0.36153	0.36177	0.36166	0.36174	0.36162	0.36184	0.36169

Table 4-59: Raw Data, $R_{\{hkl\}}$ and $I_{\{hkl\}}$, of fcc NiFe Electrodeposits on Copper Disc Substrates.

	Planes							
Thickness	**111**		**200**		**220**		**311**	
[μm]	$R_{\{hkl\}}$	$I_{\{hkl\}}$	$R_{\{hkl\}}$	$I_{\{hkl\}}$	$R_{\{hkl\}}$	$I_{\{hkl\}}$	$R_{\{hkl\}}$	$I_{\{hkl\}}$
0.3	13.8	1622	5.6	*	2.2	209	2.1	*
0.4	17.6	1440	7.2	*	2.9	132	2.7	*
0.5	21.1	1553	8.6	*	3.4	91	3.4	*
0.75	28.5	2377	11.8	*	4.8	*	4.8	*
1	34.3	6463	14.4	*	6.0	226	6.0	*
1.5	42.6	7451	18.2	*	8.0	(70)	8.1	*
2	47.8	6246	20.8	*	9.4	159	9.7	*
3	52.8	33760	23.5	*	11.3	(66)	11.9	*

* Not detectable

( ) Values in brackets are intensities below $3 \times \sqrt{\text{Background}}$

Table 4-60: Planar Distribution in per cent of fcc NiFe Electrodeposits on Copper Disc Substrates.

	Planes: *Distribution in per cent*			
[μm]	**111**	**200**	**220**	**311**
0.3	55.2	*	44.8	*
0.4	63.8	*	36.2	*
0.5	73.4	*	26.6	*
0.75	100	*	*	*
1	83.4	*	16.6	*
1.5	100	*	**	*
2	88.5	*	11.5	*
3	100	*	**	*

* Not detectable

** Intensities below $3 \times \sqrt{\text{Background}}$

Table 4-61: Raw Data: Measured 2θ Bragg Angles of fcc Nickel-Iron Deposits.

	Reflections / 2θ° Bragg Angles			
[μm]	**111**	**200**	**220**	**311**
0.3	43.58	*	74.52	*
0.4	43.63	*	74.57	*
0.5	43.65	*	74.87	*
0.75	43.74	*	*	*
1	43.72	*	74.86	*
1.5	43.75	*	(74.94)	*
2	43.77	*	75.04	*
3	42.72	*	(74.93)	*

* Not detectable

( ) Values in brackets are intensities below $3 \times \sqrt{\text{Background}}$

Table 4-62: Calculated d-Spacings of fcc NiFe Substrates of Various Thicknesses on Copper.

	Reflections / Calculated d-spacings [nm]			
[μm]	**111**	**200**	**220**	**311**
0.3	0.20751	*	0.12723	*
0.4	0.20727	*	0.12716	*
0.5	0.20721	*	0.12672	*
0.75	0.20681	*	*	*
1	0.20689	*	0.12674	*
1.5	0.20673	*	(0.12663)	*
2	0.20666	*	0.12647	*
3	0.20688	*	(0.12664)	*

* Not detectable

( ) Values in brackets are calculated from Bragg angle positions with intensities below $3 \times \sqrt{\text{Background}}$

Table 4-63: Raw Data, $R_{\{hkl\}}$ and $I_{\{hkl\}}$, of bcc NiFe Electrodeposits on Copper Disc Substrates.

Thickness	***Planes***									
	110		**200**		**211**		**310**		**222**	
[μm]	$R_{\{hkl\}}$	$I_{\{hkl\}}$	$R_{\{hkl\}}$	$I_{\{hkl\}}$	$R_{\{hkl\}}$	$I_{\{hkl\}}$	$R_{\{hkl\}}$	$I_{\{hkl\}}$	$R_{\{hkl\}}$	$I_{\{hkl\}}$
0.4	22.9	181	2.4	*	3.6	(88)	1.6	*	0.6	*
0.5	27.3	414	2.9	*	4.4	3120	1.9	*	0.7	*
0.75	36.5	552	4.0	*	6.2	519	2.7	*	1.0	*
1	43.8	598	4.9	*	7.8	693	3.4	*	1.3	(76)
1.5	53.6	333	6.3	*	10.2	810	4.6	*	1.7	309
2	59.6	249	7.3	(43)	12.0	1228	5.6	*	2.1	91
3	65.4	510	8.5	(58)	14.5	856	7.0	*	2.6	243
20	68.2	149	9.4	34	17.3	119	9.2	(18)	3.6	7032

* Not detectable

( ) Values in brackets are intensities below $3 \times \sqrt{\text{Background}}$

Table 4-64: Planar Distribution in per cent of bcc NiFe Electrodeposits on Copper Disc Substrates.

	Planes: Distribution in per cent				
[μm]	**110**	**200**	**211**	**310**	**222**
0.4	100	*	**	**	*
0.5	17.4	*	82.6	*	*
0.75	15.3	*	84.7	*	*
1	13.3	*	86.4	*	**
1.5	2.3	*	29.6	*	68.1
2	2.8	**	67.8	*	29.4
3	4.9	**	37.0	*	58.1
20	0.1	0.2	0.3	**	99.4

* Not detectable

** $I(hkl) < 3 \times \sqrt{\text{Background}}$

Table 4-65: Raw Data: Measured 2θ Bragg Angles of bcc Nickel-Iron Electrodeposits of Individual Thickness on Copper Disc Substrates.

	Reflections / 2θ° Bragg Angles				
[µm]	**110**	**200**	**211**	**310**	**222**
0.4	44.85	*	(82.66)	*	*
0.5	44.86	*	82.67	*	*
0.75	44.82	*	82.61	*	*
1	44.85	*	82.67	*	(137.52)
1.5	44.79	*	82.58	*	137.67
2	44.79	(65.37)	82.64	*	137.78
3	44.79	(65.40)	82.59	*	137.76
20	44.63	65.40	82.29	(116.70)	137.74

* Not detectable

( ) Values in brackets are Bragg angles where intensities were below $3 \times \sqrt{\text{Background}}$

Table 4-66: Calculated d-Spacings of bcc NiFe Electrodeposits of Individual Thickness on Copper Disc Substrates.

	Reflections / Calculated d-spacings [nm]				
[µm]	**110**	**200**	**211**	**310**	**222**
0.4	0.20191	*	(0.11642)	*	*
0.5	0.20190	*	0.11663	*	*
0.75	0.20207	*	0.11670	*	*
1	0.20194	*	0.11663	*	(0.08247)
1.5	0.20219	*	0.11673	*	0.08260
2	0.20217	(0.14289)	0.11667	*	0.08250
3	0.20218	(0.14296)	0.11673	*	0.08257
20	0.20287	0.14258	0.11707	(0.09049)	0.08258

* Not detectable

( ) Values in brackets are calculated from Bragg angle positions with intensities below $3 \times \sqrt{\text{Background}}$

Table 4-67: Raw Data $R_{\{hkl\}}$ and $I_{\{hkl\}}$ of 0.5μm Thick fcc NiFe Electrodeposited on Various Substrates.

Substrate	*Planes* 111		200		220		311	
	$R_{\{hkl\}}$	$I_{\{hkl\}}$	$R_{\{hkl\}}$	$I_{\{hkl\}}$	$R_{\{hkl\}}$	$I_{\{hkl\}}$	$R_{\{hkl\}}$	$I_{\{hkl\}}$
Copper Disc Substrate	21.1	1553	8.6	*	3.4	91	3.4	*
0.5μm bcc NiFe Electrodeposit	21.1	1889	8.6	*	3.4	(49)	3.4	*
2μm bcc NiFe Electrodeposit	21.1	775	8.6	*	3.4	(48)	3.4	*

* Not detectable

( ) Values in brackets are intensities below $3 \times \sqrt{\text{Background}}$

Table 4-68: Texture (Planar Distribution in per cent) of 0.5μm thick fcc NiFe Electrodeposits on Various Substrates.

Substrate	*Planes: Distribution in per cent* 111	200	220	311
Copper Disc Substrate	73.4	*	26.6	*
0.5μm bcc NiFe Electrodeposit	100	*	**	*
2μm bcc NiFe Electrodeposit	100	*	**	*

* Not detectable

** $I(hkl) < 3 \times \sqrt{\text{Background}}$

Table 4-69: Raw Data $R_{\{hkl\}}$ and $I_{\{hkl\}}$ of 2μm Thick fcc NiFe Electrodeposited on Various Substrates.

Substrate	Planes: 111		200		220		311	
	$R_{\{hkl\}}$	$I_{\{hkl\}}$	$R_{\{hkl\}}$	$I_{\{hkl\}}$	$R_{\{hkl\}}$	$I_{\{hkl\}}$	$R_{\{hkl\}}$	$I_{\{hkl\}}$
Copper Disc Substrate	47.8	6246	20.7	*	9.4	159	9.7	*
0.5μm bcc NiFe Electrodeposit	47.8	12873	20.7	*	9.4	(59)	9.7	*
2μm bcc NiFe Electrodeposit	47.8	8759	20.7	2701	9.4	133	9.7	228

* Not detectable

( ) Values in brackets are intensities below $3 \times \sqrt{\text{Background}}$

Table 4-70: Texture (Planar Distribution in per cent) of 2μm Thick fcc NiFe Electrodeposits on Various Substrates.

Substrate	Planes: Distribution in per cent 111	200	220	311
Copper Disc Substrate	88.5	*	11.5	*
0.5μm bcc NiFe Electrodeposit	100	*	**	*
2μm bcc NiFe Electrodeposit	52.1	37.3	4.0	6.6

* Not detectable

** $I(hkl) < 3 \times \sqrt{\text{Background}}$

Table 4-71: Raw Data $R_{\{hkl\}}$ and $I_{\{hkl\}}$ of 0.5μm Thick bcc NiFe Electrodeposits on Various Substrates.

Substrate	*Planes* 110		200		211		310		222	
	$R_{\{hkl\}}$	$I_{\{hkl\}}$	$R_{\{hkl\}}$	$I_{\{hkl\}}$	$R_{\{hkl\}}$	$I_{\{hkl\}}$	$R_{\{hkl\}}$	$I_{\{hkl\}}$	$R_{\{hkl\}}$	$I_{\{hkl\}}$
Copper Disc Substrate	27.3	414	2.9	*	4.4	317	1.9	*	0.7	*
0.5μm fcc NiFe Electrodeposit	27.3	889	2.9	(9)	4.4	313	1.9	*	0.7	(34)
2μm fcc NiFe Electrodeposit	27.3	1433	2.9	(4)	4.4	312	1.9	*	0.7	(50)

* Not detectable

( ) Values in brackets are intensities below $3 \times \sqrt{\text{Background}}$

Table 4-72: Texture (planar Distribution in per cent) of 0.5μm Thick bcc NiFe Electrodeposits on Various Substrates.

Substrate	*Planes: Distribution in per cent* 110	200	211	310	222
Copper Disc Substrate	17.4	*	82.6	*	*
0.5μm fcc NiFe Electrodeposit	31.5	**	68.5	*	**
2μm fcc NiFe Electrodeposit	42.6	**	57.4	*	**

* Not detectable

** $I(hkl) < 3 \times \sqrt{\text{Background}}$

Table 4-73: Raw Data $R_{\{hkl\}}$ and $I_{\{hkl\}}$ of 2μm Thick bcc NiFe Electrodeposits on Various Substrates.

Substrate	Planes 110		200		211		310		222	
	$R_{\{hkl\}}$	$I_{\{hkl\}}$	$R_{\{hkl\}}$	$I_{\{hkl\}}$	$R_{\{hkl\}}$	$I_{\{hkl\}}$	$R_{\{hkl\}}$	$I_{\{hkl\}}$	$R_{\{hkl\}}$	$I_{\{hkl\}}$
Copper Disc Substrate	59.6	249	7.3	(43)	12.0	1228	5.6	*	2.1	91
0.5μm fcc NiFe Electrodeposit	59.6	292	7.3	(38)	12.0	509	5.6	*	2.1	621
2μm fcc NiFe Electrodeposit	59.6	2200	7.3	(20)	12.0	714	5.6	*	2.1	204

* Not detectable

( ) Values in brackets are intensities below $3 \times \sqrt{\text{Background}}$

Table 4-74: Texture (planar Distribution in per cent) of 2μm Thick bcc NiFe Electrodeposits on Various Substrates.

Substrate	Planes: Distribution in per cent 110	200	211	310	222
Copper Disc Substrate	2.8	**	67.8	*	29.4
0.5μm fcc NiFe Electrodeposit	1.4	**	12.1	*	86.5
2μm fcc NiFe Electrodeposit	18.8	**	30.7	*	50.5

* Not detectable

** $I(hkl) < 3 \times \sqrt{\text{Background}}$

Table 4-75: Raw Data $R_{\{hkl\}}$ and $I_{\{hkl\}}$ of 0.5, 2, and 10μm Thick bcc NiFe Electrodeposited on 2μm thick NiFe Substrate.

	Planes									
Thickness	**110**		**200**		**211**		**310**		**222**	
	$R_{\{hkl\}}$	$I_{\{hkl\}}$	$R_{\{hkl\}}$	$I_{\{hkl\}}$	$R_{\{hkl\}}$	$I_{\{hkl\}}$	$R_{\{hkl\}}$	$I_{\{hkl\}}$	$R_{\{hkl\}}$	$I_{\{hkl\}}$
0.5 μm	27.3	1433	2.9	(4)	4.4	312	1.9	*	0.7	(50)
2 μm	59.6	2200	7.3	(20)	12.0	724	5.6	*	2.1	204
10 μm	68.7	77	9.4	60	17.5	160	9.3	79	3.6	2735

* Not detectable

( ) Values in brackets are intensities below $3 \times \sqrt{\text{Background}}$

Table 4-76: Texture (planar Distribution in per cent) of 0.5, 2, and 10μm Thick bcc NiFe Electrodeposits on 2μm thick fcc NiFe Substrate.

	Planes: *Distribution in per cent*				
Thickness	**110**	**200**	**211**	**310**	**222**
0.5 μm	42.6	*	57.4	*	**
2 μm	18.8	**	30.7	*	50.5
10 μm	0.1	0.8	1.2	1.1	96.8

* Not detectable

** $I(hkl) < 3 \times \sqrt{\text{Background}}$

Table 4-77: Raw Data: Measured 2θ Bragg Angles of 0.5µm, 2µm, and 10 µm Thick bcc NiFe Electrodeposits on 2µm fcc NiFe.

	Reflections / 2θ Bragg Angles				
Thickness	**110**	**200**	**211**	**310**	**222**
0.5 µm	44.77	(65.71)	82.61	*	(137.52)
2 µm	44.73	(65.23)	82.57	*	137.64
10 µm	44.77	65.50	82.44	116.82	137.78

Table 4-78: Calculated d-Spacings of bcc NiFe of 0.5, 2, and 10µm Thick Electrodeposits on 2µm fcc NiFe Substrates.

	Reflections / Calculated d-spacings [nm]				
Thickness	**110**	**200**	**211**	**310**	**222**
0.5 µm	0.20236	(0.14310)	0.11683	*	(0.08261)
2 µm	0.20235	(0.14383)	0.11683	*	0.08261
10 µm	0.20226	0.14302	0.11677	0.09045	0.08257

Table 4-79: Raw Data $R_{\{hkl\}}$, $I_{\{hkl\}}$ and Planar Distribution in per cent of Mild Steel Substrate.

	Planes									
Mild	**110**		**200**		**211**		**310**		**222**	
Steel	$R_{\{hkl\}}$	$I_{\{hkl\}}$	$R_{\{hkl\}}$	$I_{\{hkl\}}$	$R_{\{hkl\}}$	$I_{\{hkl\}}$	$R_{\{hkl\}}$	$I_{\{hkl\}}$	$R_{\{hkl\}}$	$I_{\{hkl\}}$
Raw Data	262.2	700	37.4	39	68.3	99	37.3	64	14.6	18
%	32.9		12.7		17.8		21.1		15.5	

Table 4-80: Raw Data: Measured 2θ Bragg Angles. Calculated Interplanar Spacings 'd' and Lattice Parameter 'a' of Mild Steel Substrate.

Mild	***Reflections***					
Steel	**110**	**200**	**211**	**220**	**310**	**222**
°2θ	44.82	65.08	82.39	98.77	116.27	136.98
d [nm]	0.20205	0.14322	0.11696	1.01470	0.09070	0.08280
a [nm]	0.285738	0.28643	0.28650	0.28703	0.28682	0.28682

Table 4-81: Calculated $R_{\{hkl\}}$ Values of an Untextured Nickel-Zinc Powder Specimen of Similar Nominal Composition and Thickness to the Electrodeposit formed at 10 mA cm^{-2}.

Thickness	***Planes: $R_{\{hkl\}}$-Values***										
[μm]	**222**	**321**	**330**	**332**	**510**	**521**	**600**	**631**	**552**	**741**	**820**
0.1	12.4	54.9	8.2	10.6	7.3	10.5	0.8	3.8	1.3	1.7	0.8
0.2	24.3	107.2	16.0	20.8	14.3	20.6	1.7	7.3	2.5	3.2	1.5
0.5	56.6	253.9	38.1	49.7	34.4	49.6	4.0	17.9	6.1	7.9	3.7
1	105.2	474.3	71.7	94.1	65.4	94.7	7.7	34.5	11.8	15.2	7.1
2	183.4	837.3	128.4	175.1	119.1	173.5	14.3	64.3	22.1	28.6	13.5
10	407.2	1939	318.4	457.7	324.7	489.9	42.2	199.8	70.8	95.2	45.1
20	420.6	2025	340.6	497.2	362.3	556.4	49.3	240.3	86.9	120.4	57.3

Table 4-82: Measured Intensities $I_{\{hkl\}}$ of NiZn, Electrodeposited at 10 mA cm^{-2}, on Mild Steel Substrates.

Thickness	*Planes: $I_{\{hkl\}}$-Values*										
[μm]	**222**	**321**	**330**	**332**	**510**	**521**	**600**	**631**	**552**	**741**	**820**
0.1	*	*	2205	*	*	*	*	*	*	*	*
0.2	*	*	1053	*	*	*	*	*	*	*	*
0.5	125	*	1169	*	*	*	*	*	69	*	*
1	305	*	1965	*	*	*	*	*	121	*	*
2	1356	*	2473	(50)	*	*	*	*	91	*	*
10	4990	*	2155	322	*	*	217	*	71	*	*
20	2143	*	14390	417	*	*	404	*	215	*	*

* Not detectable

( ) Values in brackets are intensities below $3 \times \sqrt{\text{Background}}$

Table 4-83: Planar Distribution of Nickel-Zinc Deposit of Various Thicknesses, Electrodeposited at 10 mA cm^{-2}, on Mild Steel Substrates.

	Planes: *Distribution in per cent*										
[μm]	**222**	**321**	**330**	**332**	**510**	**521**	**600**	**631**	**552**	**741**	**820**
0.1	*	*	100	*	*	*	*	*	*	*	*
0.2	*	*	100	*	*	*	*	*	*	*	*
0.5	5.0	*	69.4	*	*	*	*	*	25.6	*	*
1	7.2	*	67.6	*	*	*	*	*	25.2	*	*
2	24.0	*	62.6	**	*	*	*	*	13.4	*	*
10	47.4	*	26.2	2.7	*	*	19.9	*	3.8	*	*
20	8.7	*	71.8	1.4	*	*	13.9	*	4.2	*	*

* Not detectable

** $I(hkl) < 3 \times \sqrt{\text{Background}}$

Table 4-84: Raw Data: Bragg Angles of bcc Nickel-Zinc, Electrodeposited at 10 mA cm^{-2}, on Mild Steel Substrates.

	Reflections / 2θ Bragg Angles										
[μm]	**222**	**321**	**330**	**332**	**510**	**521**	**600**	**631**	**552**	**741**	**820**
0.1	*	*	44.24	*	*	*	*	*	*	*	*
0.2	*	*	43.98	*	*	*	*	*	*	*	*
0.5	35.42	*	43.62	*	*	*	*	*	80.2	*	*
1	35.34	*	43.52	*	*	*	*	*	79.95	*	*
2	35.35	*	43.48	(48)	*	*	*	*	79.84	*	*
10	35.32	*	43.44	47.9	*	*	63.07	*	79.81	*	*
20	35.3	*	43.41	47.95	*	*	62.96	*	79.80	*	*

* Not detectable

( ) Values in brackets are intensities below $3 \times \sqrt{\text{Background}}$

Table 4-85: Calculated d-Spacings of bcc Nickel-Zinc (i = 10 mA cm^{-2}) at Various Thicknesses.

	Reflections / Calculated d-Spacings [nm]										
[μm]	**222**	**321**	**330**	**332**	**510**	**521**	**600**	**631**	**552**	**741**	**820**
0.1	*	*	0.20456	*	*	*	*	*	*	*	*
0.2	*	*	0.20571	*	*	*	*	*	*	*	*
0.5	0.25391	*	0.20732	*	*	*	*	*	0.11970	*	*
1	0.25449	*	0.20779	*	*	*	*	*	0.11997	*	*
2	0.25471	*	0.20796	(0.1881)	*	*	*	*	0.12007	*	*
10	0.25491	*	0.20814	0.18827	*	*	0.14717	*	0.12017	*	*
20	0.25509	*	0.20828	0.18840	*	*	0.14728	*	0.12025	*	*

* Not detectable

( ) Values in brackets are calculated from 2θ Bragg angles with intensities below $3 \times \sqrt{\text{Background}}$

Table 4-86: Calculated $R_{\{hkl\}}$ Values of an Untextured Nickel-Zinc Powder Specimen of Similar Nominal Composition and Thickness to the Electrodeposit Formed at 60 mA cm^{-2}.

Thickness	*Planes: $R_{\{hkl\}}$-Values*										
[μm]	**222**	**321**	**330**	**332**	**510**	**521**	**600**	**631**	**552**	**741**	**820**
0.1	12.3	54.2	8.1	10.4	7.2	10.3	0.8	3.7	1.3	1.6	0.8
0.2	23.2	104.7	15.6	19.9	14.0	20.1	1.6	7.2	2.4	3.2	1.5
0.5	55.1	249.4	37.4	50.0	33.8	48.7	4.1	17.6	5.9	7.9	3.6
1	104.0	468.1	71.5	96.1	64.4	93.3	7.8	34.0	11.7	15.3	7.0
2	178.4	820.3	125.8	171.6	116.8	170.1	14.2	63.0	21.6	28.2	13.1
10	390.8	1839	302.3	422.8	313.4	462.7	40.2	189.3	67.7	90.6	43.6
20	412.9	1968	331.2	473.5	352.6	514.8	47.9	234.0	84.4	116.9	55.4

Table 4-87: Measured Intensities $I_{\{hkl\}}$ of NiZn, Electrodeposited at 60 mA cm^{-2}, on Mild Steel Substrates.

Thickness	*Planes: $I_{\{hkl\}}$-Values*										
[μm]	**222**	**321**	**330**	**332**	**510**	**521**	**600**	**631**	**552**	**741**	**820**
0.1		*	2256	*	*	*	*	*	*	*	*
0.2	249	*	2352	(29)	*	*	*	*	(18)	*	*
0.5	428	*	5994	106	*	*	(30)	*	265	(32)	*
1	1463	*	12685	253	*	*	243	*	303	98	*
2	410	*	28807	111	*	*	301	*	507	227	*
10	*	*	19870	*	456	(62)	627	109	947	499	336
20	*	*	355824	*	*	*	(86)	*	392	137	*

* Not detectable

( ) Values in brackets are intensities below $3 \times \sqrt{\text{Background}}$

Table 4-88: Planar Distribution of Nickel-Zinc Deposit of Various Thicknesses, Electrodeposited at 60 mA cm^{-2}, on Mild Steel Substrates.

	Planes: *Distribution in per cent*										
[μm]	**222**	**321**	**330**	**332**	**510**	**521**	**600**	**631**	**552**	**741**	**820**
0.1	*	*	100	*	*	*	*	*	*	*	*
0.2	6.6	*	93.4	**	*	*	*	*	**	*	*
0.5	3.6	*	74.6	1.0	*	*	**	*	20.8	**	*
1	5.5	*	68.9	1.0	*	*	12.1	*	10.0	2.5	*
2	0.8	*	80.4	0.2	*	*	7.5	*	8.3	2.8	*
10	*	*	59.4	*	1.3	**	14.1	0.5	12.7	5.0	7.0
20	*	*	99.5	*	*	*	**	*	0.4	0.1	*

* Not detectable

** $I(hkl) < 3 \times \sqrt{\text{Background}}$

Table 4-89: Raw Data: Bragg Angles of bcc Nickel-Zinc, Electrodeposited at 60 mA cm^{-2}, on Mild Steel Substrates.

	Reflections / 2θ Bragg Angles										
[μm]	**222**	**321**	**330**	**332**	**510**	**521**	**600**	**631**	**552**	**741**	**820**
0.1	*	*	44.20	*	*	*	*		*	*	*
0.2	35.56	*	43.71	(48.86)	*	*	*	*	80.50	*	*
0.5	35.40	*	43.50	48.09	*	*	(63.63)	*	80.10	(89.72)	*
1	35.40	*	43.49	48.09	*	*	62.63	*	80.10	89.72	*
2	35.28	*	43.31	47.82	*	*	62.75	*	79.54	89.56	*
10	*	*	43.16	*	52.26	(56.81)	62.65	72.12	79.11	89.41	90.57
20	*	*	43.17	*	*	*	62.63	*	79.32	89.49	*

* Not detectable

( ) Values in brackets are calculated from 2θ Bragg angles with intensities below $3 \times \sqrt{\text{Background}}$

Table 4-90: Calculated d-Spacings of bcc Nickel-Zinc (i = 60 mA cm^{-2}) at Various Thicknesses.

	Reflections / Calculated d-Spacings [nm]										
[µm]	**222**	**321**	**330**	**332**	**510**	**521**	**600**	**631**	**552**	**741**	**820**
0.1	*	*	0.20474	*	*	*	*		*	*	*
0.2	0.25345	*	0.20694	(0.18728)	*	*	*	*	(0.11948)	*	*
0.5	0.25463	*	0.20790	0.18806	*	*	(0.14822)	*	0.12003	(0.10920)	*
1	0.25463	*	0.20790	0.18806	*	*	0.14822	*	0.12003	0.10920	*
2	0.25565	*	0.20874	0.18881	*	*	0.14796	*	0.12052	0.10936	*
10	*	*	0.20942	*	0.17424	(0.16922)	0.14815	0.13087	0.12097	0.10950	0.10840
20	*	*	0.20939	*	*	*	0.14806	*	0.12089	0.19352	*

* Not detectable

( ) Values in brackets are calculated from 2θ Bragg angles with intensities below $3 \times \sqrt{\text{Background}}$

Table 5-1: Interplanar Spacings of Substrate Metals, Alloy Electrodeposits Investigated, and Individual Metals Contained in Alloy Electrodeposits Investigated, based on JCPDS Data [88].

		Cu	NiFe	NiFe	Ni	Fe	Fe	Ni_5Zn_{21}
	lattice	fcc	fcc	bcc	fcc	fcc	bcc	bcc
	JCPDS	4-836	23-297	37-474	4-850	31-619	6-696	6-653
$h^2+k^2+l^2$	plane	*d-spacings [nm]*						
1	100	**0.3615**	**0.3596**	**0.28681**	**3.5238**	**0.36**	**0.28664**	**0.892**
2	110	0.25562	0.25428	0.20281	0.24917	0.25456	0.20269	0.63074
3	111	0.20871	0.20762	0.16559	0.20345	0.20785	0.16550	0.515
5	210	0.16167	0.16082	0.12827	0.15759	0.161	0.12819	0.39892
6	211	0.14758	0.14681	0.11709	0.14386	0.14697	0.11702	0.36416
9	221	0.1205	0.11987	0.09560	0.11746	0.12	0.09555	0.29733
10	310	0.11432	0.11372	0.0907	0.11143	0.11384	0.09064	0.28208
11	311	0.1090	0.10842	0.08648	0.10625	0.10854	0.08643	0.26895
13	320	0.10026	0.09974	0.07955	0.09773	0.09985	0.07950	0.2474
14	321	0.09661	0.09611	0.07665	0.09418	0.09621	0.07661	0.2384

Table 5-2: Crystallographic Planes (Directions) with Corresponding Perpendicular Planes (Directions) in the Cubic System [119].

{hkl}	Planes Perpendicular (⊥) to {hkl}
100	100; 110; 210; 310; 320
110	110; 211; 221
111	110; 211; 321
210	100; 210; 221; 321
211	110; 111; 311; 321
221	110; 210; 221
310	100; 110; 310
311	110; 211; 310
320	100; 320
321	111; 210; 211

Table 5-3: Interplanar Spacings of fcc and bcc Nickel-Iron Compatible for Initial Deposition on Copper Substrate According to Finch's 15 per Cent Criterion. Data are Based on JCPDS Lattice Parameters.

	Substrate	Electrodeposit	
	Cu	NiFe	NiFe
Lattice	*fcc*	*fcc*	*bcc*
	100	100	-
	110	110	100
	111	111	110
	210	210; 211	111
	211	210; 211	111; 210
	221	221; 310; 311	210; 211
	310	221; 310; 311	210; 211
	311	221; 310; 311; 320; 321	211; 221

Table 5-4: Interplanar Spacings of fcc and bcc Nickel-Iron Compatible for Initial Deposition According to Finch's 15 per Cent Criterion. Data are Based on JCPDS Lattice Parameters.

	NiFe	NiFe
Lattice	*fcc*	*bcc*
	100	-
	110	100
	111	110
	210	111
	211	111; 210
	221	210; 211
	310	210; 211; 220
	311	211; 221
	320	211; 221; 310; 311
	321	221; 310; 311

Table 5-5: Interplanar Spacings of Ni_5Zn_{21}, that Fulfil Finch's 15 per cent Criterion and Fit on the d-Spacings of the Copper and Iron Substrate Multiplied by Three.

	Substrate	Electrodeposit
	Cu	Ni_5Zn_{21}
Lattice	*fcc*	*bcc*
	100	-
	110	300
	111	330
	210	333
	211	333; 630
	221	630; 633
	310	630; 633; 663
	311	633 ;663; 930
	320	663; 930; 933
	321	663; 930; 933; 960

Substrate	Electrodeposit
Fe	Ni_5Zn_{21}
bcc	*bcc*
100	300
110	330
111	333
210	630; 633
211	630; 633; 663
221	663; 930;933; 960
310	663; 930;933; 960; 963
311	663; 930; 933; 960; 963
320	930, 933, 960; 963
321	933; 960;963

Table 5-6: Atomic Density $\delta_{(hkl)}$ of Different Crystal Planes {hkl} in the fcc Lattice.

{hkl}	{111}	{100}	{110}	{311}	{210}	{211}
$\delta_{\{hkl\}}$ (at/a^2)	2.3094	2	1.4142	0.9177	0.8944	0.6666
$\delta_{\{hkl\}}$ (at/nm^2)	17.8591	15.4664	10.9364	7.0965	6.9168	5.1555

Table 5-7: Atomic Density $\delta_{(hkl)}$ of Different Crystal Planes {hkl} in the bcc Lattice.

{hkl}	{110}	{100}	{310}	{111}	{211}
$\delta_{\{hkl\}}$ (at/a^2)	1.4142	1	0.6325	0.5774	0.3333
$\delta_{\{hkl\}}$ (at/nm^2)	17.1920	12.1566	7.6885	7.0186	4.0522

8. 2 Figures

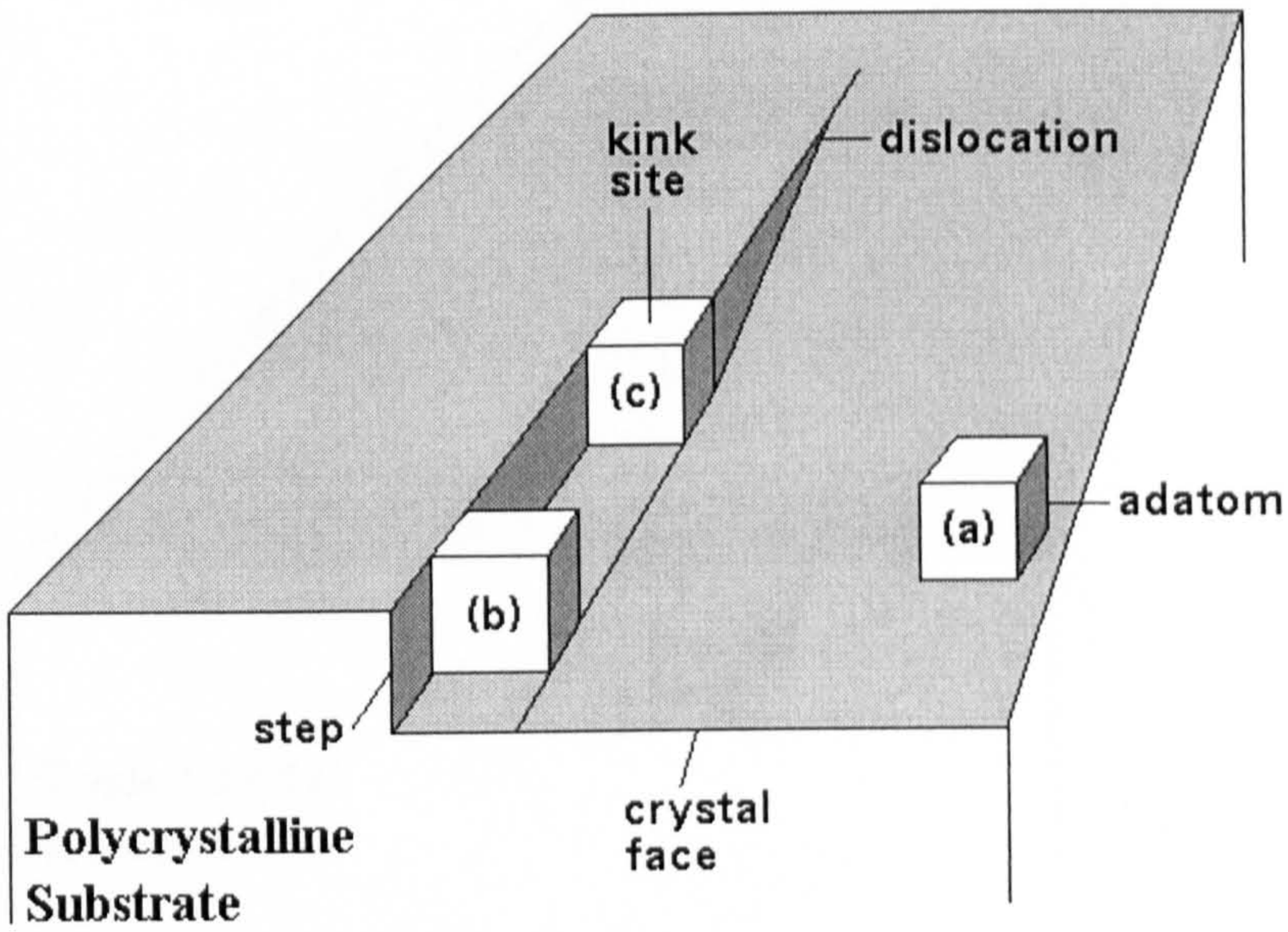

Fig. 2-1: Schematic Drawing of the Electrocrystallization Process of an Atom on a polycrystalline Substrate from (a) being discharged, (b) diffusing over the Surface to a Step, and (c) diffusing along the Step to kink Site in a Screw Dislocation.

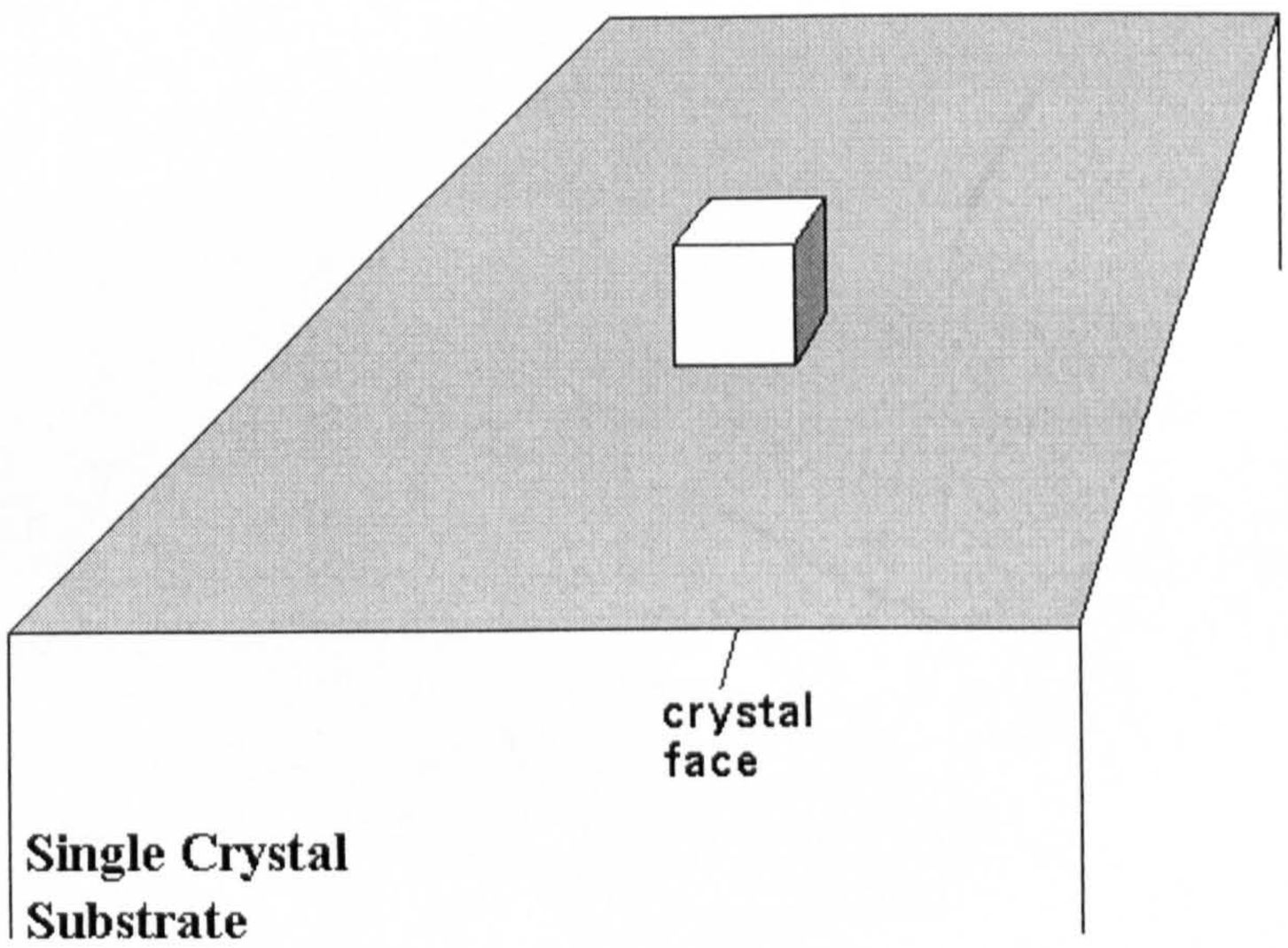

Fig. 2-2: Schematic Drawing of the three-dimensional Electrocrystallization Process of an Atom on a single Crystal Substrate (Island Growth).

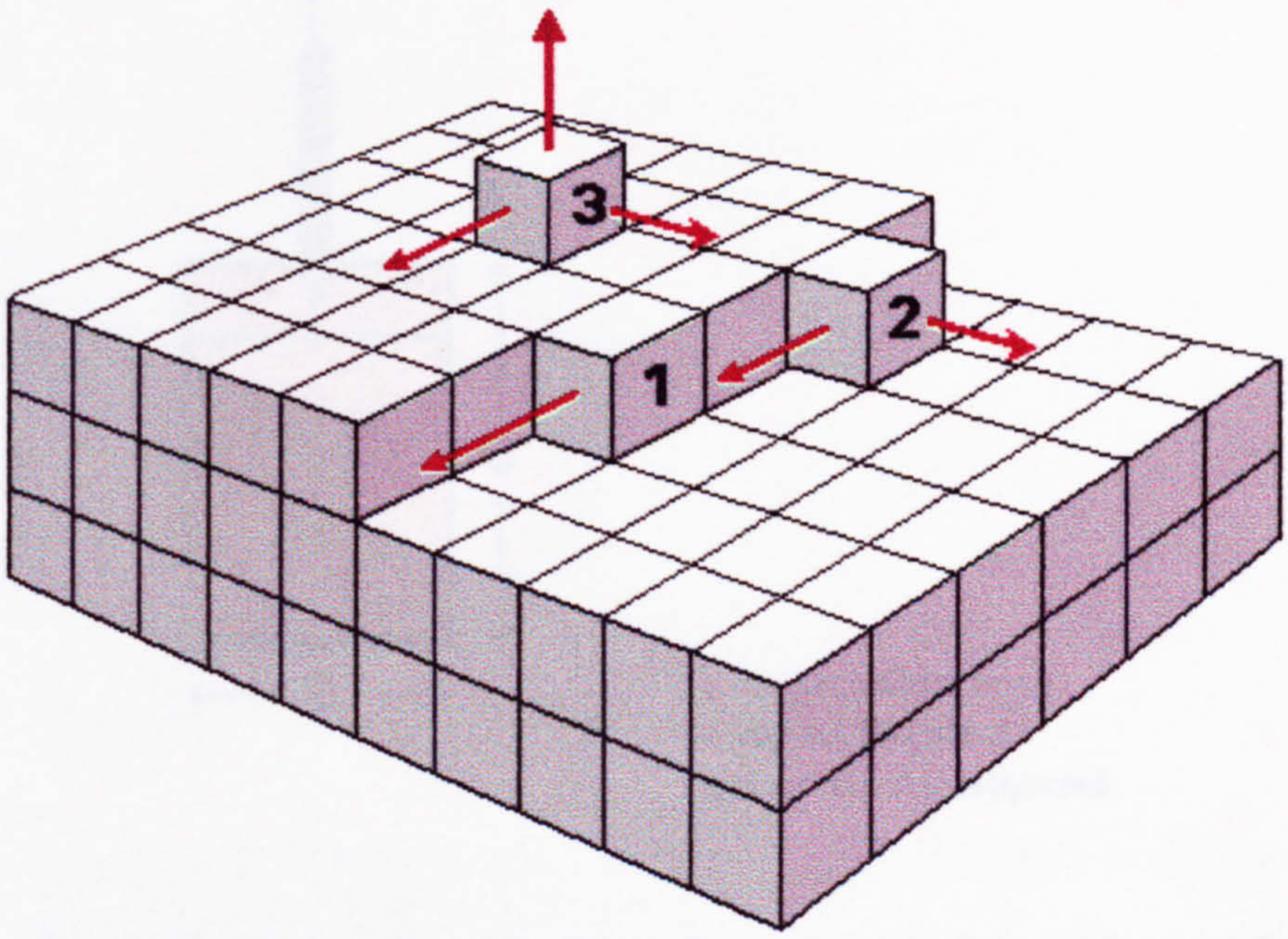

Fig. 2-3: Schematic Drawing of linear Growth at Kink Site '1', two-dimensional Growth '2', and three-dimensional Growth '3'.

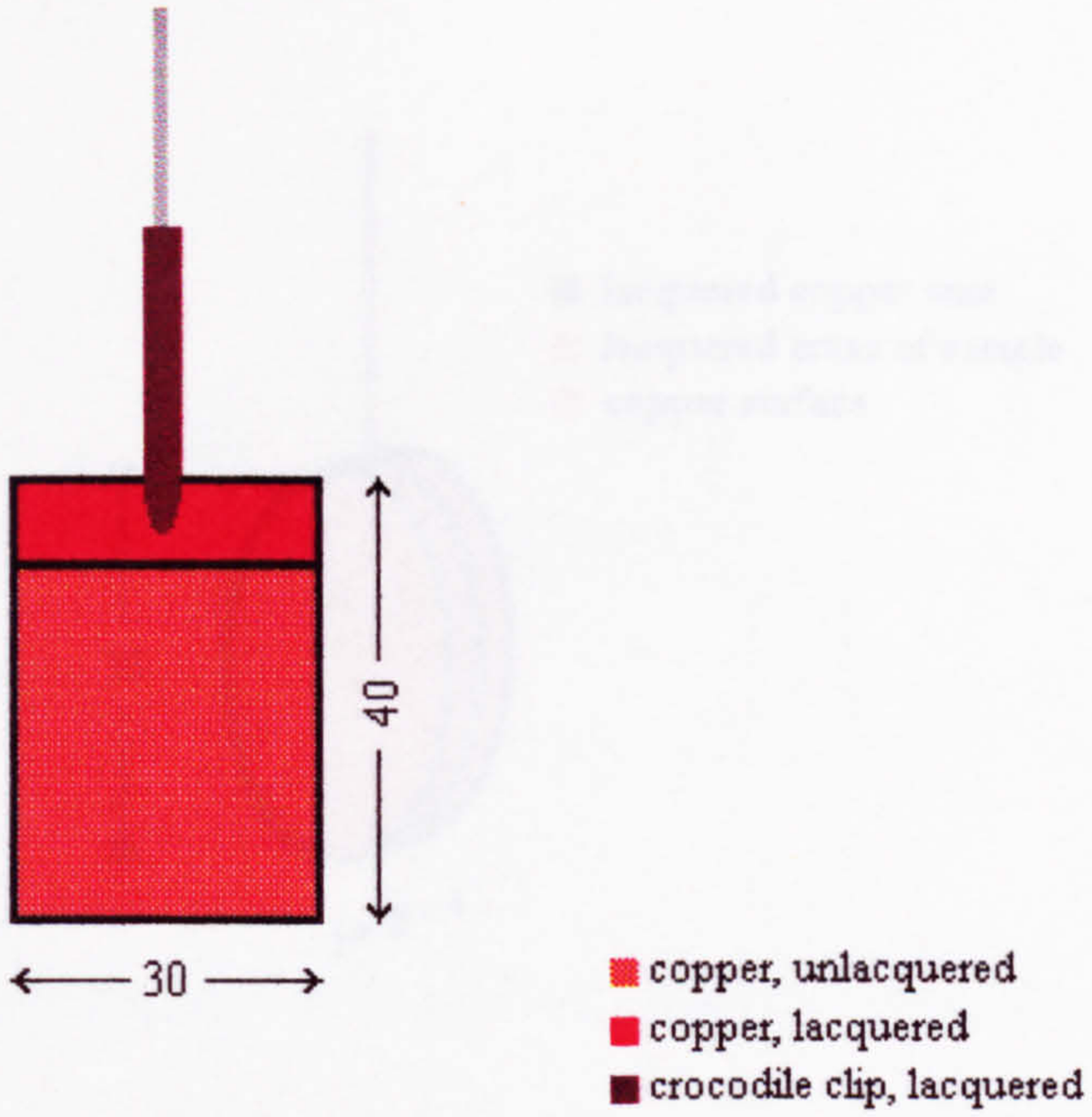

Fig. 3-1: Copper Cathodes, Used for Thick Deposits at Individual Current Densities for subsequent XRD, GDOES, EDX Investigations.

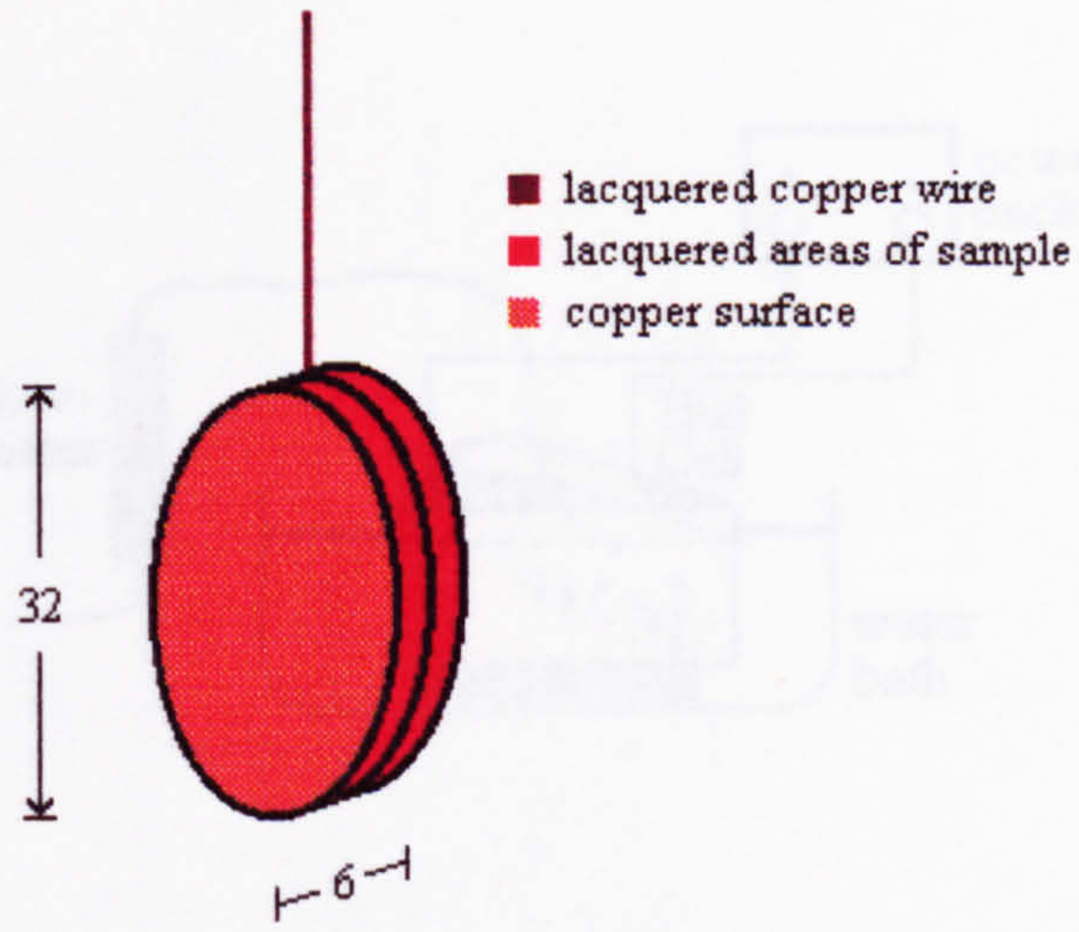

Fig. 3-2: Copper Disc Cathodes, Used to Deposit Thin Deposits for Subsequent XRD, GDOES, EDX Investigations.

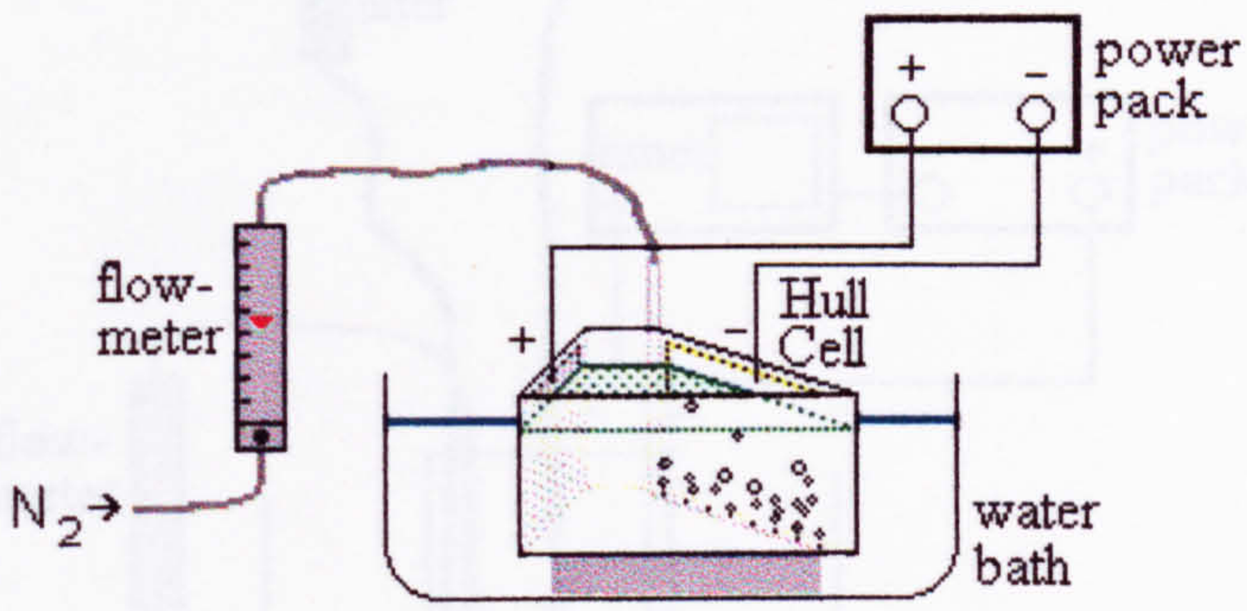

Fig. 3-3: Schematic Diagram of Experimental Electroplating Set-up with the Hull Cell.

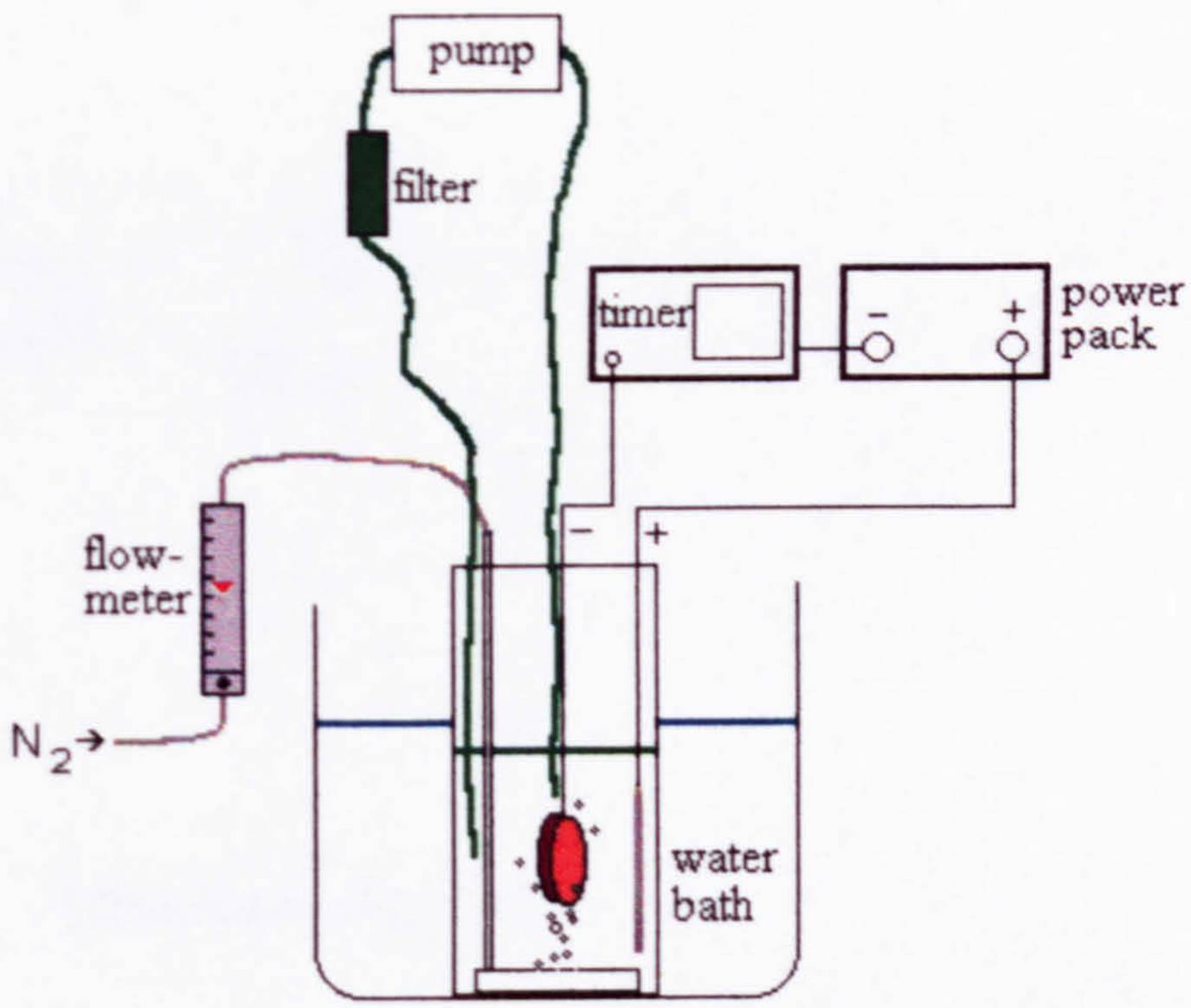

Fig. 3-4: Schematic Diagram of Experimental Electroplating Set-up.

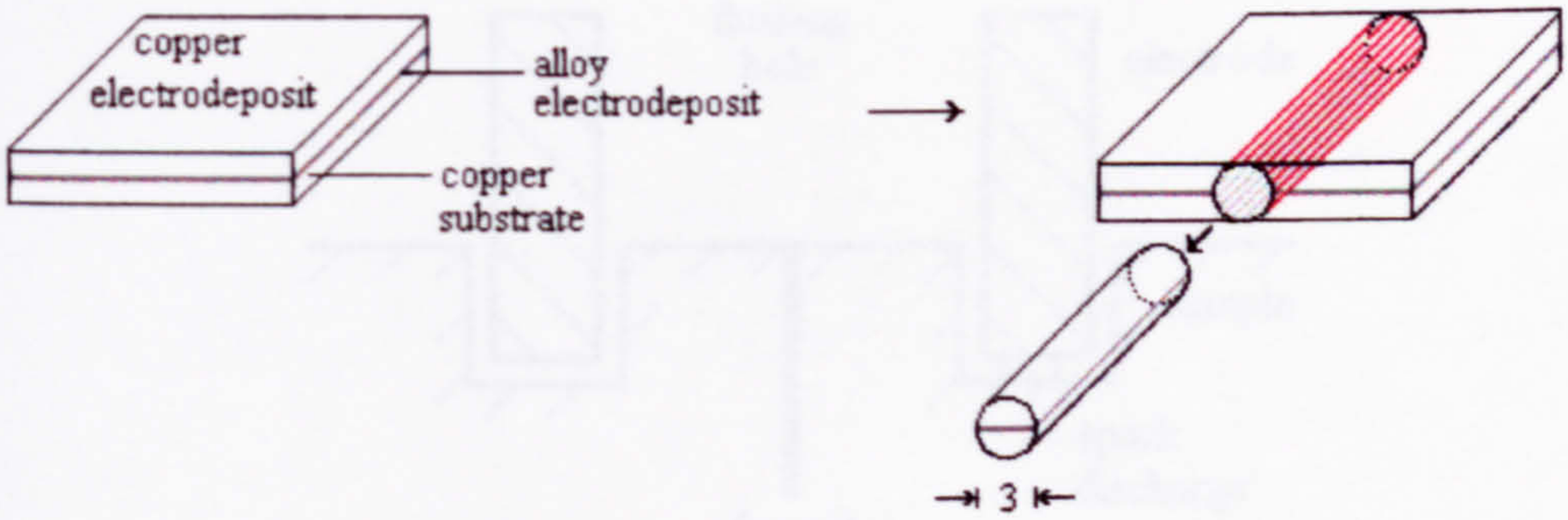

Fig. 3-5: Spark Erosion of a Cylinder.

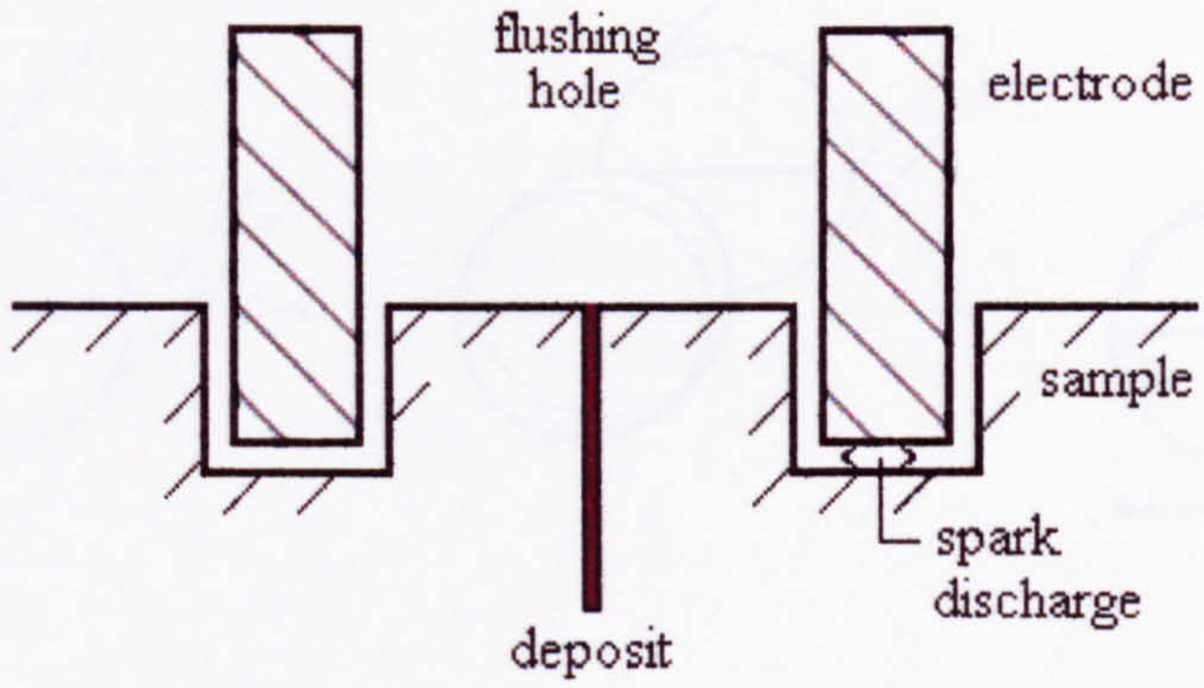

Fig. 3-6: Cross-sectional View of Spark Erosion Process.

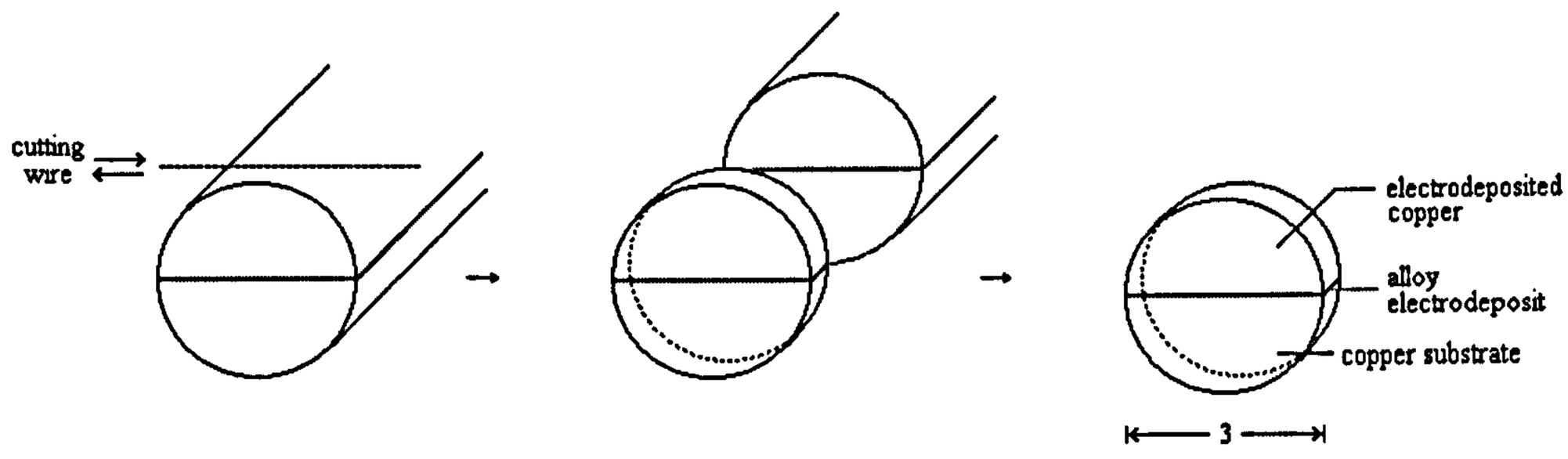

Fig. 3-7: Cutting off Discs.

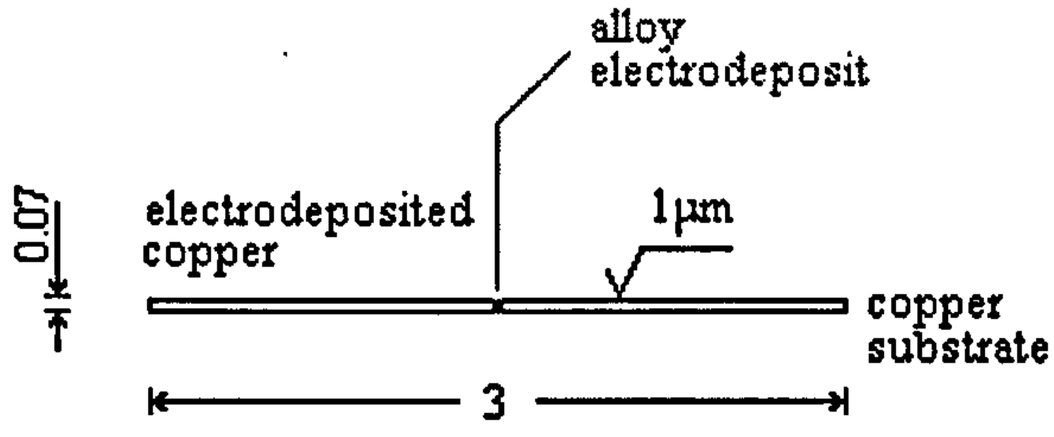

Fig. 3-8: Ground 3 mm Diameter Disc, Ready for Dimpling.

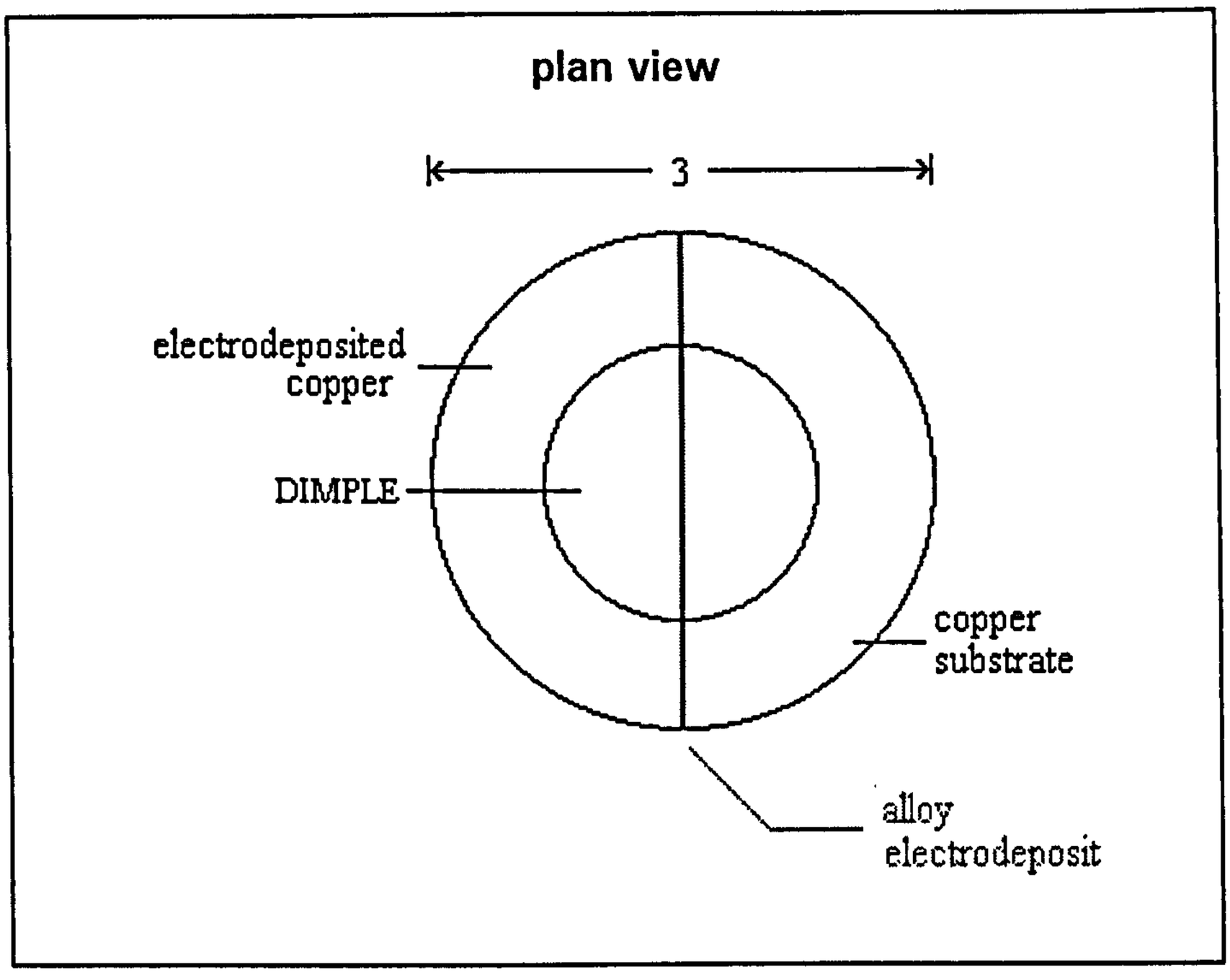

Fig. 3-9: Dimpled 3 mm Diameter Disc.

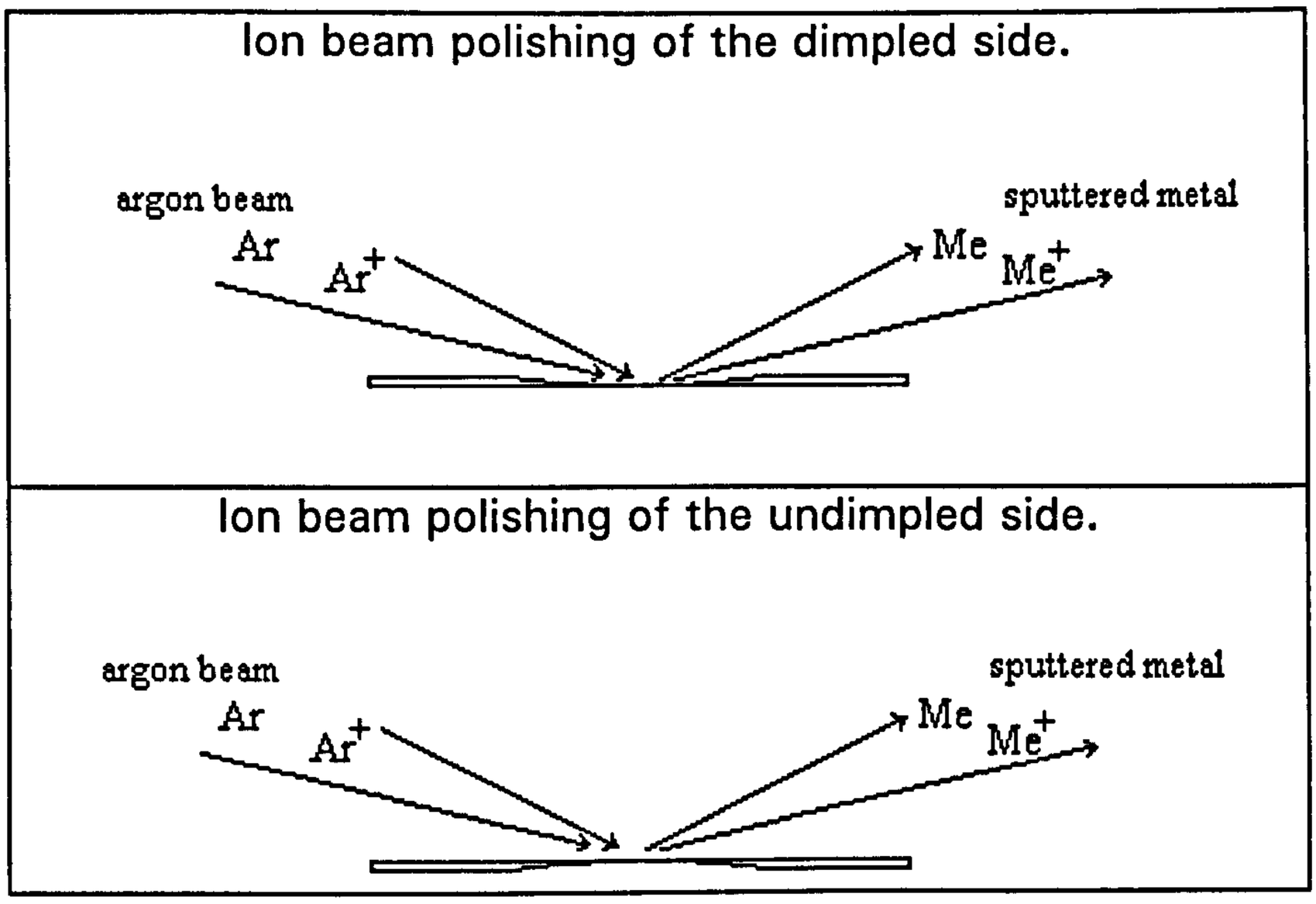

Fig. 3-10: Ion Beam Thinning.

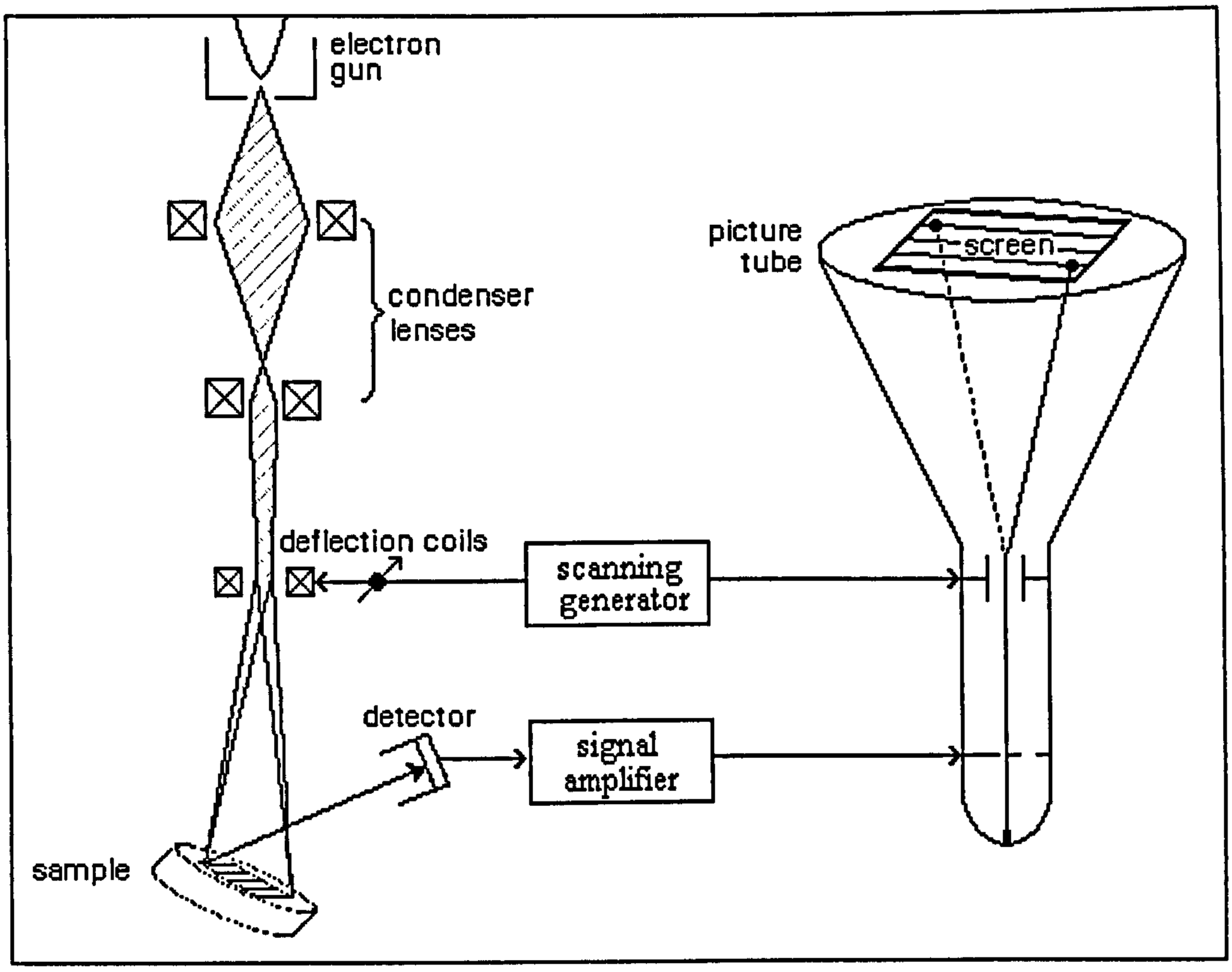

Fig. 3-11: Schematic Diagram of the SEM [81].

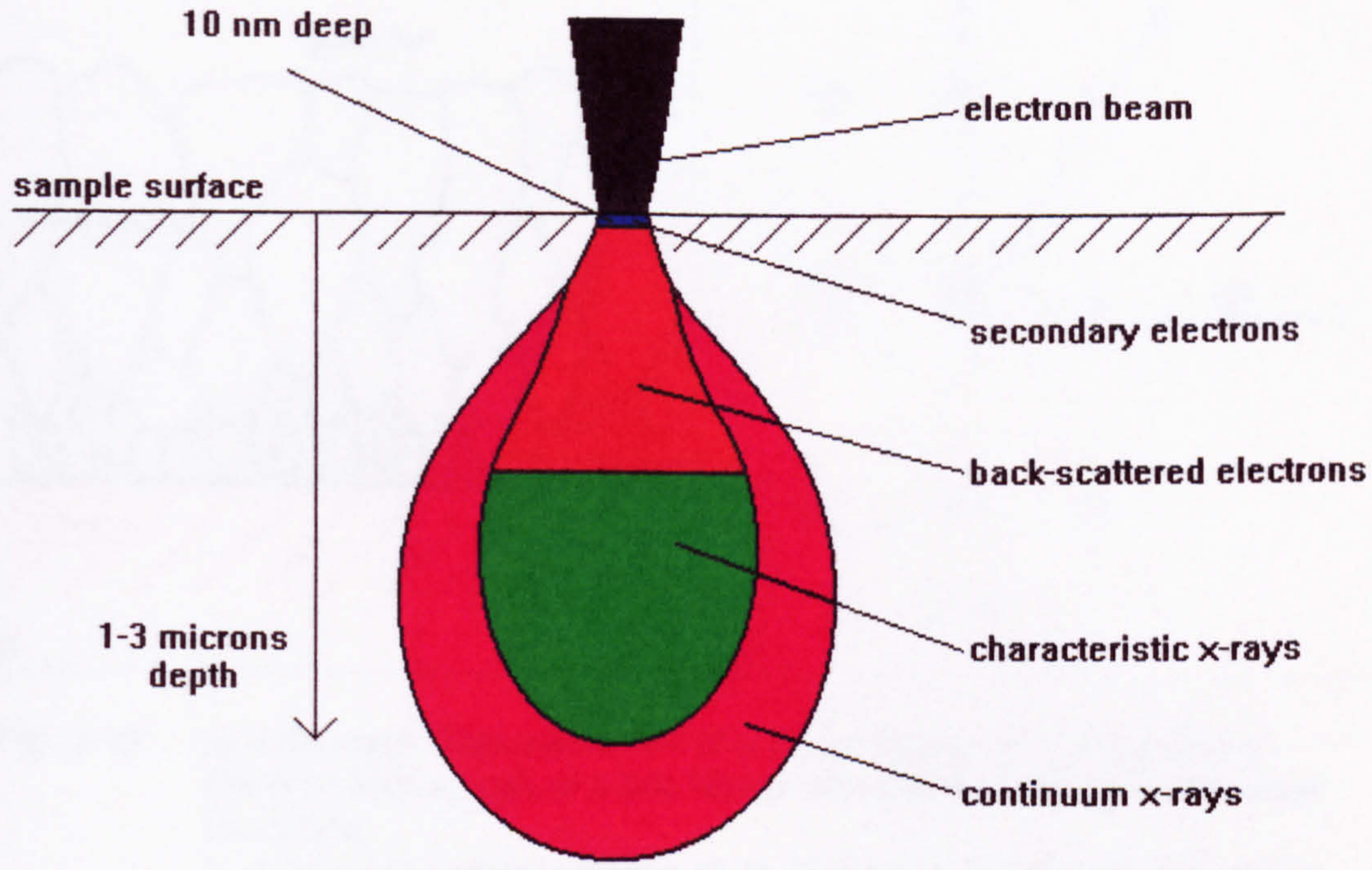

Fig. 3-12 [82]: Schematic Diagram of Excitation Volume for Major SEM Sample Emissions.

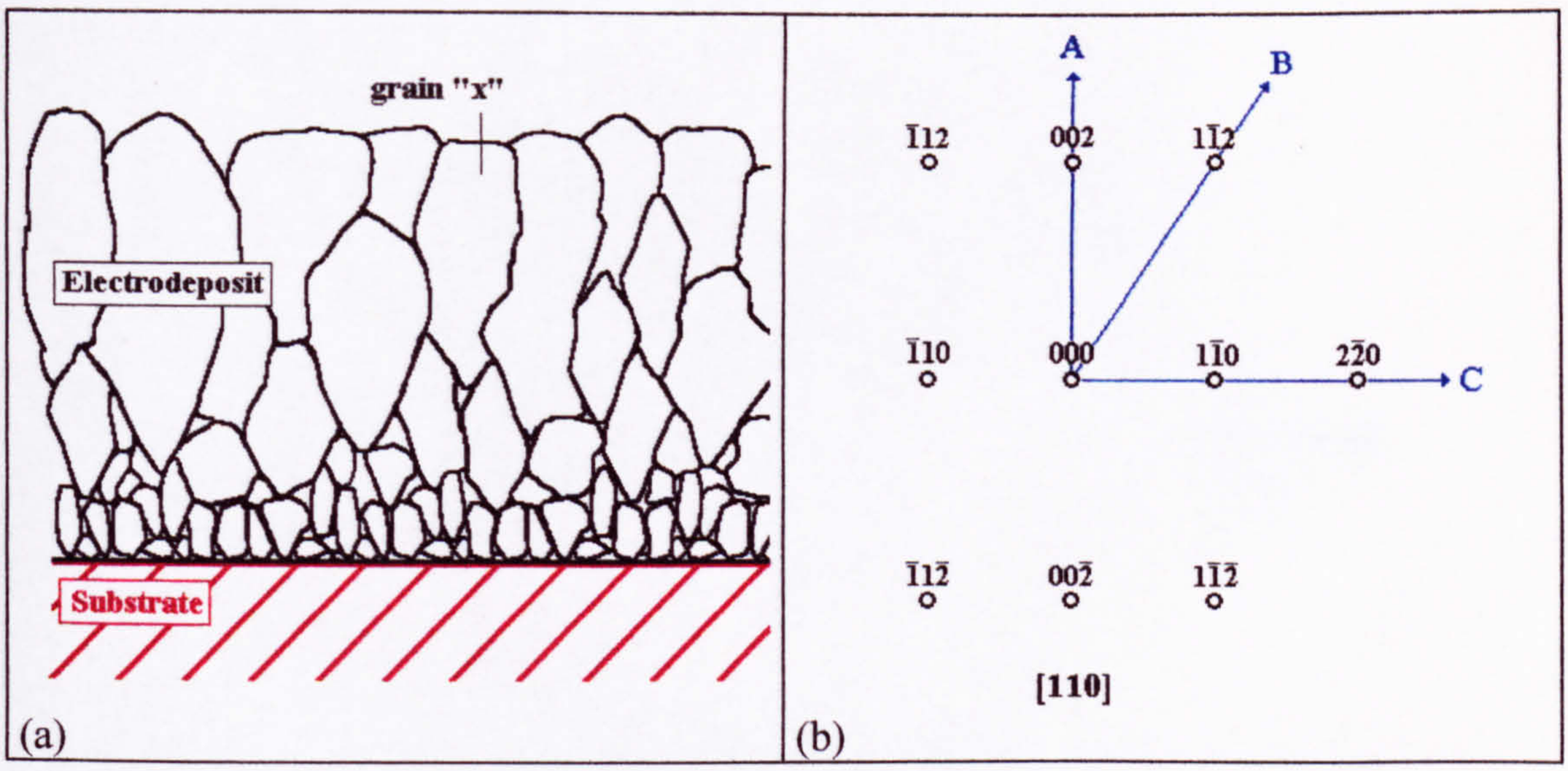

Fig. 3-13: a) Schematic Representation of a Cross-Sectional Transmission Electron Micrograph of a bcc Nickel-Iron Electrodeposit on a Copper Substrate.
b) Schematic Representation of an Electron Diffraction Pattern from Grain 'x' in a).

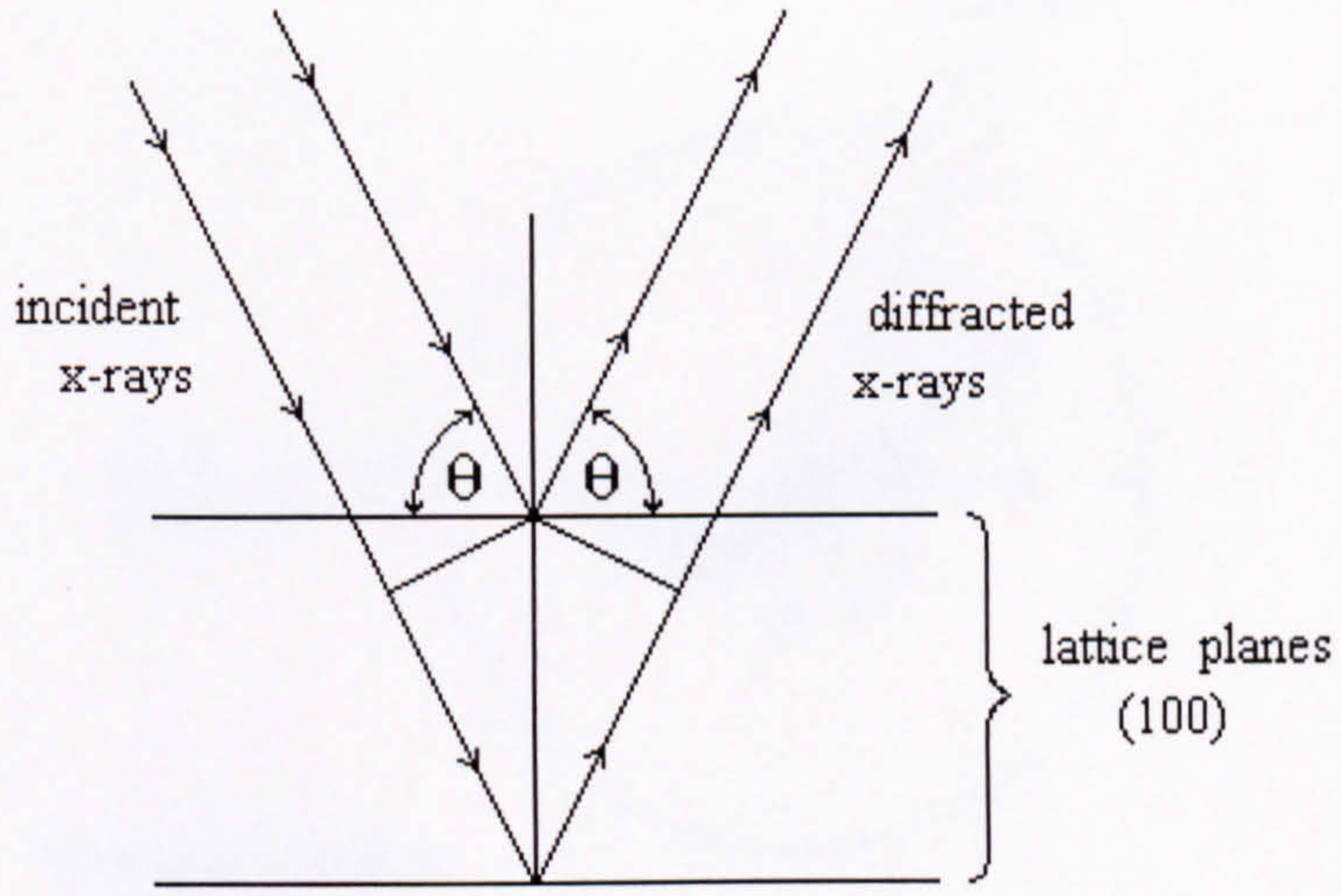

Fig. 3-14: Diffraction of X-rays by Lattice Planes.

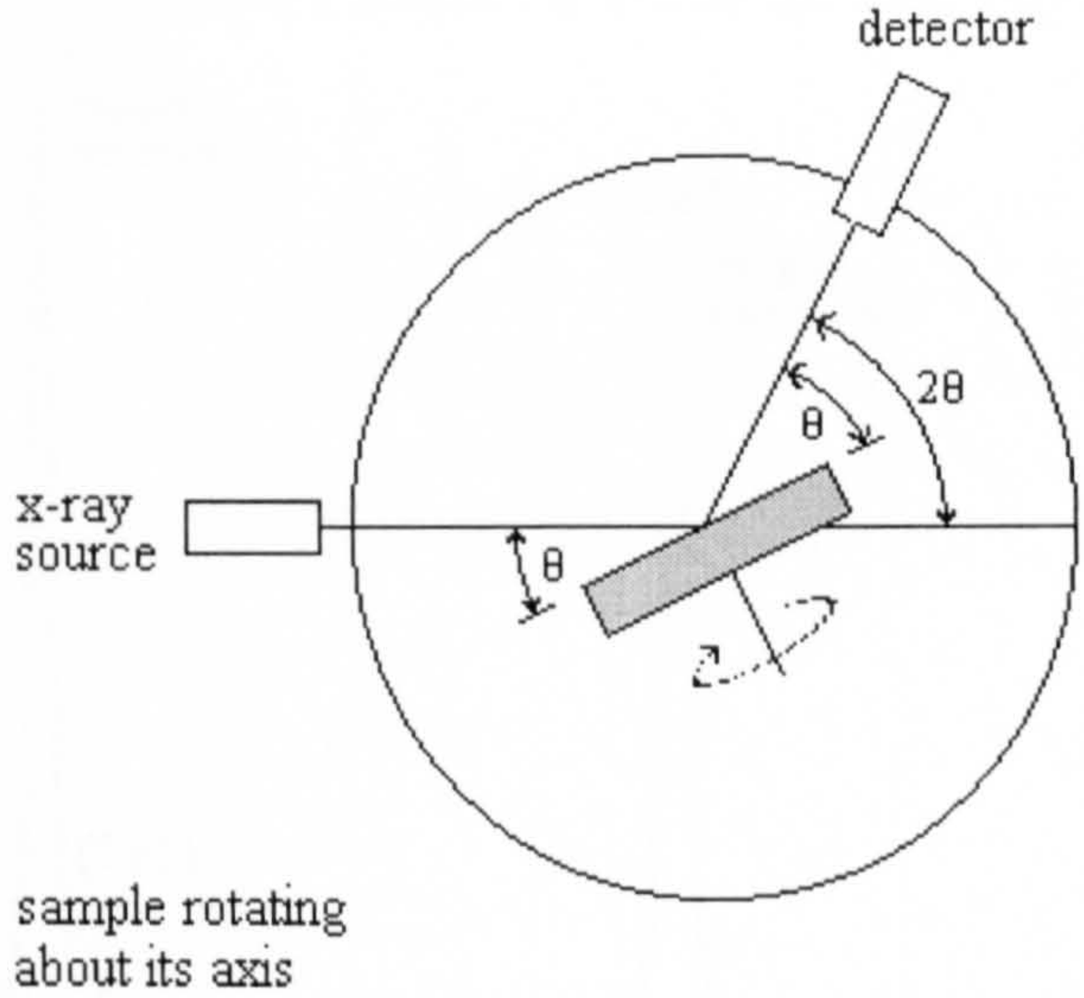

Fig. 3-15: X-ray Spectrometer Operated under Bragg-Brentano Conditions.

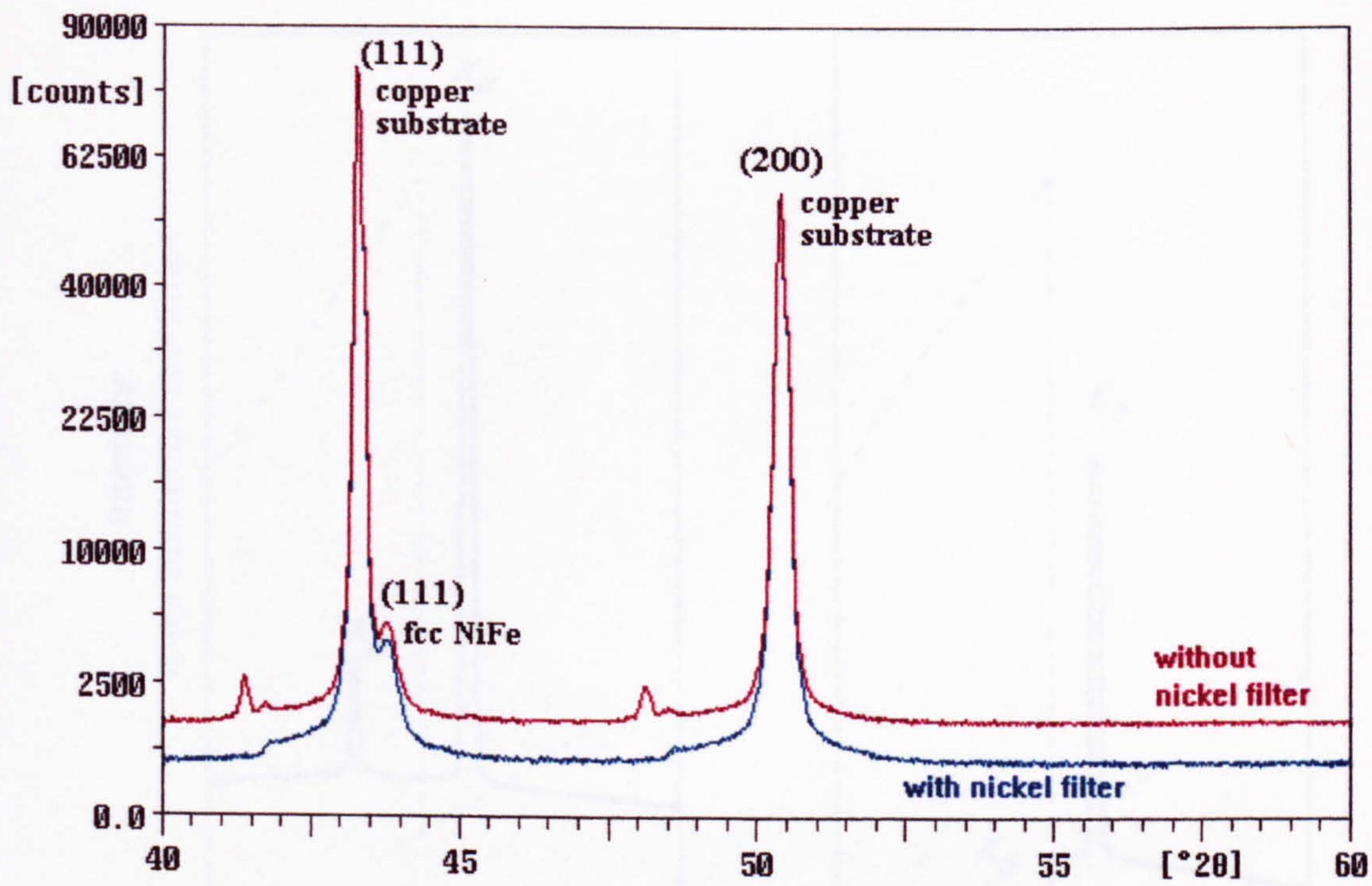

Fig. 3-16: X-ray Diffraction Spectra of Nickel-Iron Electrodeposit on Copper Substrate. Filtering Monochromatic CuK_{α} Radiation Through a Nickel Foil Resulted in Lower Background Noise.

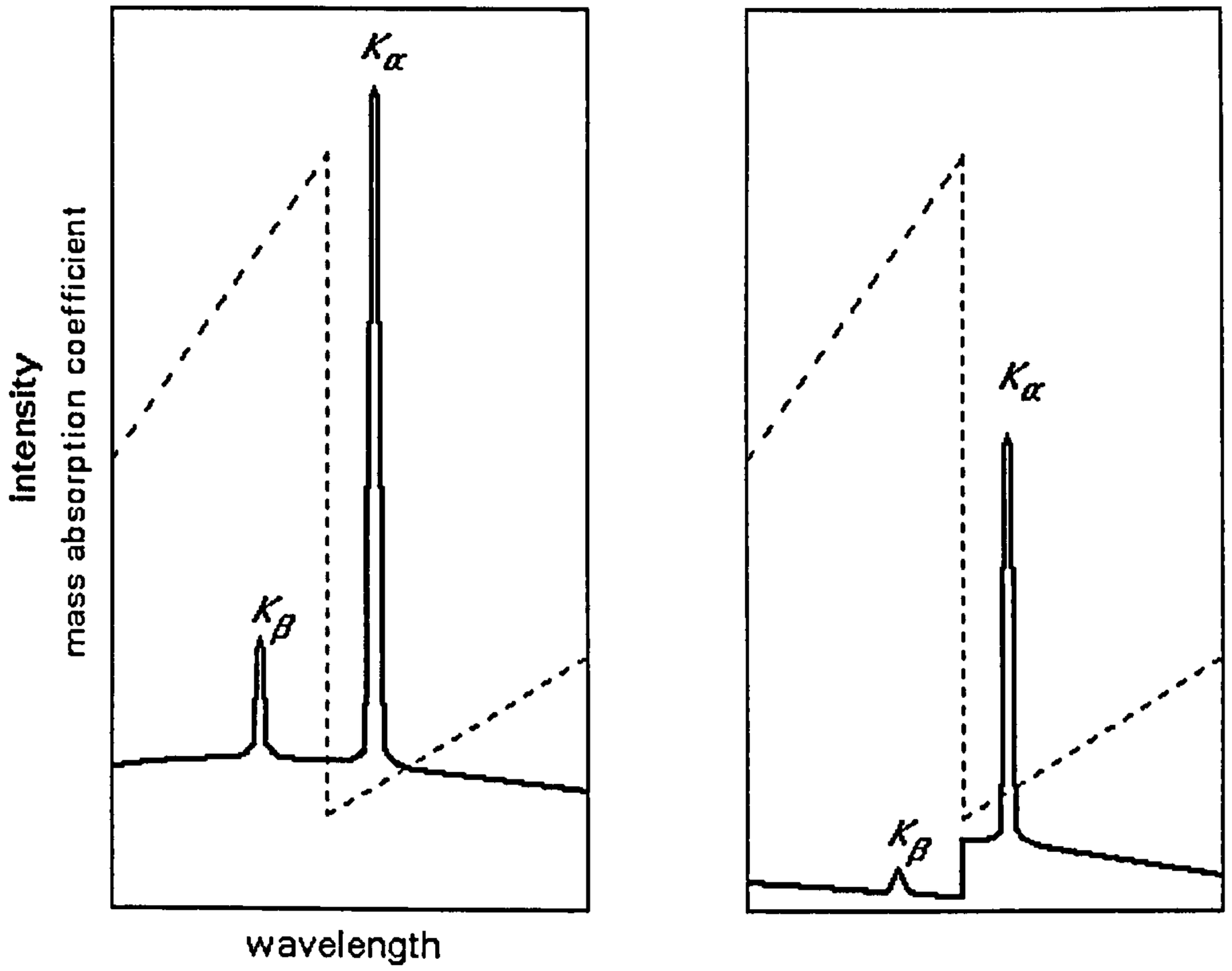

(a) No filter *(b) Nickel filter*

Fig. 3-17[87]: Schematic Comparison of the Spectra of Copper Radiation *(a)* Before and *(b)* After Passage Through a Nickel Filter. The Dashed Line Is the Mass Absorption Coefficient of Nickel.

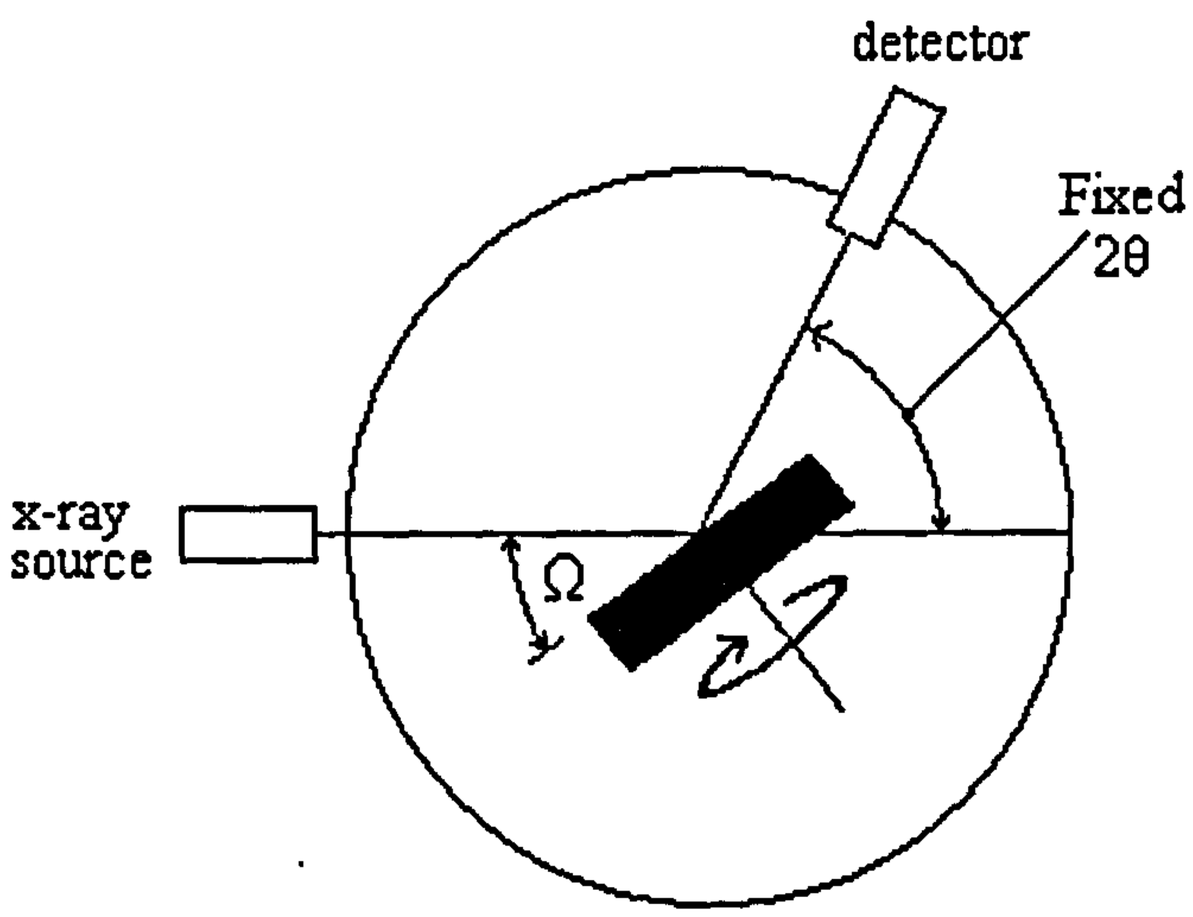

Fig. 3-18: X-ray Spectrometer operated under Omega Scan Conditions.

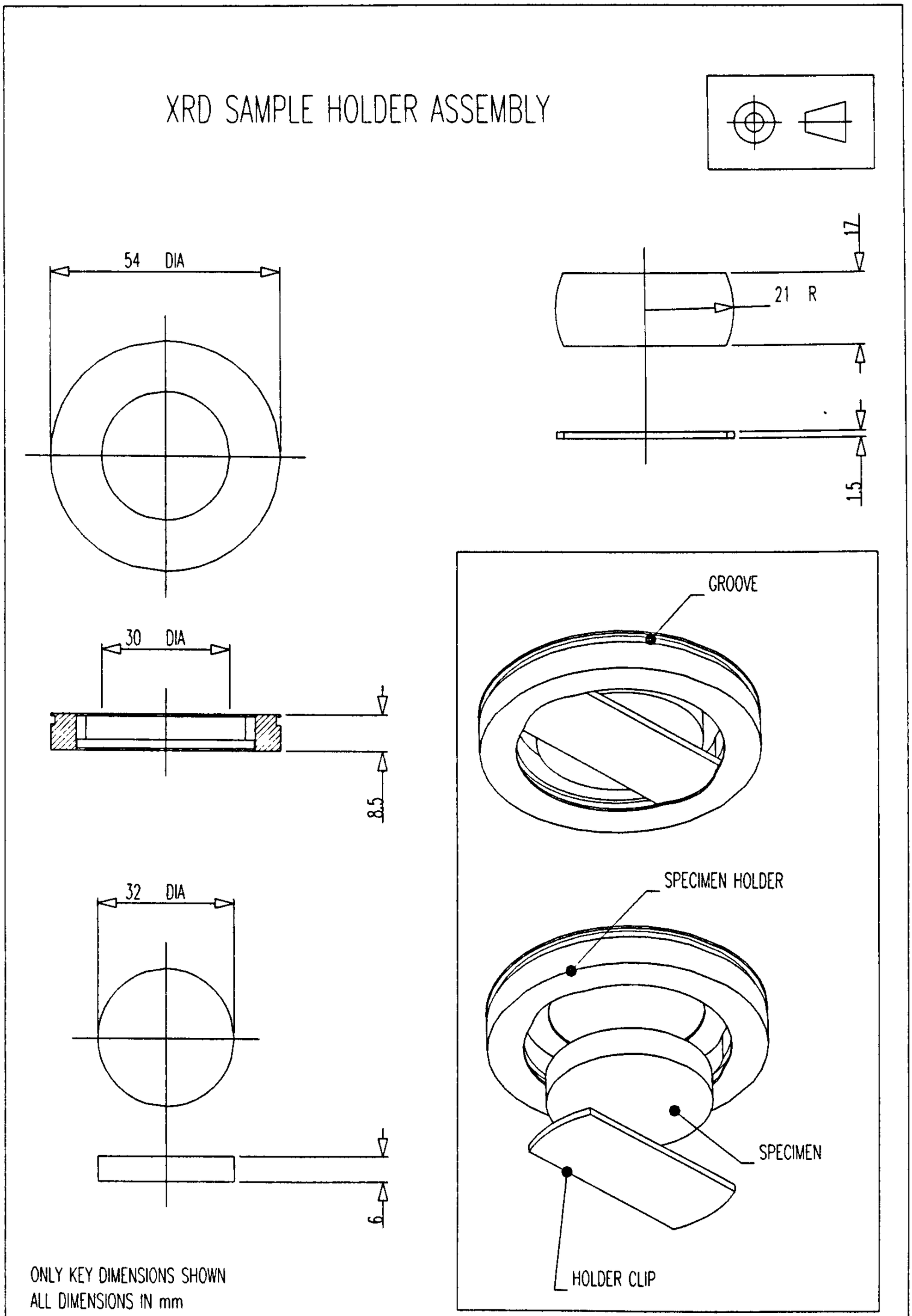

Fig. 3-19: Specimen Holder Assembly for X-ray Diffraction Investigations of Disc Samples.

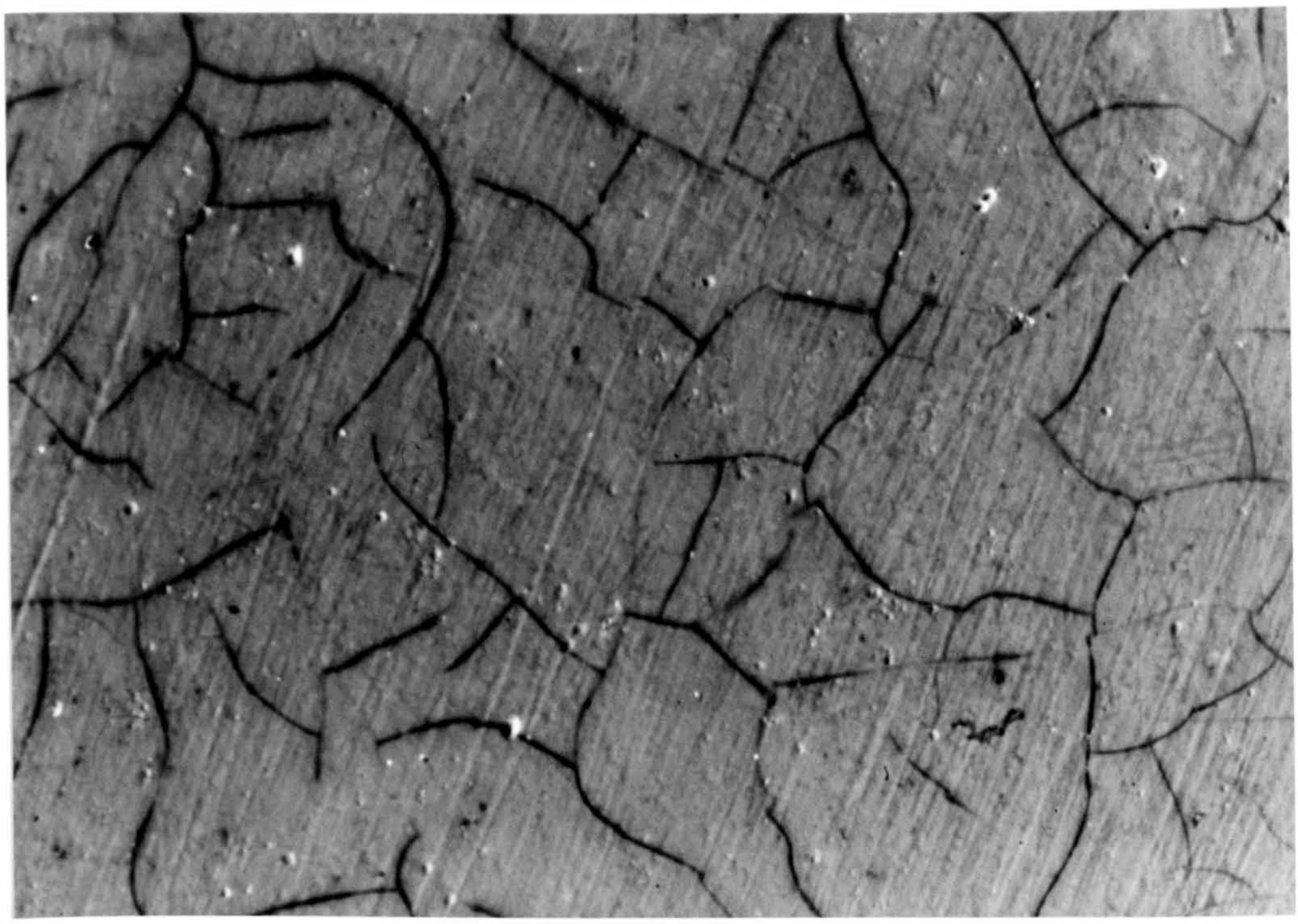

Fig. 4-1: Surface Morphology of Deposit Produced in NiFe Solution 4 at 10 mA cm^{-2}.

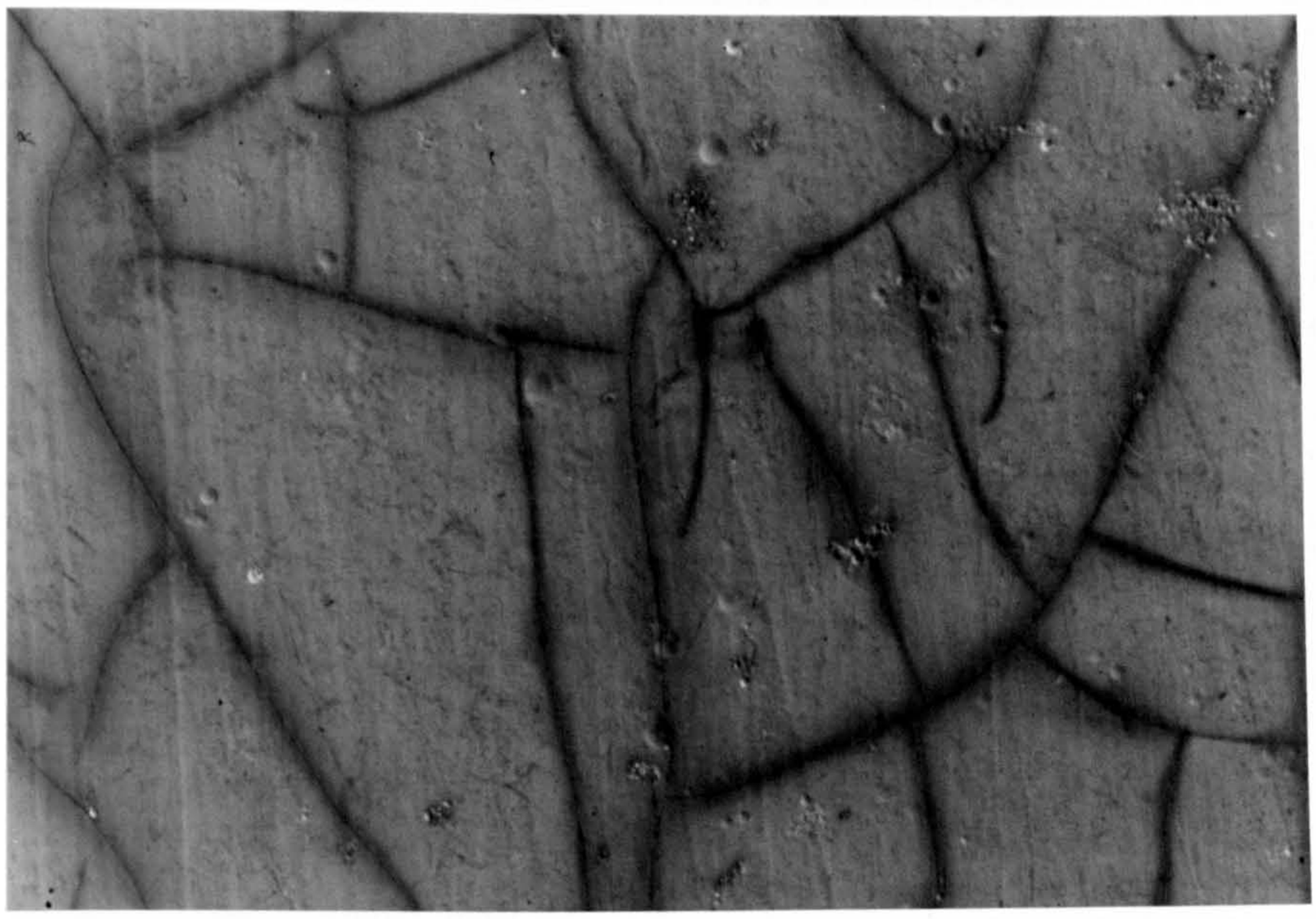

Fig. 4-2: Surface Morphology of Deposit Produced in NiFe Solution 4 at 30 mA cm^{-2}. 10 µm

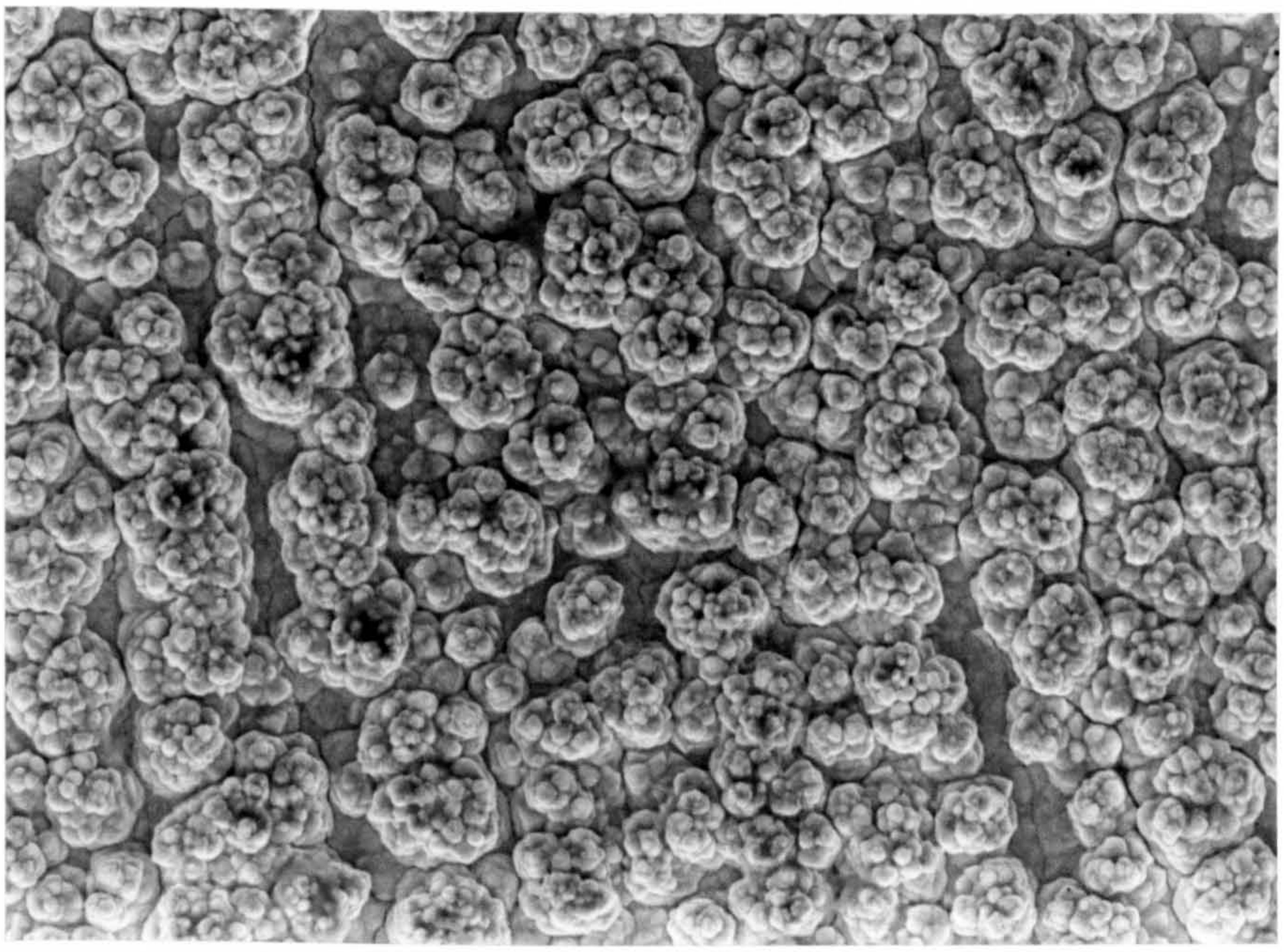

Fig. 4-3: Surface Morphology of Deposit Produced in NiZn Solution 8 at 10 mA cm^{-2}.

1 µm

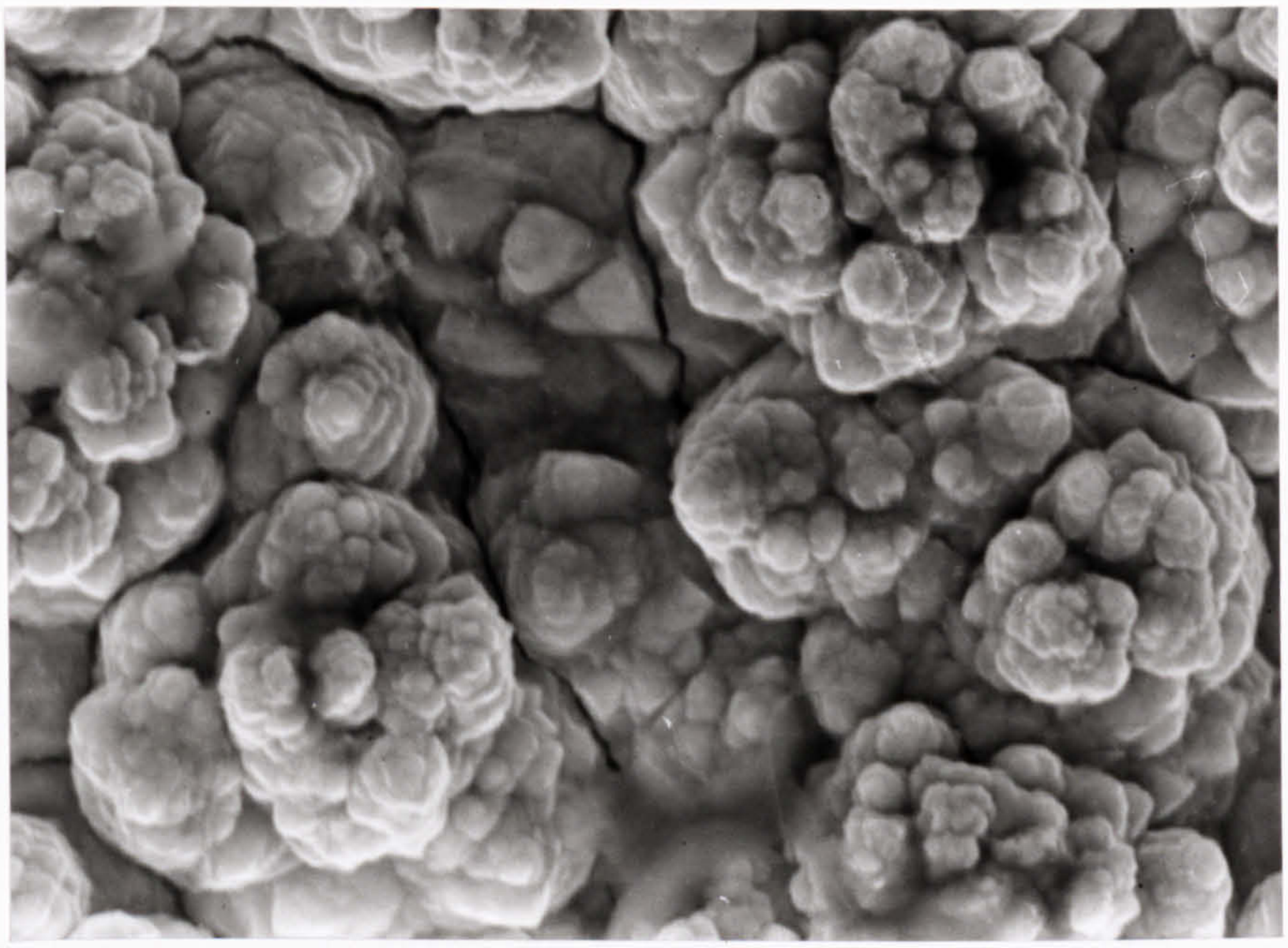

Fig. 4-4: Surface Morphology of Deposit Produced in NiZn Solution 8 at 10 mA cm^{-2}.

2 µm

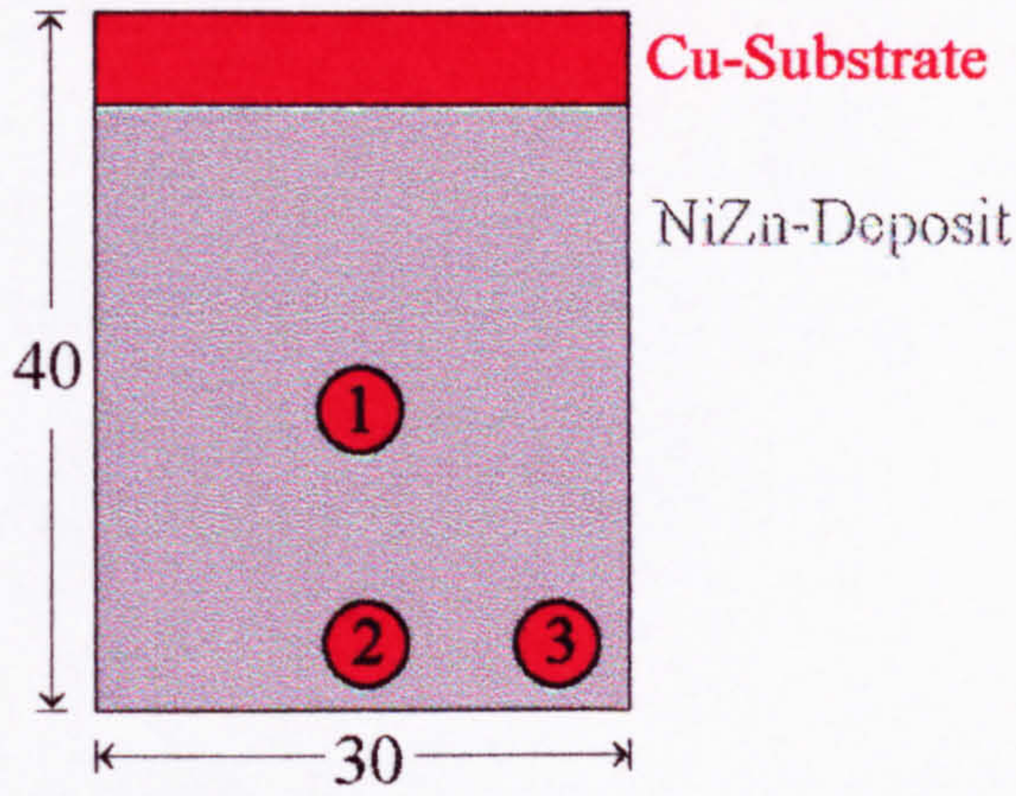

Fig. 4-5: Schematic Diagram of Nickel-Zinc Deposited Sample, Analyzed Areas Indicated with Numbers.

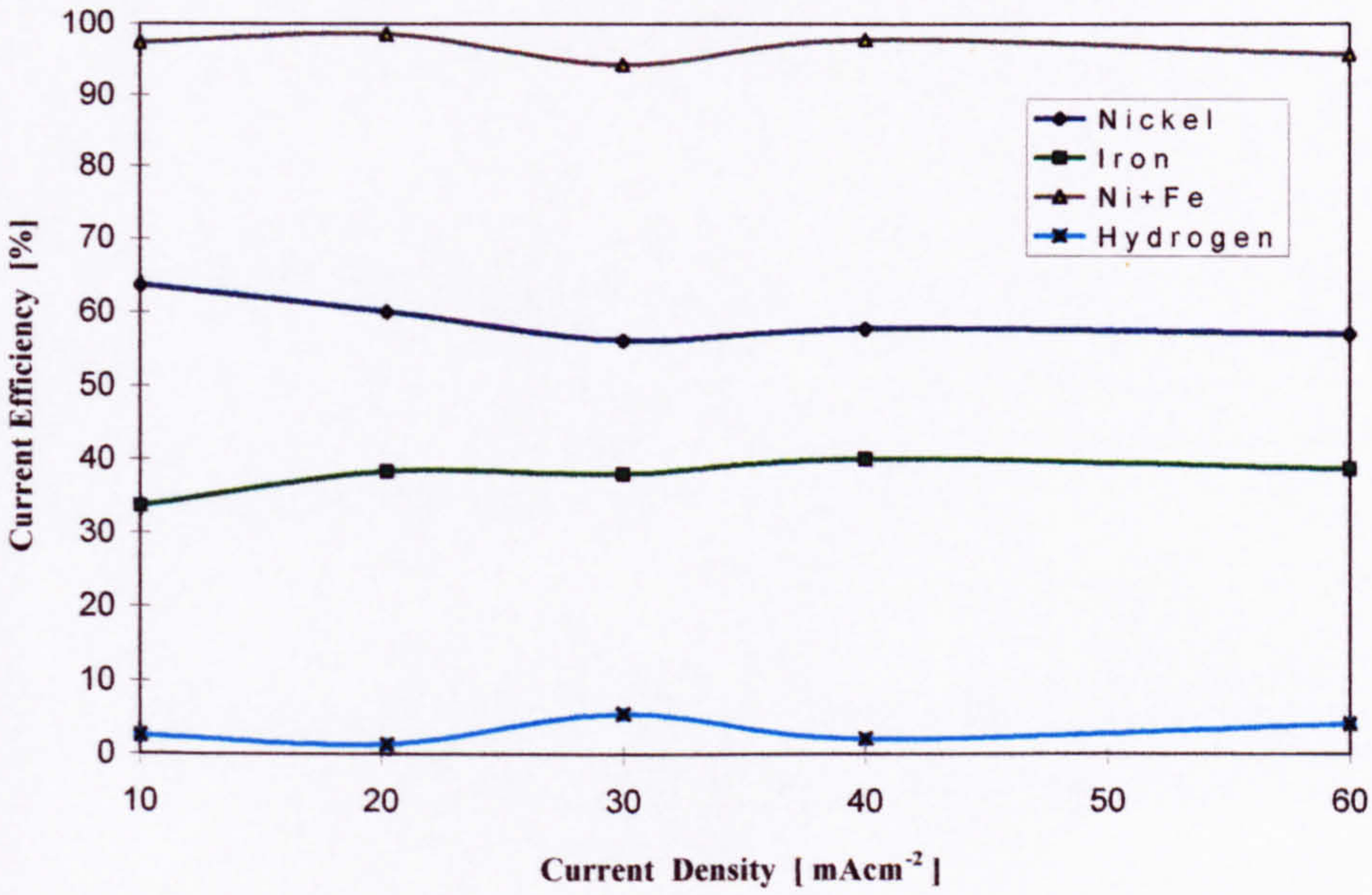

Fig. 4-6: Partial Current Efficiencies of Nickel-Iron Solution 1 at Individual Current Densities Using Compositional Results from EDX.

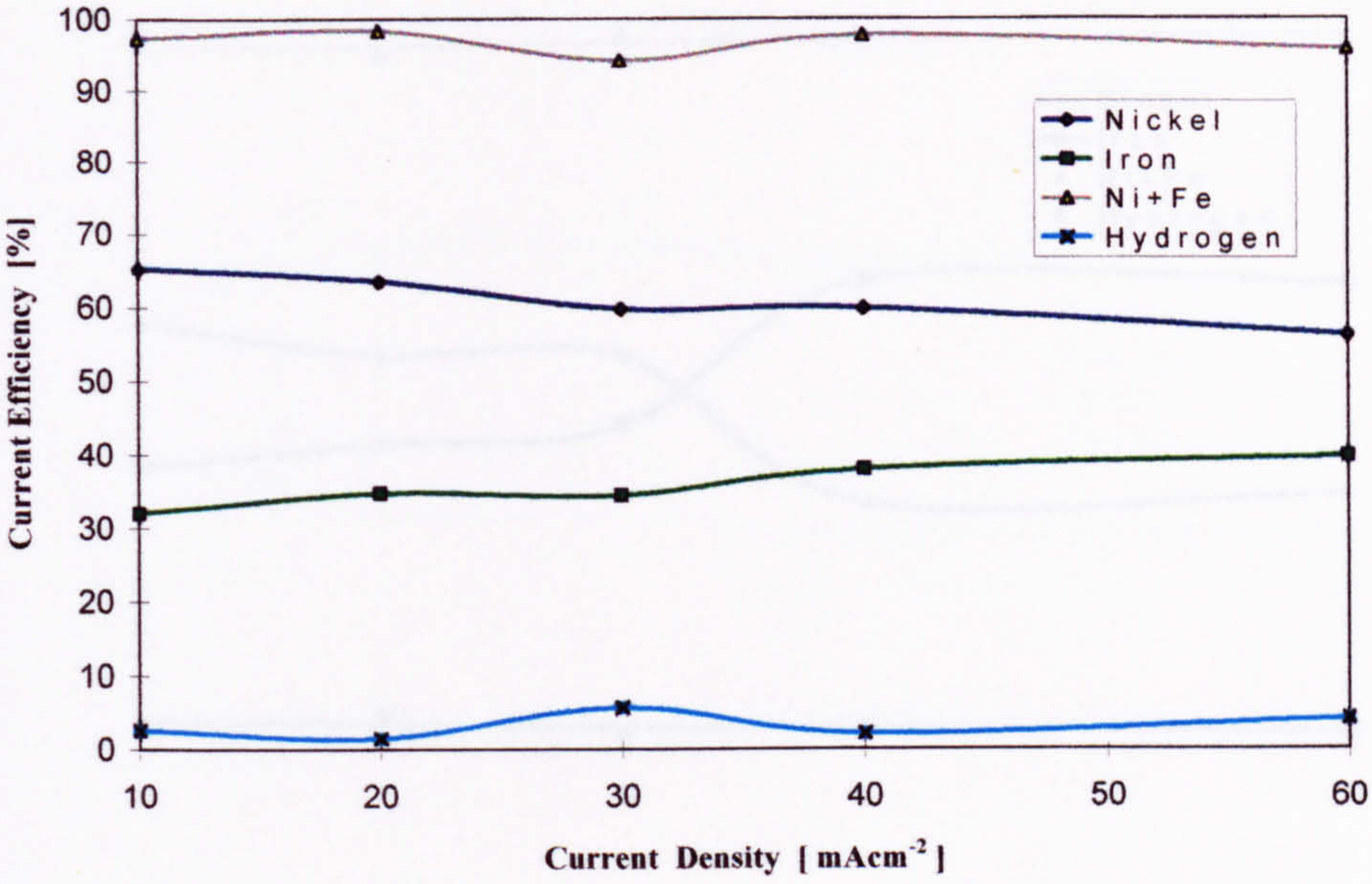

Fig. 4-7: Partial Current Efficiencies of Nickel-Iron Solution 1 at Individual Current Densities Using Compositional Results from GDOES.

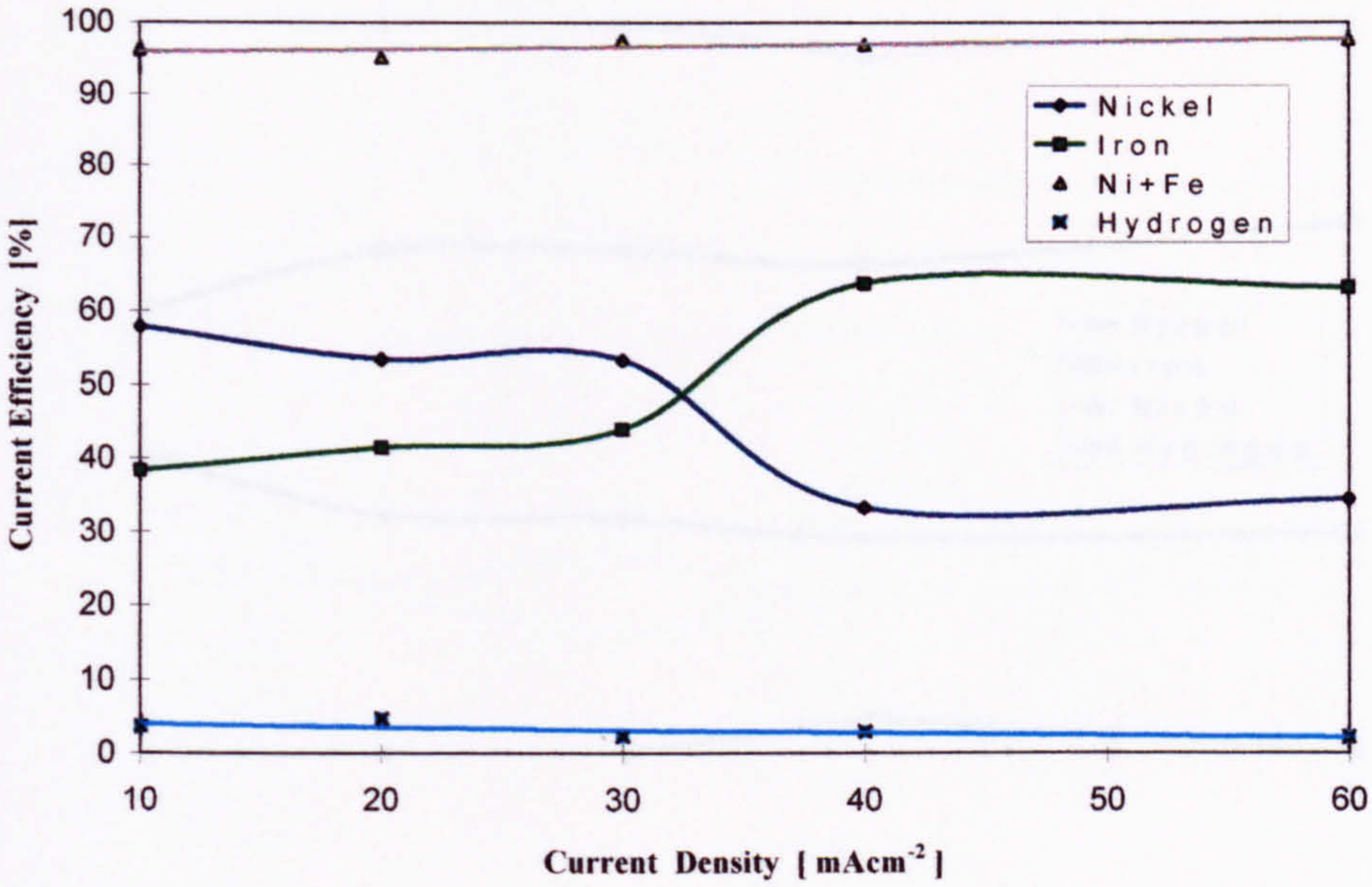

Fig. 4-8: Partial Current Efficiencies of Nickel-Iron Solution 3 at Individual Current Densities Using Compositional Results from GDOES.

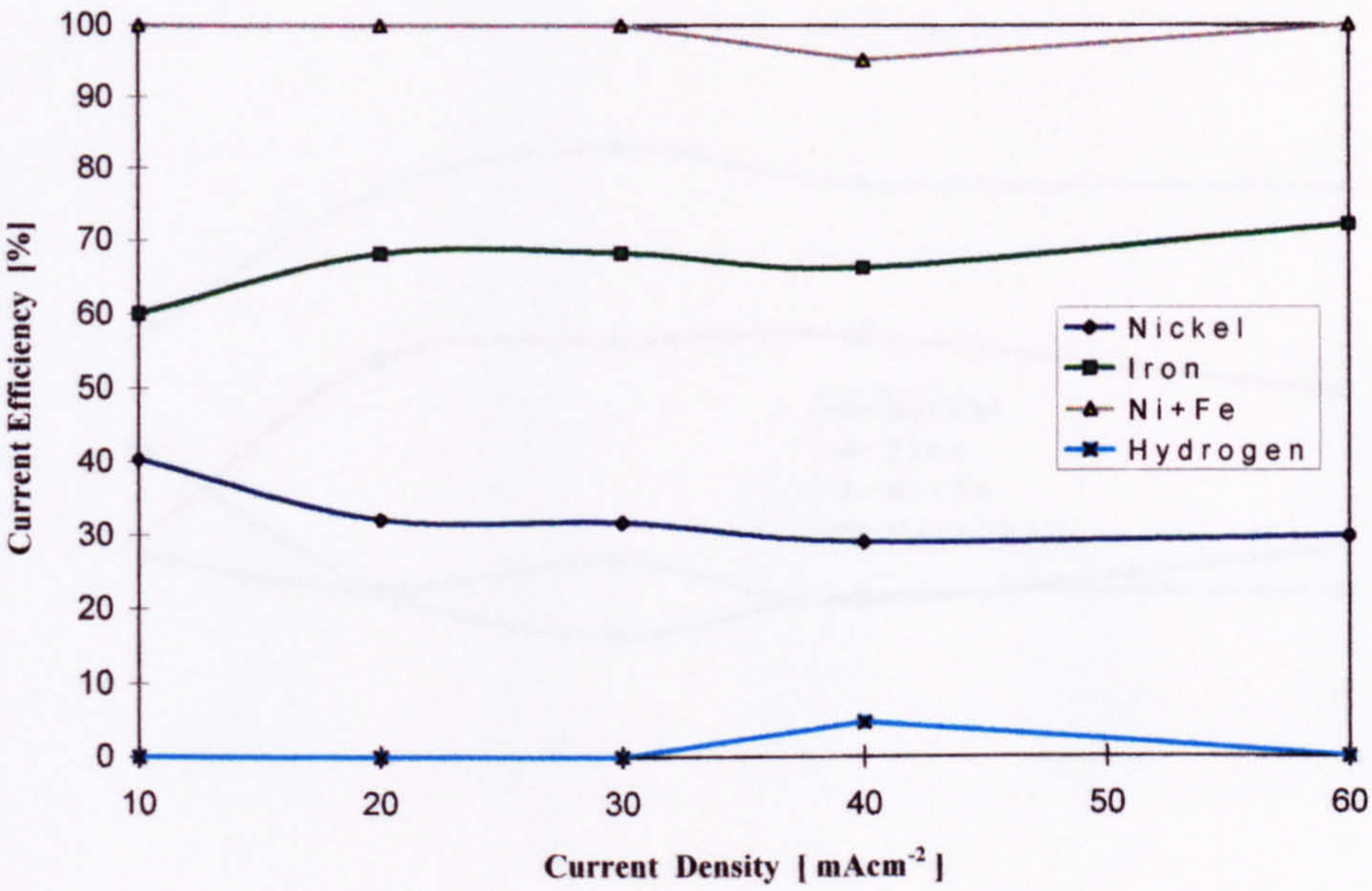

Fig. 4-9: Partial Current Efficiencies of Nickel-Iron Solution 4 at Individual Current Densities Using Compositional Results from GDOES.

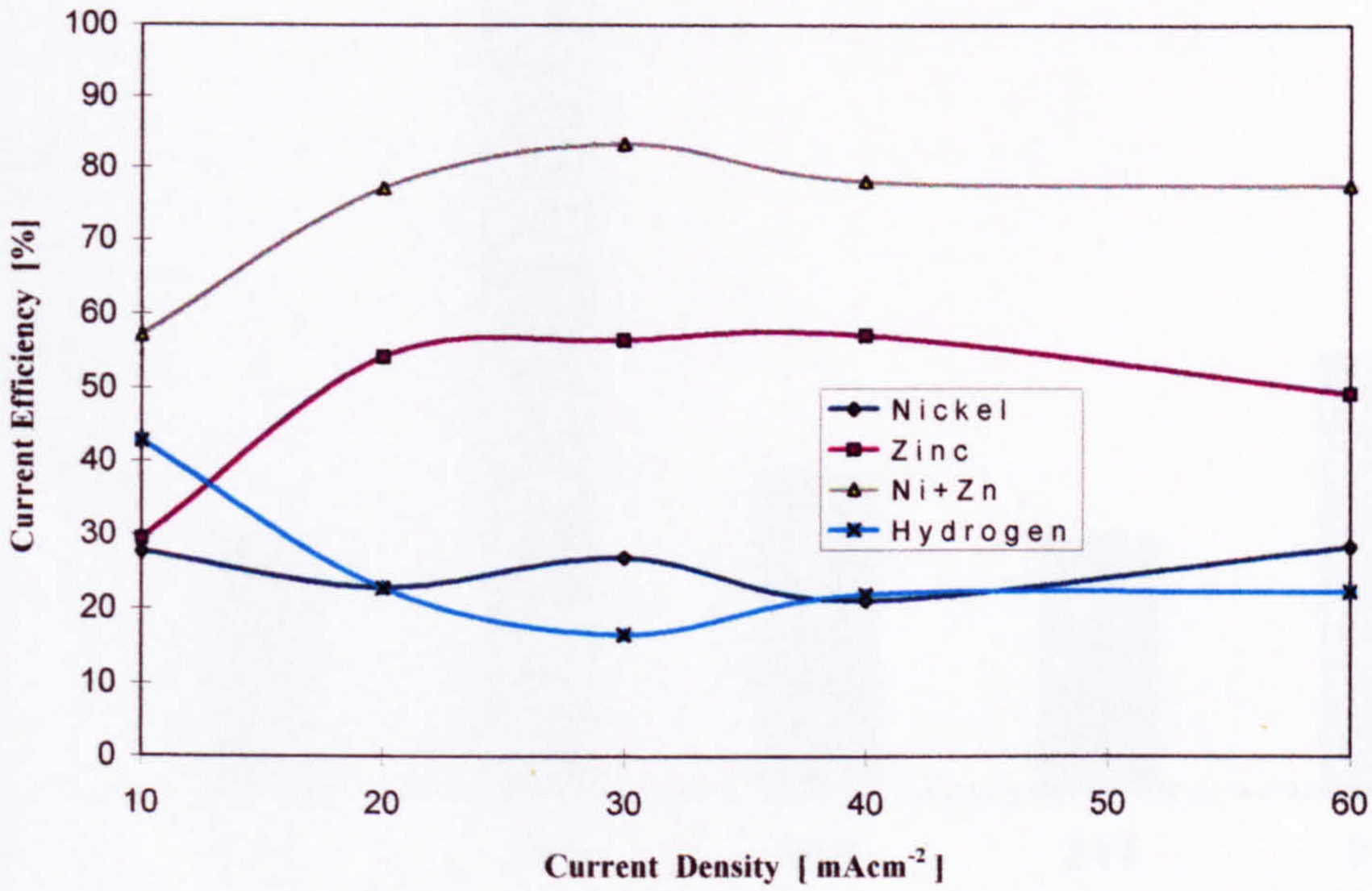

Fig. 4-10: Partial Current Efficiencies of Nickel-Zinc Solution 8 at Individual Current Densities Using Compositional Results from GDOES.

Fig. 4-11: Distribution of Reflecting Planes Detected in the Copper Sheet Substrate.

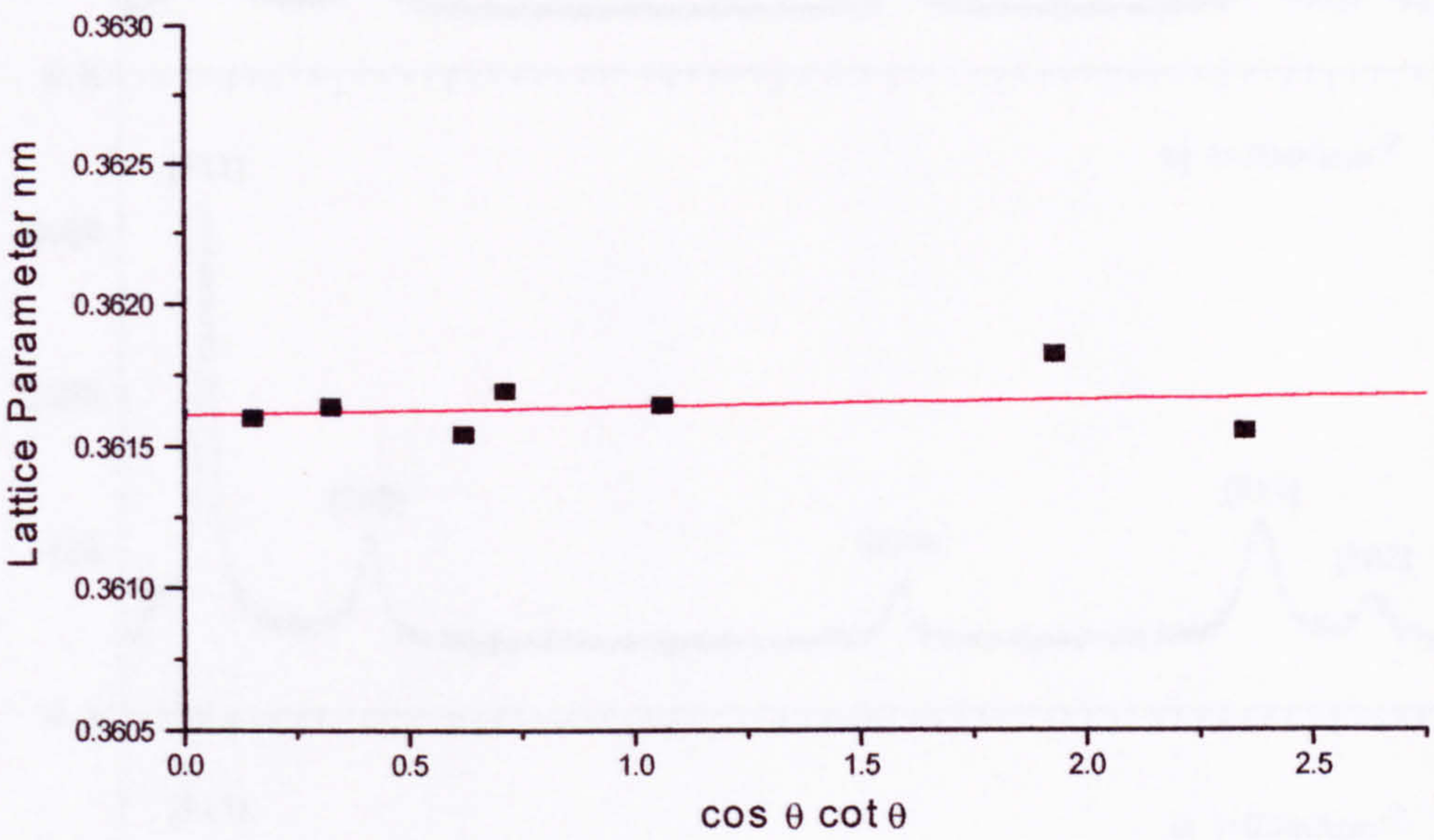

Fig. 4-12: Copper Sheet Substrate: Lattice Parameter [nm] Versus cosθ cotθ; Cohen-Wagner Plot for Extrapolation of Lattice Parameter 'a'.

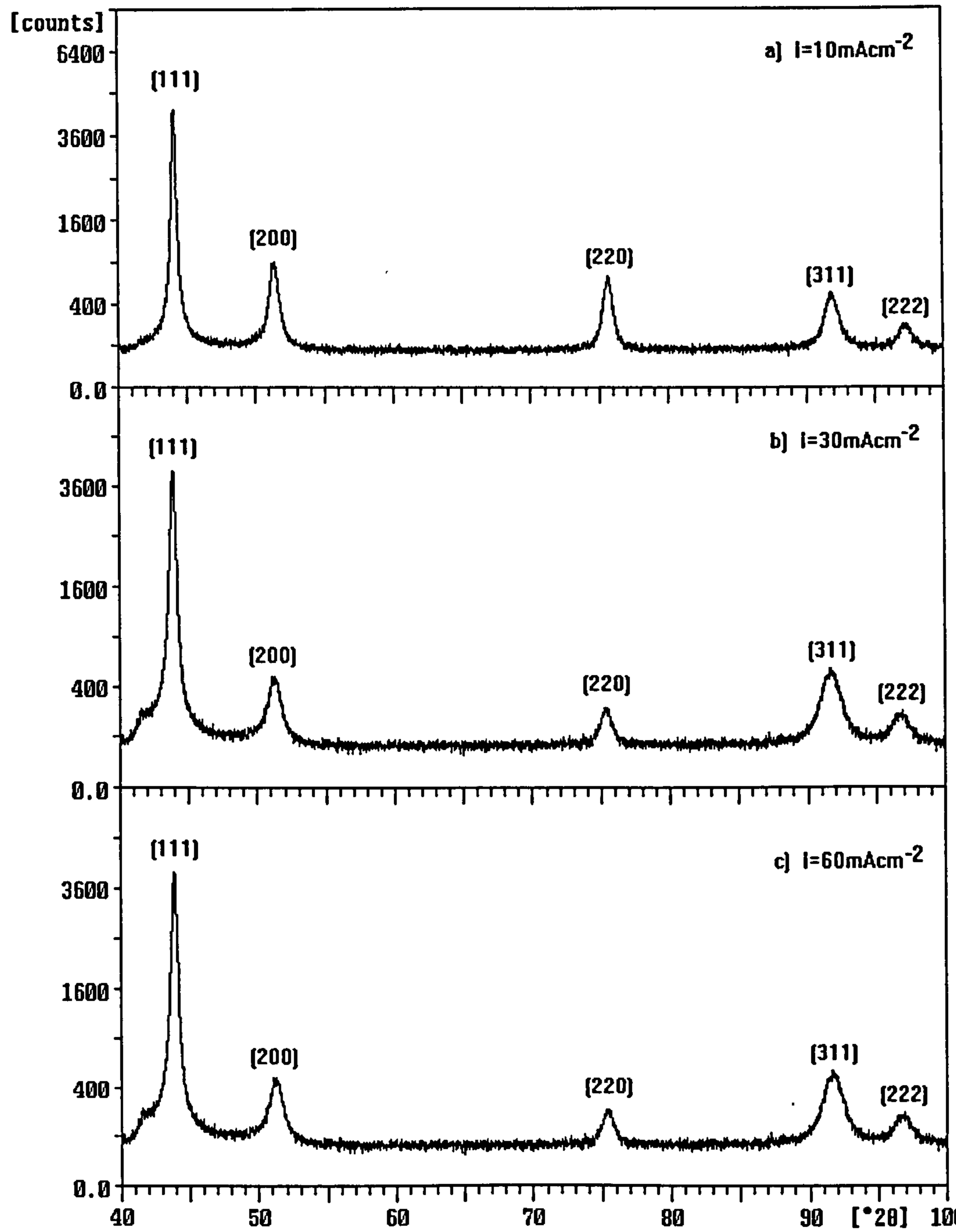

Fig. 4-13: X-Ray Diffraction Spectra of fcc Structured NiFe Deposits Obtained from Solution 1 at Different Current Densities:
a) i = 10 mA cm^{-2}, b) i = 30 mA cm^{-2}, c) i = 60 mA cm^{-2}.

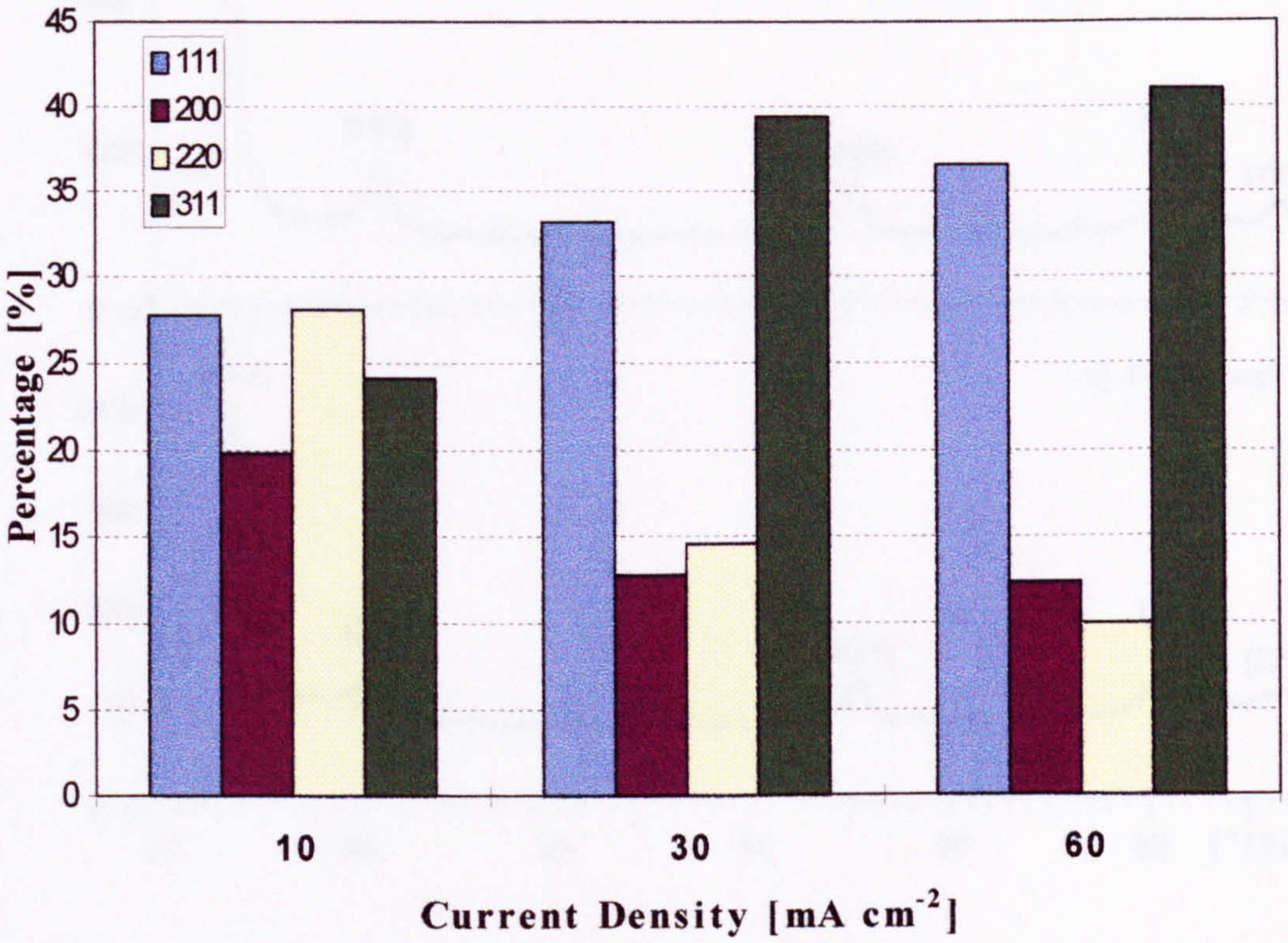

Fig. 4-14: Distribution of Reflections Detected in fcc NiFe Electrodeposits on Copper Sheet Substrates Deposited in NiFe Solution 1 at 10, 30 and 60 mA cm^{-2}.

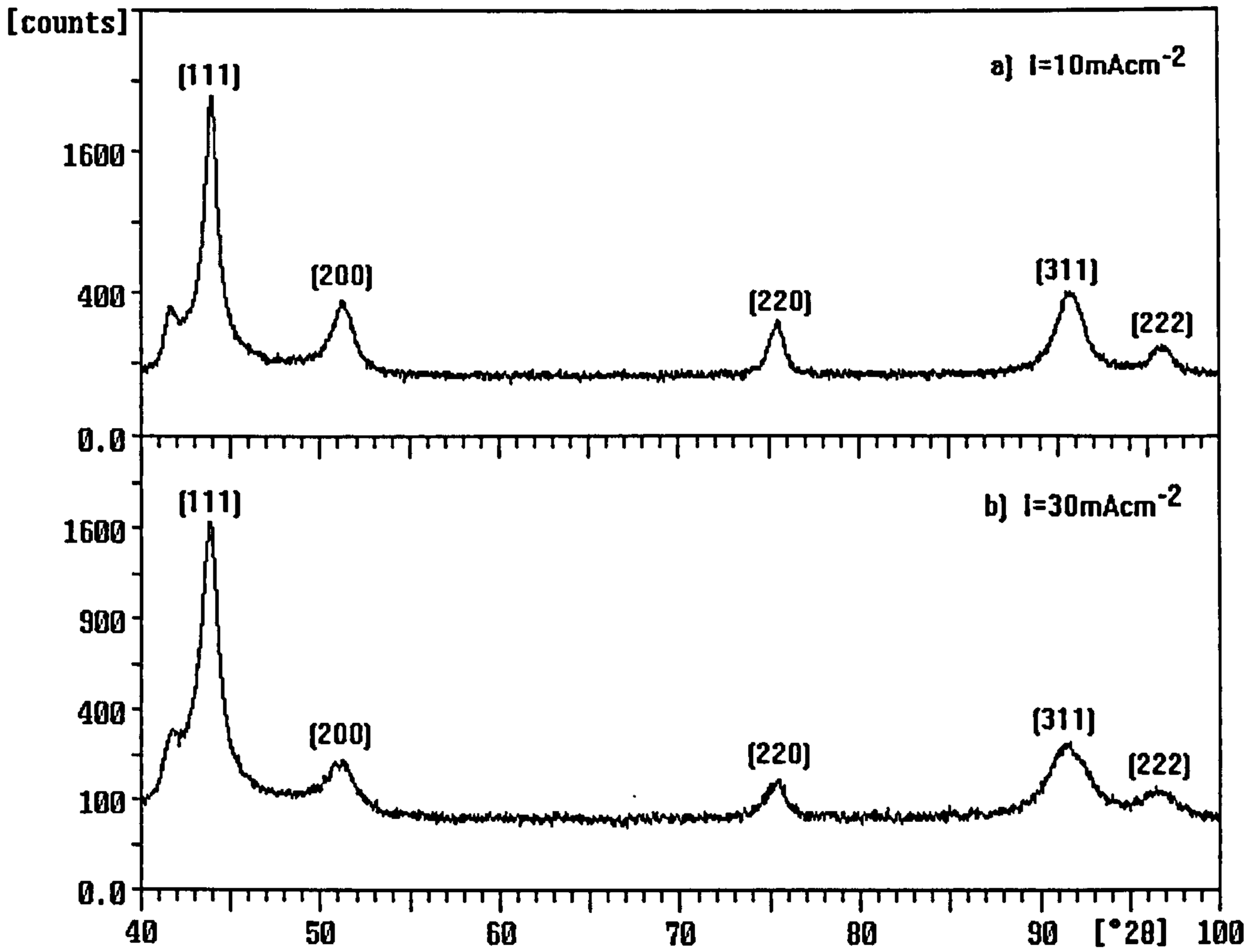

Fig. 4-15: X-Ray Diffraction Spectra of fcc Structured NiFe Deposits Obtained from Solution 3 at Different Current Densities:
a) i = 10 mA cm^{-2}, b) i = 30 mA cm^{-2}.

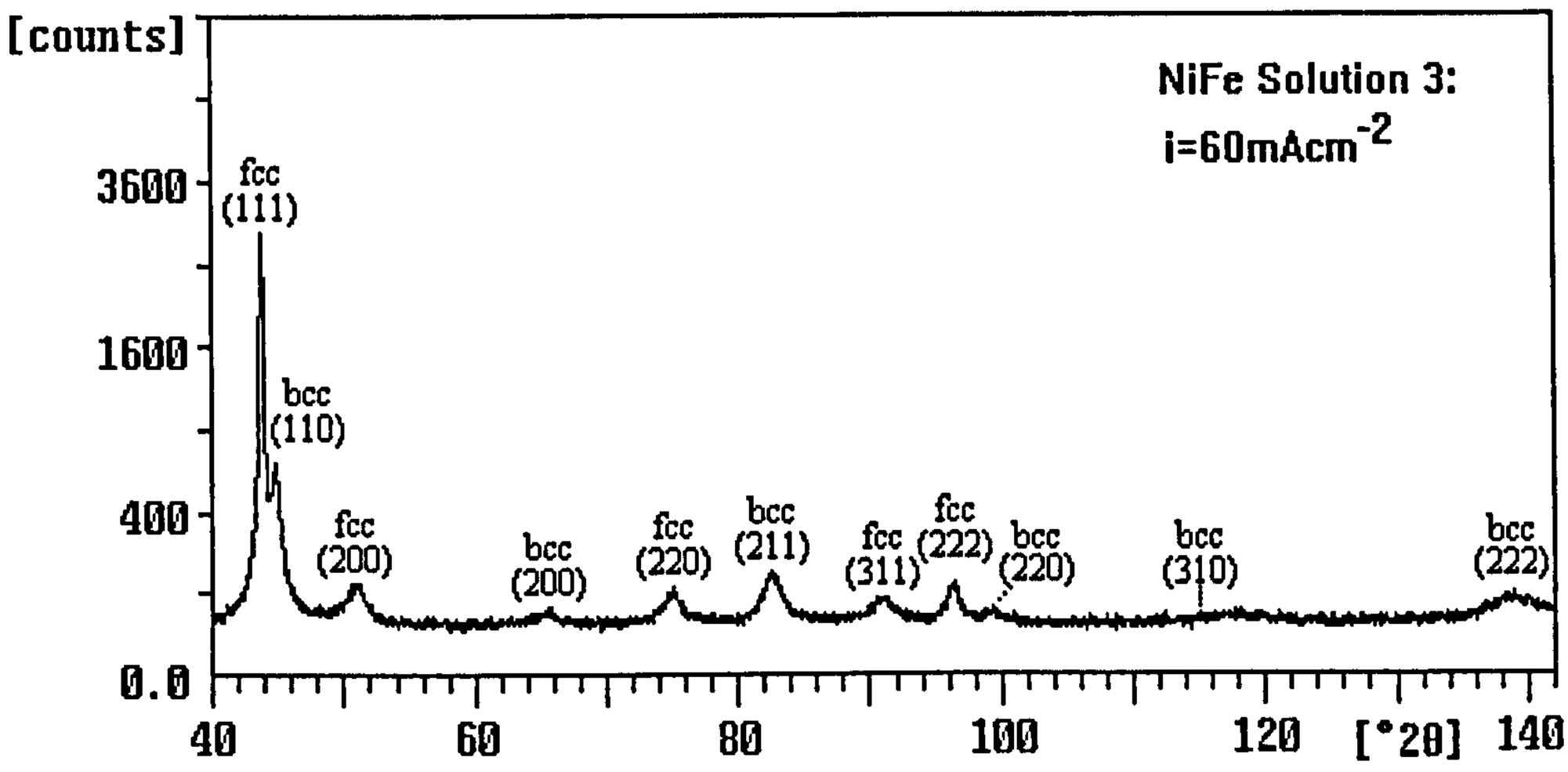

Fig. 4-16: X-Ray Diffraction Spectrum of Mixed fcc/bcc Structured NiFe Deposits Obtained from Solution 3 at i = 60 mA cm^{-2}.

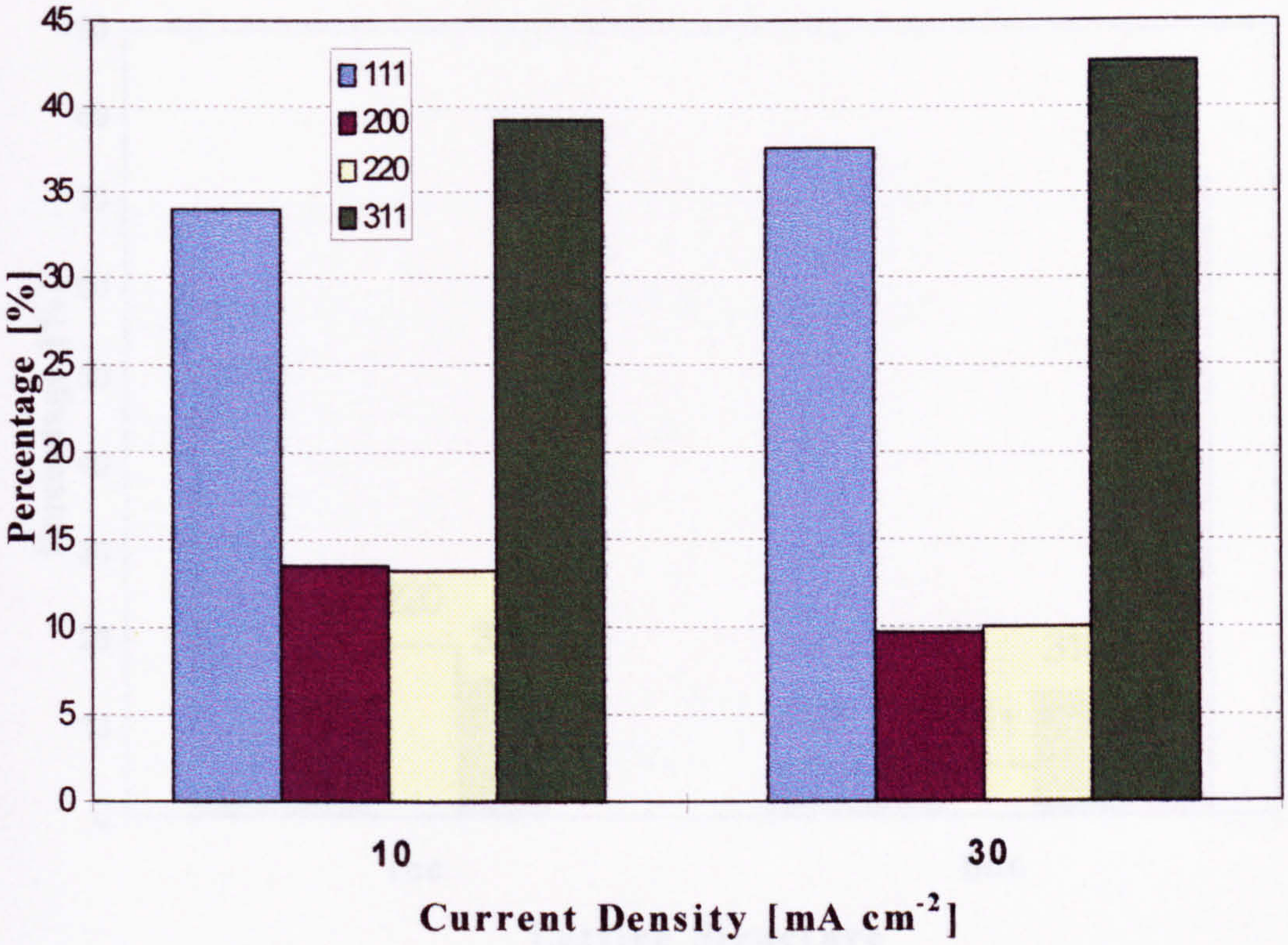

Fig. 4-17: Distribution of Reflections Detected in fcc NiFe Electrodeposits on Copper Sheet Deposited at 10 and 30 mA cm^{-2} in NiFe Solution 3.

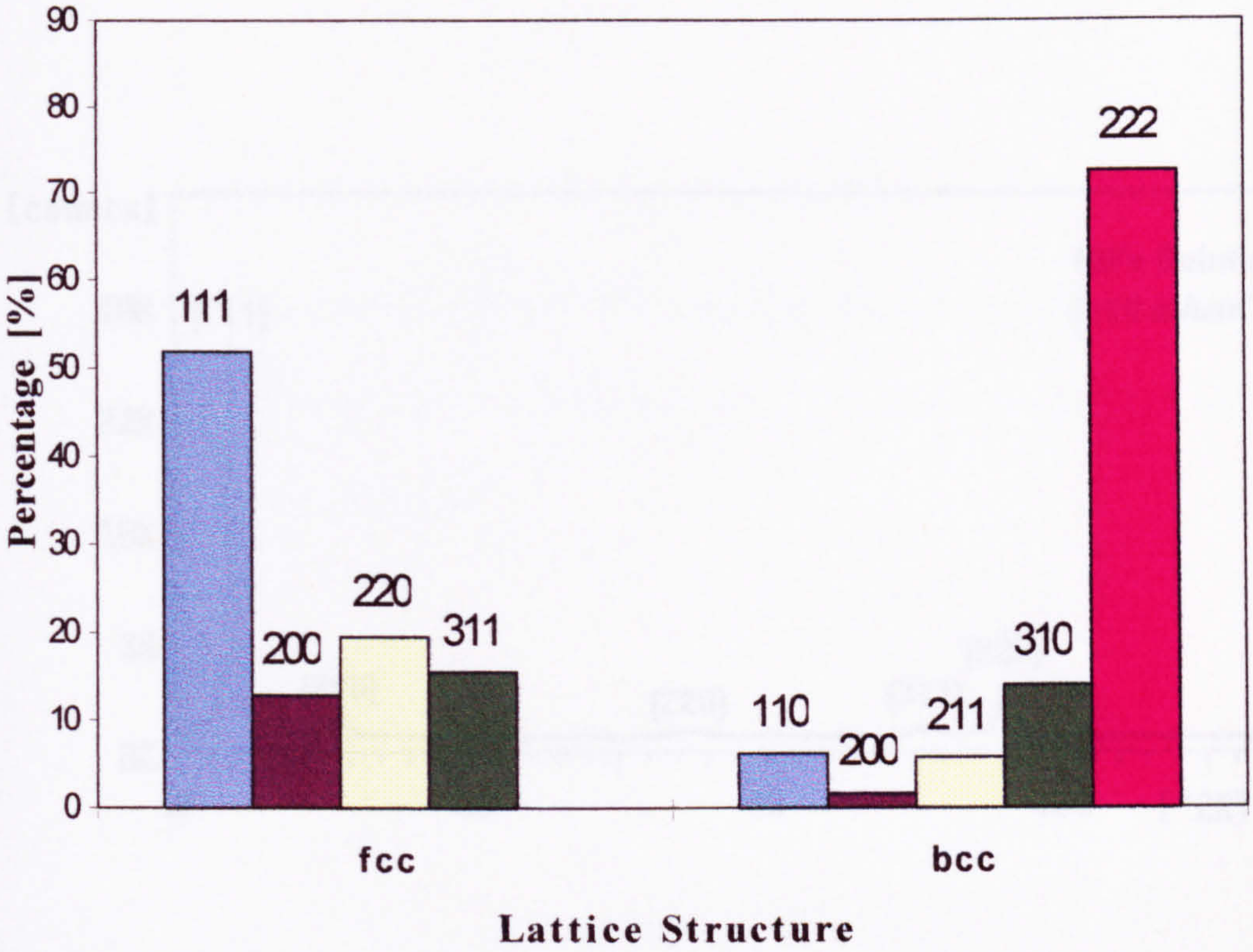

Fig. 4-18: Distribution of Reflections Detected in fcc/bcc NiFe Electrodeposits on Copper Sheet Deposited at 60 mA cm^{-2} in NiFe Solution 3.

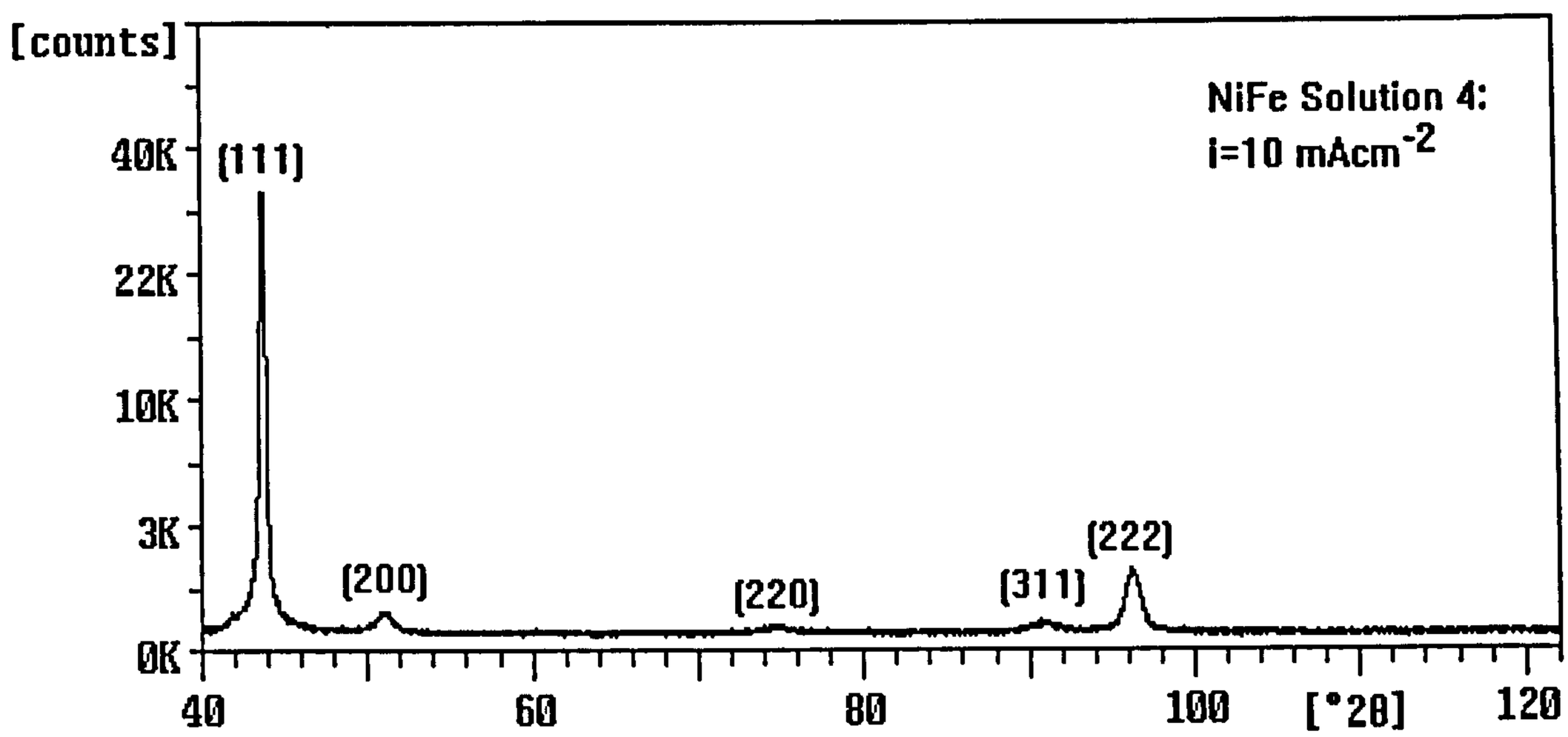

Fig. 4-19: X-Ray Diffraction Spectrum of fcc Structured NiFe Deposits Obtained from Solution 4 (i = 10 mA cm^{-2}).

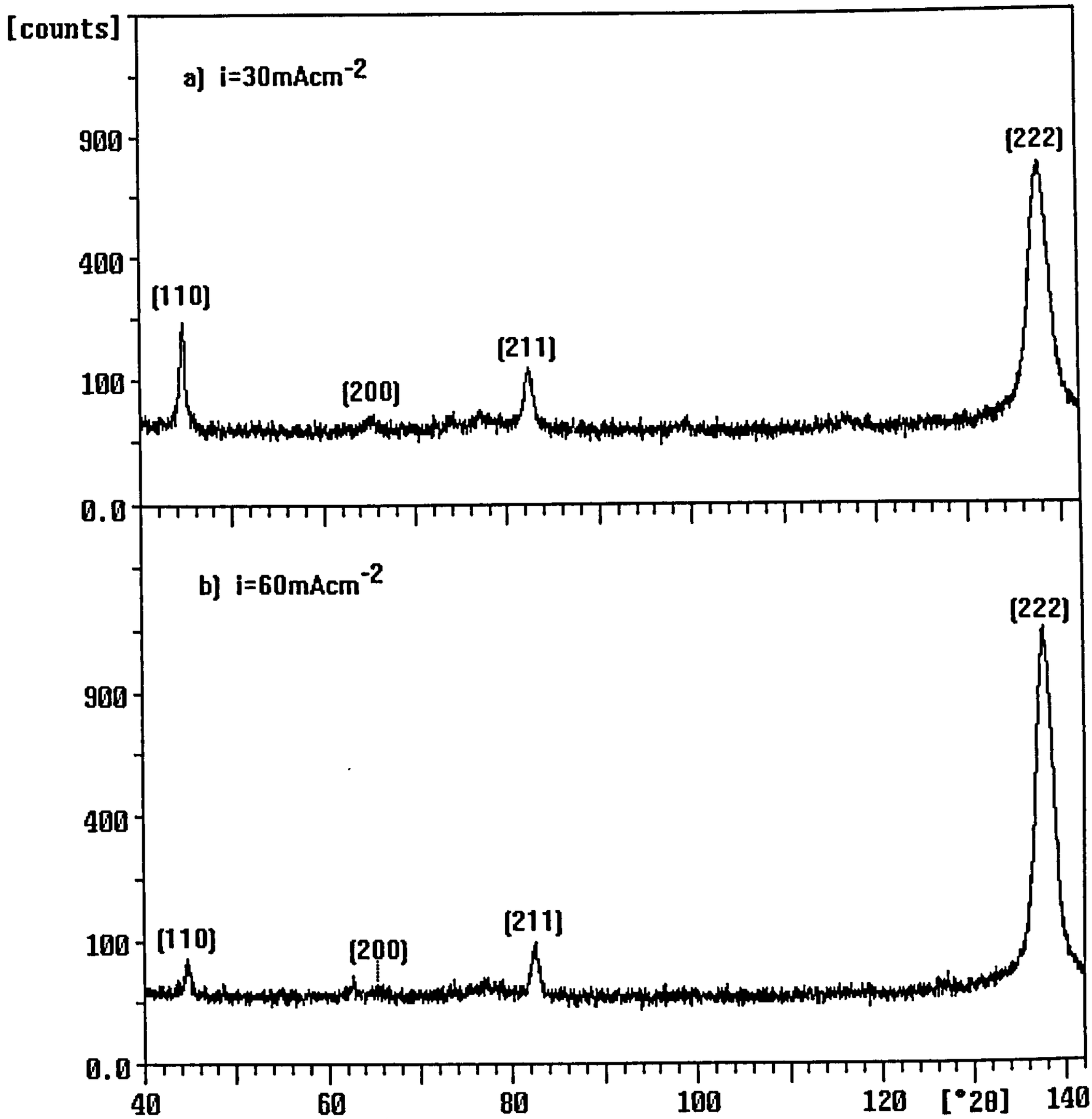

Fig. 4-20: X-Ray Diffraction Spectra of bcc Structured NiFe Deposits Obtained from Solution 4 at Different Current Densities:
a) i = 30 mA cm^{-2}, b) i = 60 mA cm^{-2}.

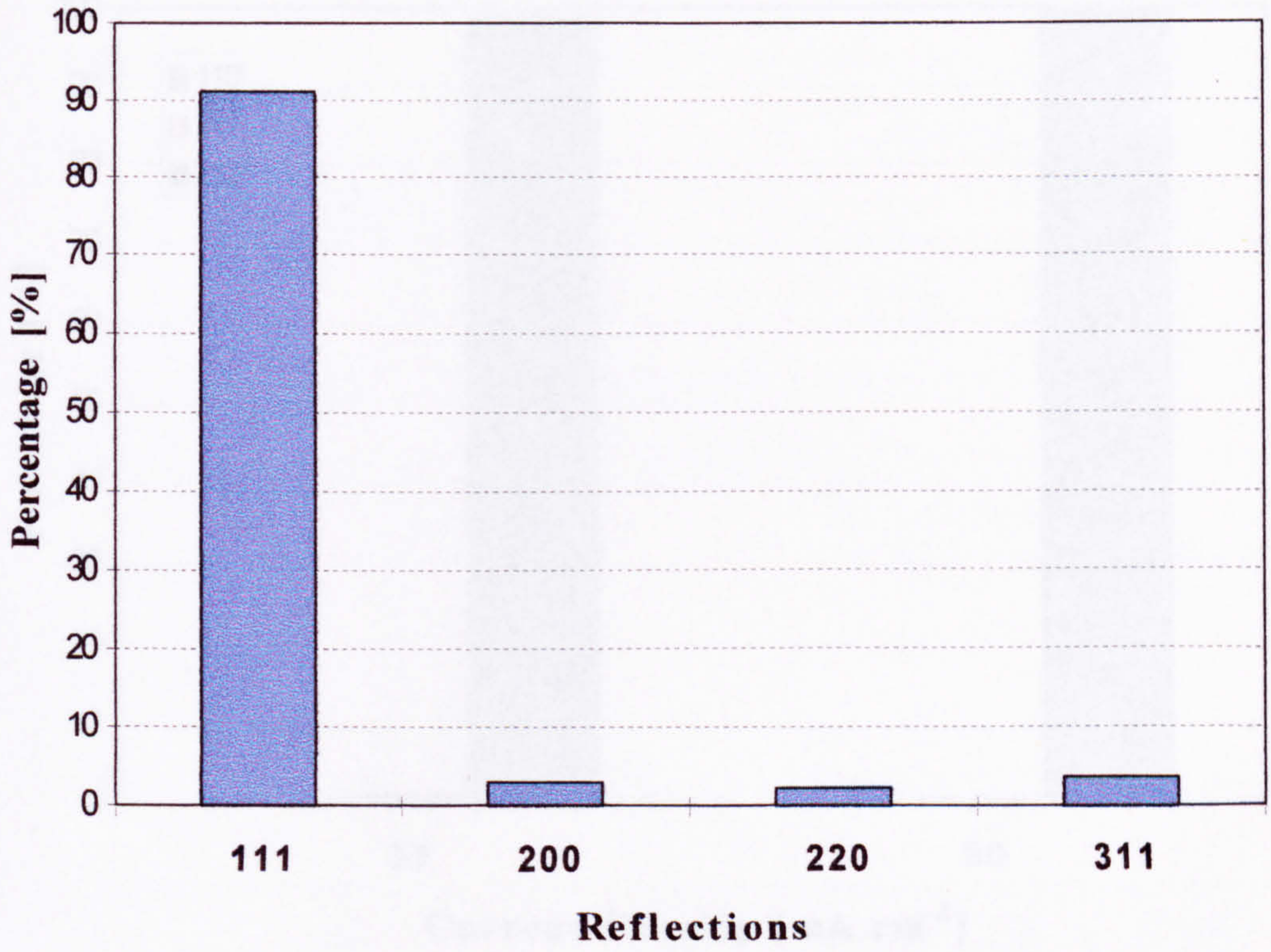

Fig. 4-21: Distribution of Reflections Detected in fcc NiFe Electrodeposit on Copper Sheet Deposited at 10 mA cm^{-2} in NiFe Solution 4.

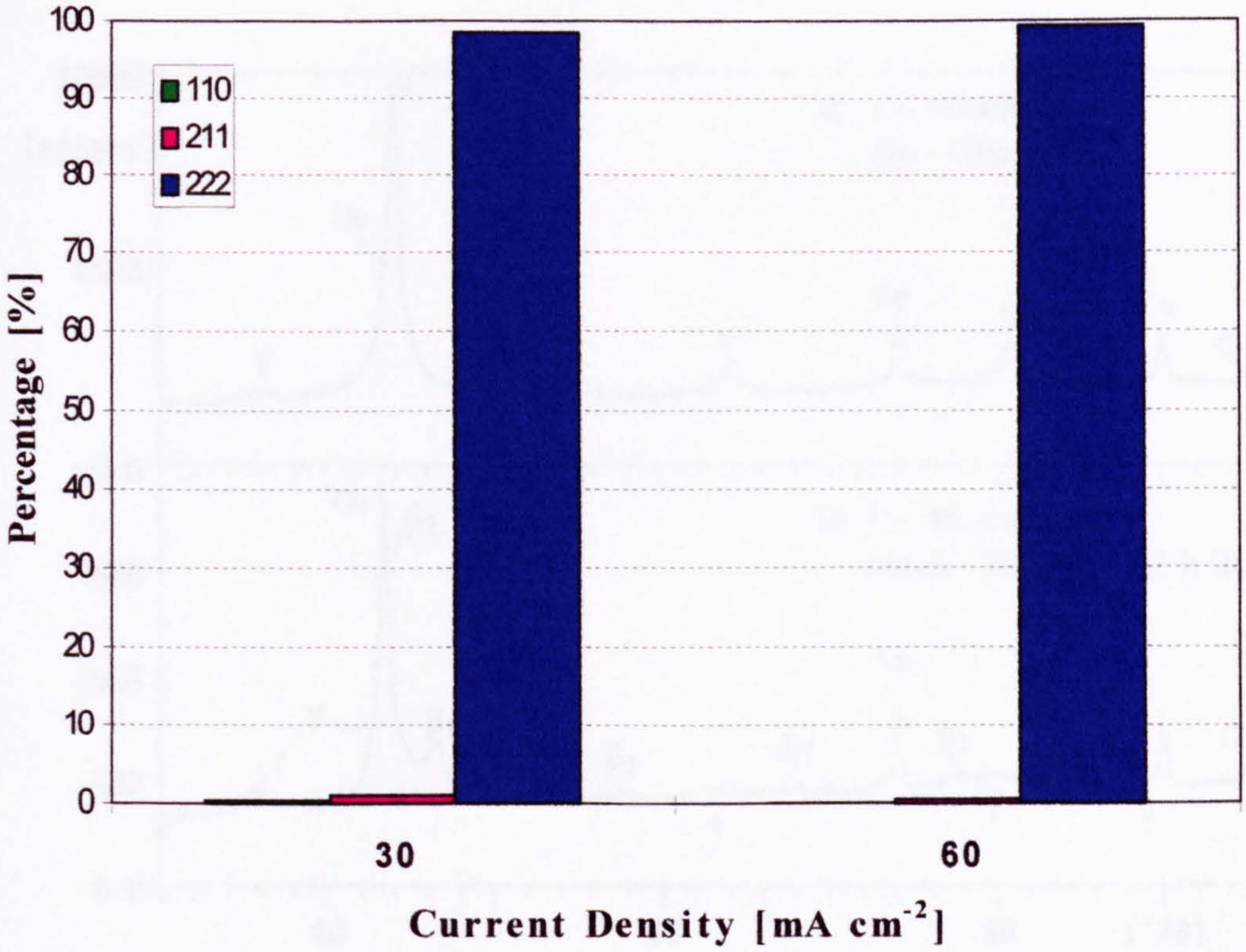

Fig. 4-22: Distribution of Reflections Detected in bcc NiFe Electrodeposit on Copper Sheet Deposited at 30 and 60 mA cm^{-2} in NiFe Solution 4.

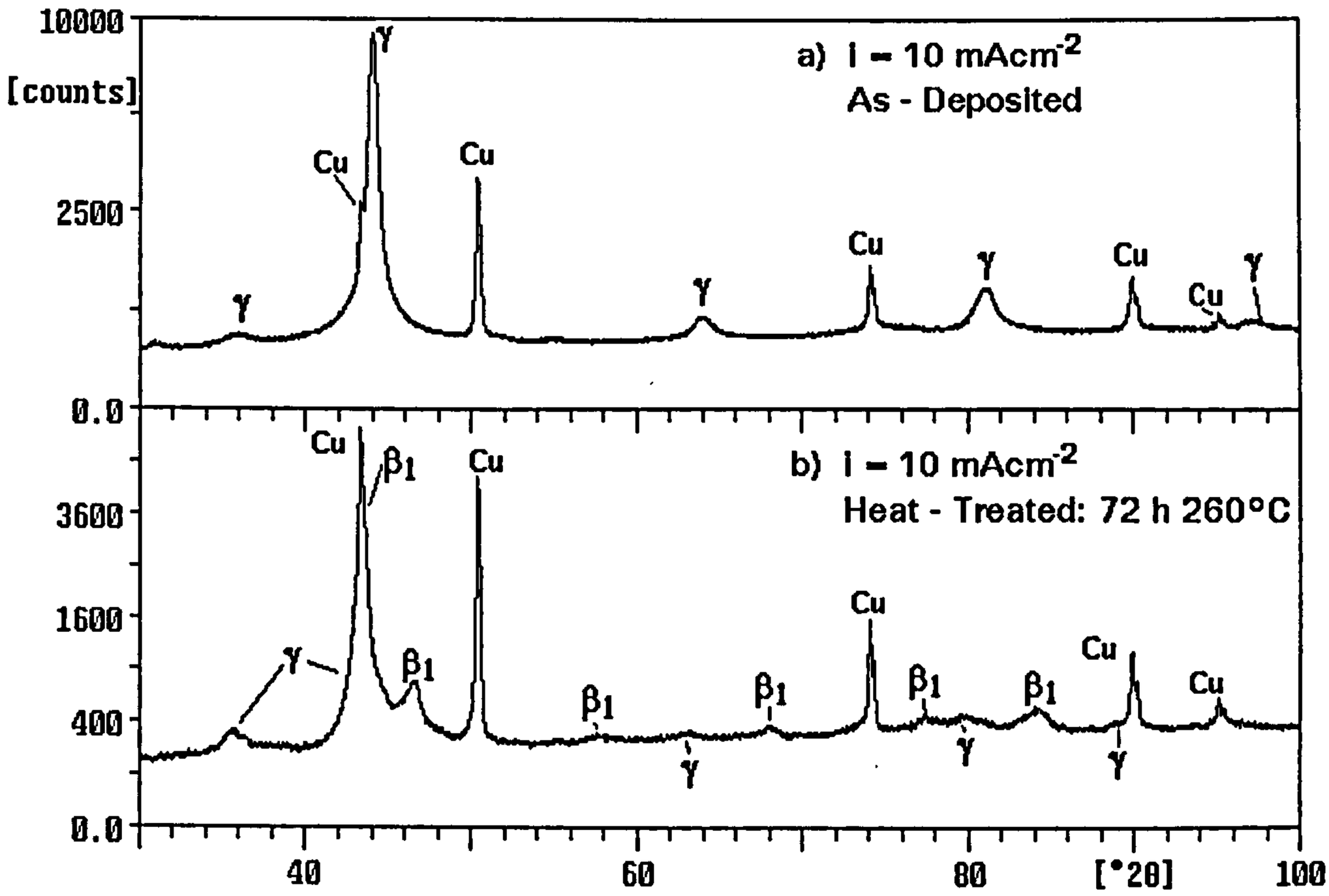

Fig. 4-23: XRD Spectra of Deposit Produced in Nickel-Zinc Solution 8, (i = 10 mA cm^{-2}) in a) As-Deposited, b) Heat-Treated Condition.

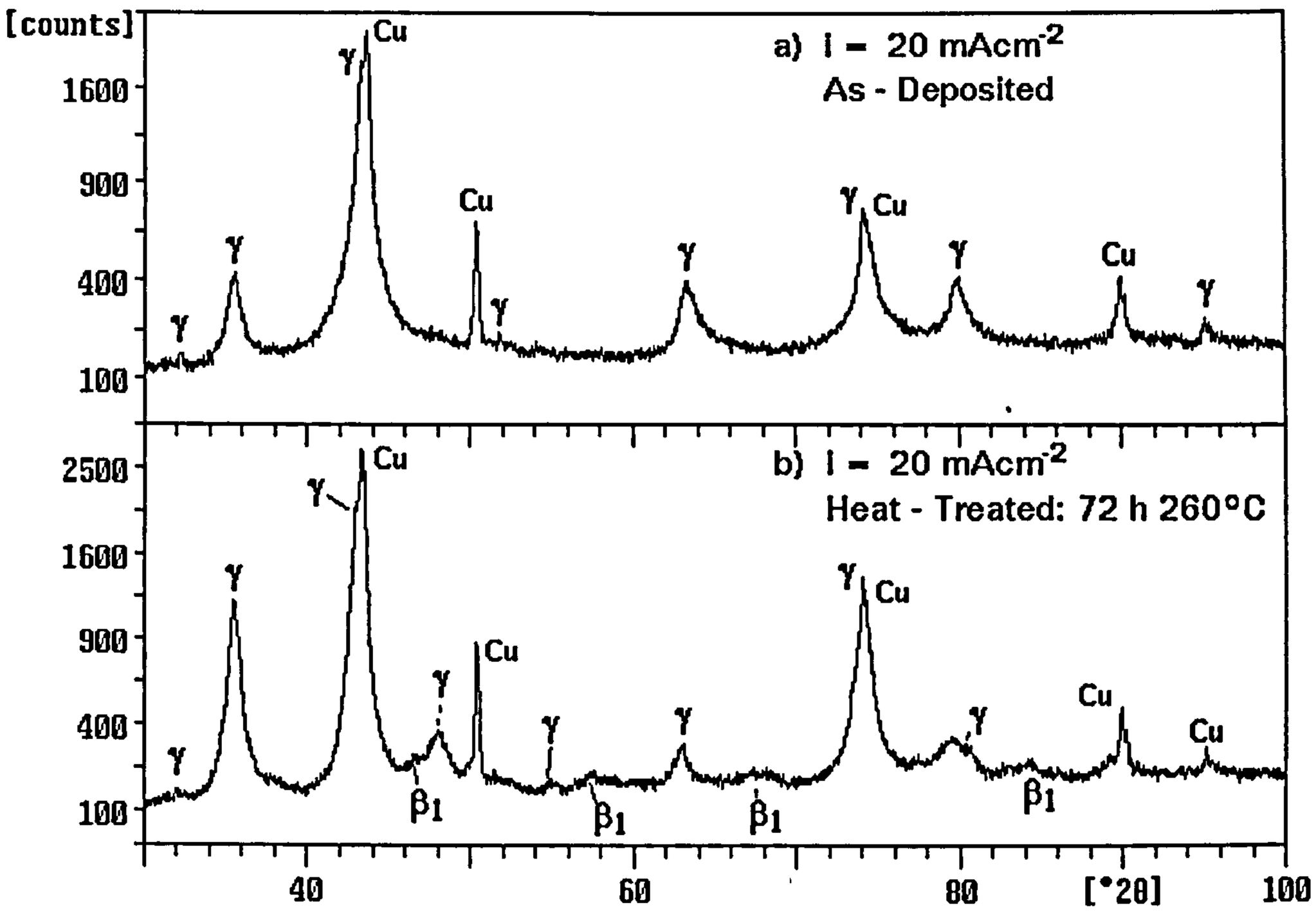

Fig. 4-24: XRD Spectra of Deposit Produced in Nickel-Zinc Solution 8, ($i = 20$ mA cm^{-2}) in a) As-Deposited, b) Heat-Treated Condition.

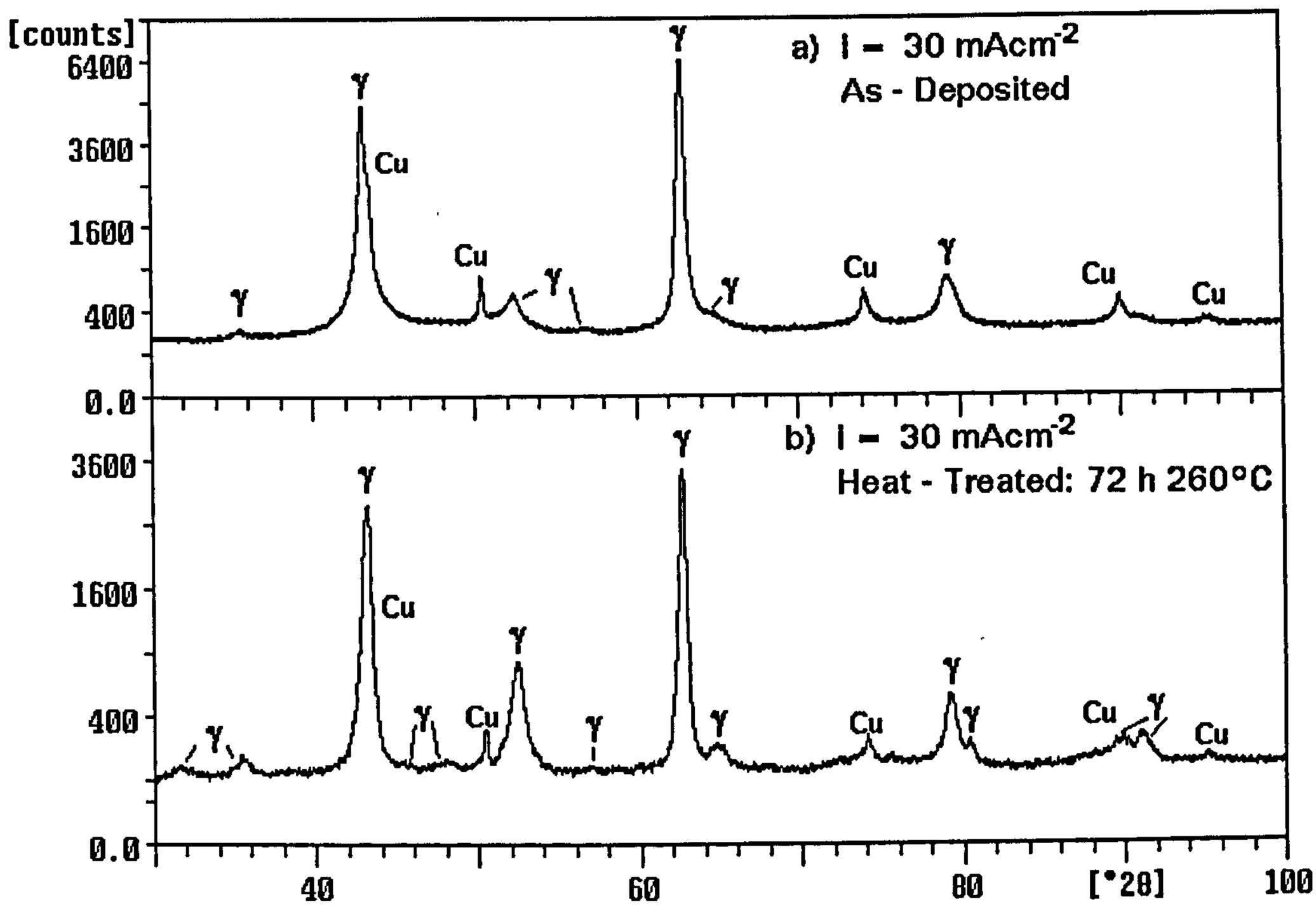

Fig. 4-25: XRD Spectra of Deposit Produced in Nickel-Zinc Solution 8, (i = 30 mA cm^{-2}) in a) As-Deposited, b) Heat-Treated Condition.

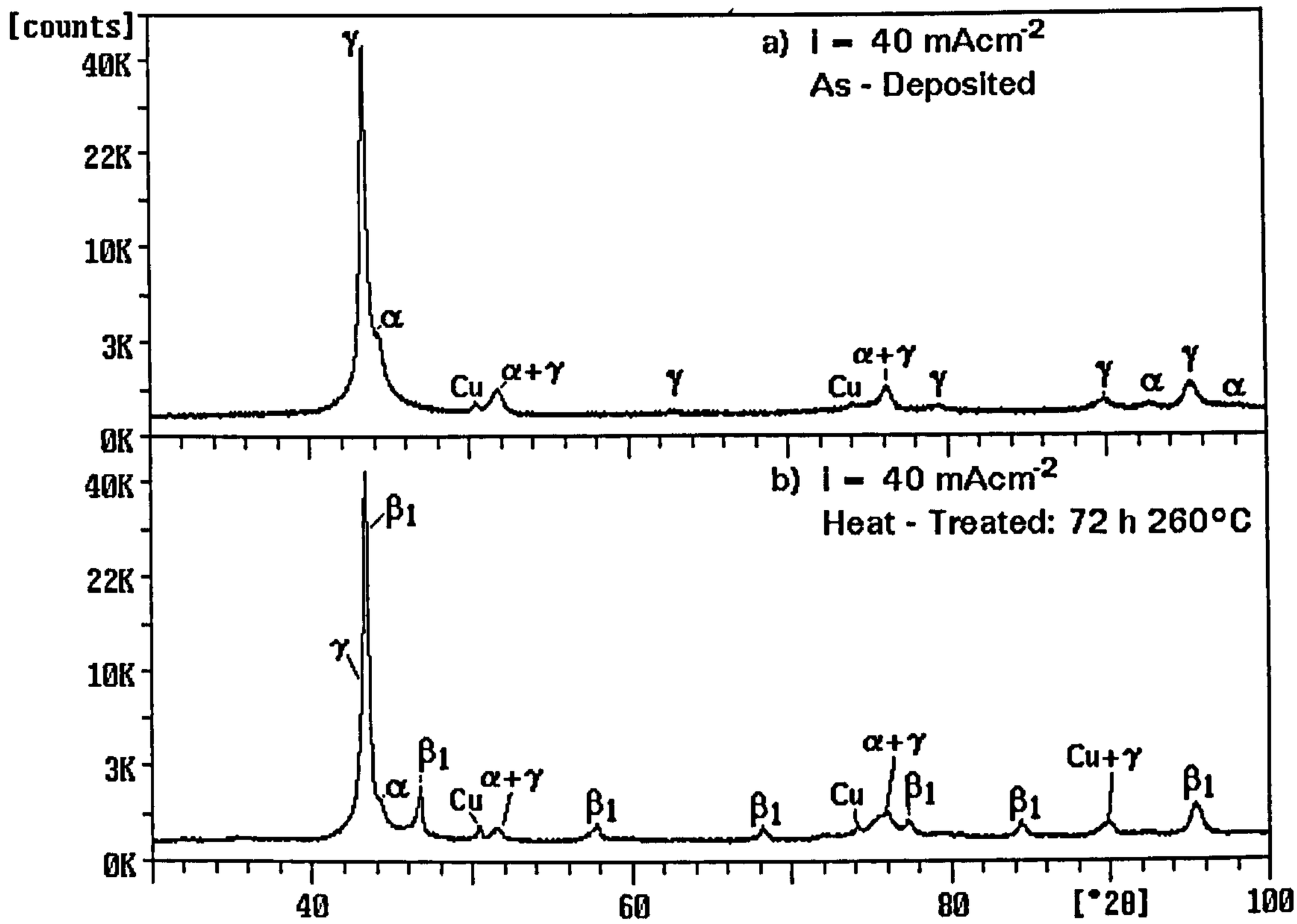

Fig. 4-26: XRD Spectra of Deposit Produced in Nickel-Zinc Solution 8, (i = 40 mA cm^{-2}) in a) As-Deposited, b) Heat-Treated Condition.

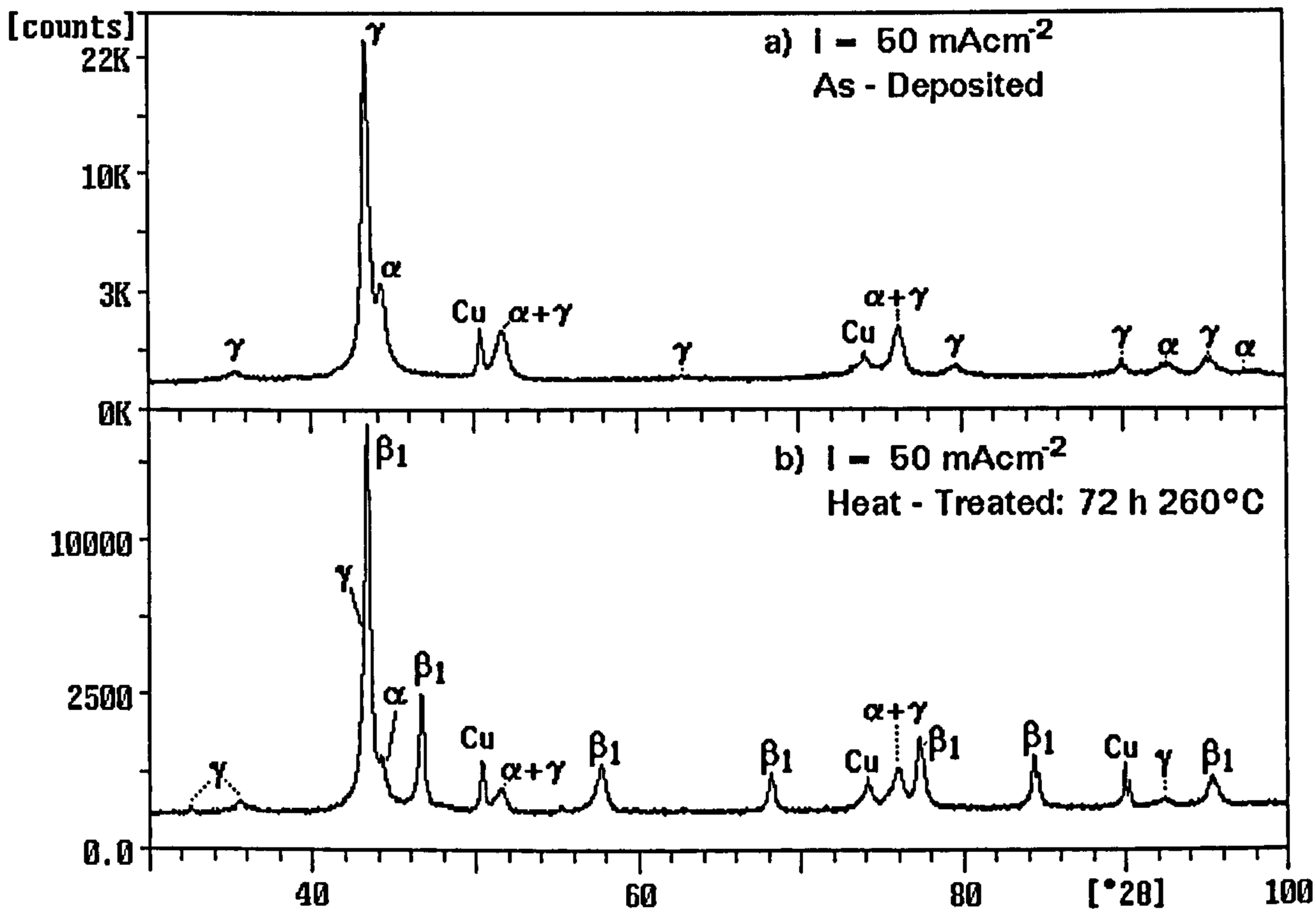

Fig. 4-27: XRD Spectra of Deposit Produced in Nickel-Zinc Solution 8, (i = 50 mA cm^{-2}) in a) As-Deposited, b) Heat-Treated Condition.

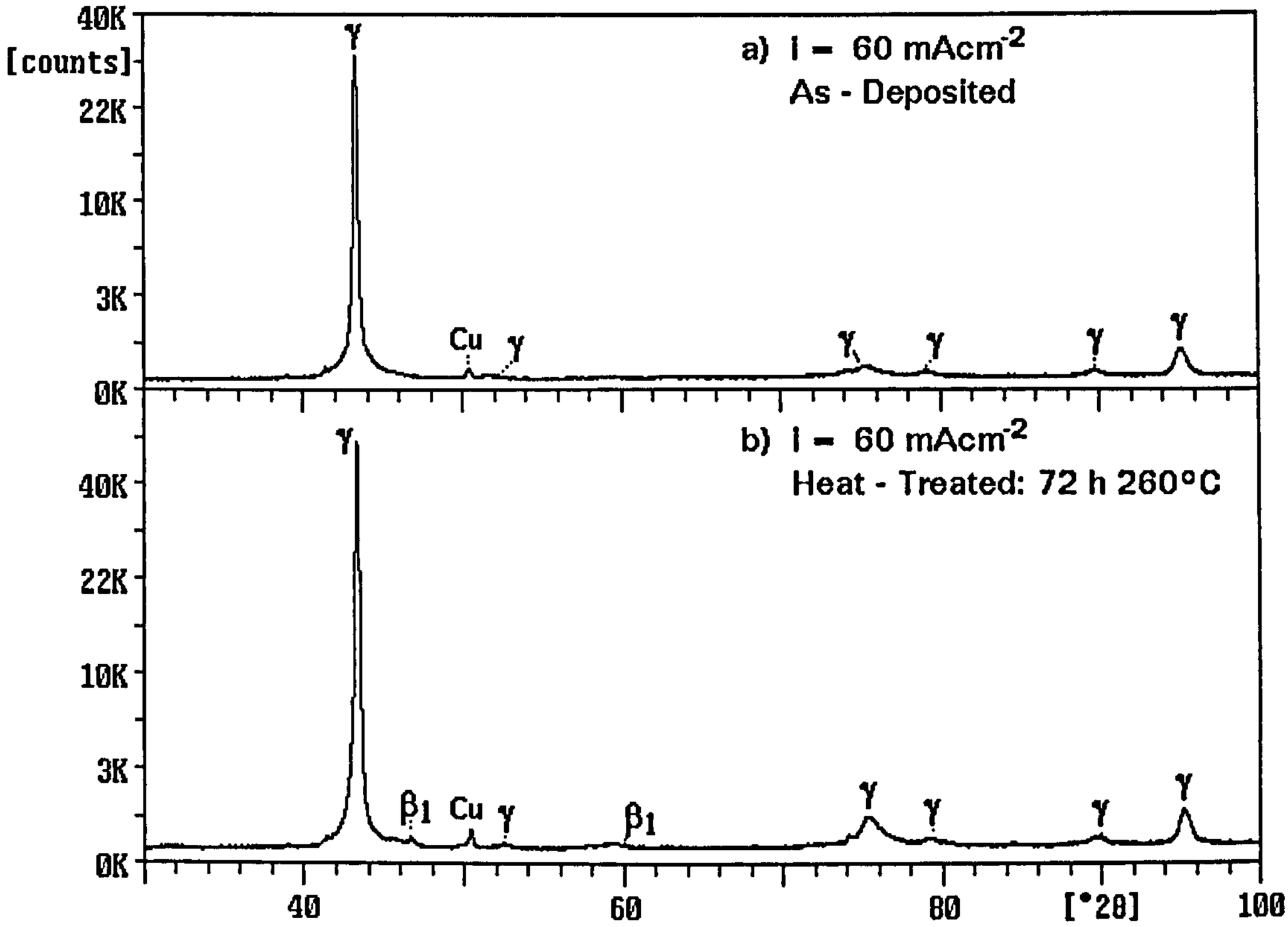

Fig. 4-28: XRD Spectra of Deposit Produced in Nickel-Zinc Solution 8, (i = 60 mA cm^{-2}) in a) As-Deposited, b) Heat-Treated Condition.

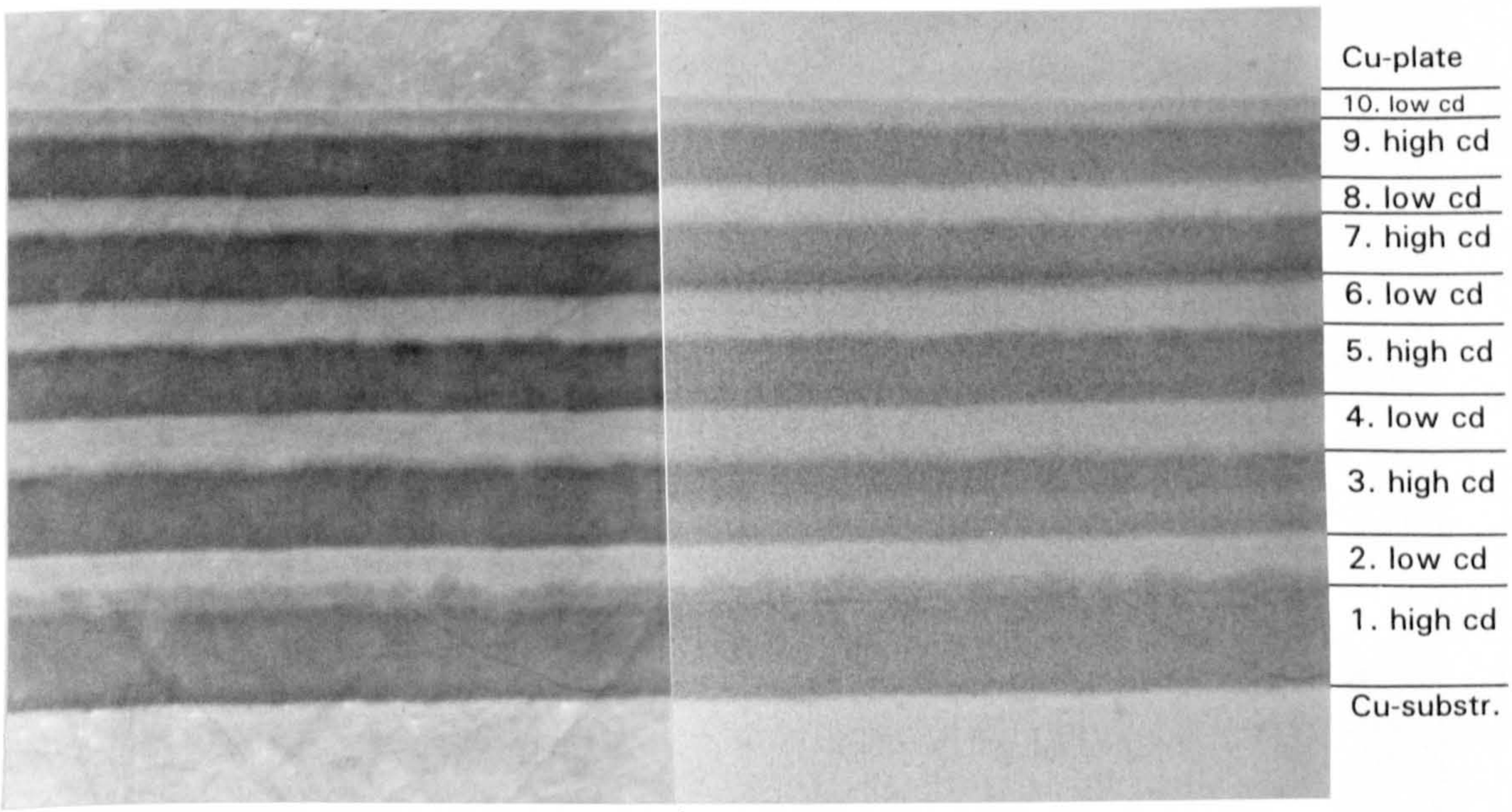

Fig. 4-29:
a) SEI
of Multilayered NiFe Deposit.

b) BSI
of Multilayered NiFe Deposit.

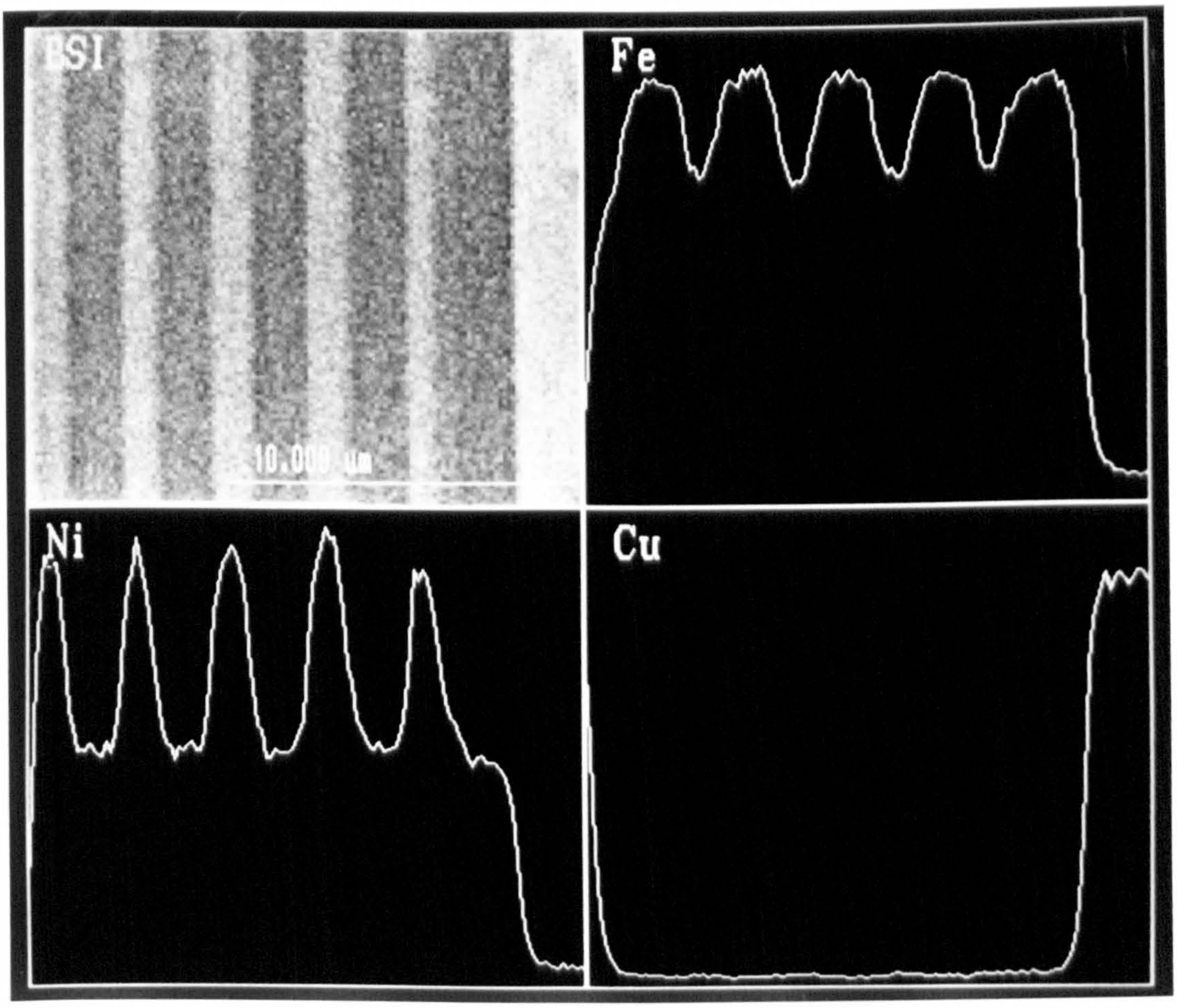

Fig. 4-30: Cross-sectioned Nickel-Iron Electrodeposit.
Digitized BSI (top left).
Energy Dispersive Line-Scans of Multilayered Nickel-Iron Electrodeposit: Iron (top right); Nickel (bottom left); Copper (bottom right).

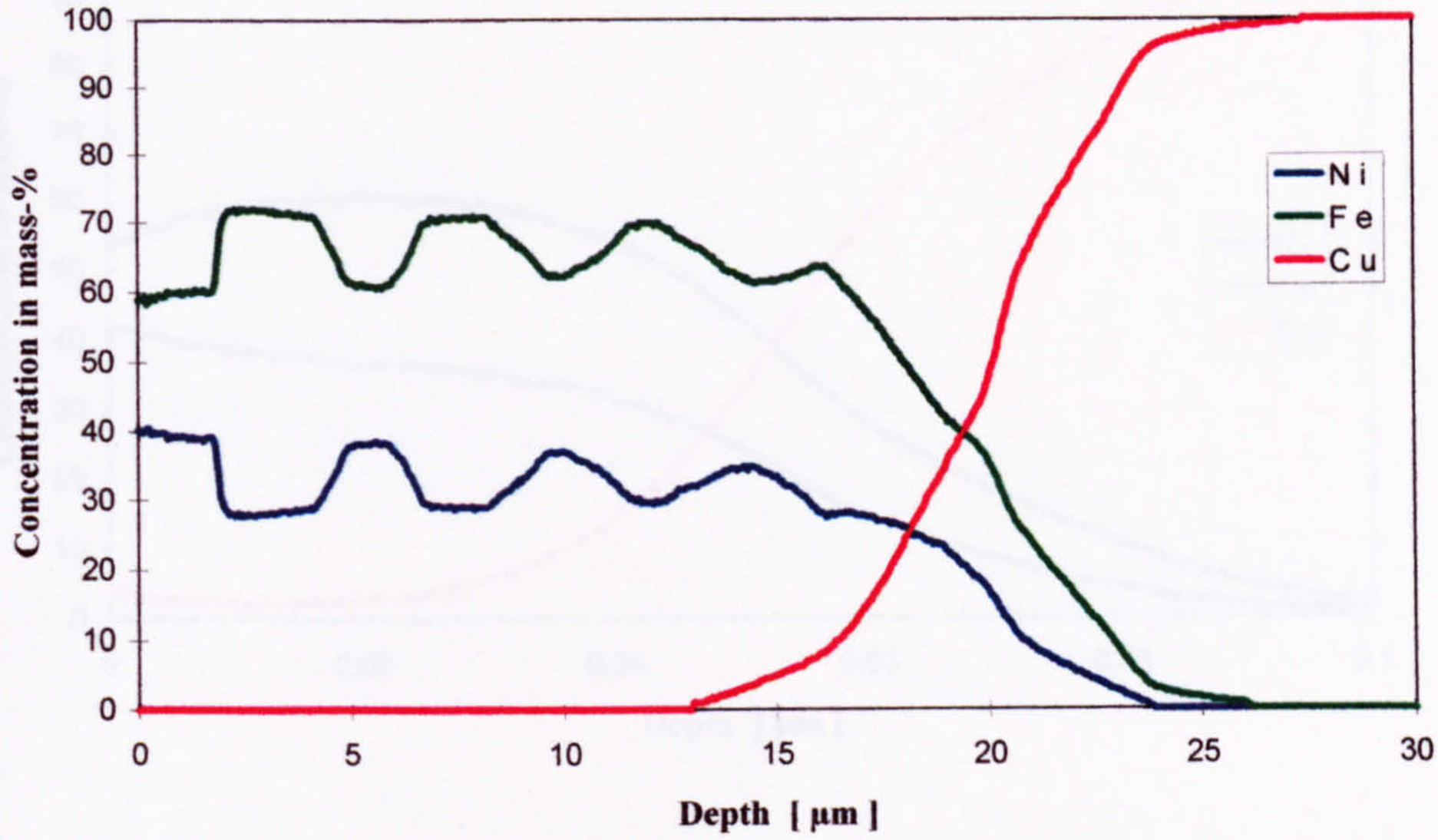

Fig. 4-31: Quantitative Depth Profile of Nickel-Iron Multilayer Obtained by GDOES.

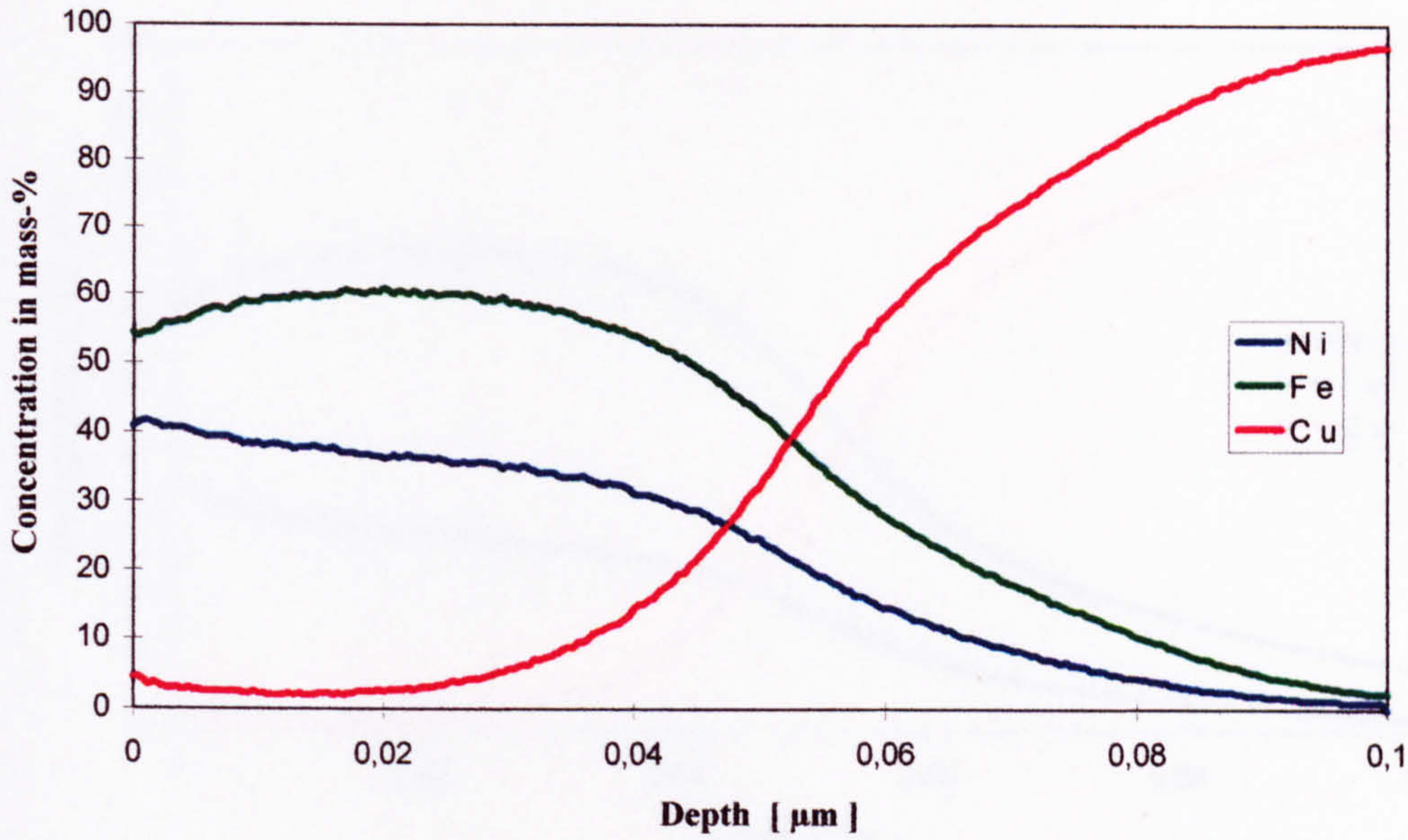

Fig. 4-32: Quantitative Depth Profile of 0.05 µm Thick fcc Nickel-Iron Electrodeposit (i = 10 mA cm^{-2}).

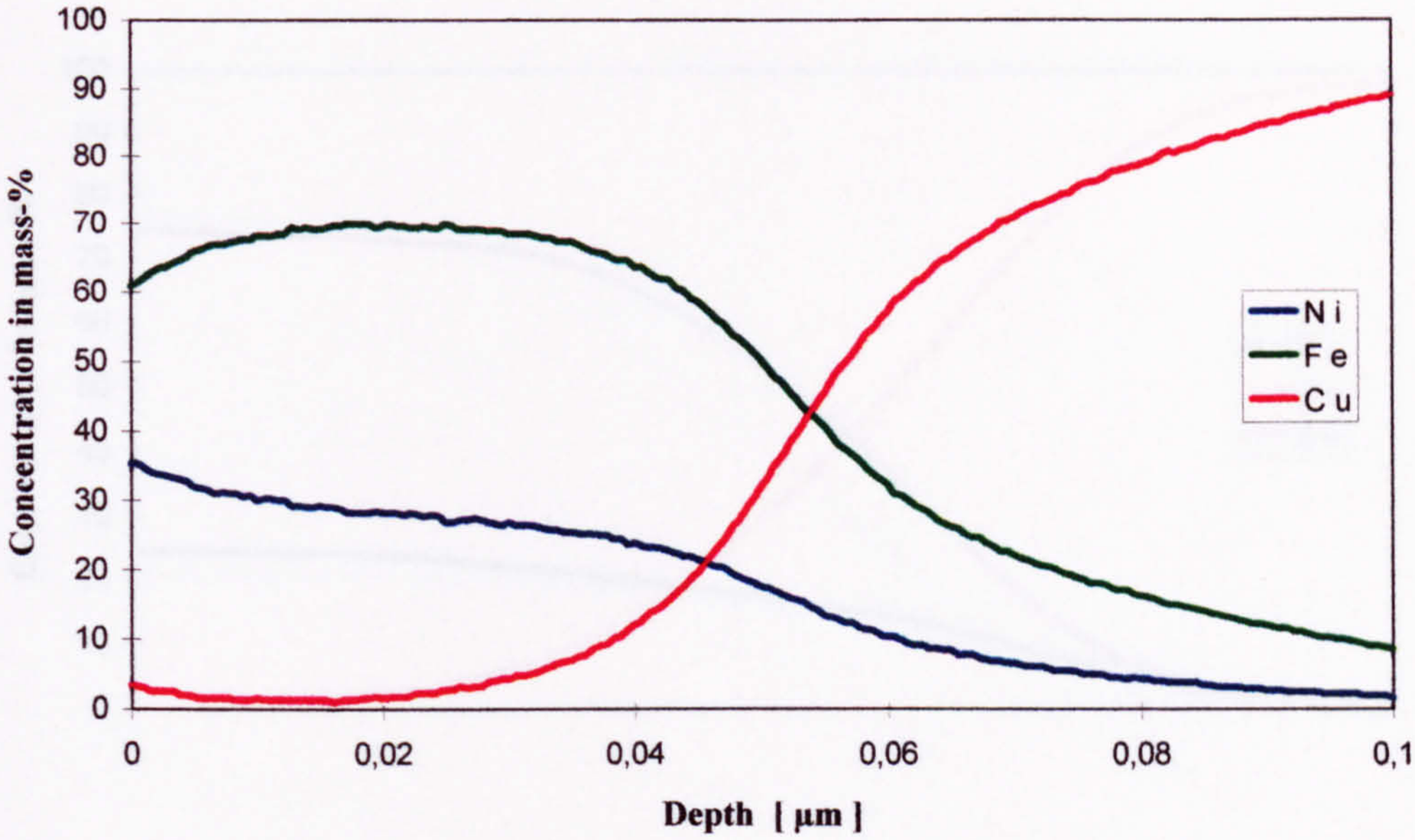

Fig. 4-33: Quantitative Depth Profile of 0.05 µm Thick bcc Nickel-Iron Electrodeposit (i = 60 mA cm^{-2}).

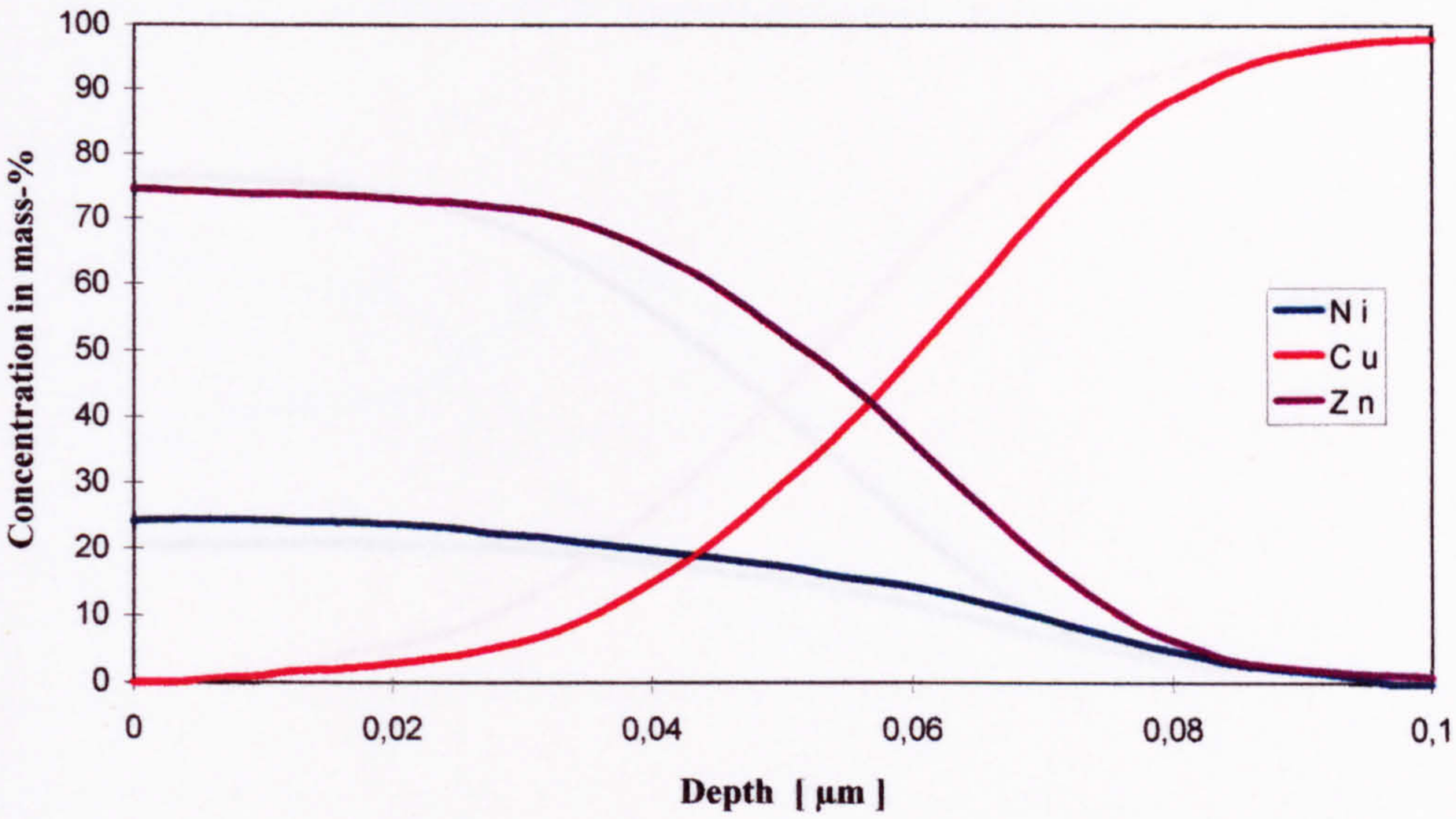

Fig. 4-34: Quantitative Depth Profile of 0.05 µm Thick Nickel-Zinc Electrodeposited with 10 mA cm^{-2} onto Copper Substrate.

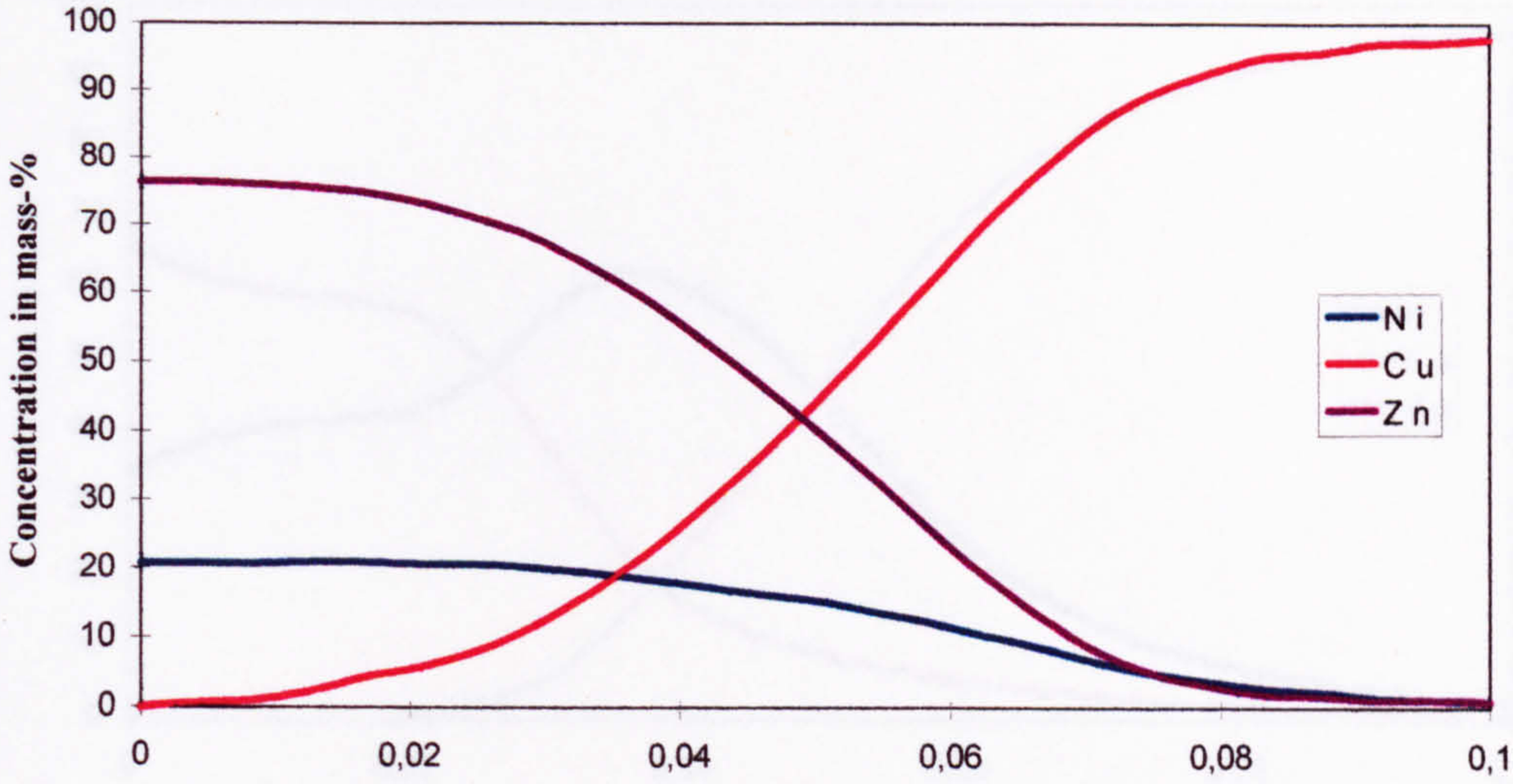

Fig. 4-35: Quantitative Depth Profile of 0.05 µm thick Nickel-Zinc Electrodeposited with 60 mA cm^{-2} onto Copper Substrate.

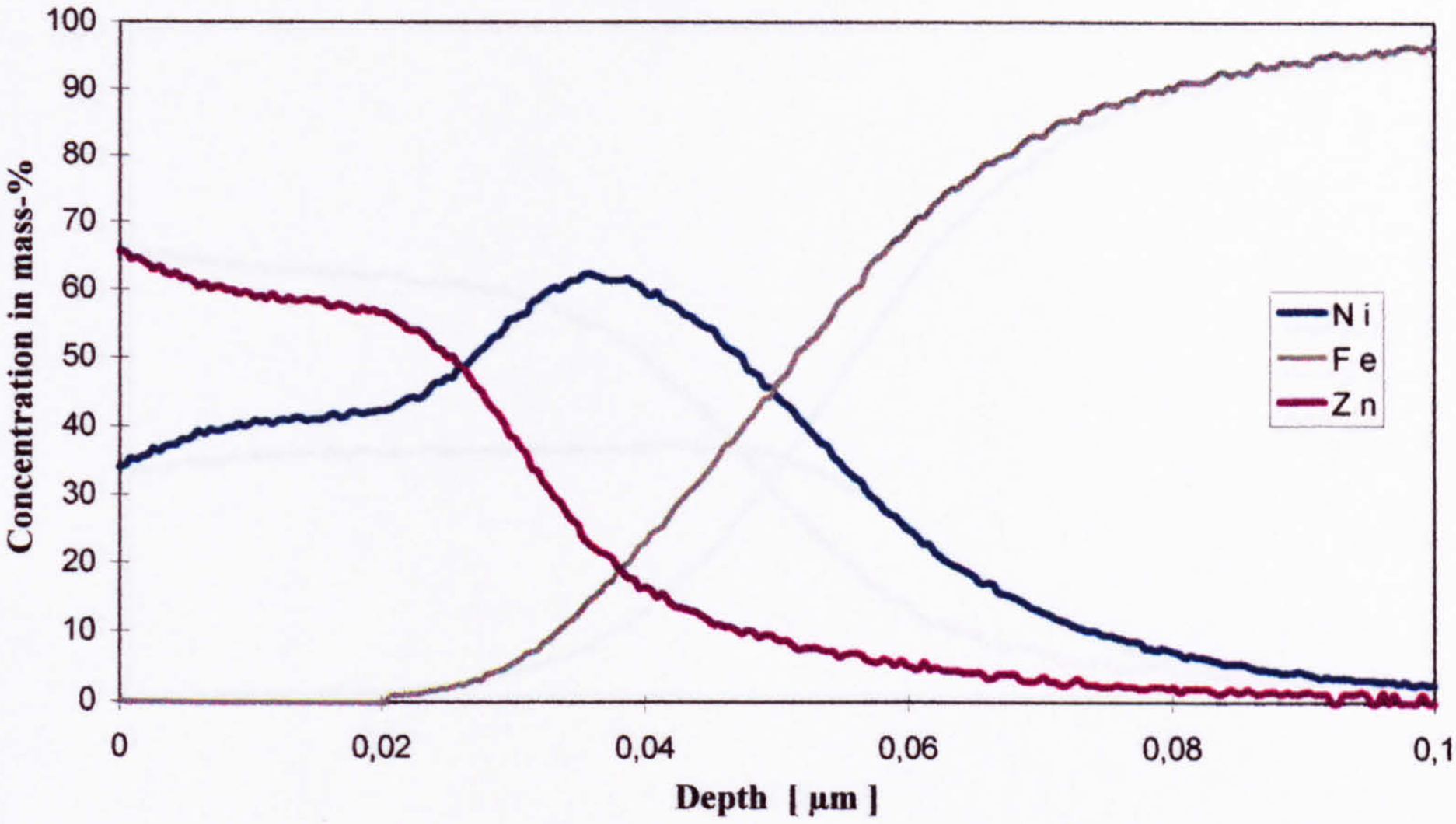

Fig. 4-36: Quantitative Depth Profile of 0.05 µm Thick Nickel-Zinc Electrodeposited with 10 mA cm^{-2} onto Steel Substrate.

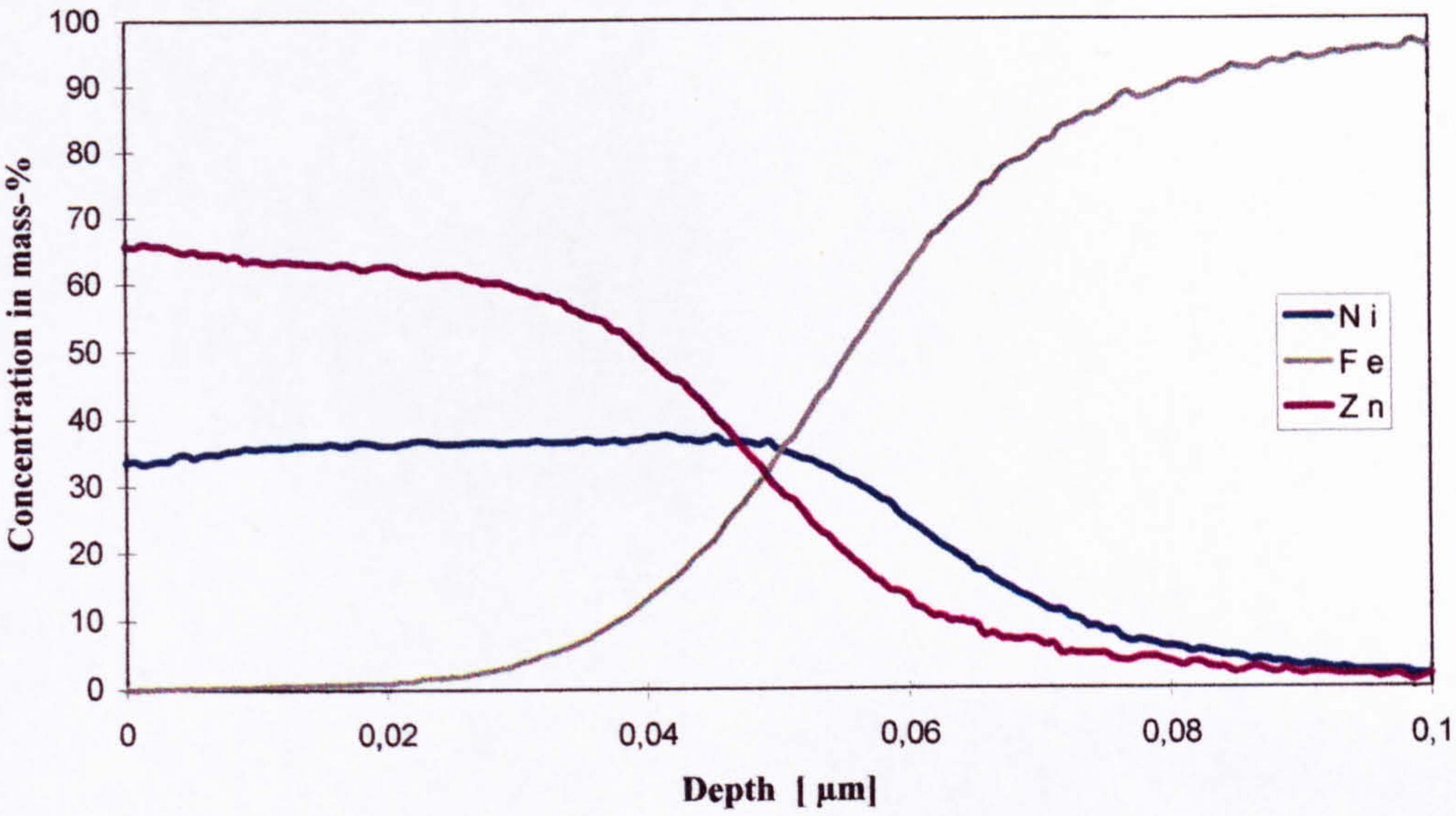

Fig. 4-37: Quantitative Depth Profile of 0.05 µm Thick Nickel-Zinc Electrodeposited with 60 mA cm^{-2} onto Steel Substrate.

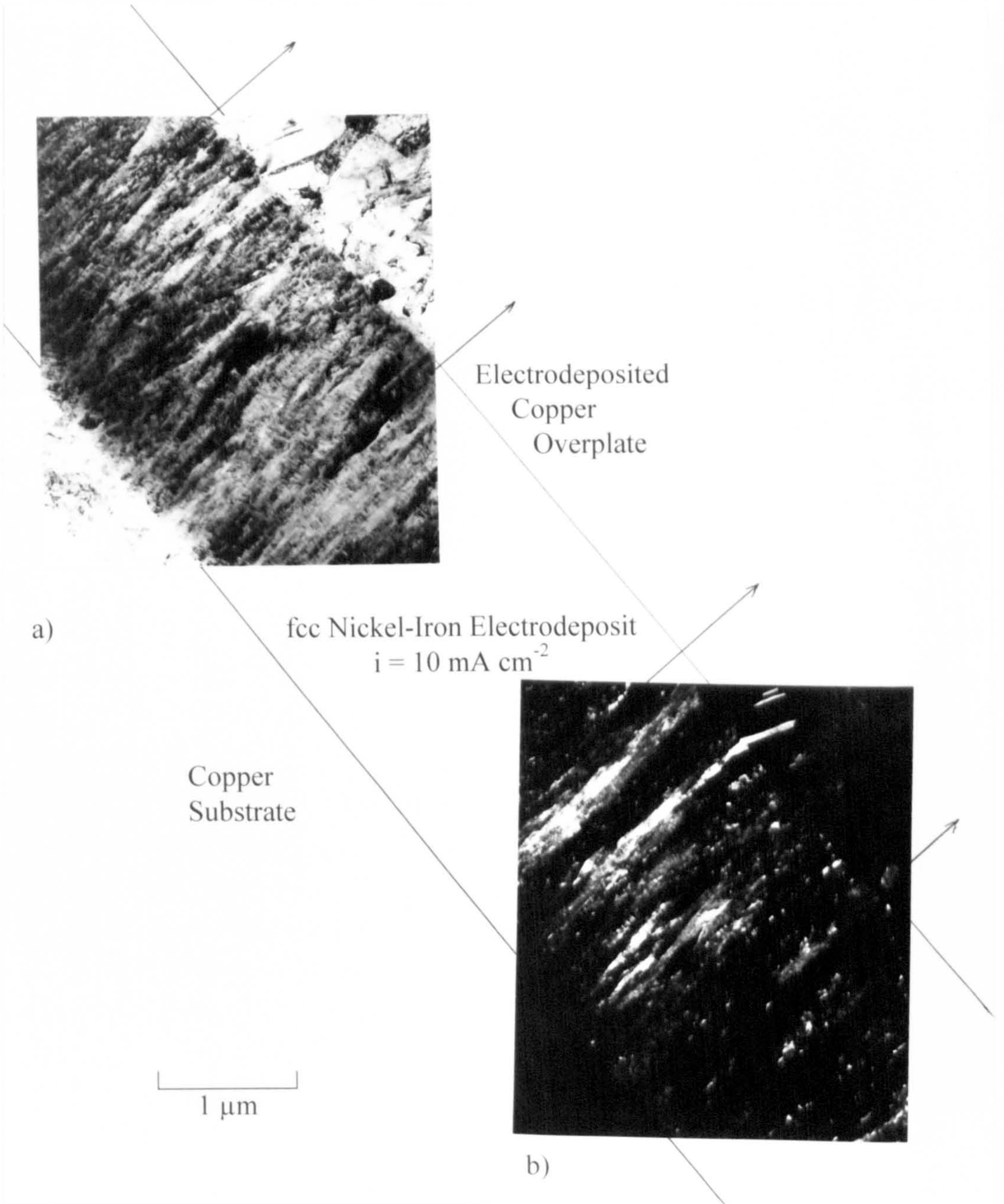

Fig. 4-38: (a) Bright and (b) Dark Field Image of Cross-Sectioned fcc Nickel-Iron Electrodeposit.

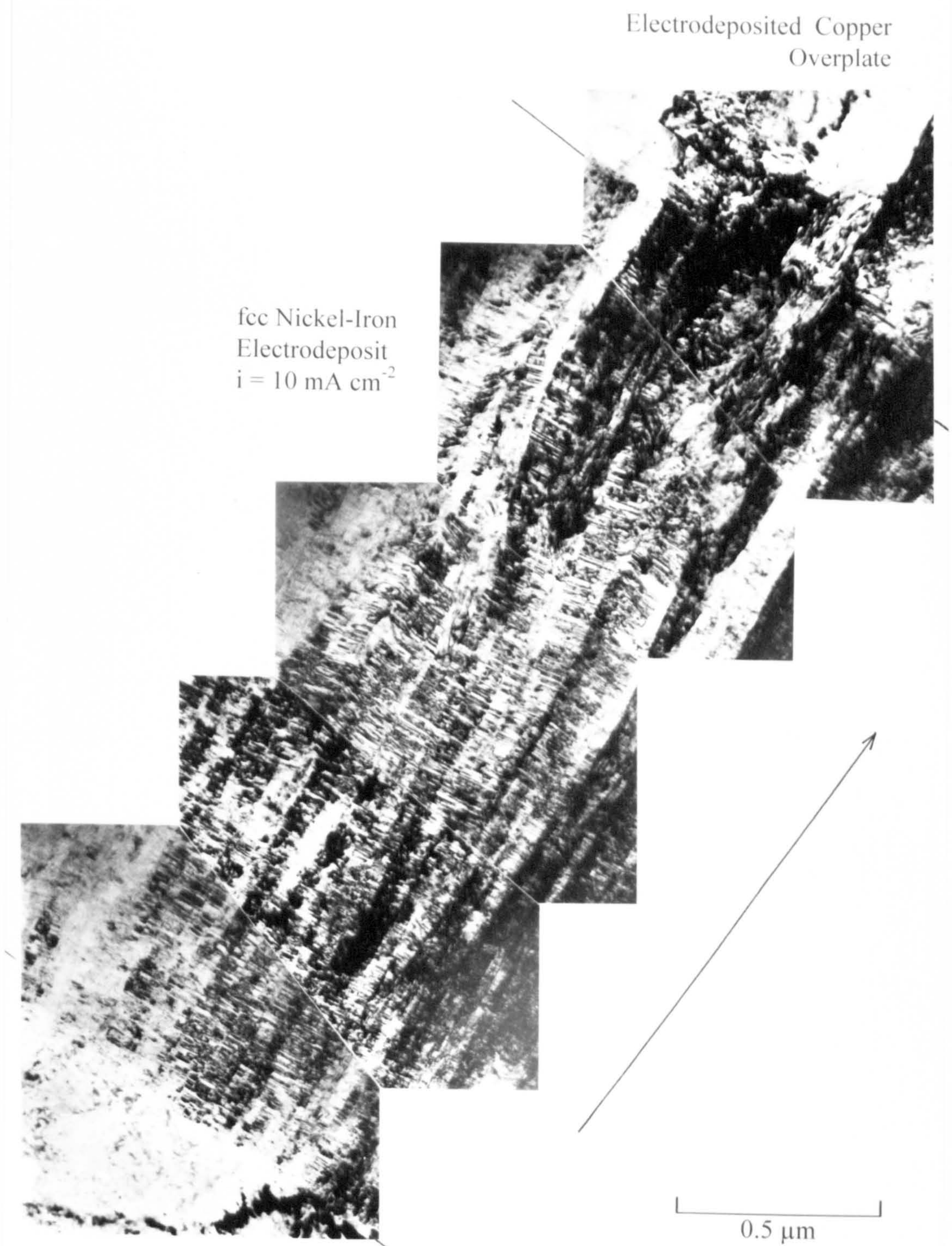

Fig. 4-39a: Montage of Bright Field Images Across Cross-Sectioned fcc Nickel-Iron Electrodeposit.

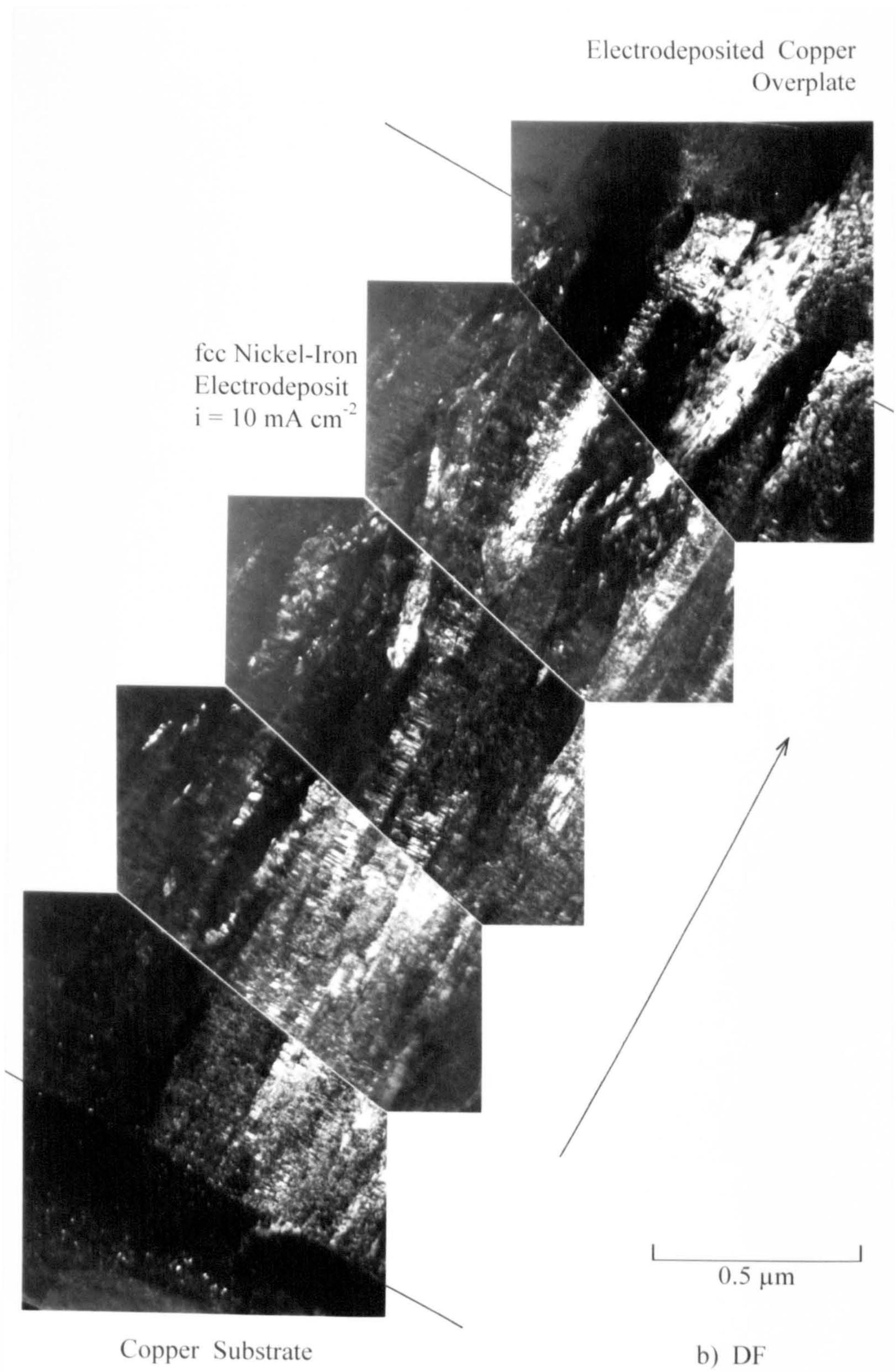

Fig. 4-39b: Montage of Dark Field Images Across Cross-Sectioned fcc Nickel-Iron Electrodeposit.

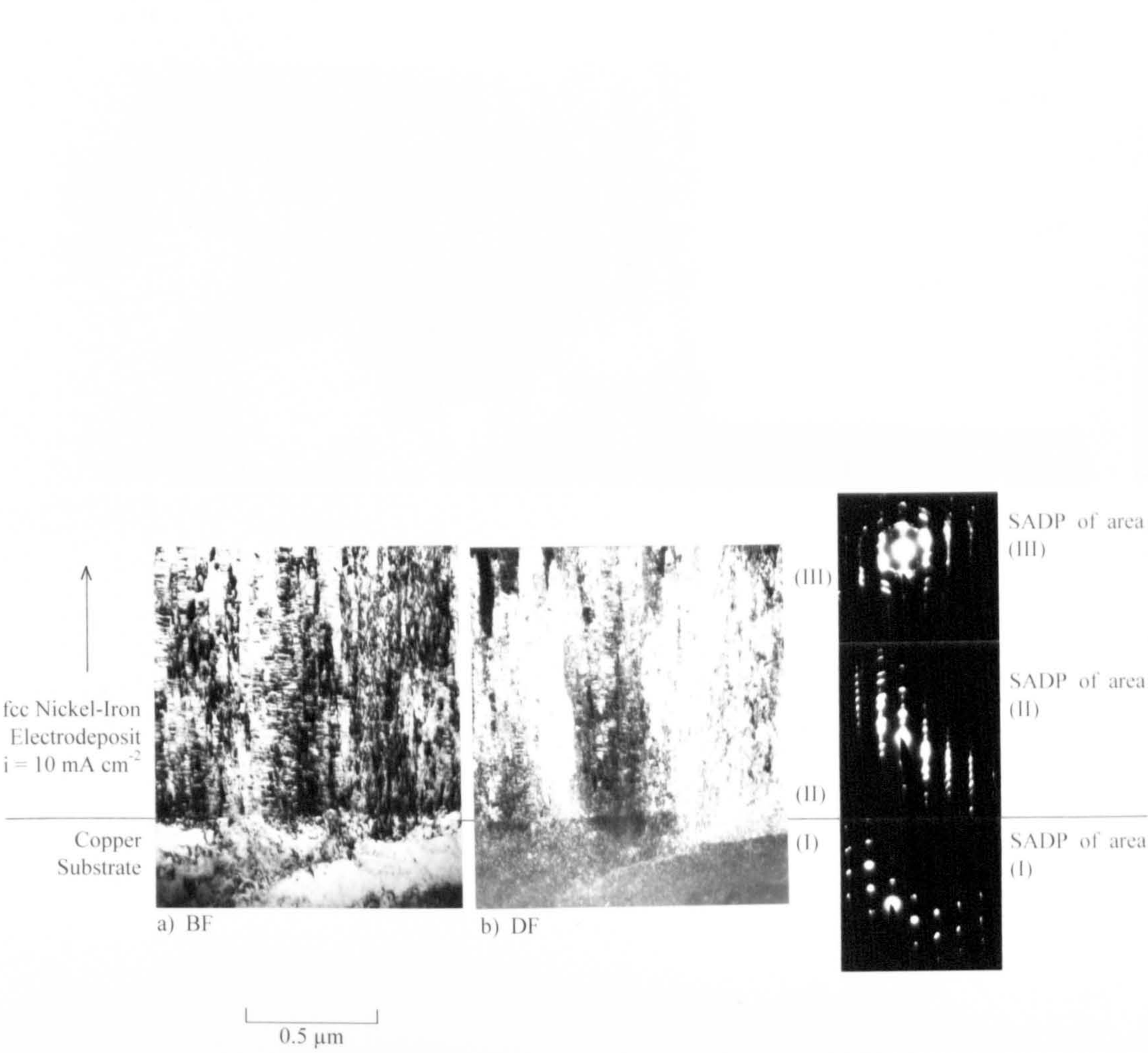

Fig. 4-40: (a) Bright and (b) Dark Field Pair of Interface Between Copper Substrate and fcc Nickel-Iron Electrodeposit.
SADPs: (I) Copper Substrate, (II) Nucleation Site of fcc Nickel-Iron Deposit, (III) Advanced Developed fcc Nickel-Iron Deposit.

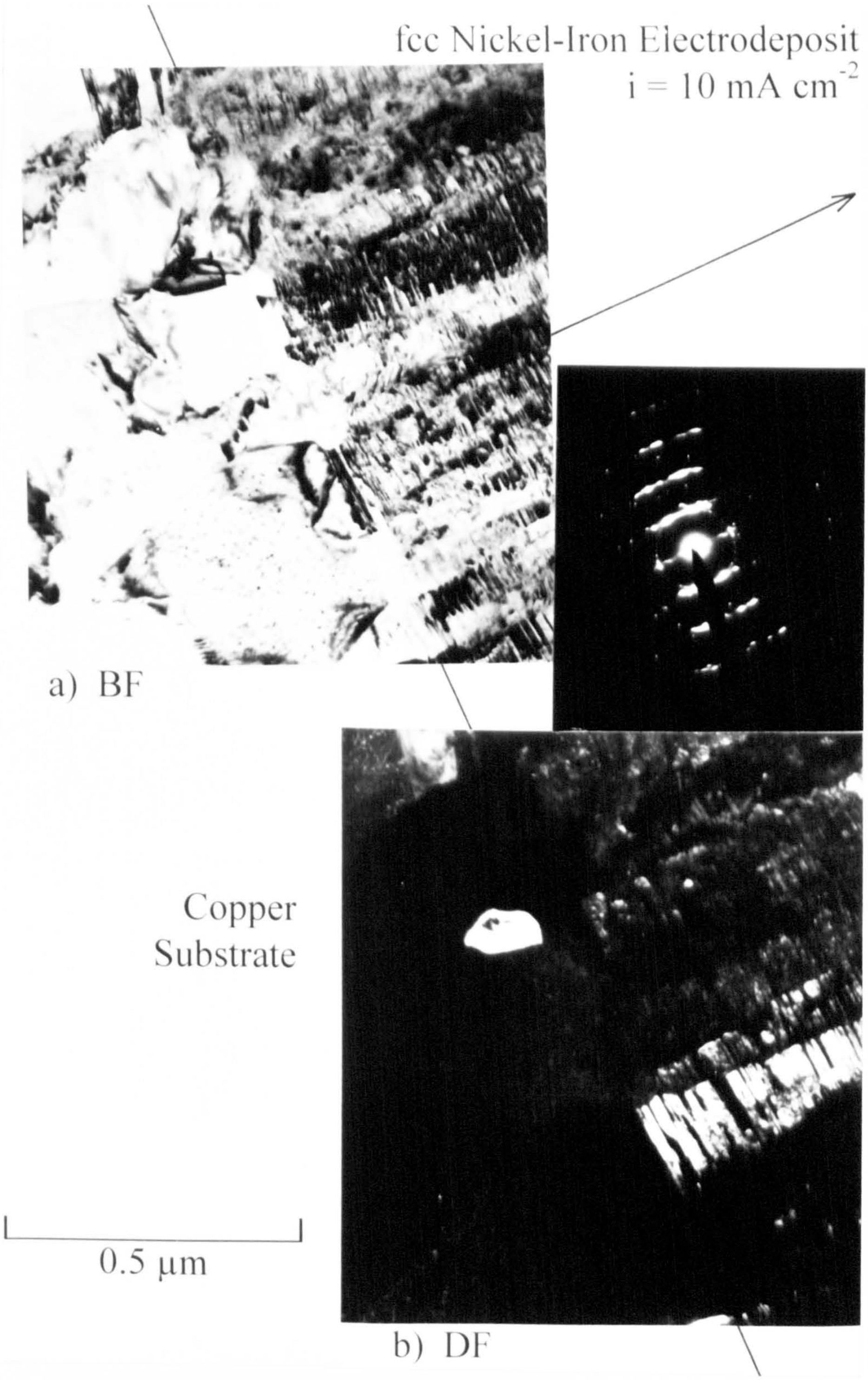

Fig. 4-41: (a) Bright and (b) Dark Field Pair of Initial Nucleation Site of fcc Nickel-Iron Electrodeposit on Copper Substrate, Including SADP of fcc Coating.

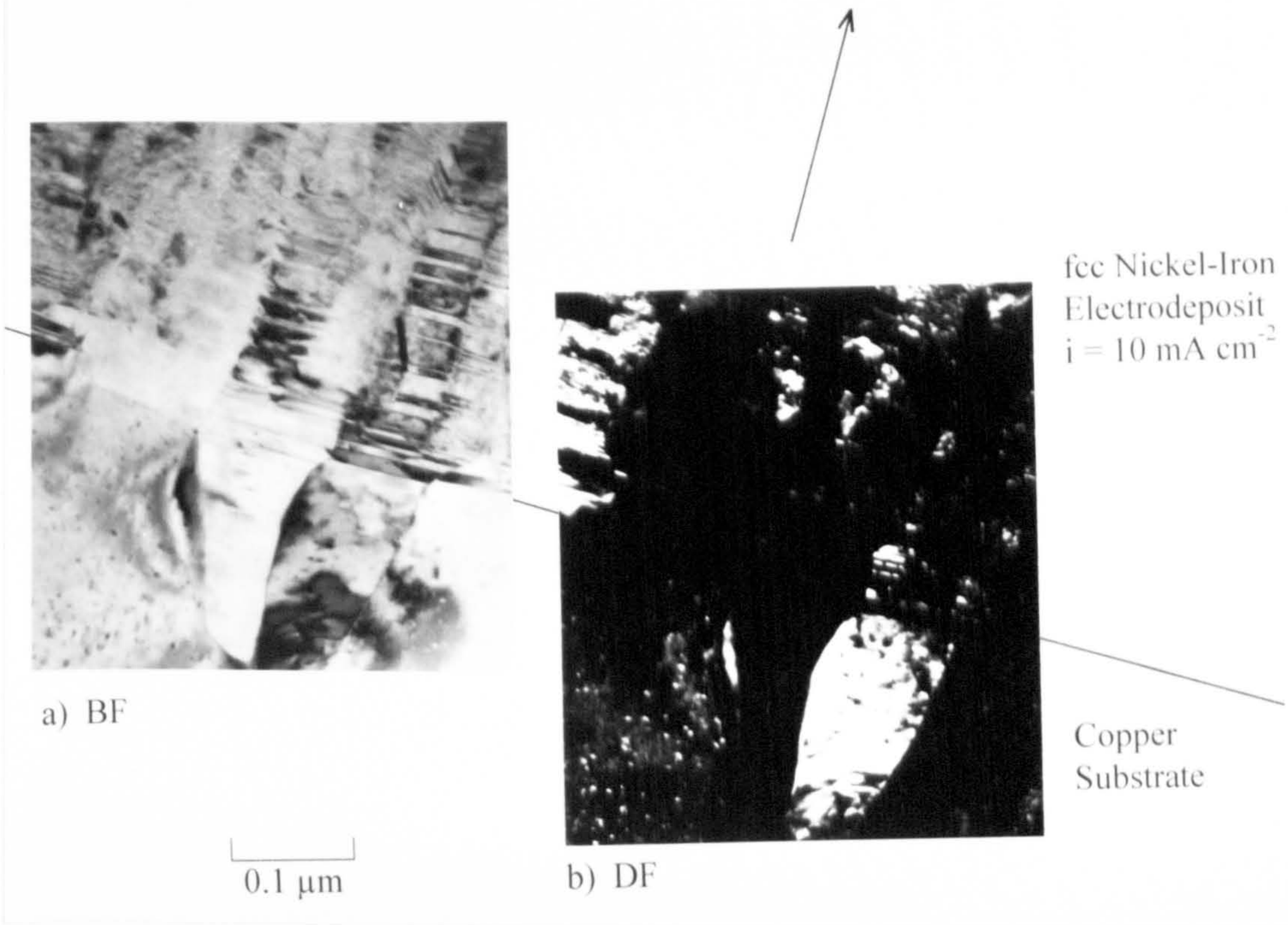

Fig. 4-42: (a) Bright and (b) Dark Field Pair of Interface Copper Substrate/fcc Nickel-Iron Electrodeposit.

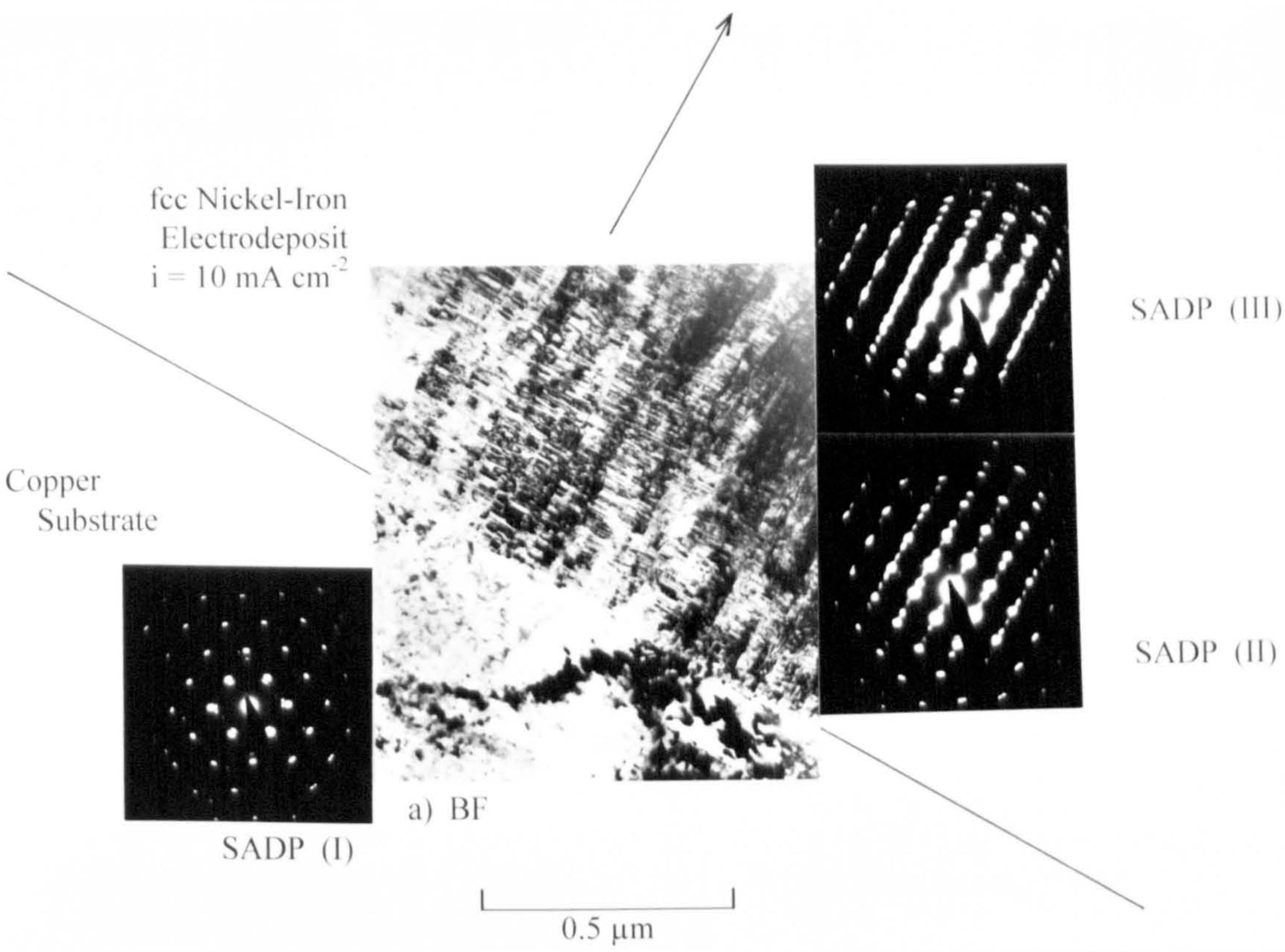

Fig. 4-43: (a) Bright Field Image of Interface Copper Substrate/fcc Nickel-Iron Electrodeposit.
SADPs: (I) Copper Substrate, (II) Interface Copper Substrate/fcc NiFe Deposit, (III) Advanced Developed fcc NiFe Deposit.

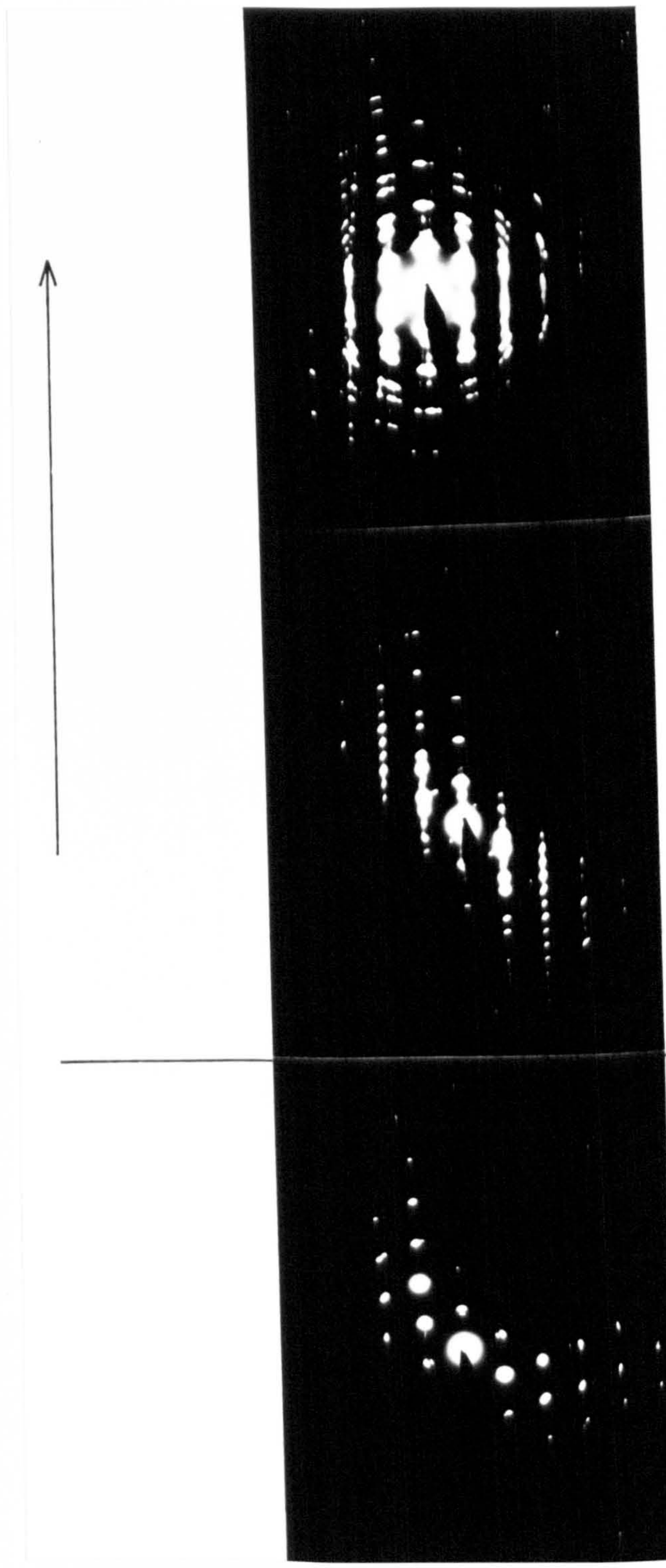

Fig. 4-44: Series of Selected Area Diffraction Patterns Indicating Initial Epitaxial Growth and 'Arcing' of Twin Spots in Advanced Developed fcc NiFe Deposit.
SADPs: (I) Copper Substrate, (II) fcc Nickel-Iron Electrodeposit at Nucleation Site, (III) Advanced Developed fcc NiFe Electrodeposit.

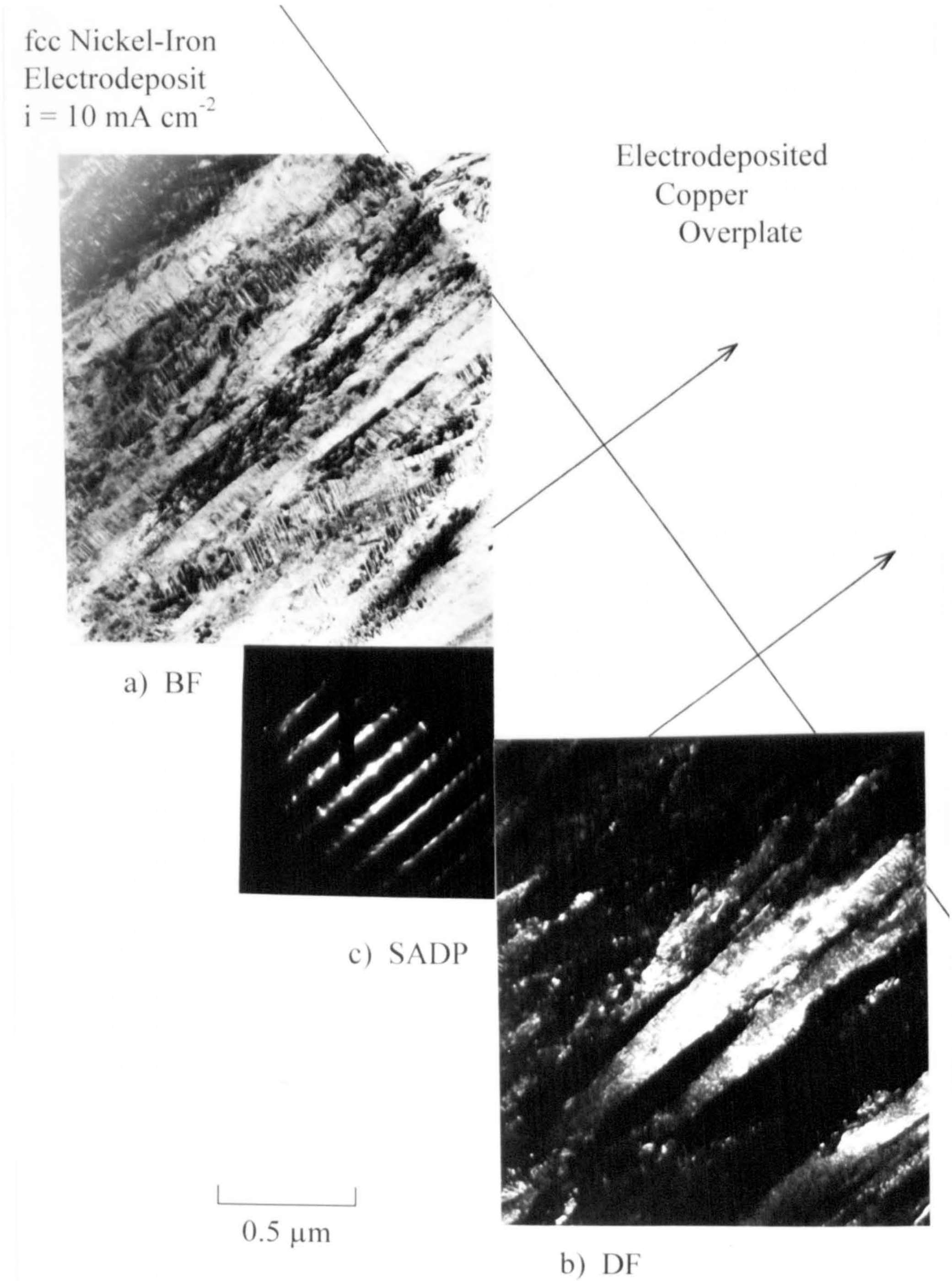

Fig. 4-45: a) Bright, (b) Dark Field Image and (c) Selected Area Diffraction Pattern of Advanced Developed fcc Nickel-Iron Electrodeposit.

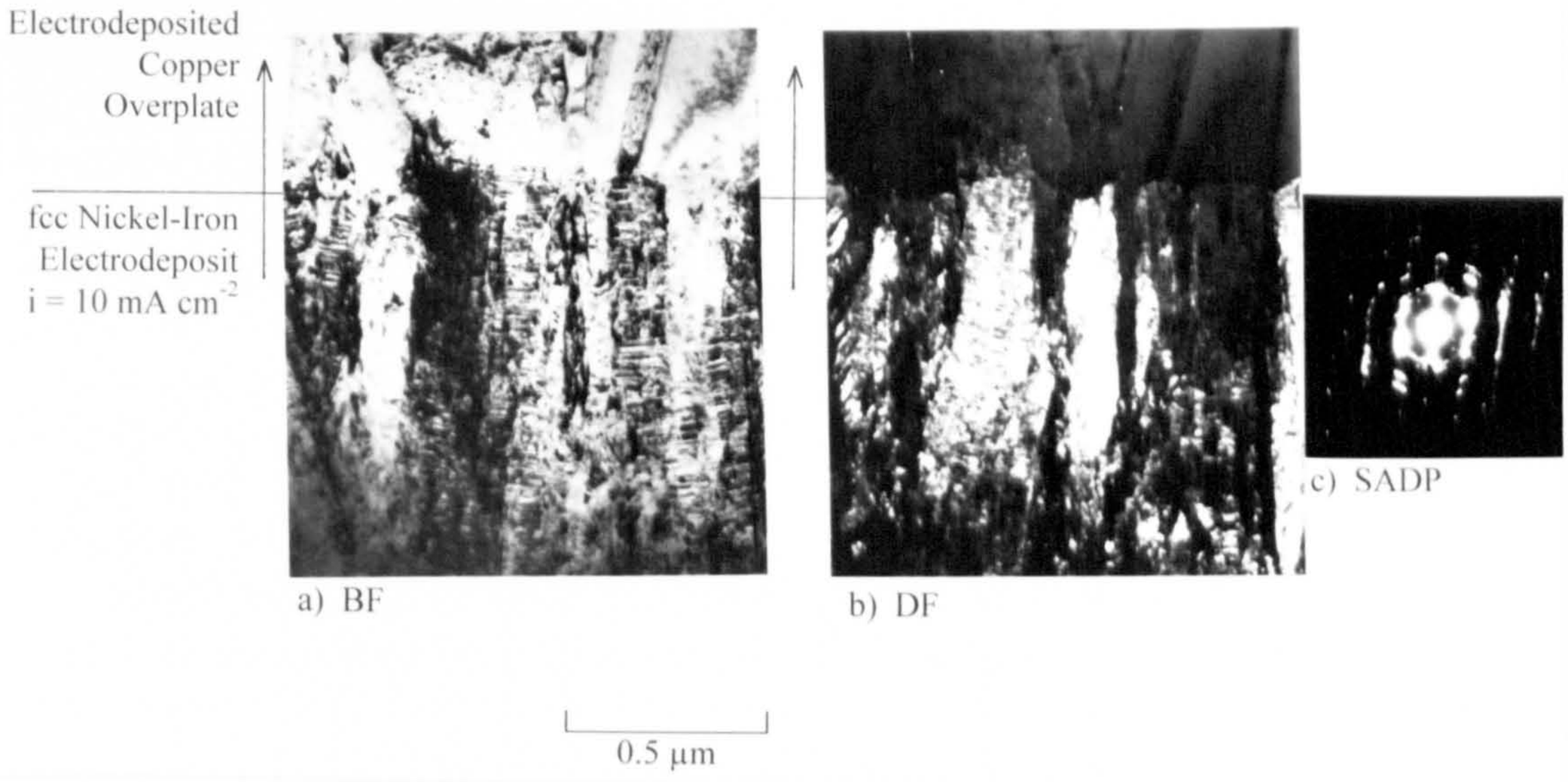

Fig. 4-46: (a) Bright, (b) Dark Field Image and (c) Selected Area Diffraction Pattern of Advanced Developed fcc Nickel-Iron Electrodeposit.

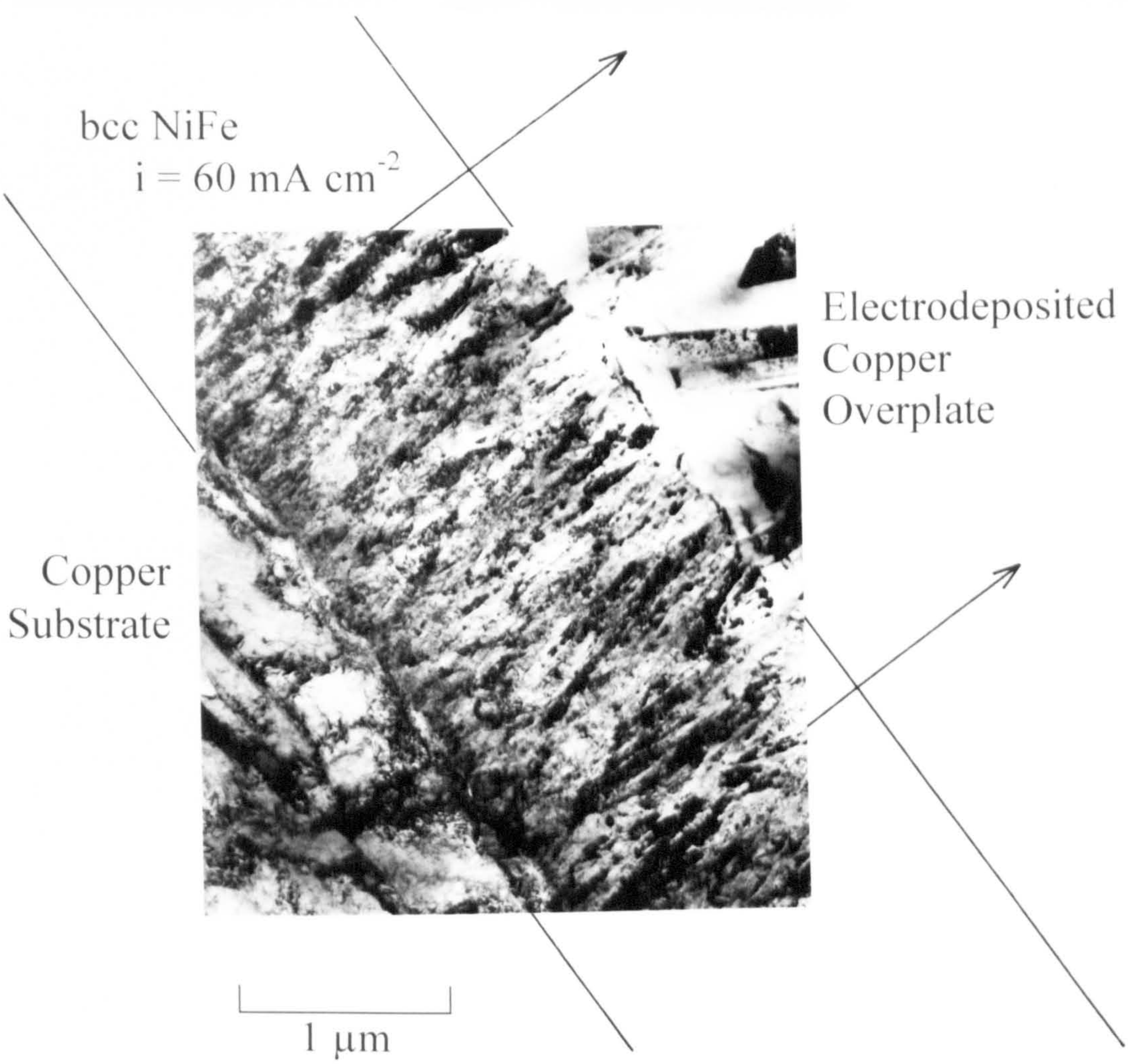

Fig. 4-47: Bright Field Image Showing General Overall View of Cross-Sectioned bcc Nickel-Iron Electrodeposit Nucleated on a Copper Substrate, Overplated with Copper.

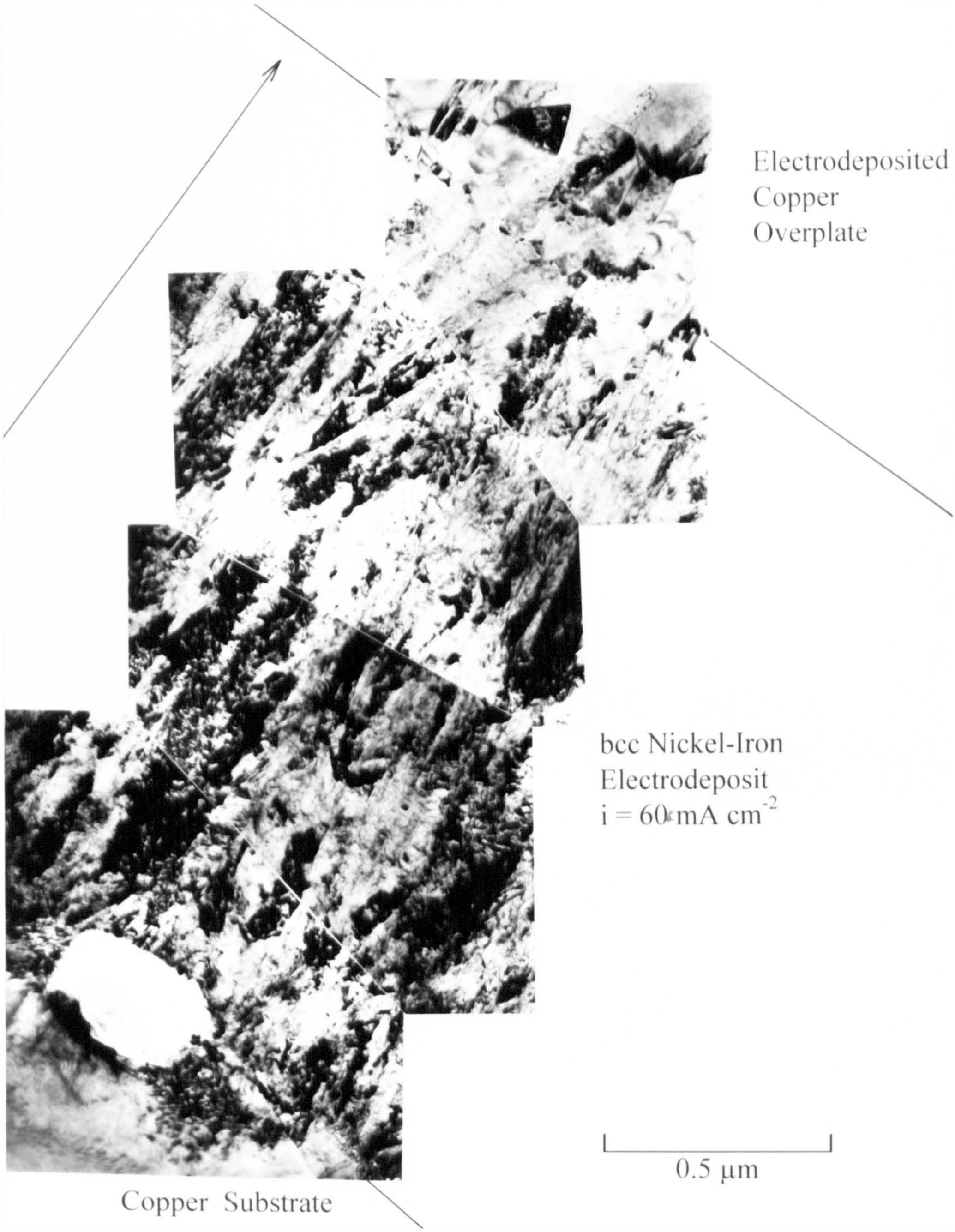

Fig. 4-48: Montage of Bright Field Images Showing General Overall View of Cross-Sectioned bcc Nickel-Iron Electrodeposit Nucleated on a Copper Substrate, Overplated with Copper.

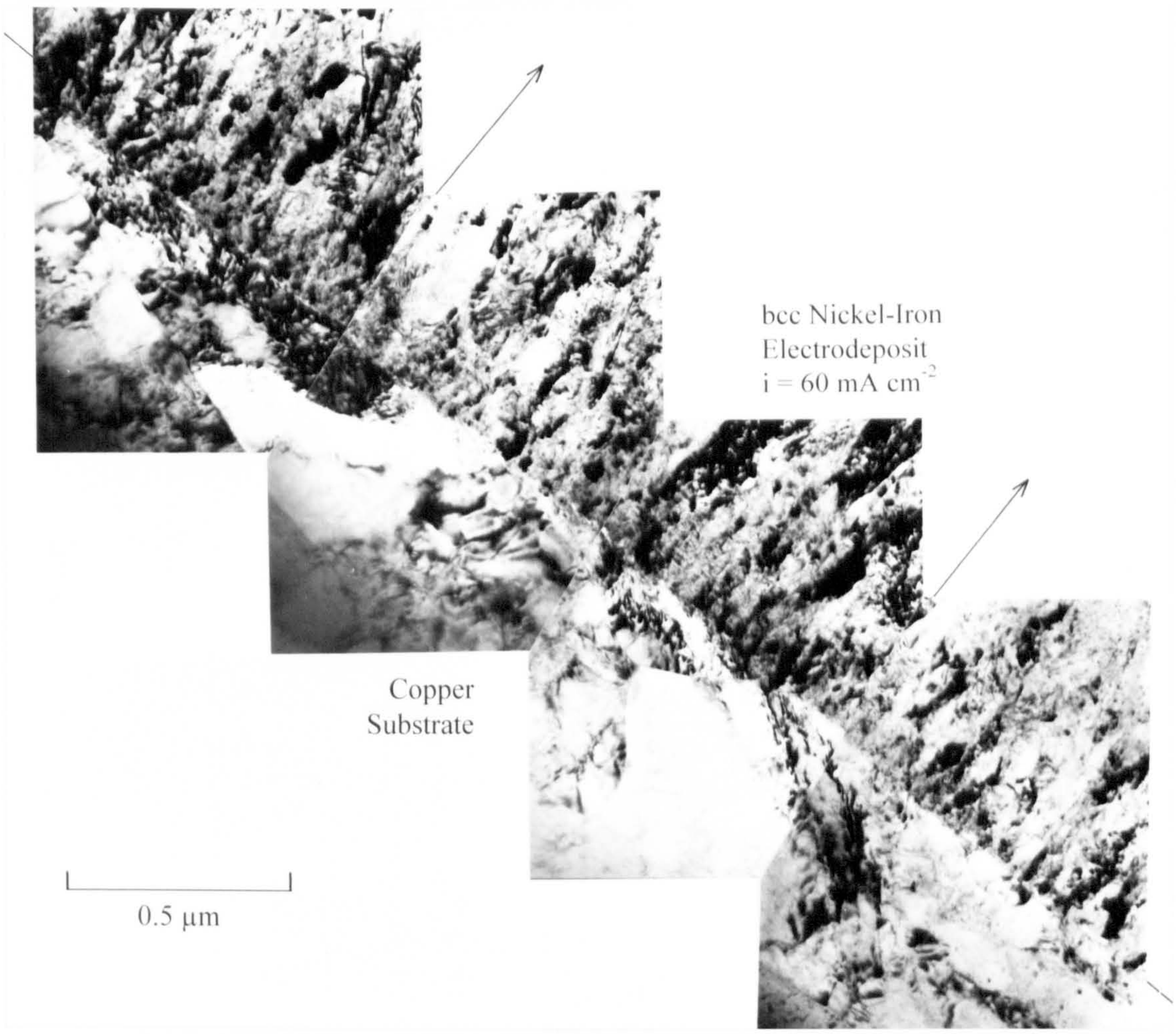

Fig. 4-49: Montage of Bright Field Images Along the Interface Between the bcc Nickel-Iron Electrodeposit and the Copper Substrate.

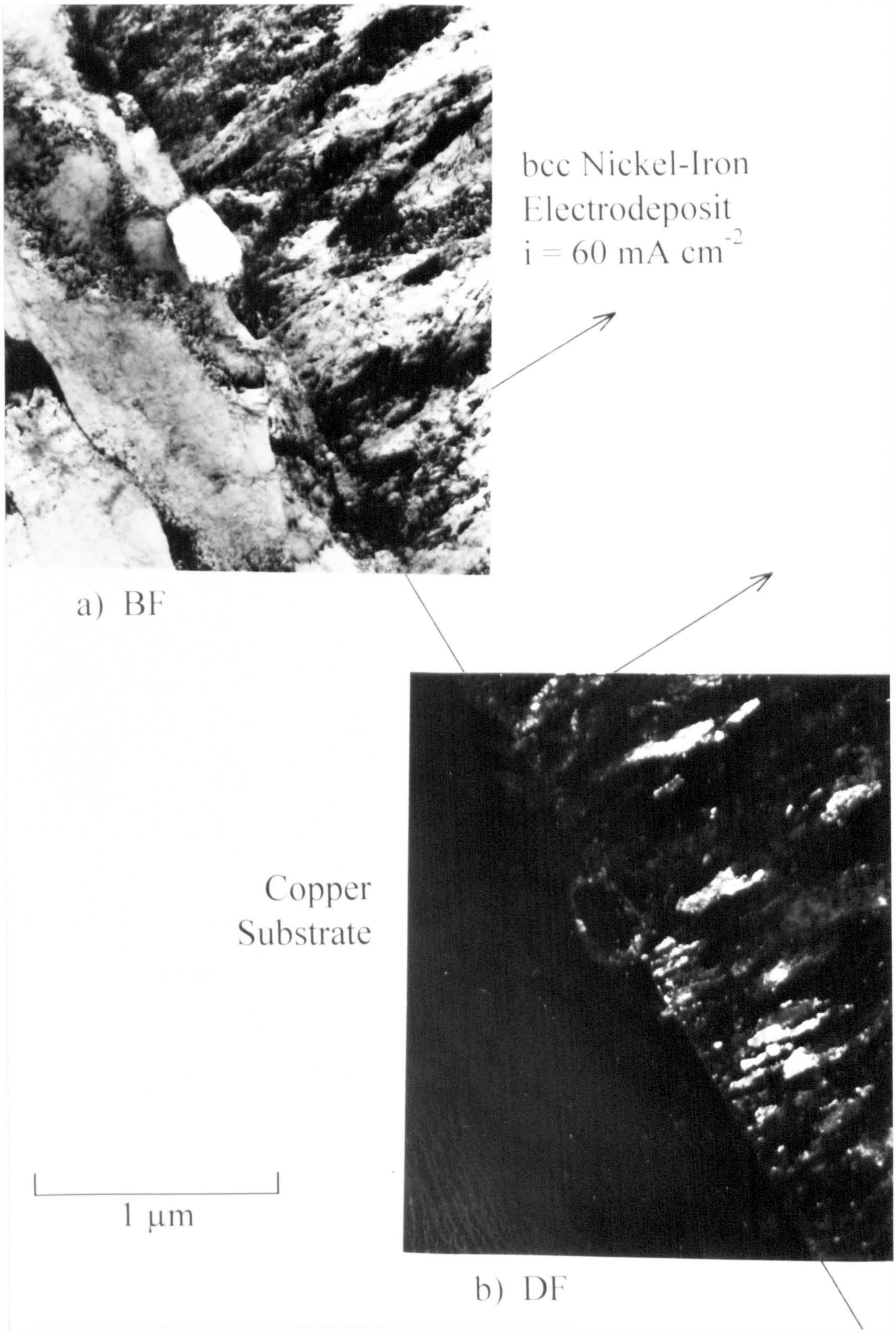

Fig. 4-50: (a) Bright and (b) Dark Field Micrograph of Copper Substrate/bcc Nickel-Iron Electrodeposit Interface.

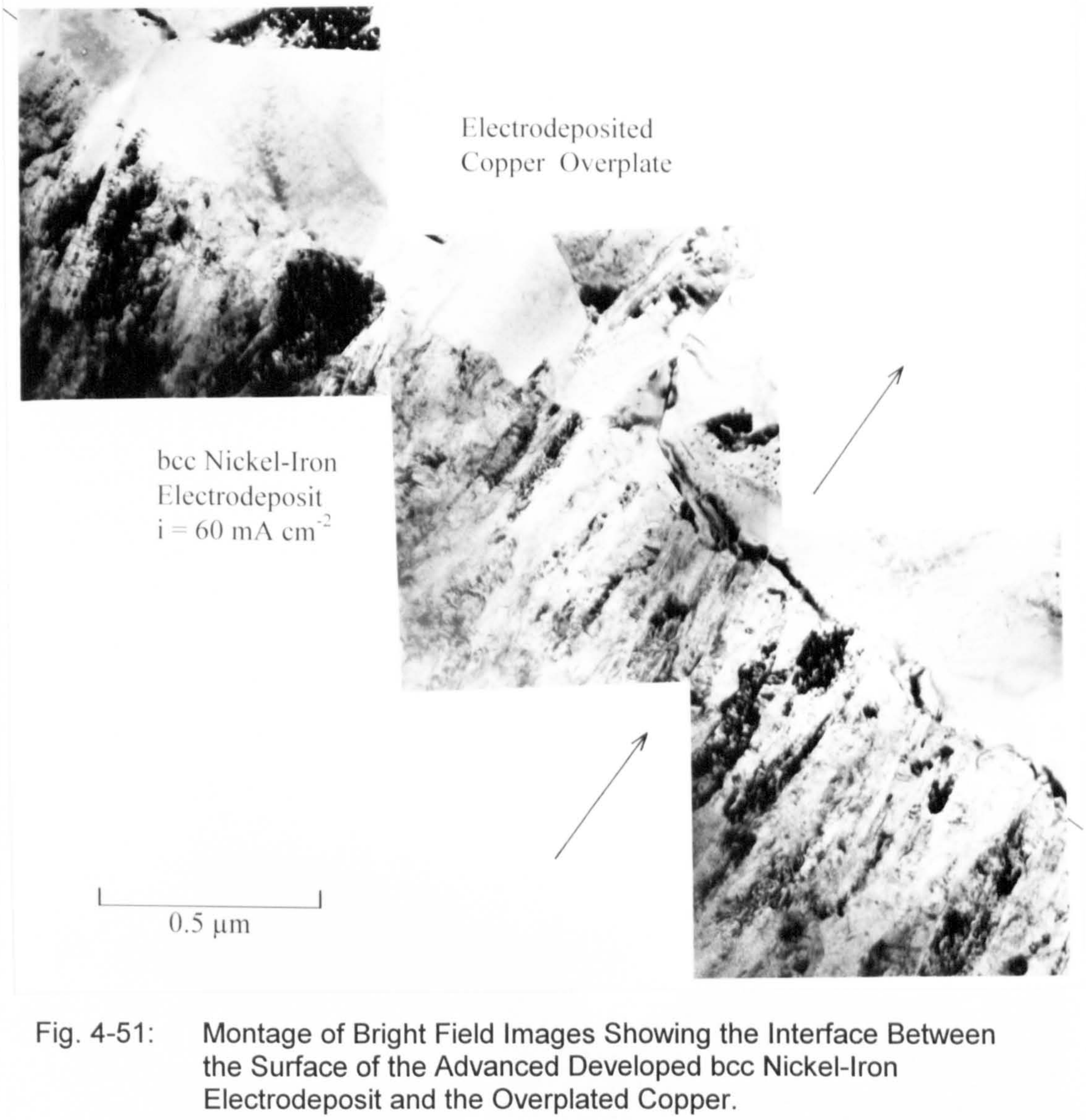

Fig. 4-51: Montage of Bright Field Images Showing the Interface Between the Surface of the Advanced Developed bcc Nickel-Iron Electrodeposit and the Overplated Copper.

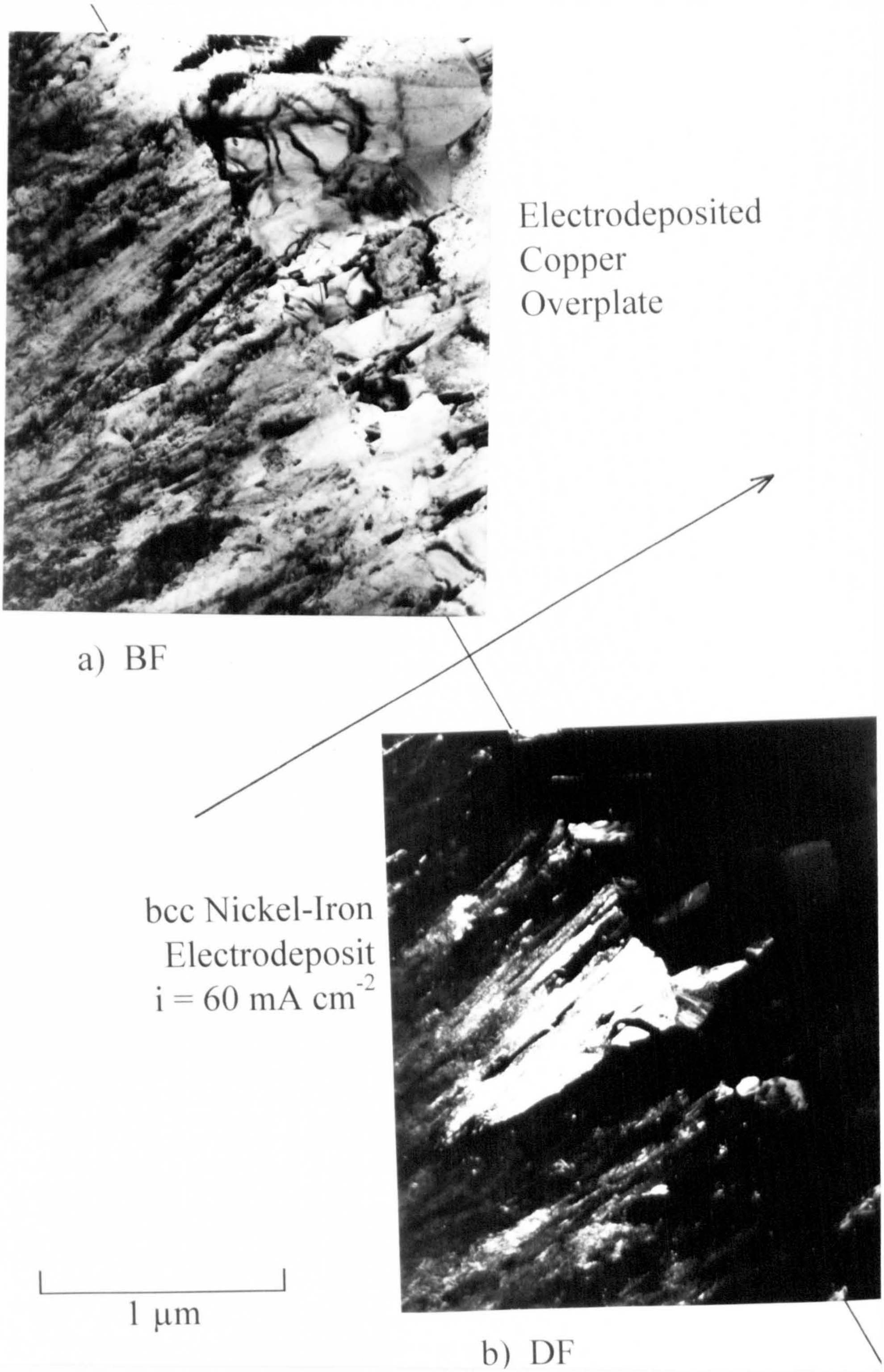

Fig. 4-52: (a) Bright and (b) Dark Field Pair of bcc Nickel-Iron Deposit/Copper Overplate Interface. Bright Grains in (b) Have <211> Growth Direction.

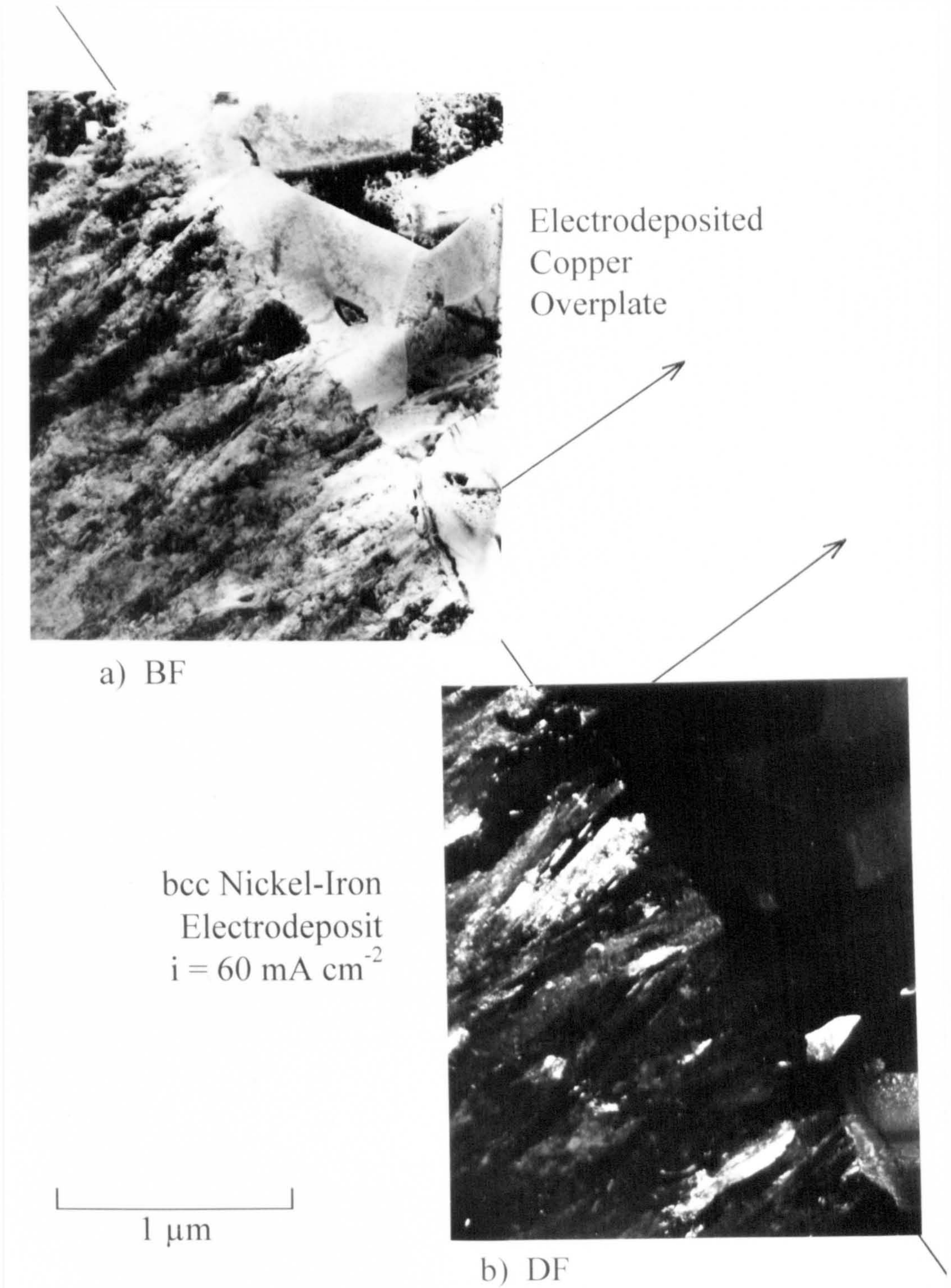

Fig. 4-53: (a) Bright and (b) Dark Field Pair of bcc Nickel-Iron Deposit/Copper Overplate Interface. Bright Grains in (b) Have <211> Growth Direction.

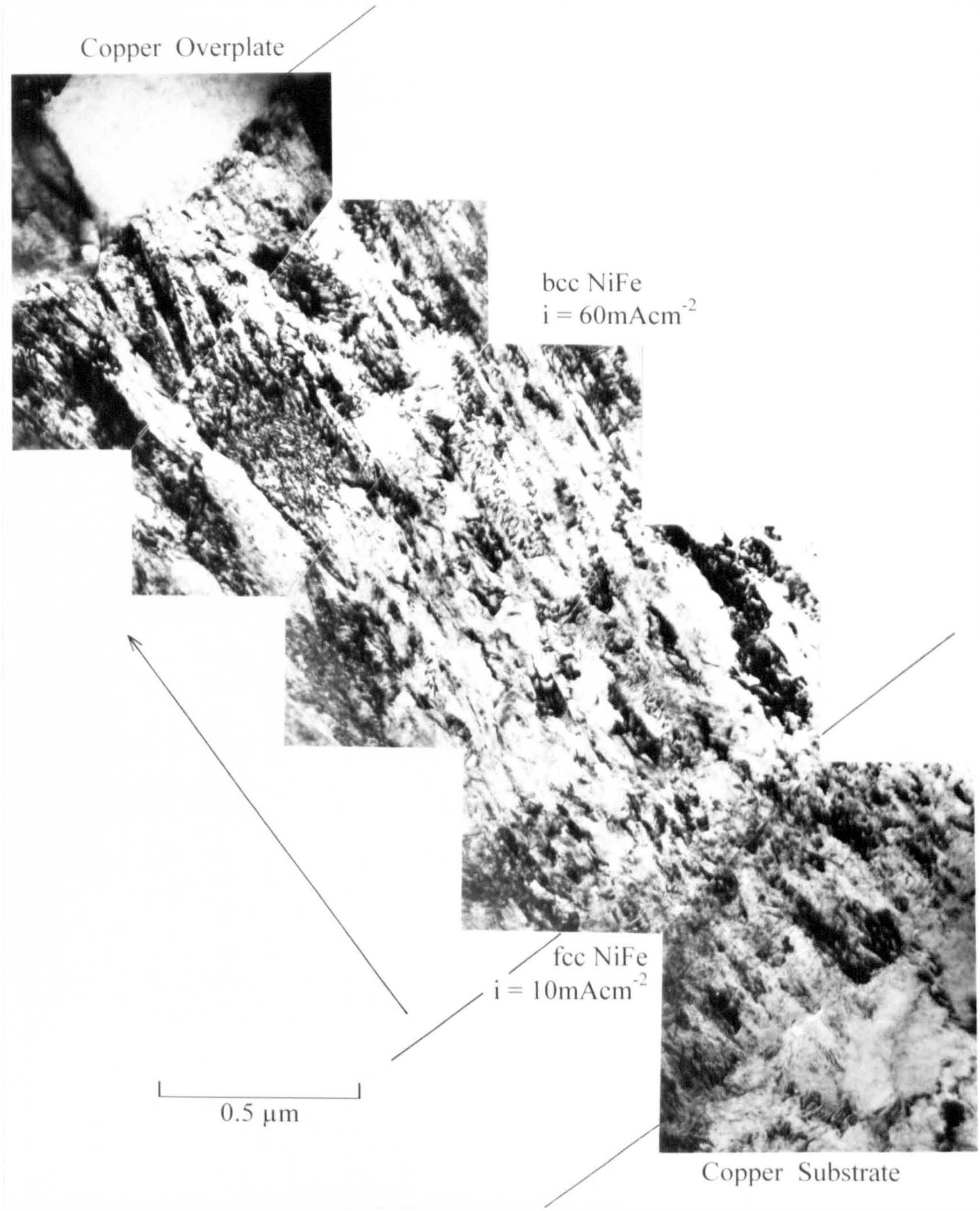

Fig. 4-54a: Montage of Bright Field Images Showing Double Layered 2µm Thick bcc NiFe Nucleated on 0.5µm Thick fcc NiFe Deposit.

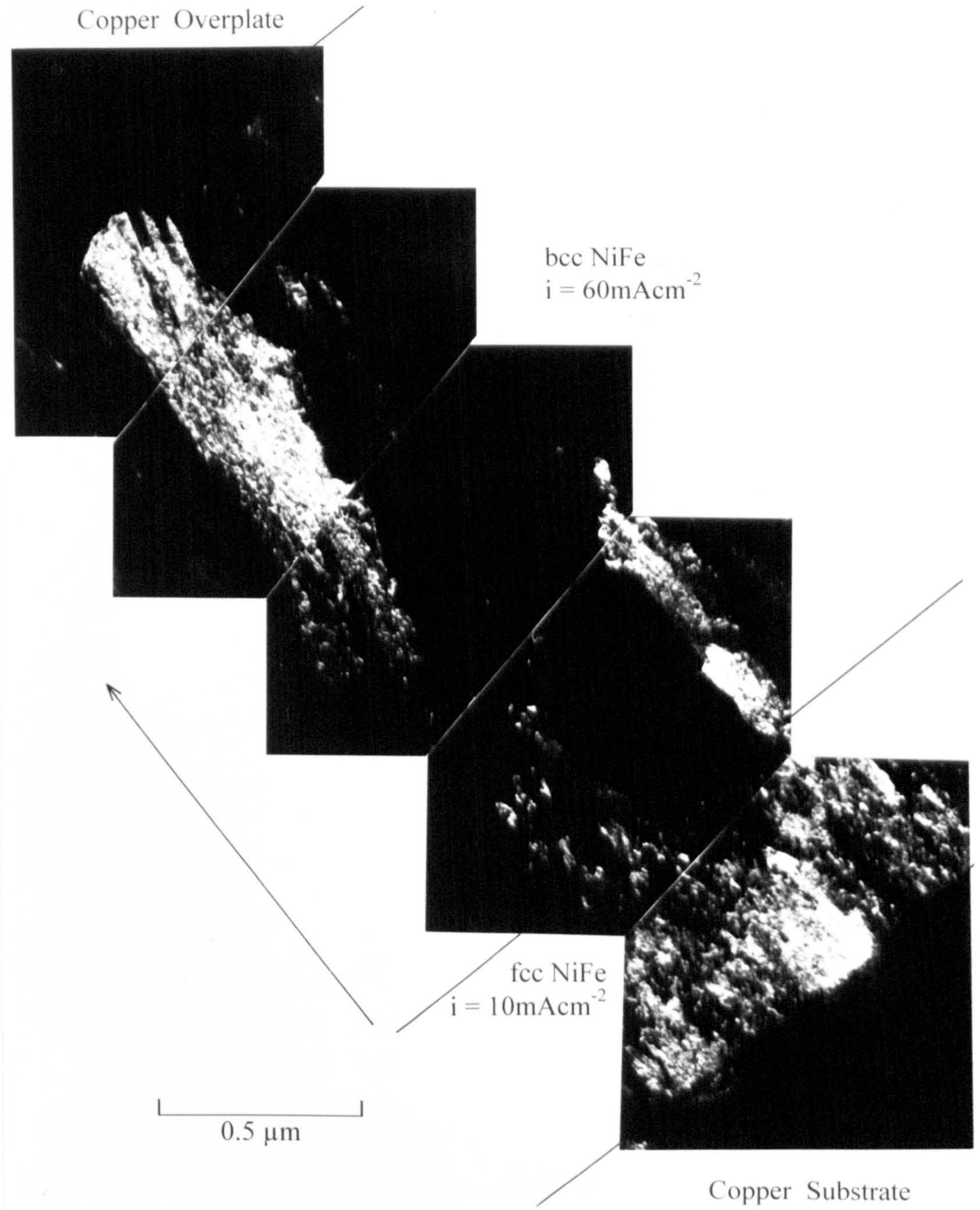

Fig. 4-54b: Montage of Dark Field Images Showing Double Layered 2µm Thick bcc NiFe Nucleated on 0.5µm Thick fcc NiFe Deposit.

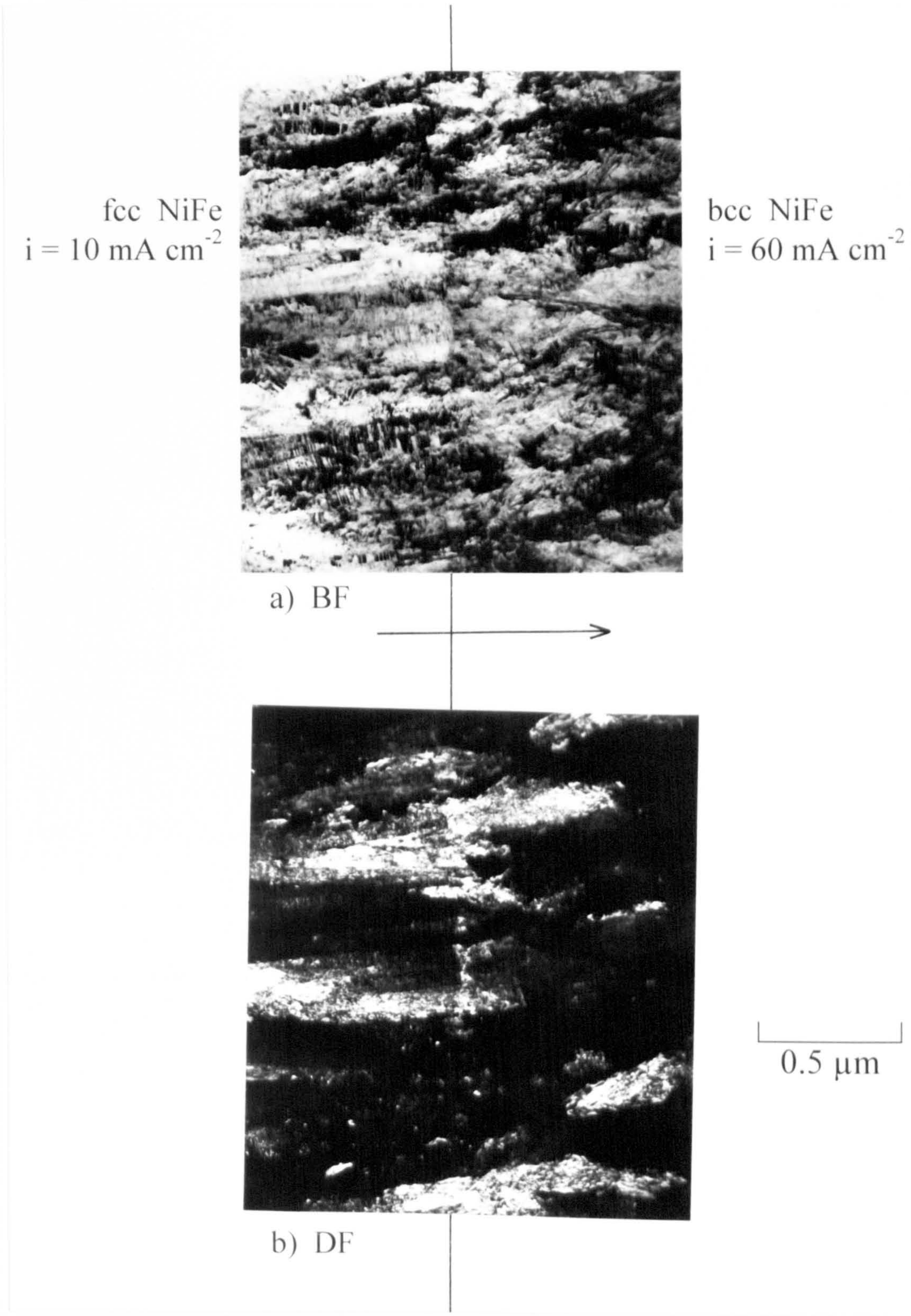

Fig. 4-55: (a) Bright and (b) Dark Field Pair of Interface Between Advanced Developed, 2µm Thick fcc NiFe Deposit and Nucleation Site of bcc NiFe Deposit.

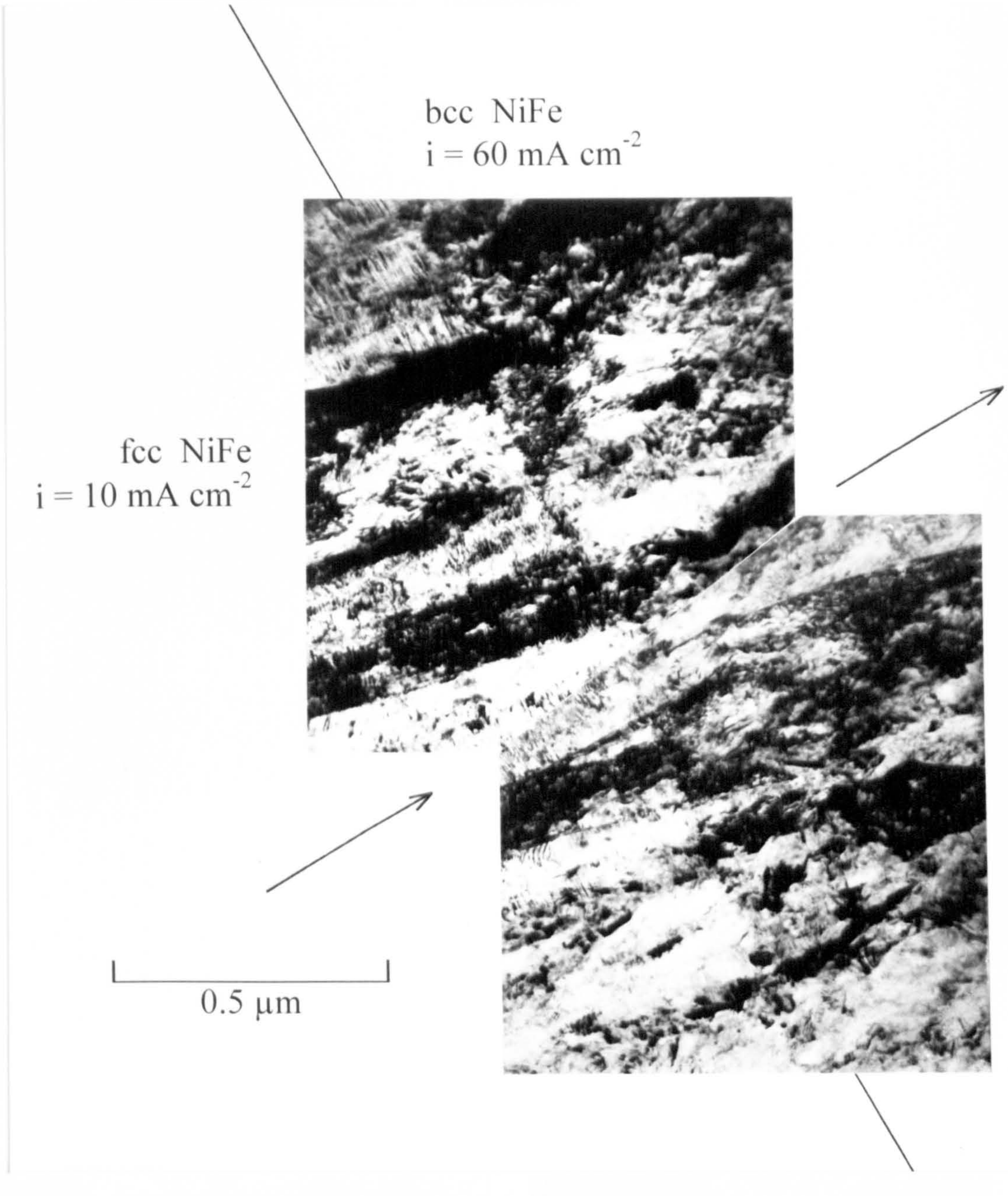

Fig. 4-56: Montage of Bright Field Image Showing Interface Between 2µm Thick, Advanced Developed fcc NiFe Deposit and Nucleation Site of bcc NiFe Deposit.

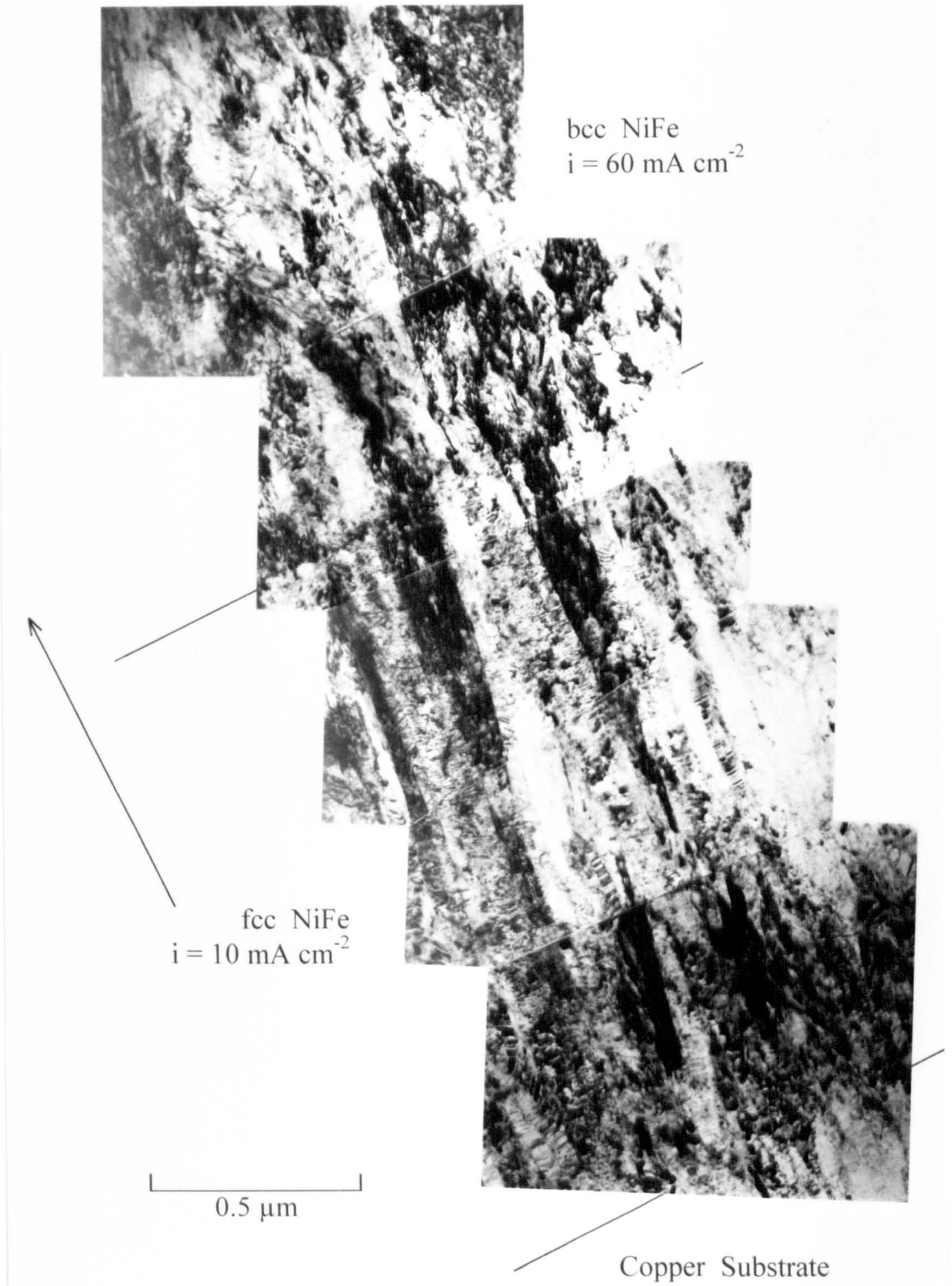

Fig. 4-57a: Bright Field Images of Double Layered 2μm Thick bcc NiFe-Nucleated on 2μm Thick fcc NiFe Deposit.

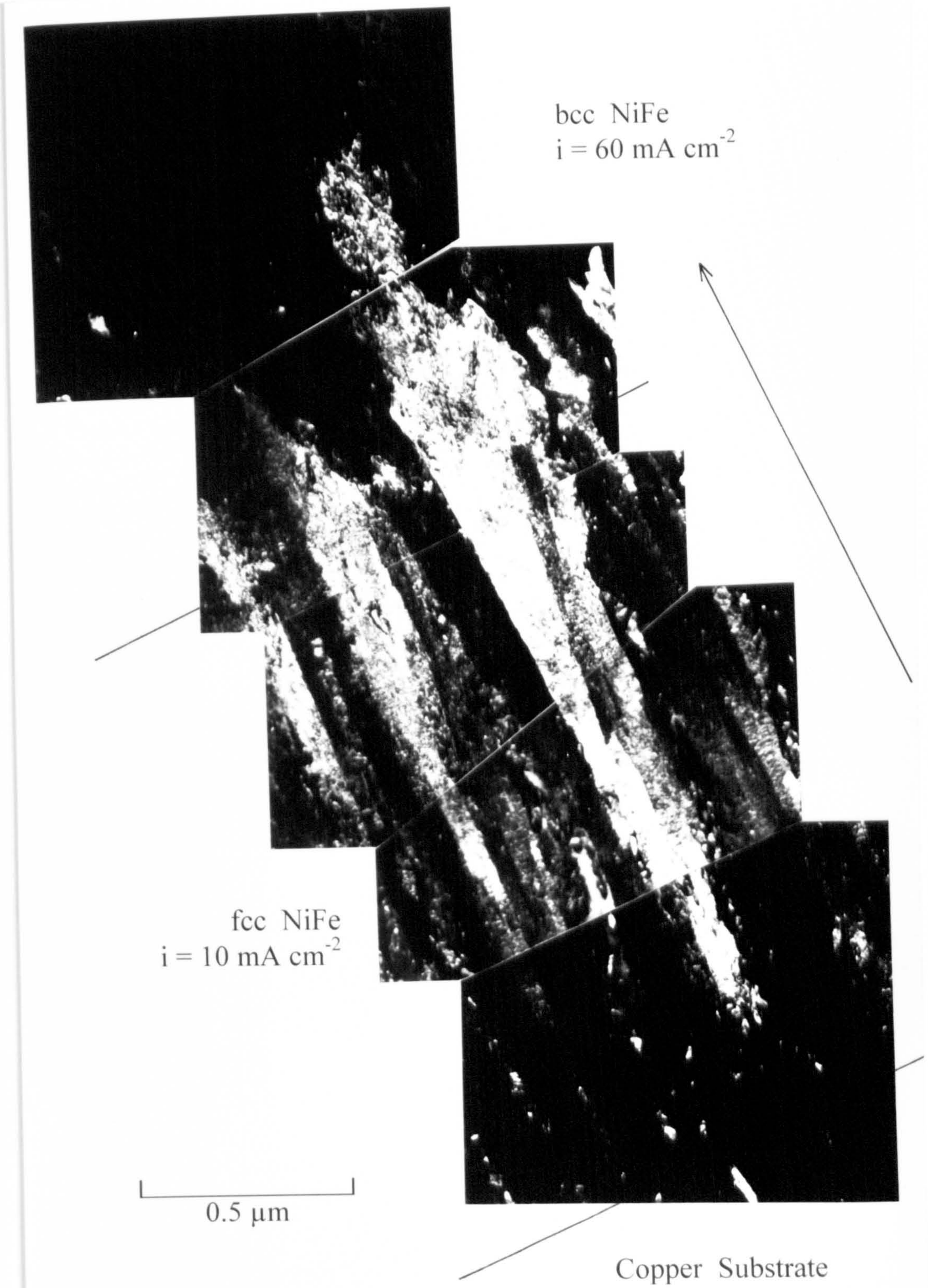

Fig. 4-57b: Dark Field Images of Double Layered 2μm Thick bcc NiFe-Nucleated on 2μm Thick fcc NiFe Deposit.

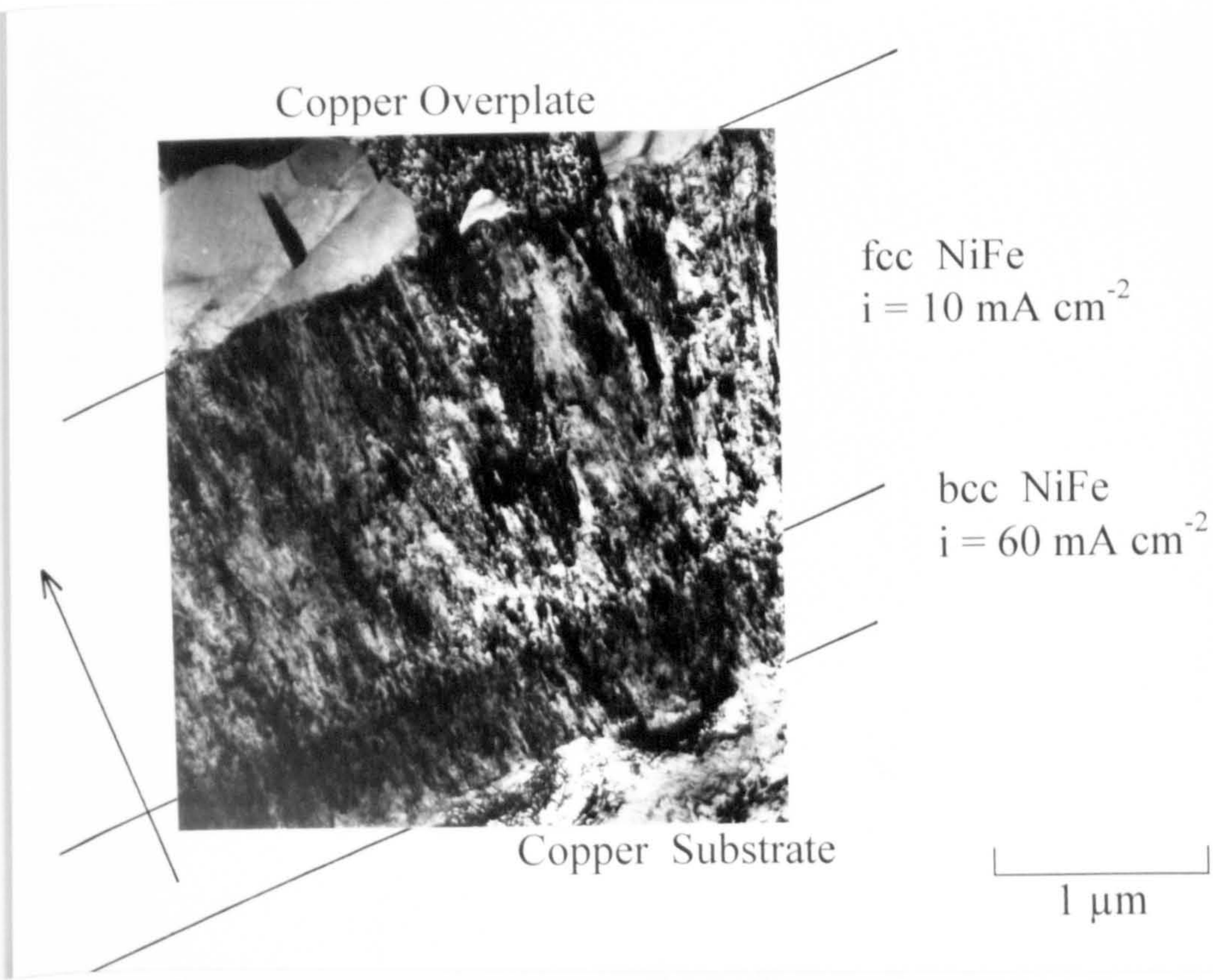

Fig. 4-58: Bright Field Image of Double Layered 2μm Thick fcc NiFe Nucleated on 0.5μm Thick bcc NiFe Deposit.

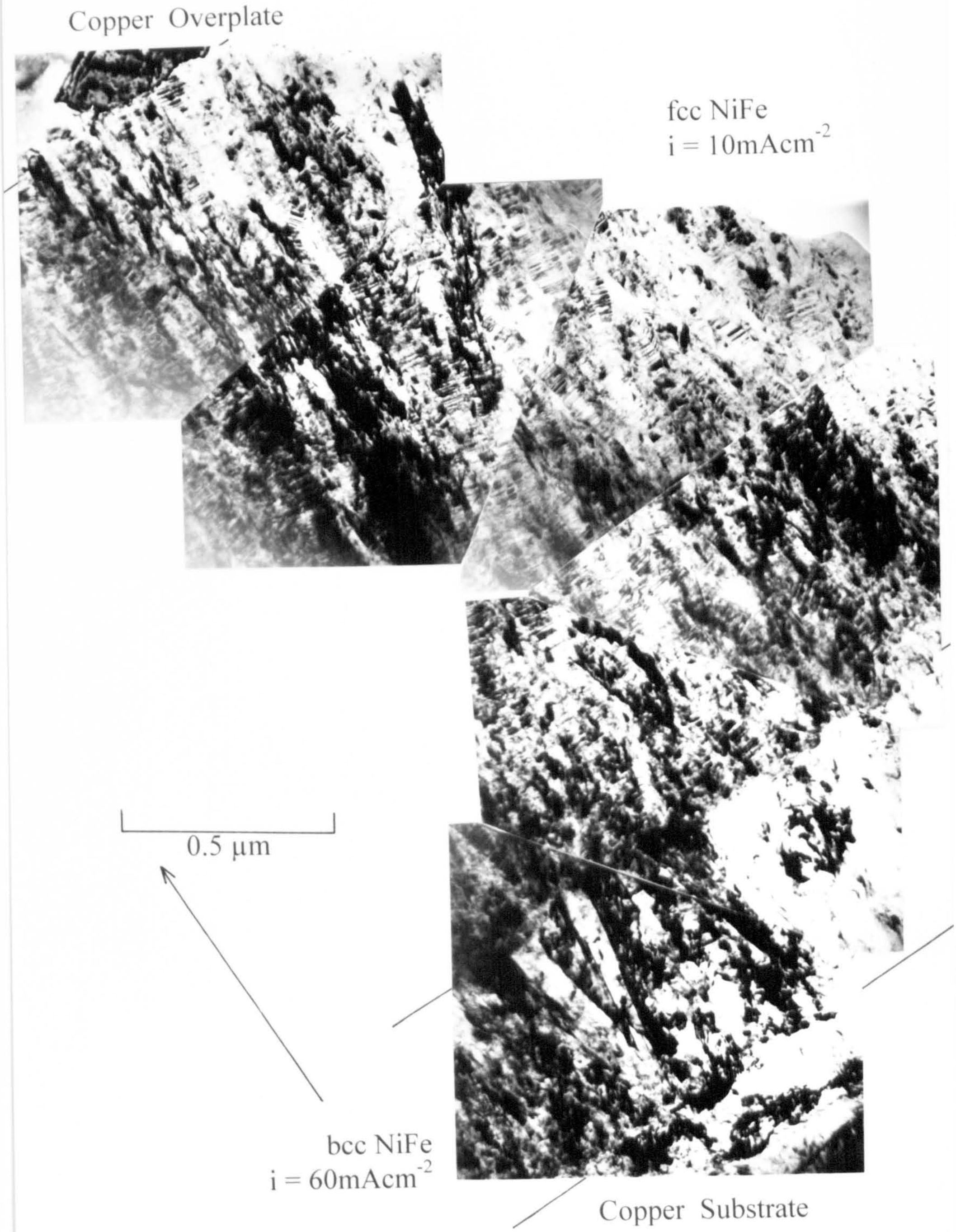

Fig. 4-59: Montage of Bright Field Images of Double Layered 2μm thick fcc NiFe Nucleated on 0.5μm Thick bcc NiFe Deposit.

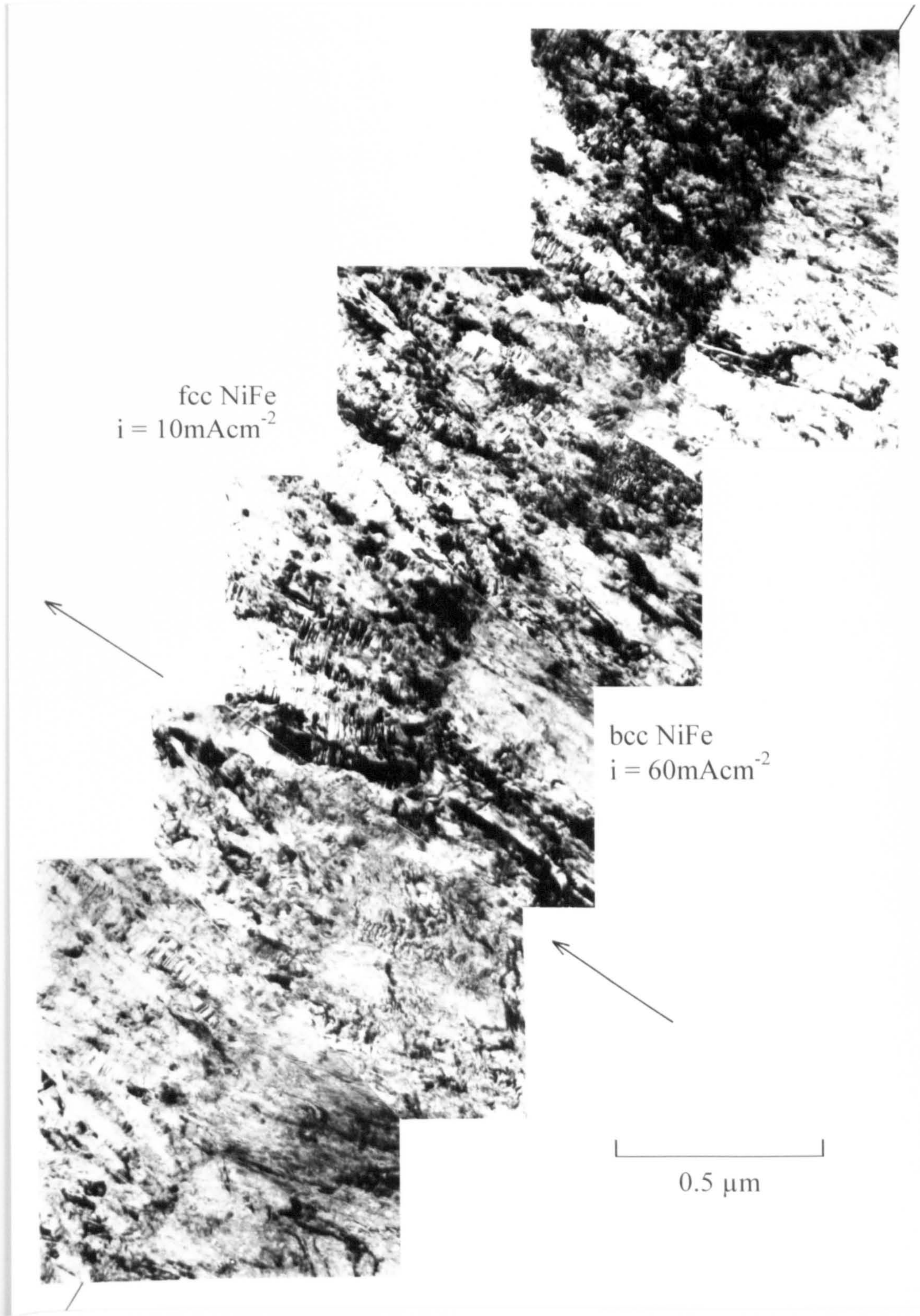

Fig. 4-60a: Montage of Bright Fields Along Interface of Double Layered, 2μm Thick fcc NiFe Deposit Nucleated on 2μm Thick bcc NiFe Deposit.

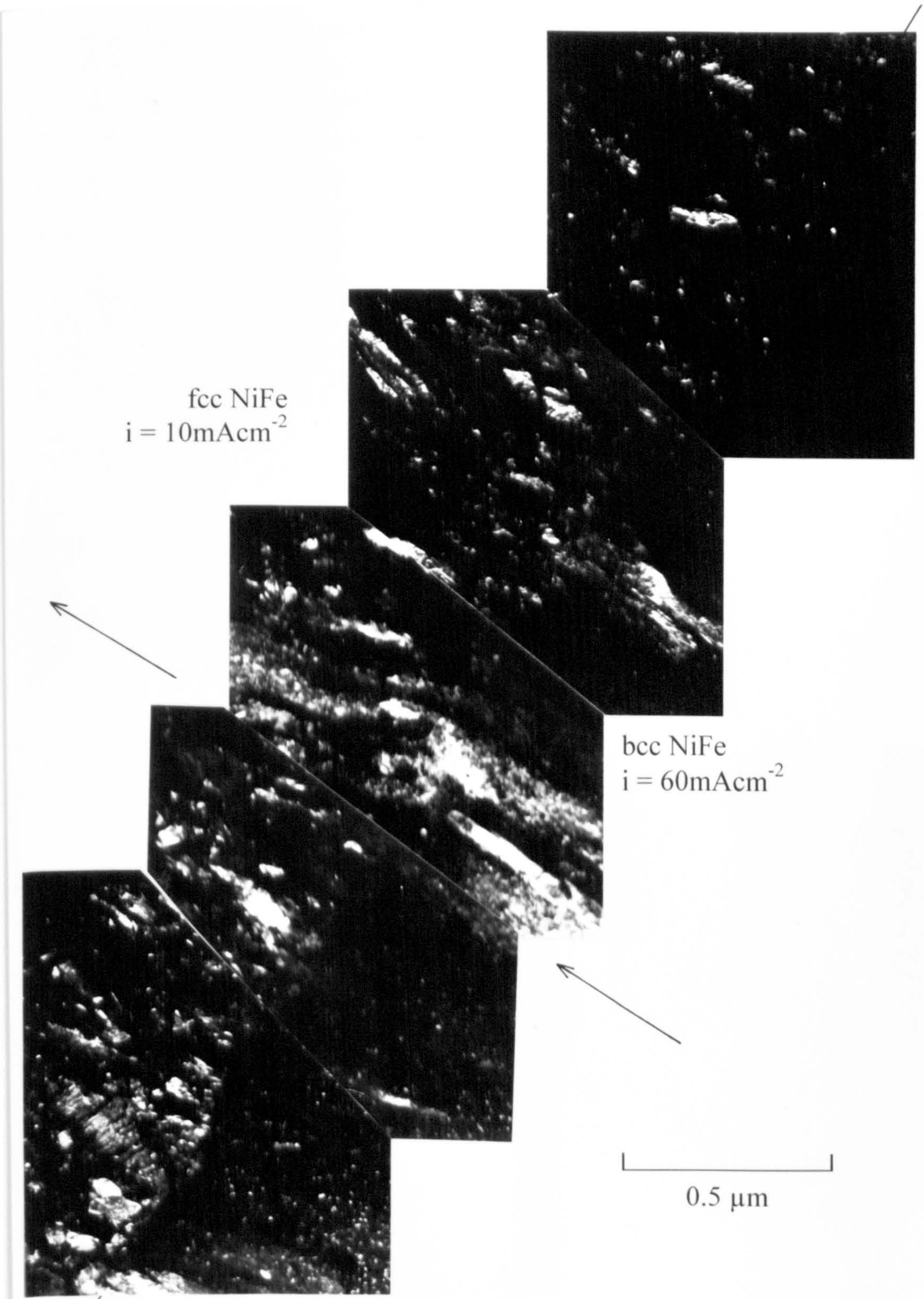

Fig. 4-60b: Montage of Dark Fields Along Interface of Double Layered, 2μm Thick fcc NiFe Deposit Nucleated on 2μm Thick bcc NiFe Deposit.

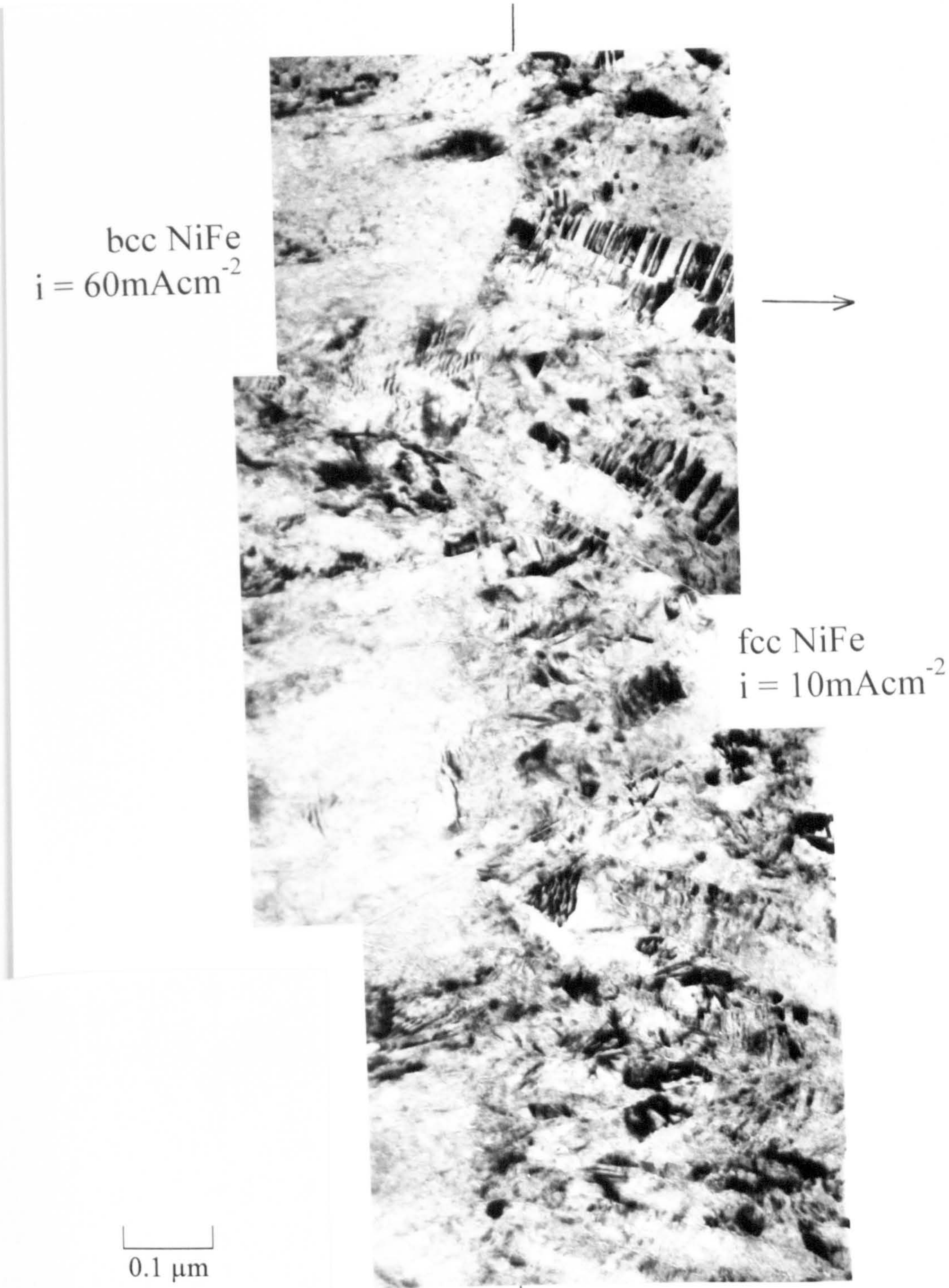

Fig. 4-61: Montage of Bright Fields Along Interface of Double Layered 2μm Thick fcc NiFe Deposit Nucleated on 2μm Thick bcc NiFe Deposit.

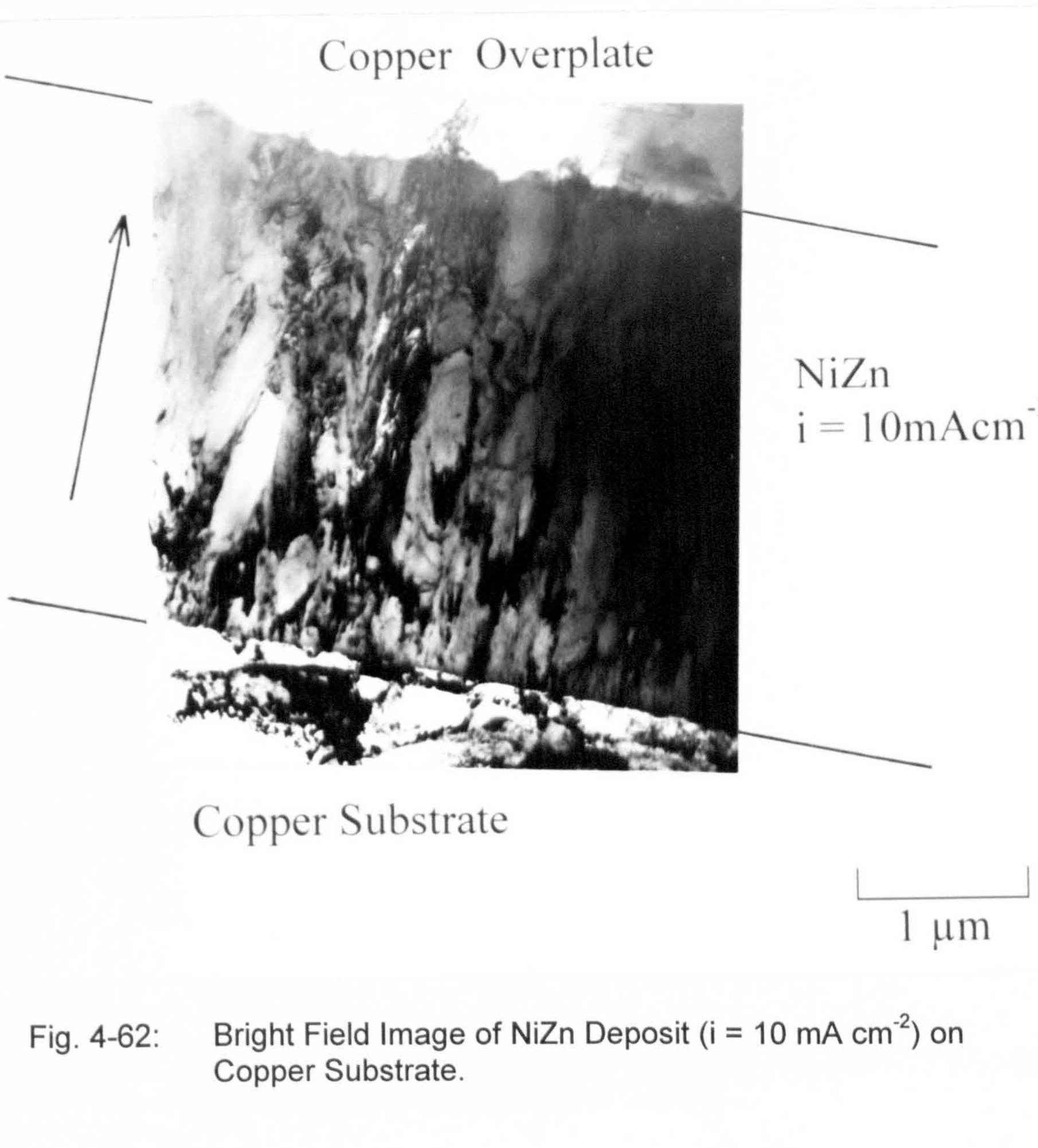

Fig. 4-62: Bright Field Image of NiZn Deposit (i = 10 mA cm^{-2}) on Copper Substrate.

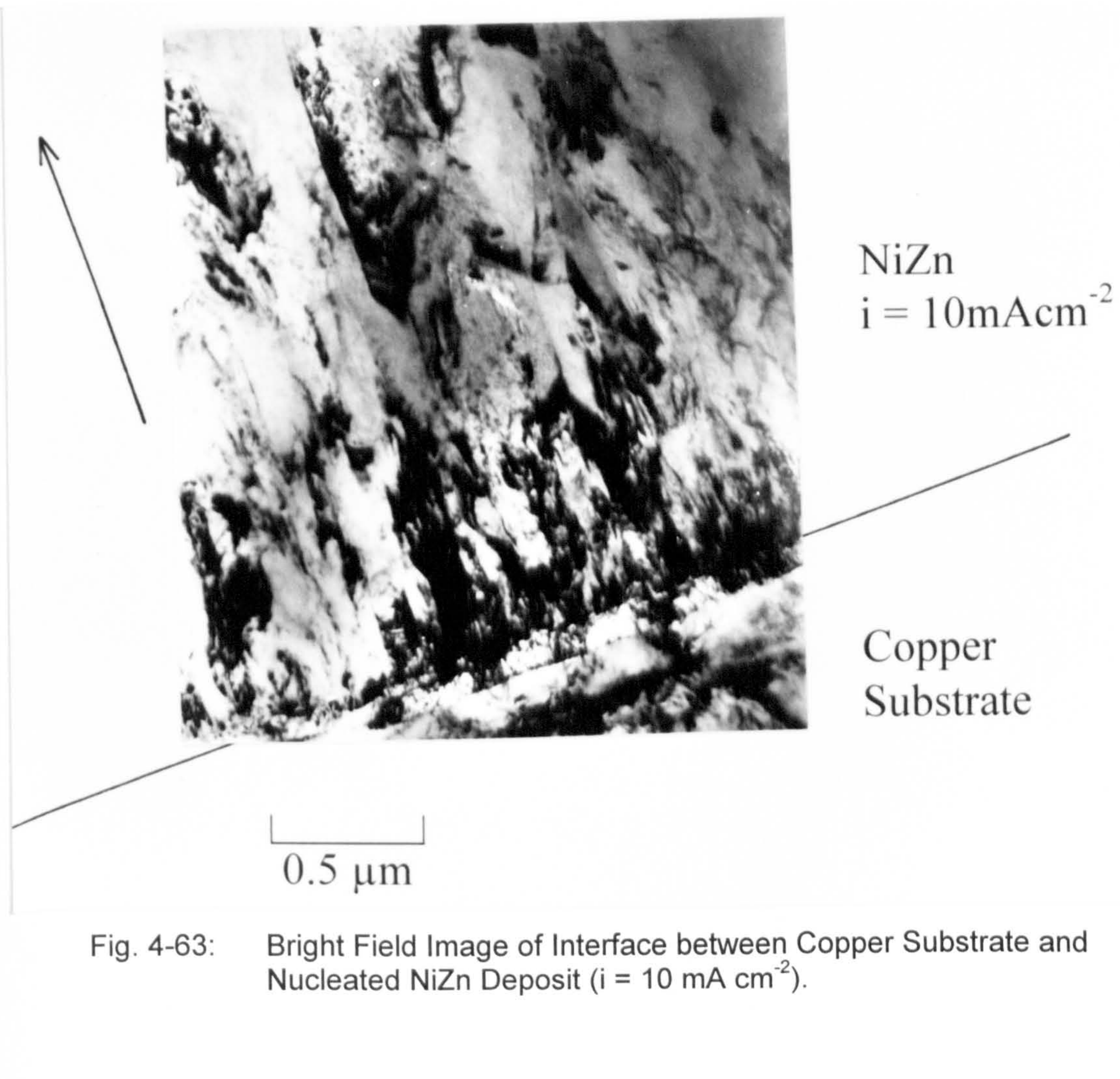

Fig. 4-63: Bright Field Image of Interface between Copper Substrate and Nucleated NiZn Deposit (i = 10 mA cm^{-2}).

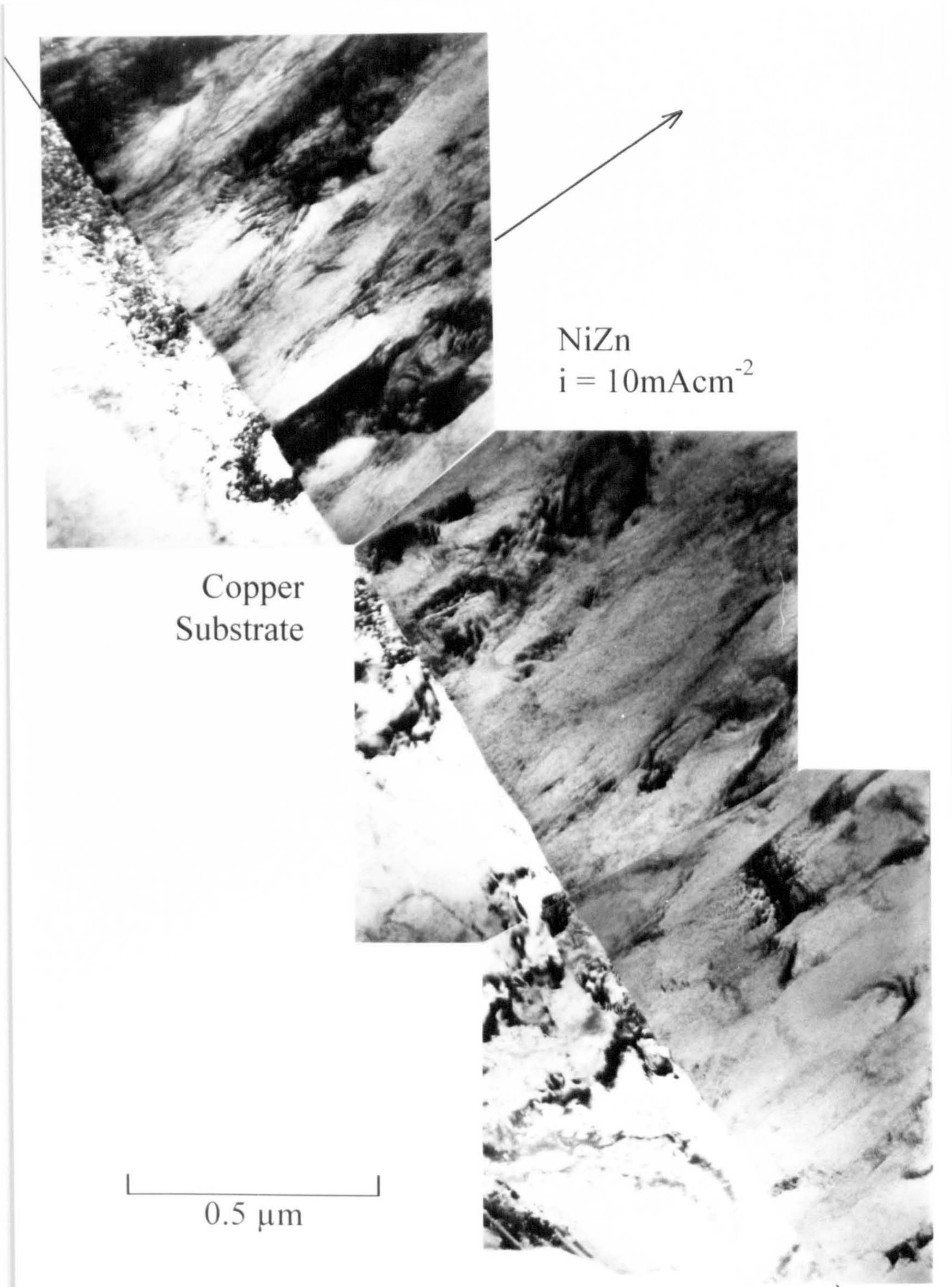

Fig. 4-64: Bright Field Images Along Interface Between Copper Substrate and Nucleated NiZn Deposit (i = 10 mA cm^{-2}).

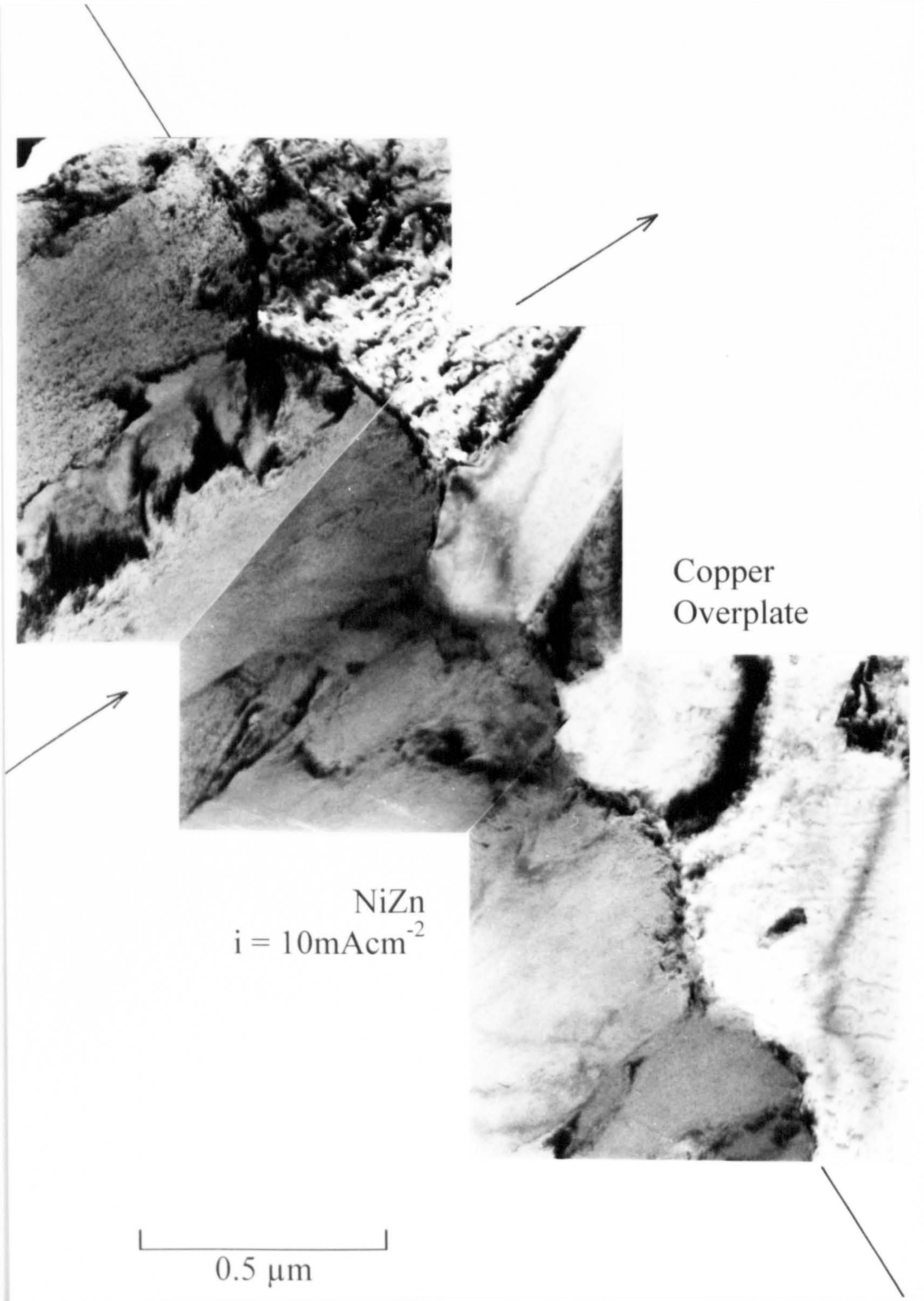

Fig. 4-65: Bright Field Images Along Interface Between Advanced Developed, Approximately 2µm Thick, Coarse Grained NiZn Deposit (i = 10 mA cm^{-2}) and Copper Overplate.

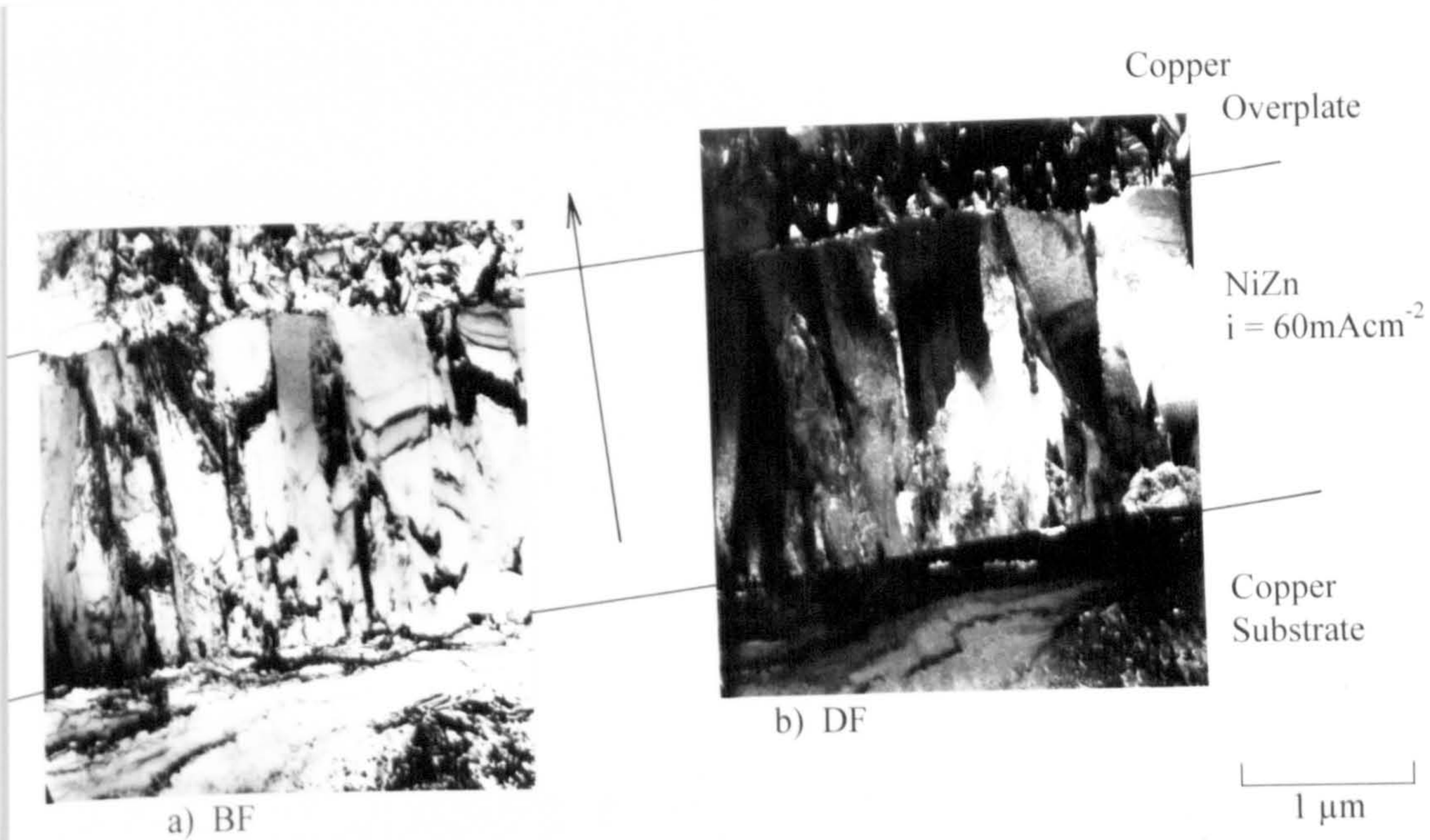

Fig. 4-66: (a) Bright Field and (b) Dark Field Image of Cross-Sectioned NiZn Deposit (i = 60 mA cm^{-2}) Nucleated on Copper.

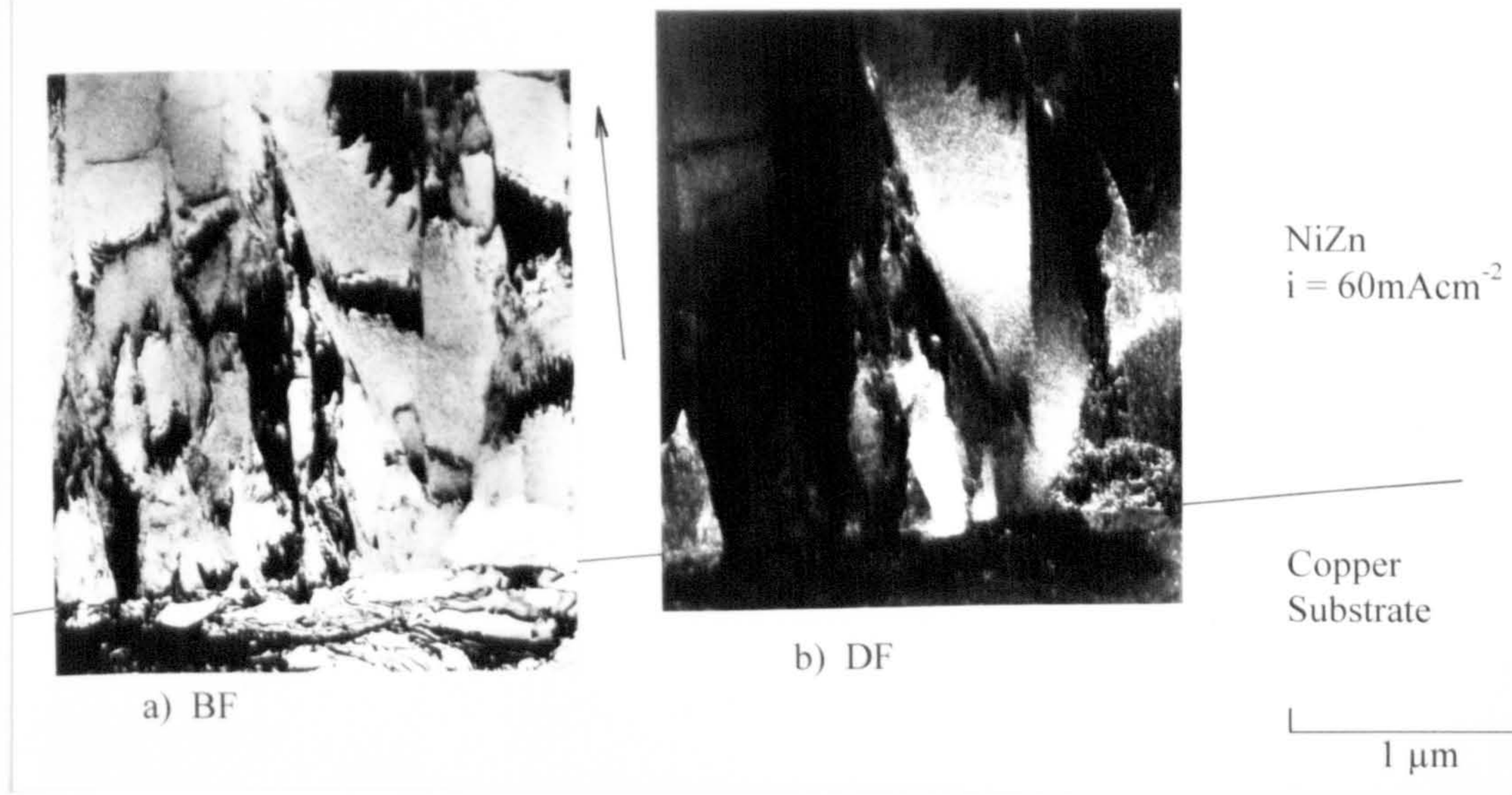

Fig. 4-67: (a) Bright and (b) Dark Field Image of Nucleation Site of NiZn Deposit (i = 60 mA cm^{-2}) on Copper.

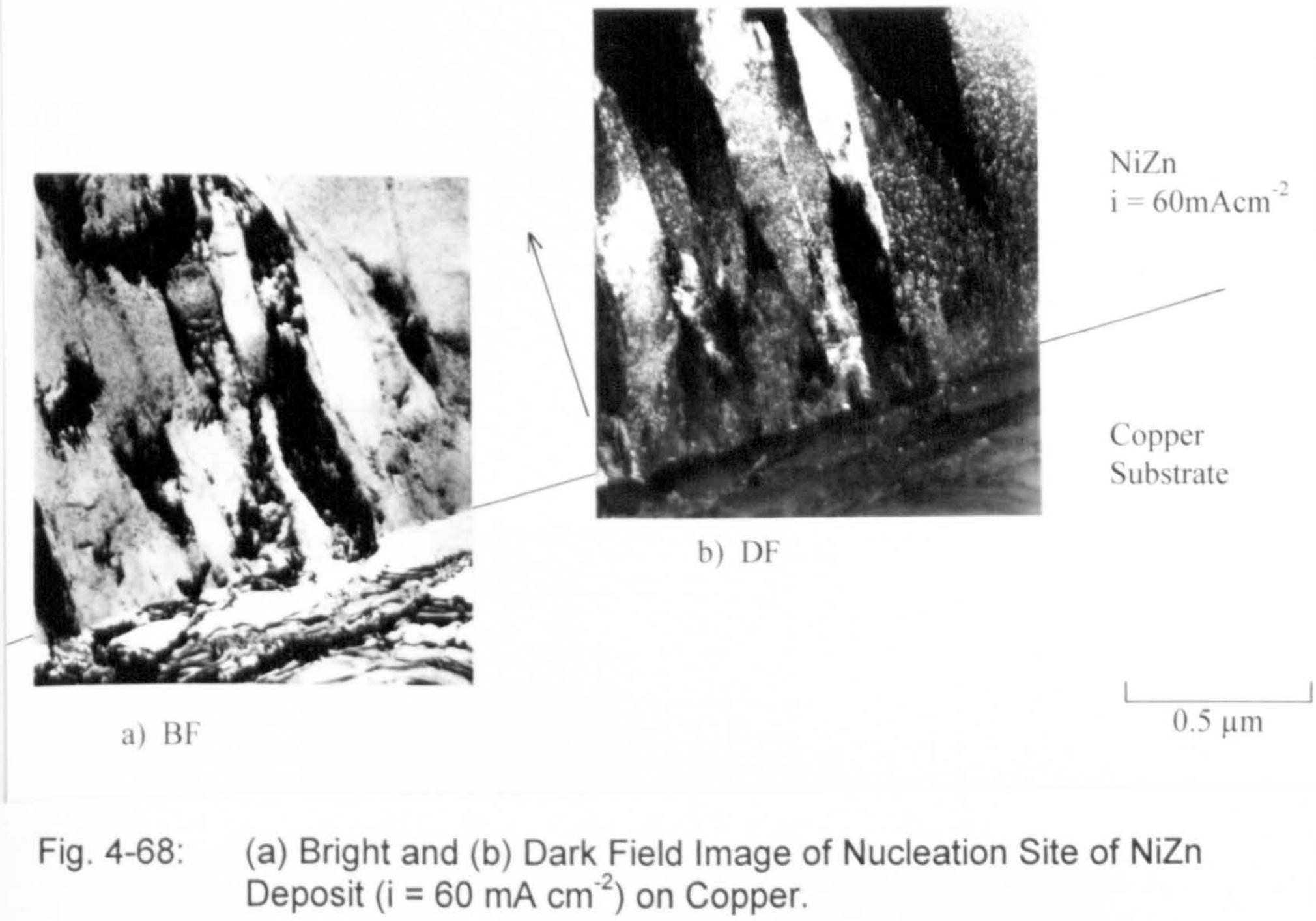

Fig. 4-68: (a) Bright and (b) Dark Field Image of Nucleation Site of NiZn Deposit (i = 60 mA cm^{-2}) on Copper.

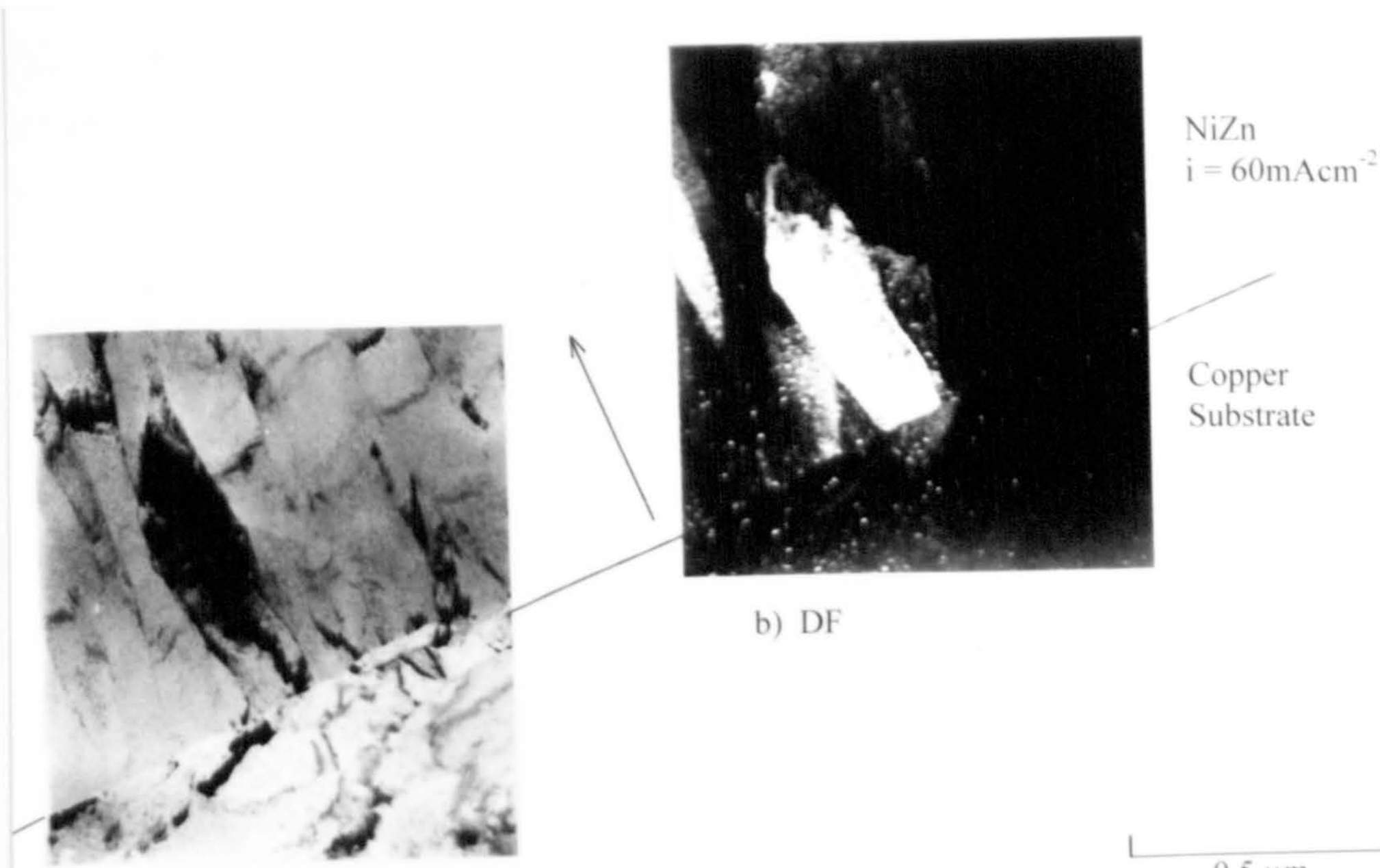

Fig. 4-69: (a) Bright and (b) Dark Field Image of Nucleation Site of NiZn Deposit (i = 60 mA cm^{-2}) on Copper.

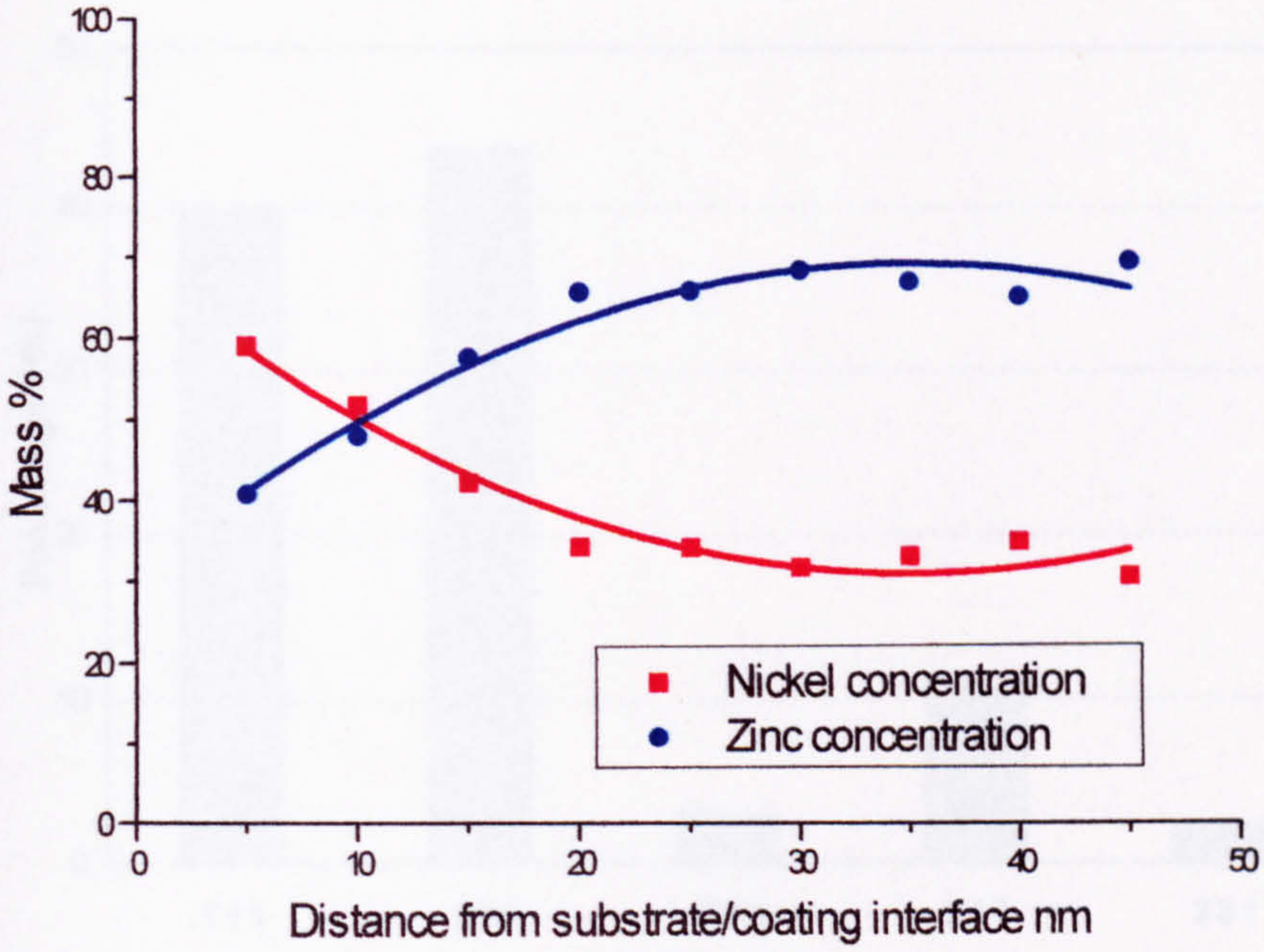

Fig. 4-70: Composition of Nickel Zinc Deposit (i = 10 mA cm^{-2}) versus Distance from Interface Steel Substrate/Nickel Zinc Deposit.

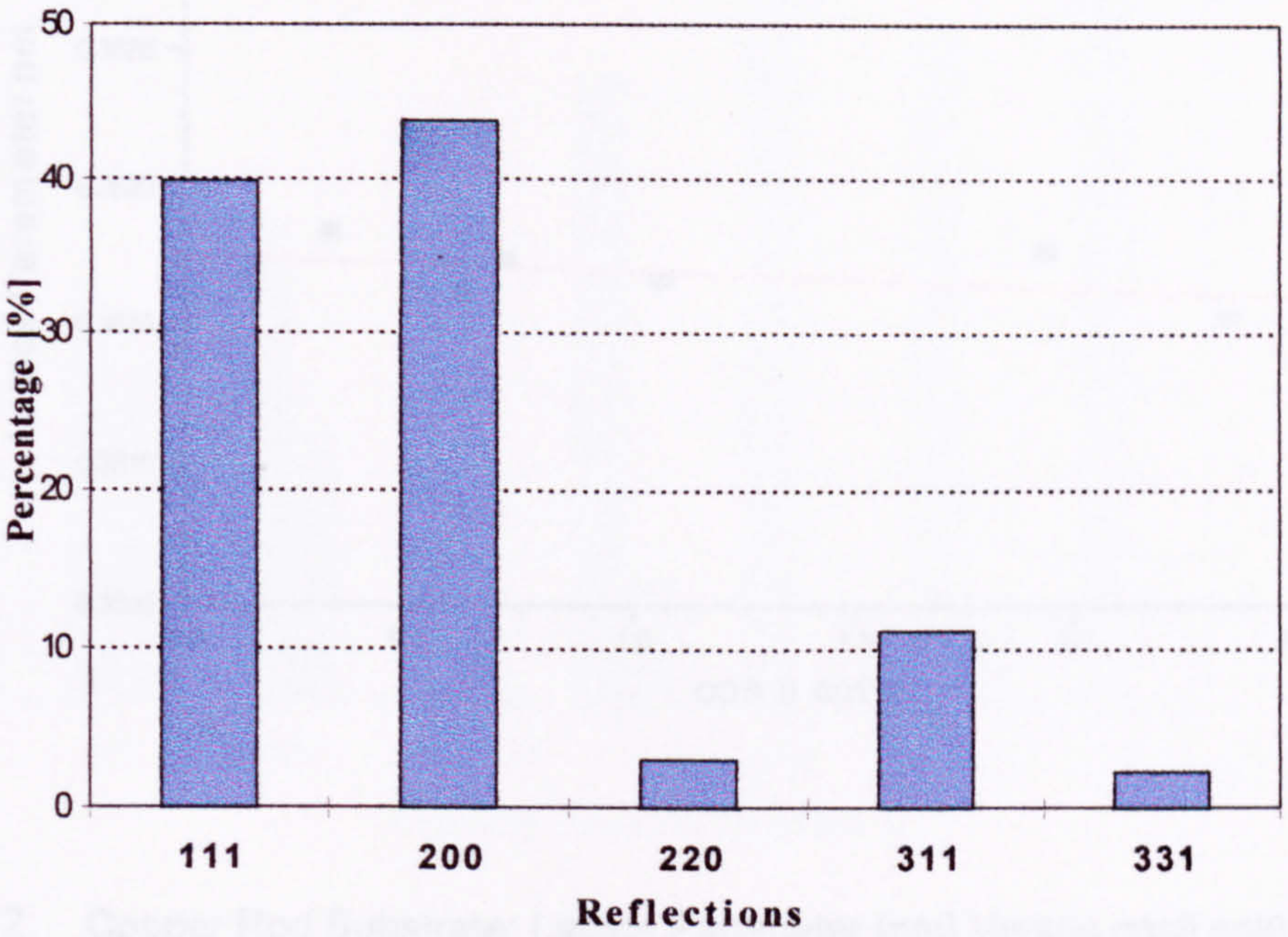

Fig. 4-71: Distribution of Reflections Detected in the Copper Disc Substrate.

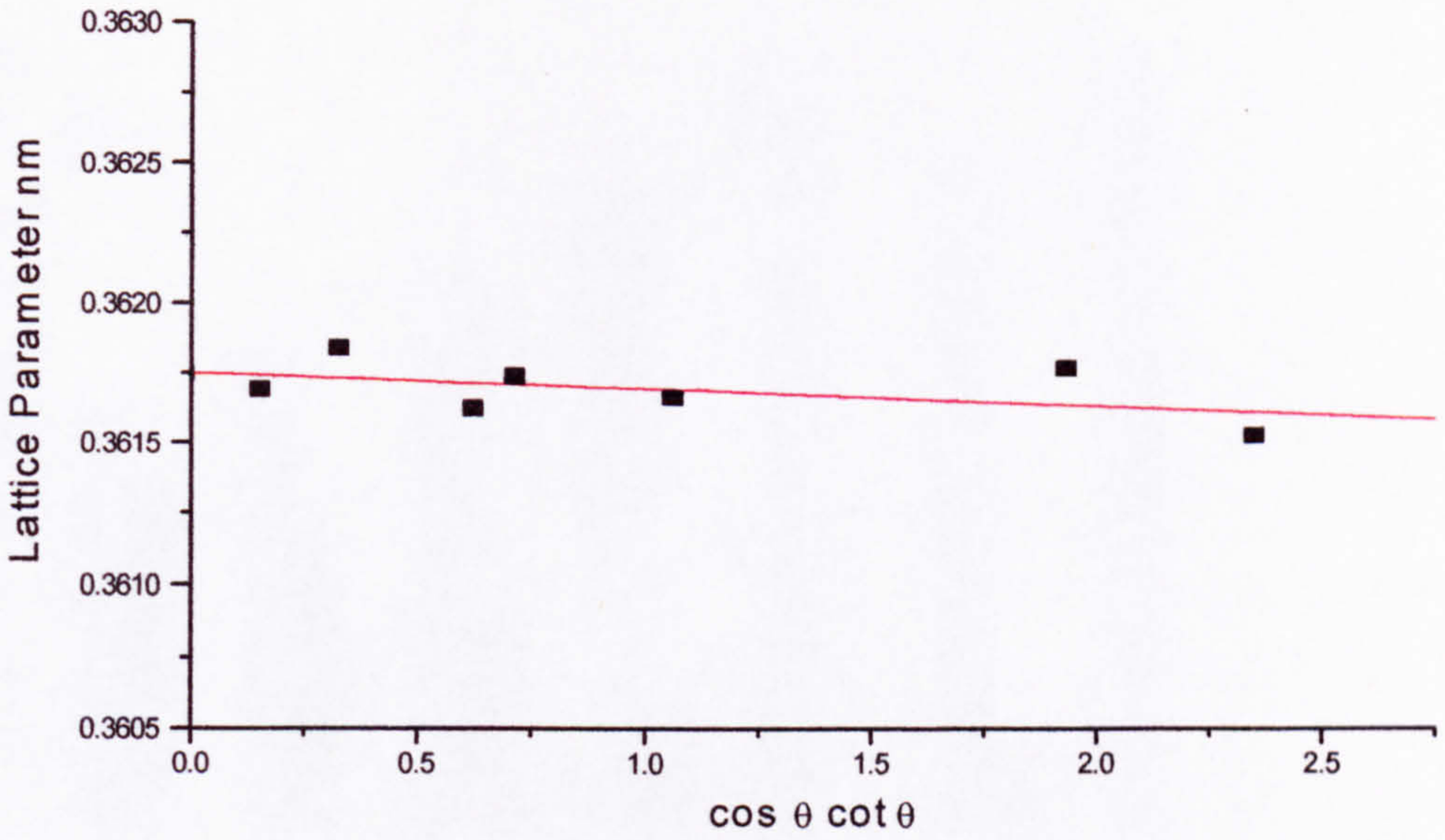

Fig. 4-72: Copper Rod Substrate: Lattice Parameter [nm] Versus cosθ cotθ; Cohen-Wagner Plot for Extrapolation of Lattice Parameter 'a'.

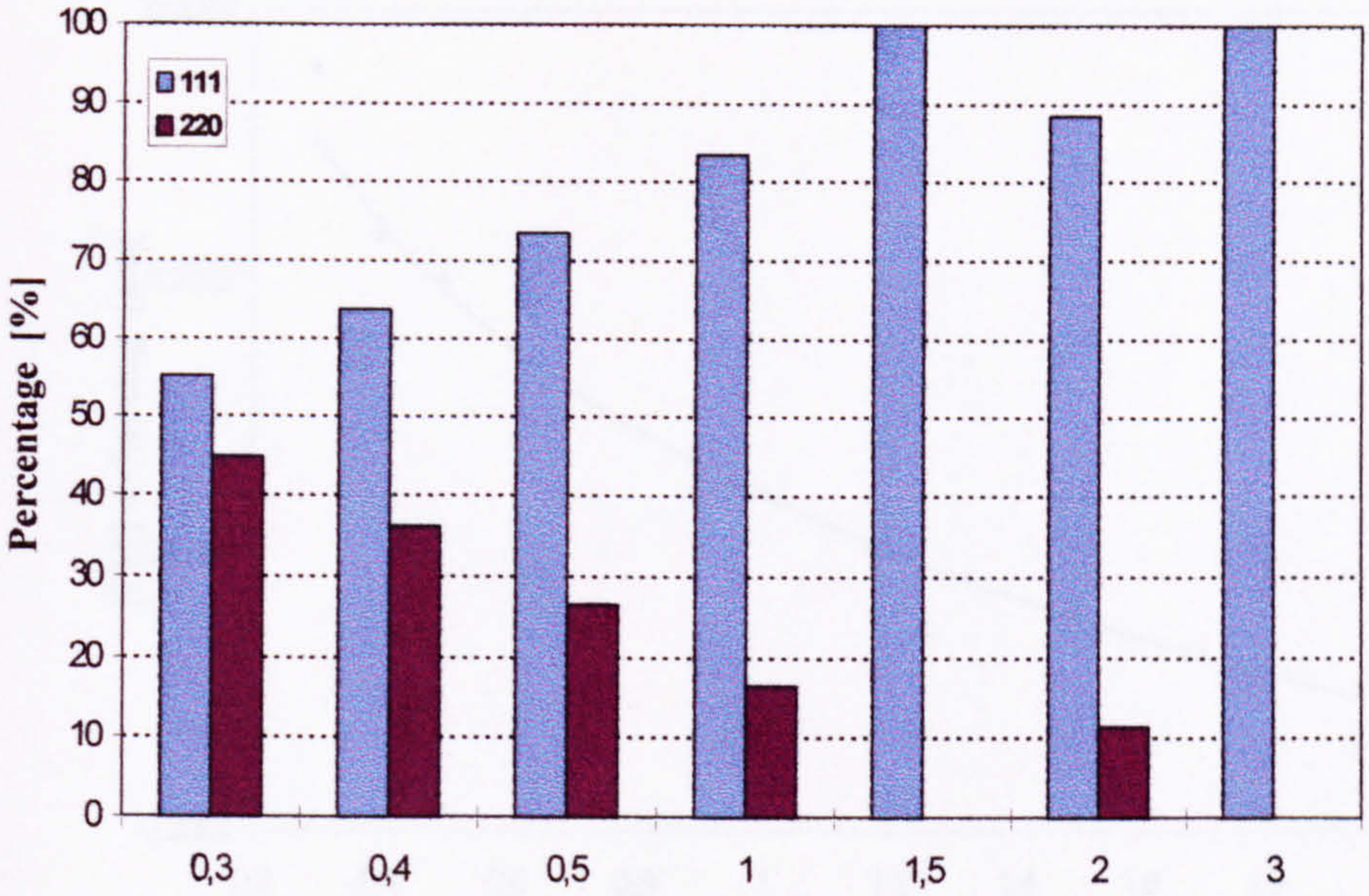

Fig. 4-73: Distribution of Reflections Detected at Various Thicknesses in the fcc NiFe Electrodeposits.

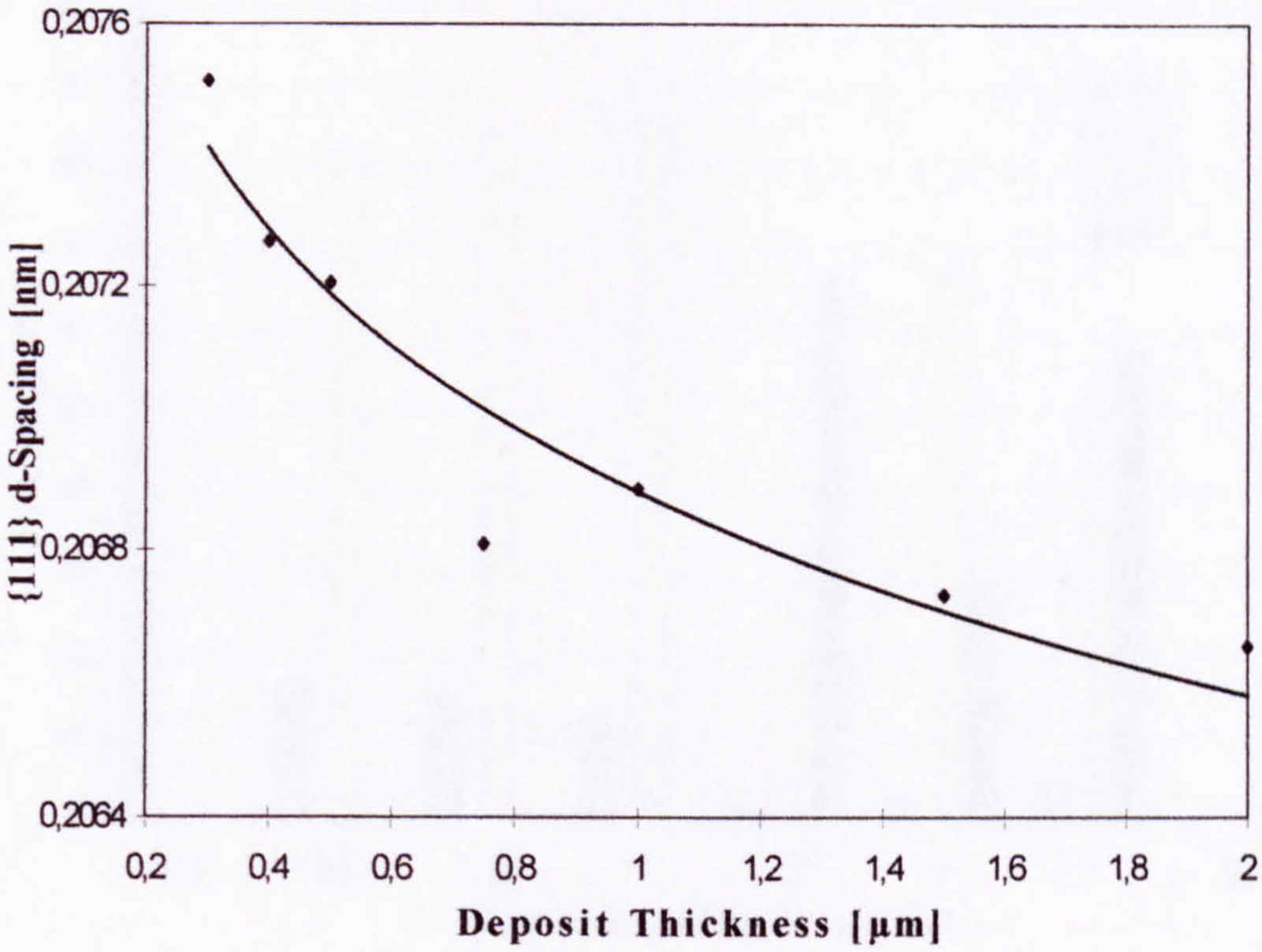

Fig. 4-74: Deposit Thickness Versus {111} Interplanar d-Spacing in fcc NiFe Electrodeposit.

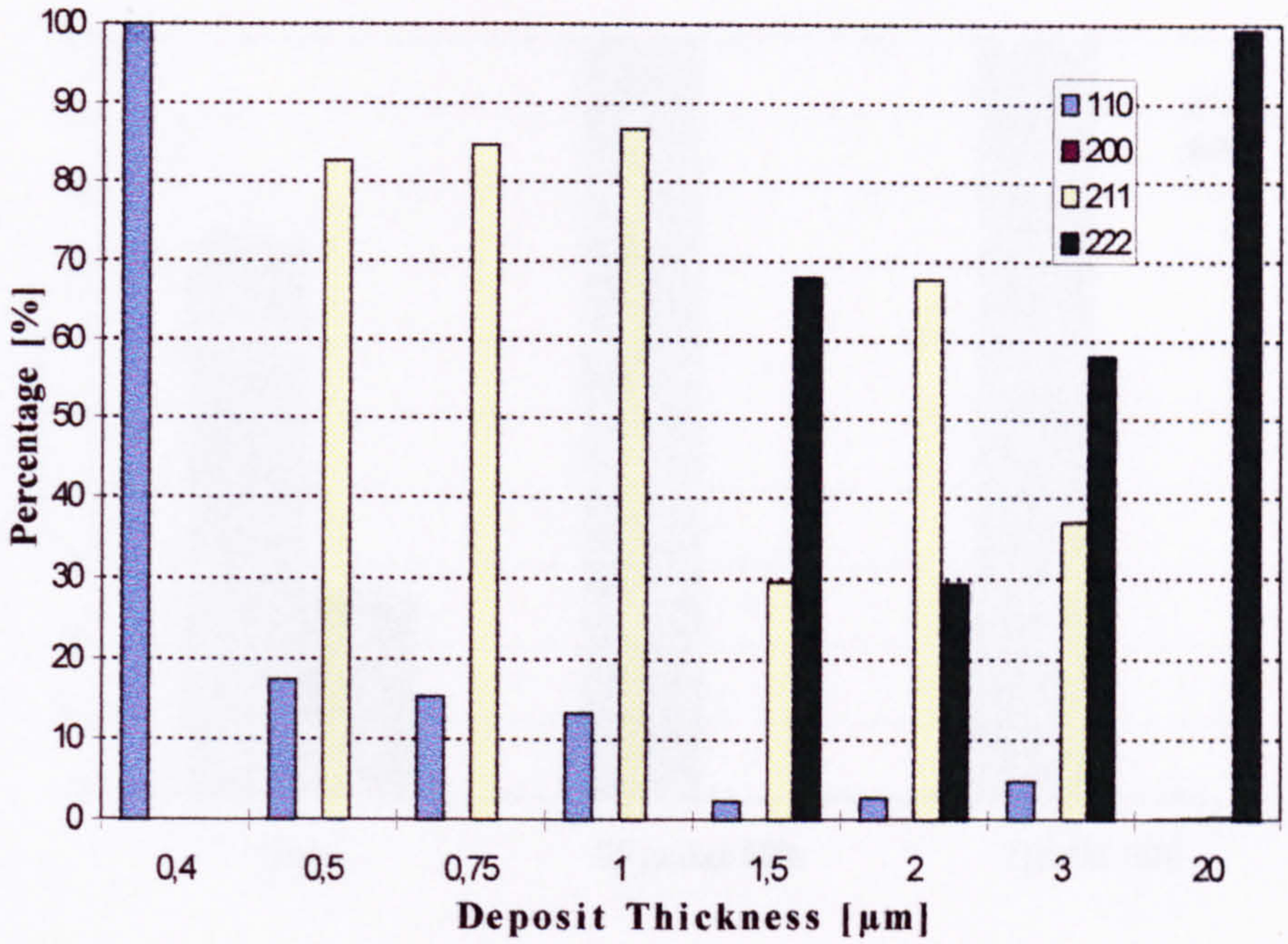

Fig. 4-75: Distribution of Reflections Detected at Various Thicknesses in the bcc NiFe Electrodeposits.

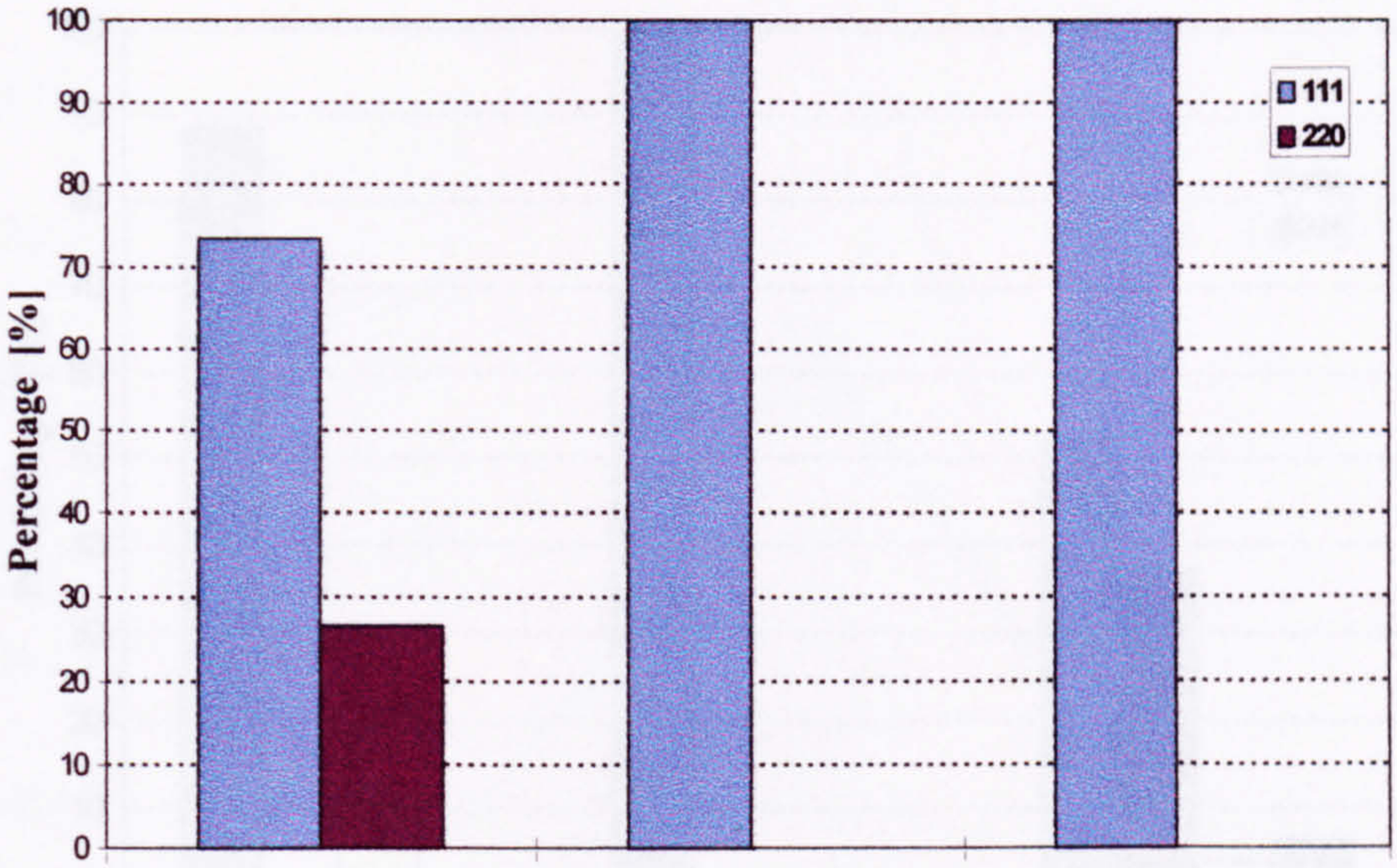

Fig. 4-76: Planar Distribution of 0.5µm Thick fcc NiFe on Copper, 0.5µm bcc NiFe, and 2µm bcc NiFe Electrodeposited Substrates.

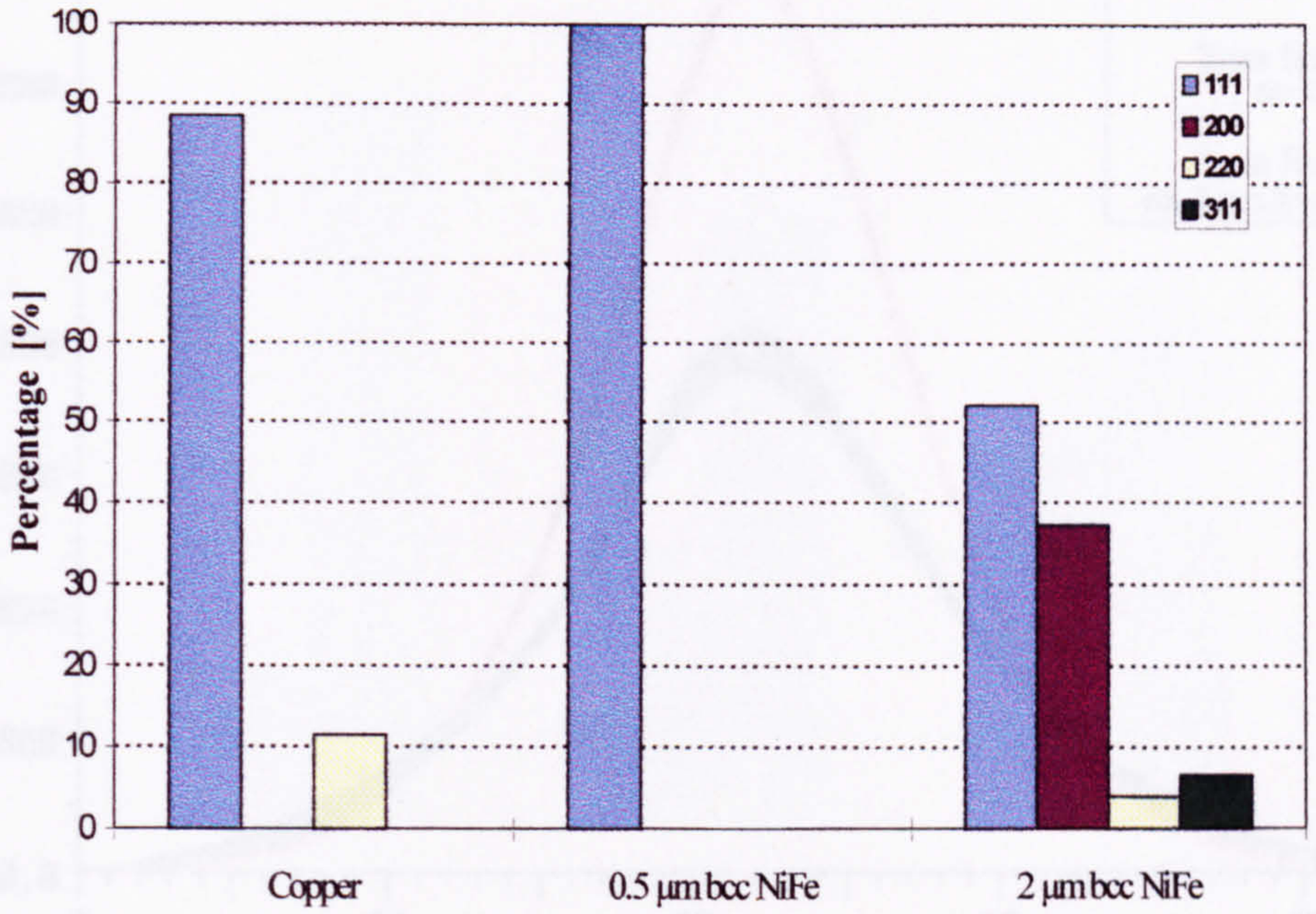

Fig. 4-77: Planar Distribution in per cent of 2µm Thick fcc NiFe Electrodeposits on Copper, 0.5µm bcc NiFe, and 2µm bcc NiFe Electrodeposited Substrates.

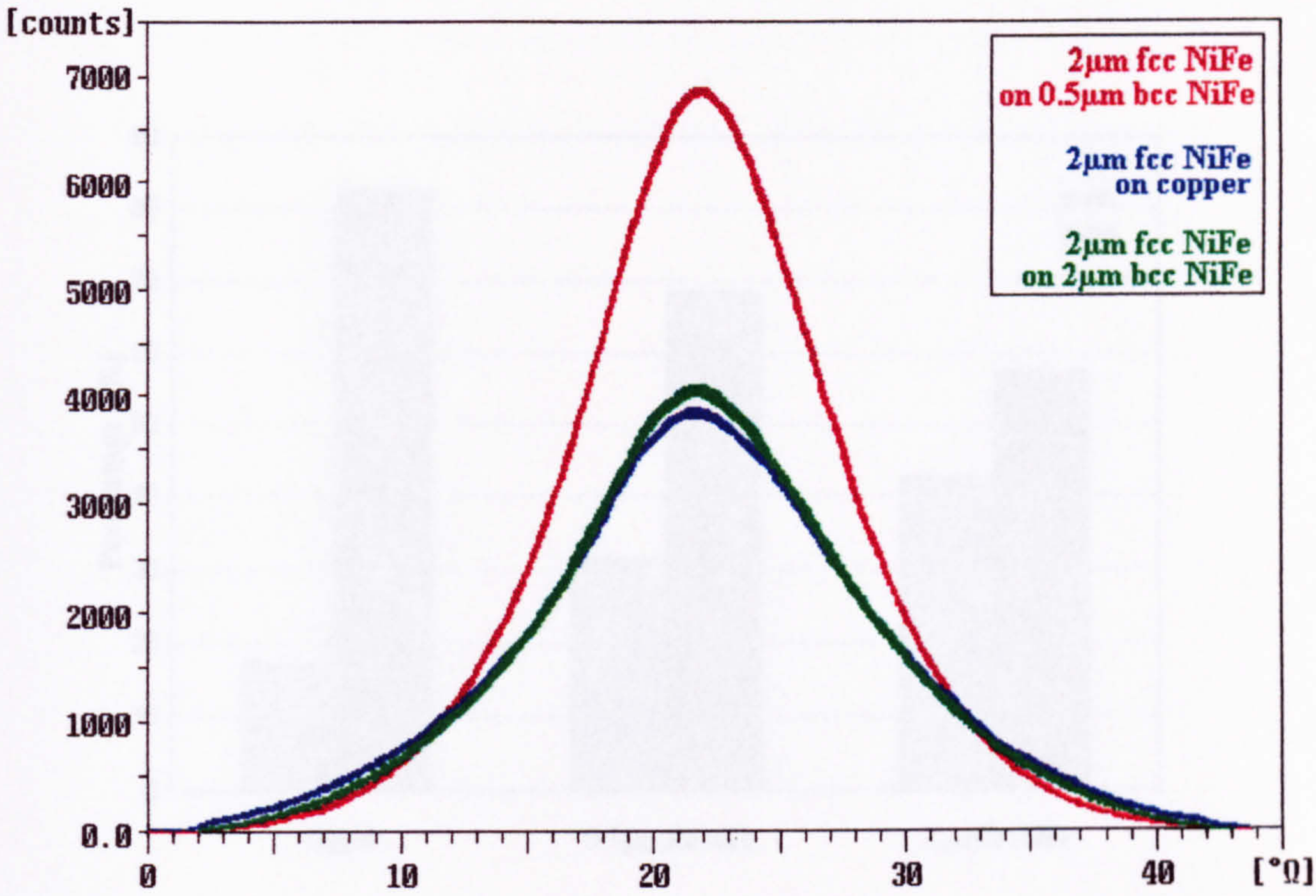

Fig. 4-78: Ω-Scan Spectra of 2µm Thick fcc Structured Nickel-Iron Deposit Electrocrystallized onto Different Substrates, i.e. Copper, 0.5µm bcc NiFe, and 2µm bcc NiFe Electrodeposits.

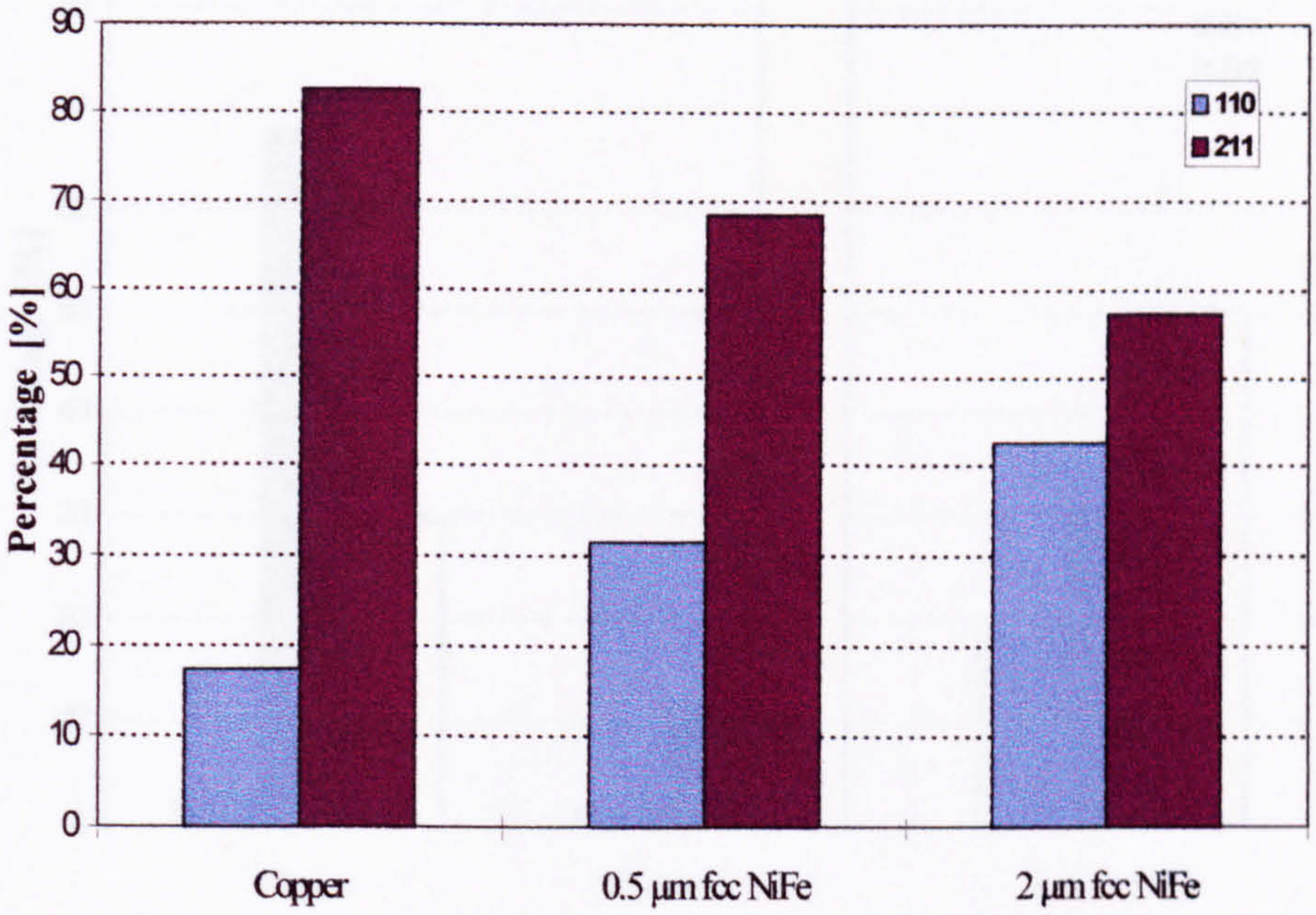

Fig. 4-79: Planar Distribution of 0.5µm Thick bcc NiFe on Copper, 0.5µm fcc NiFe, and 2µm fcc NiFe Electrodeposited Substrates.

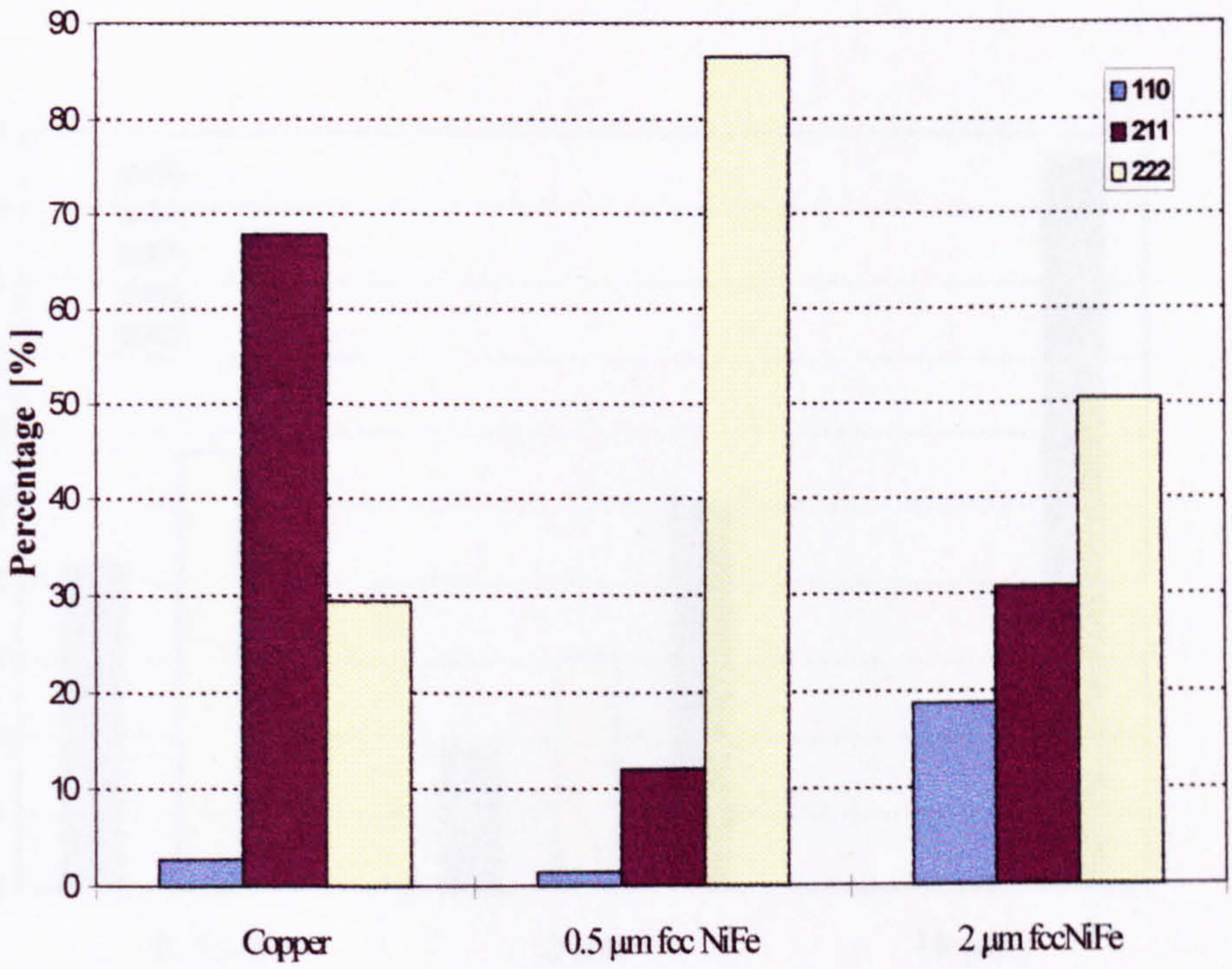

Fig. 4-80: Planar Distribution of 2µm Thick bcc NiFe on Copper, 0.5µm fcc NiFe, and 2µm fcc NiFe Electrodeposited Substrates.

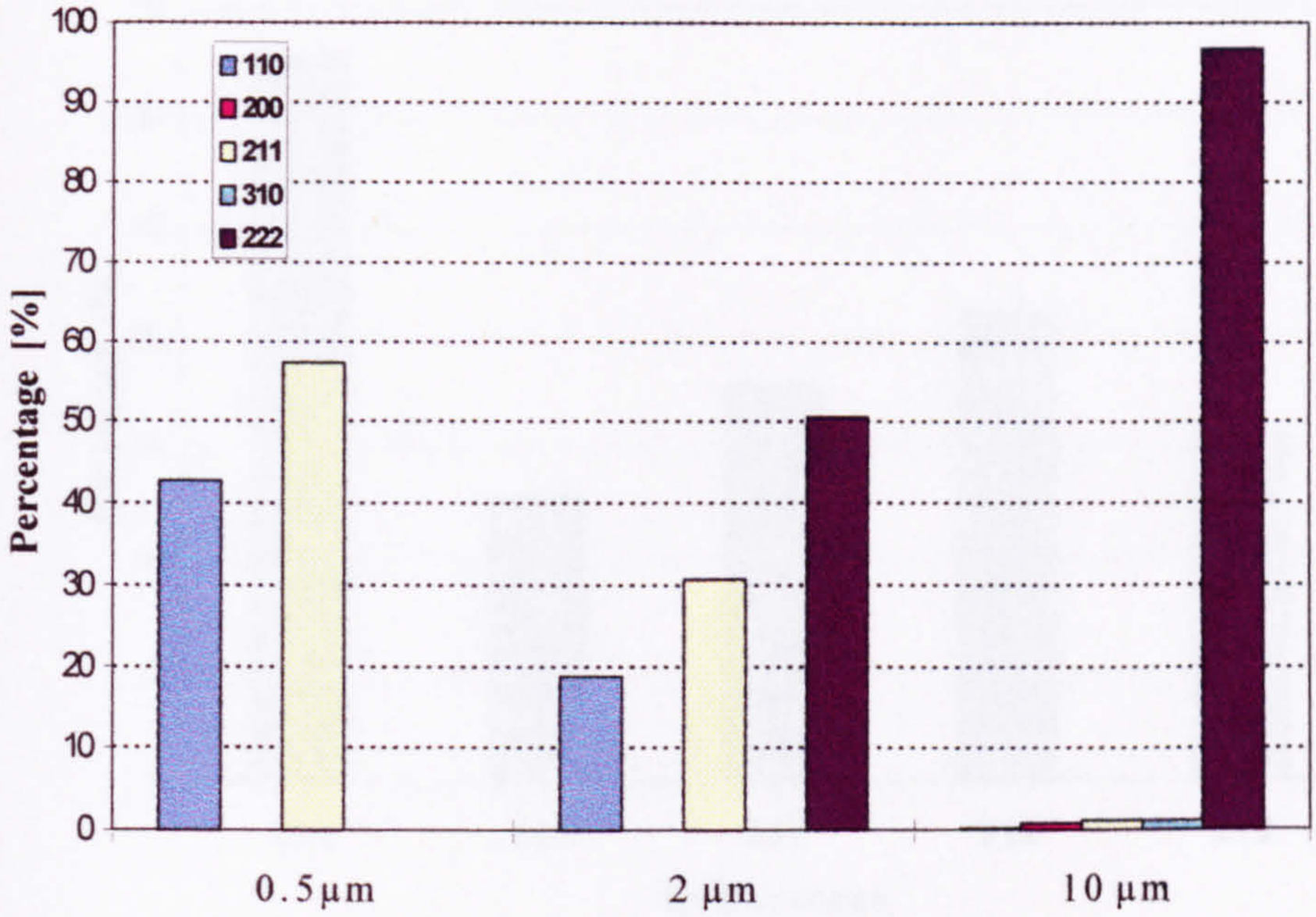

Fig. 4-81: Planar Distribution of 0.5µm, 2µm, and 10µm thick bcc NiFe Electrodeposit on 2µm fcc NiFe Substrate.

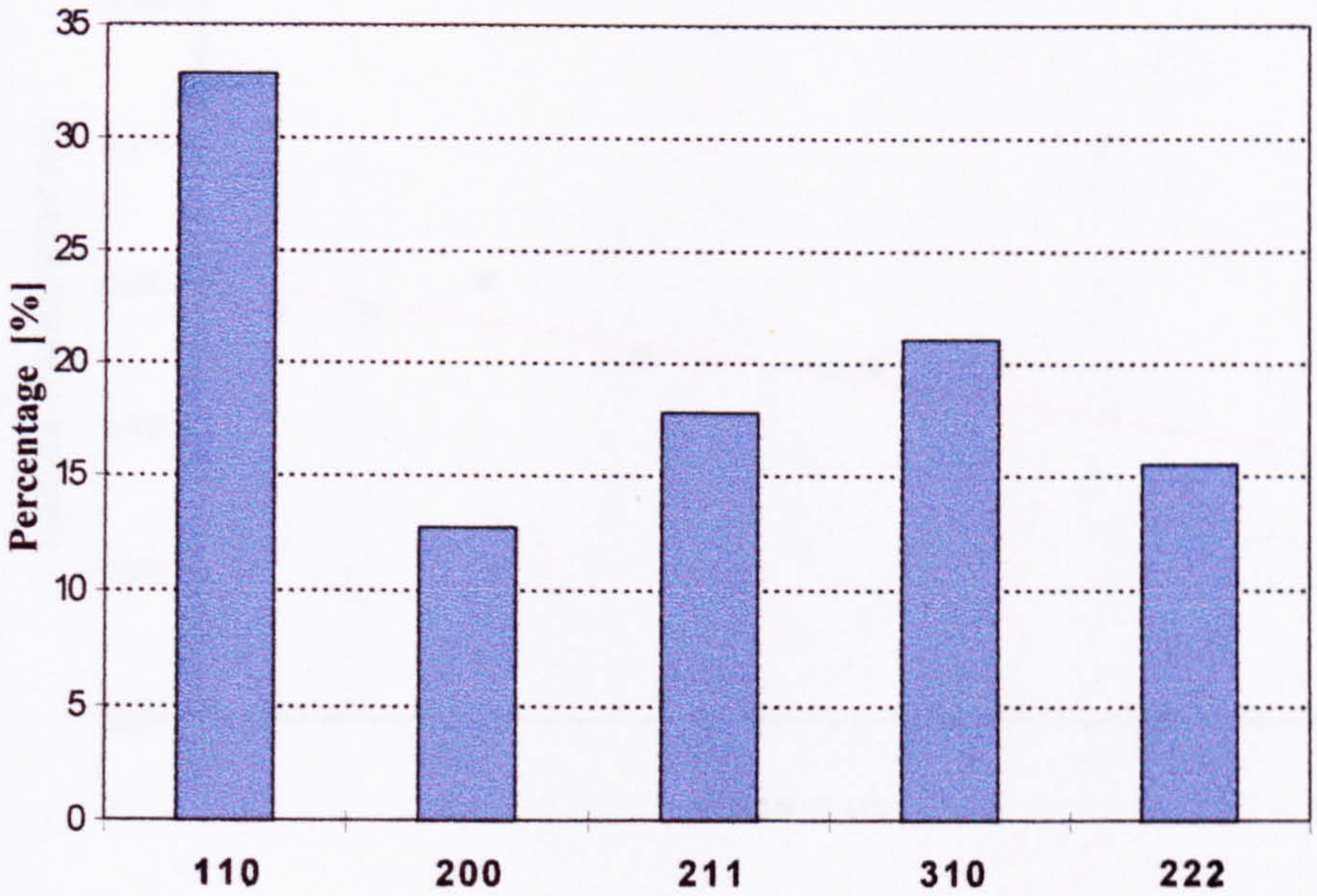

Fig. 4-82: Distribution of Reflections detected in the Mild Steel Disc Substrate.

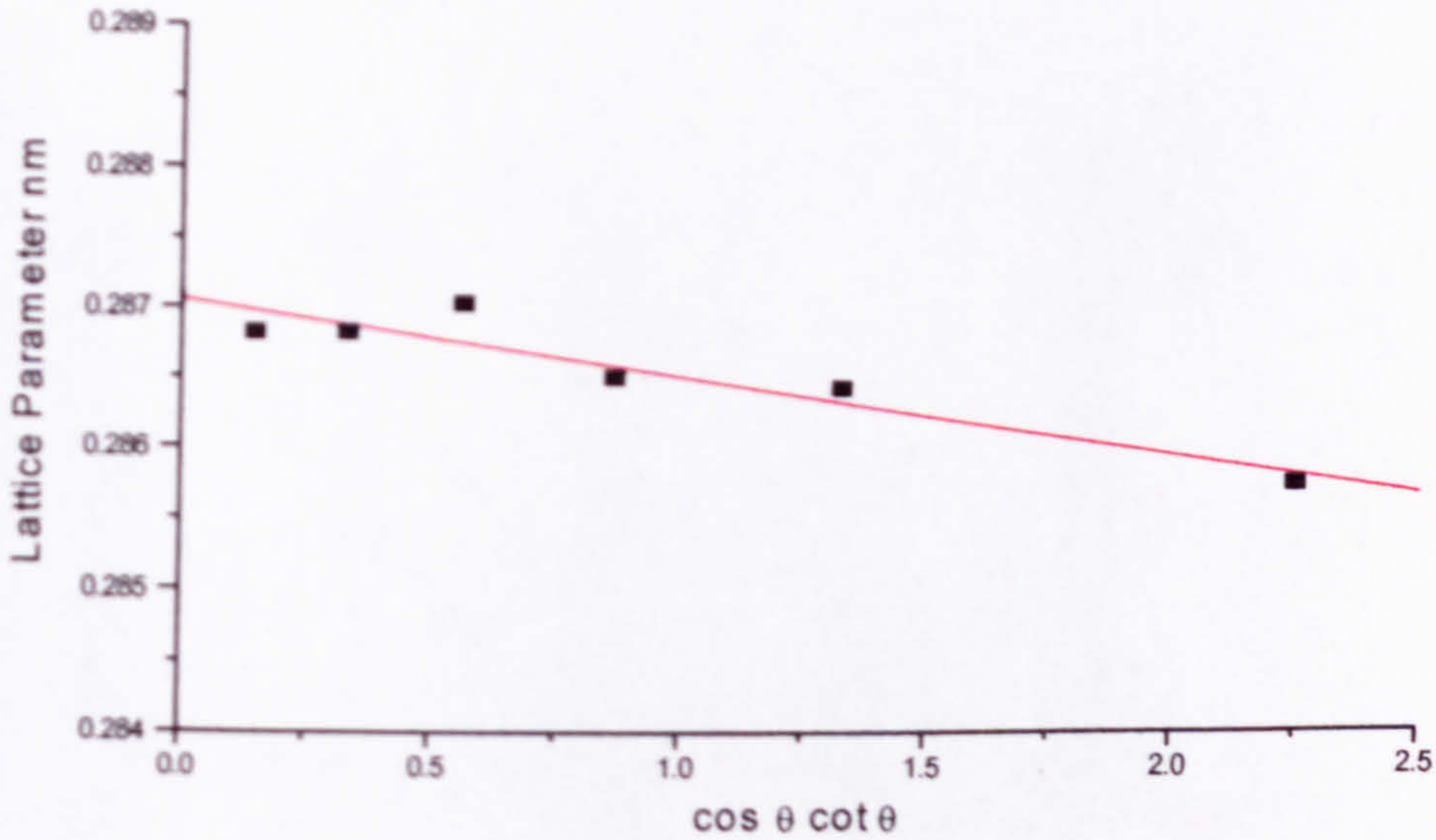

Fig. 4-83: Mild Steel Substrate: Lattice Parameter [nm] Versus cosθ cotθ; Cohen-Wagner Plot for Extrapolation of Lattice Parameter 'a'.

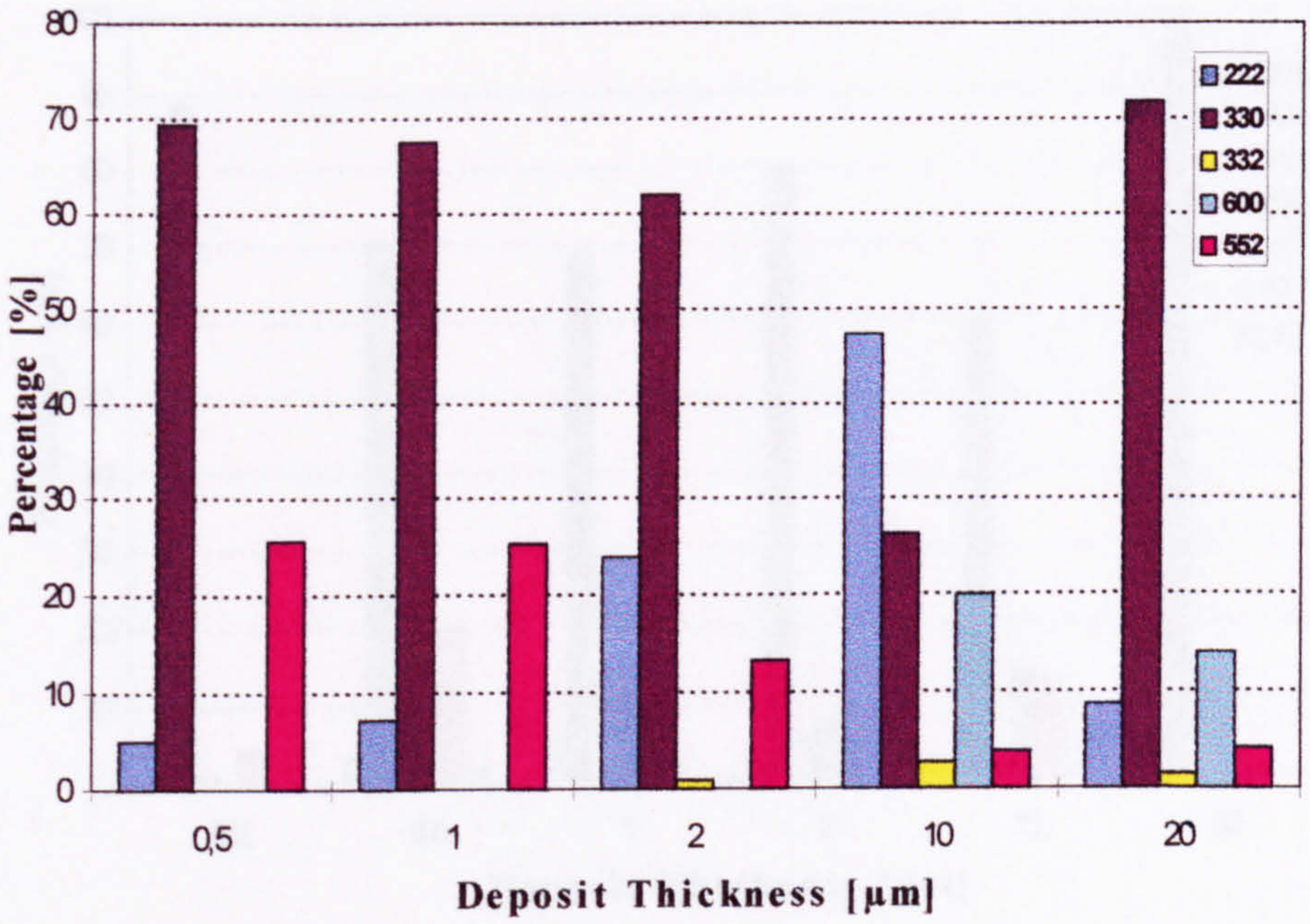

Fig. 4-84: Distribution of Reflections Detected in Nickel-Zinc of Various Thicknesses, Deposited with 10 mA cm^{-2} on Mild Steel Substrates.

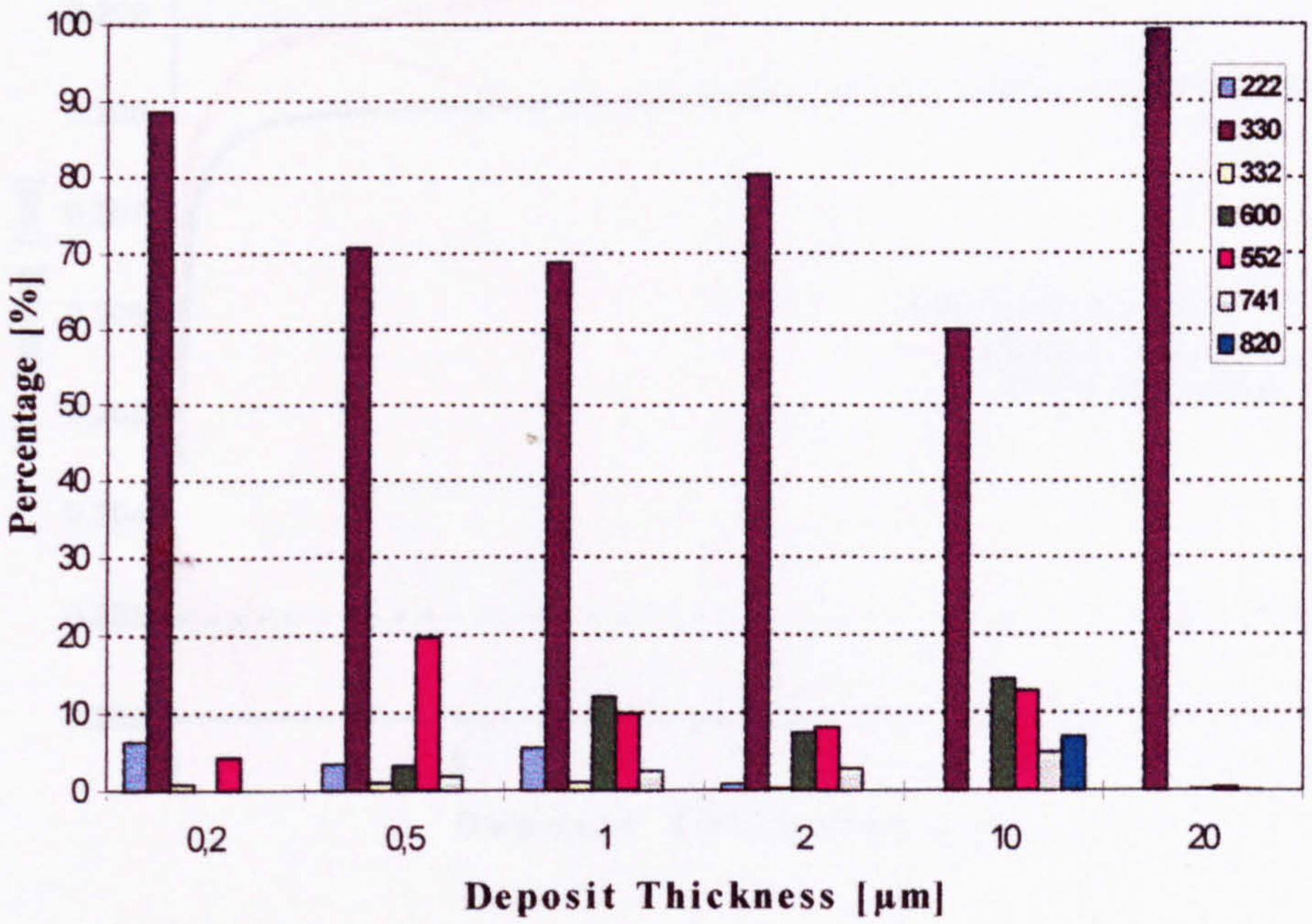

Fig. 4-85: Distribution of Reflections Detected in Nickel-Zinc of Various Thicknesses, Deposited with 60 mA cm^{-2} on Mild Steel Substrates.

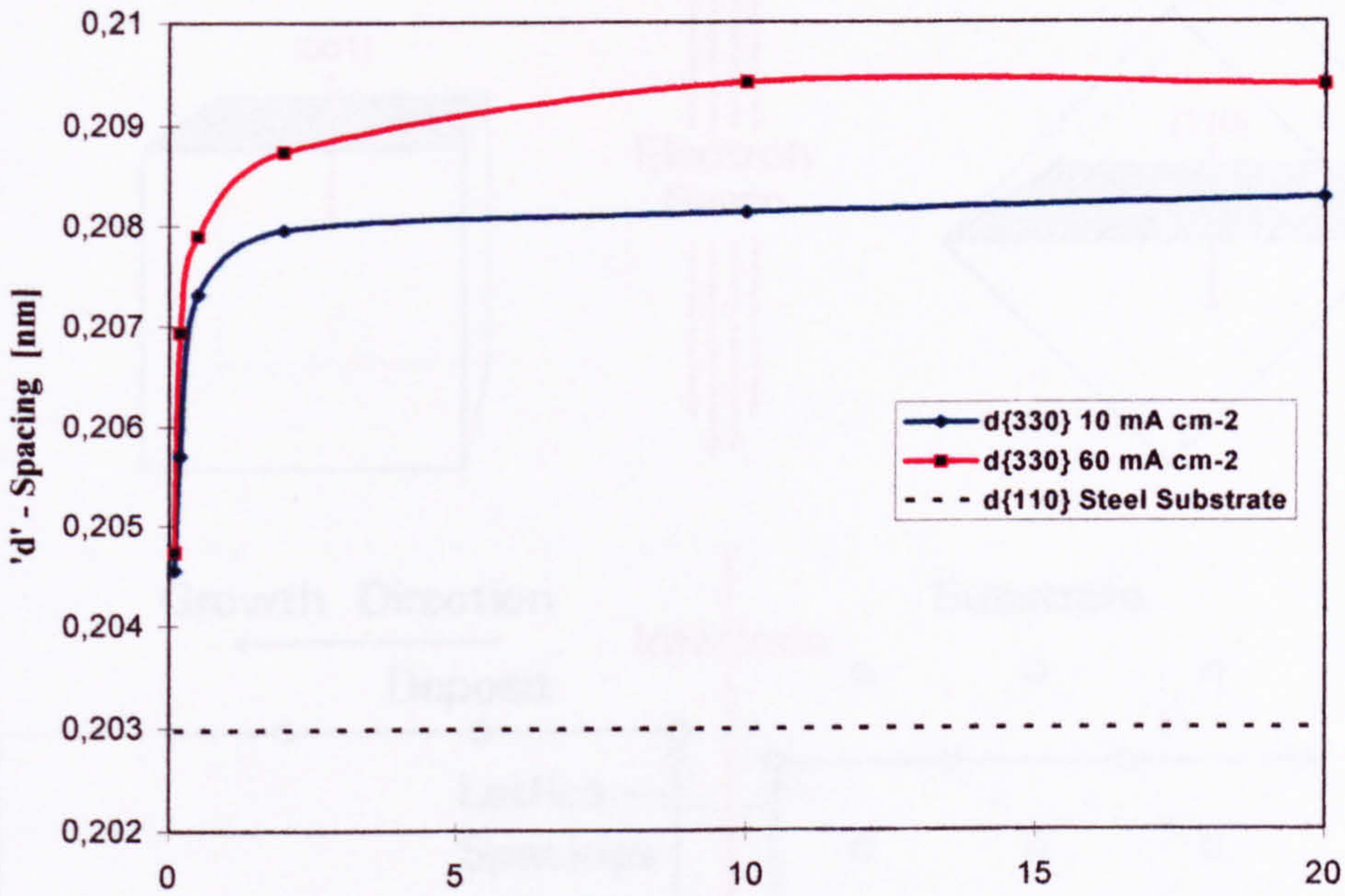

Fig. 4-86: Interplanar {330} d-Spacings of γ-Phase NiZn Deposits Formed at 10 and 60 mA cm^{-2} Versus Deposit Thickness and {110} d-Spacing of Steel Substrate.

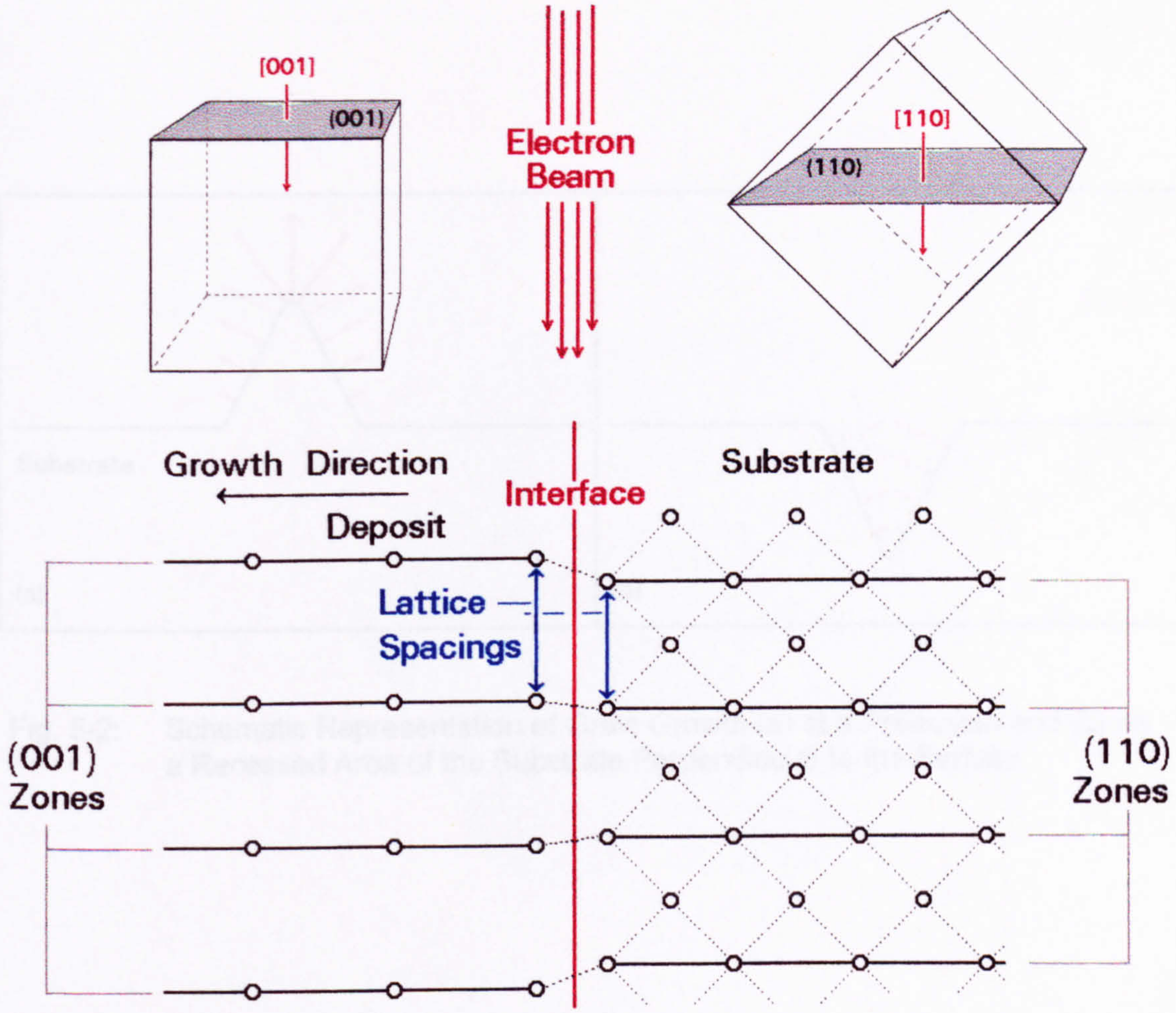

Fig. 5-1: Model of the Electron Beam Interacting with a Cross-Sectioned Specimen, i.e. bcc Nickel-Iron Electrodeposited on a Copper Substrate.

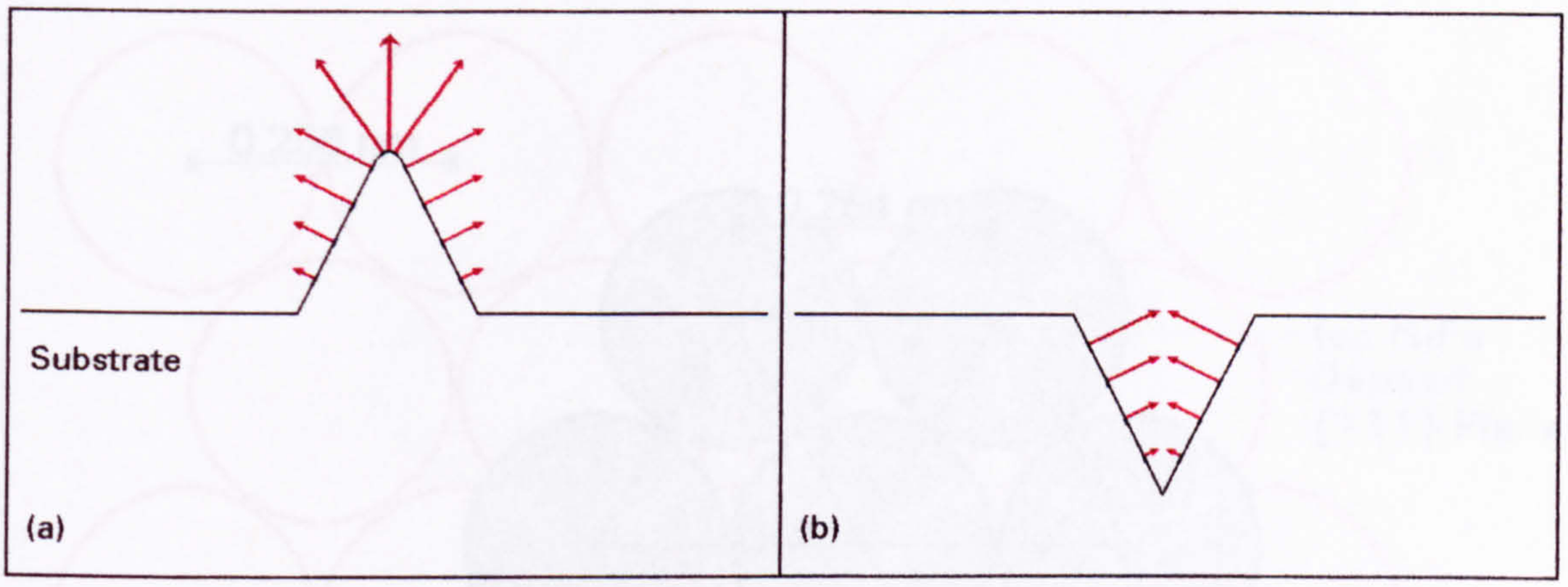

Fig. 5-2: Schematic Representation of Grain Growth (a) at a Protrusion and (b) on a Recessed Area of the Substrate Perpendicular to the Surface.

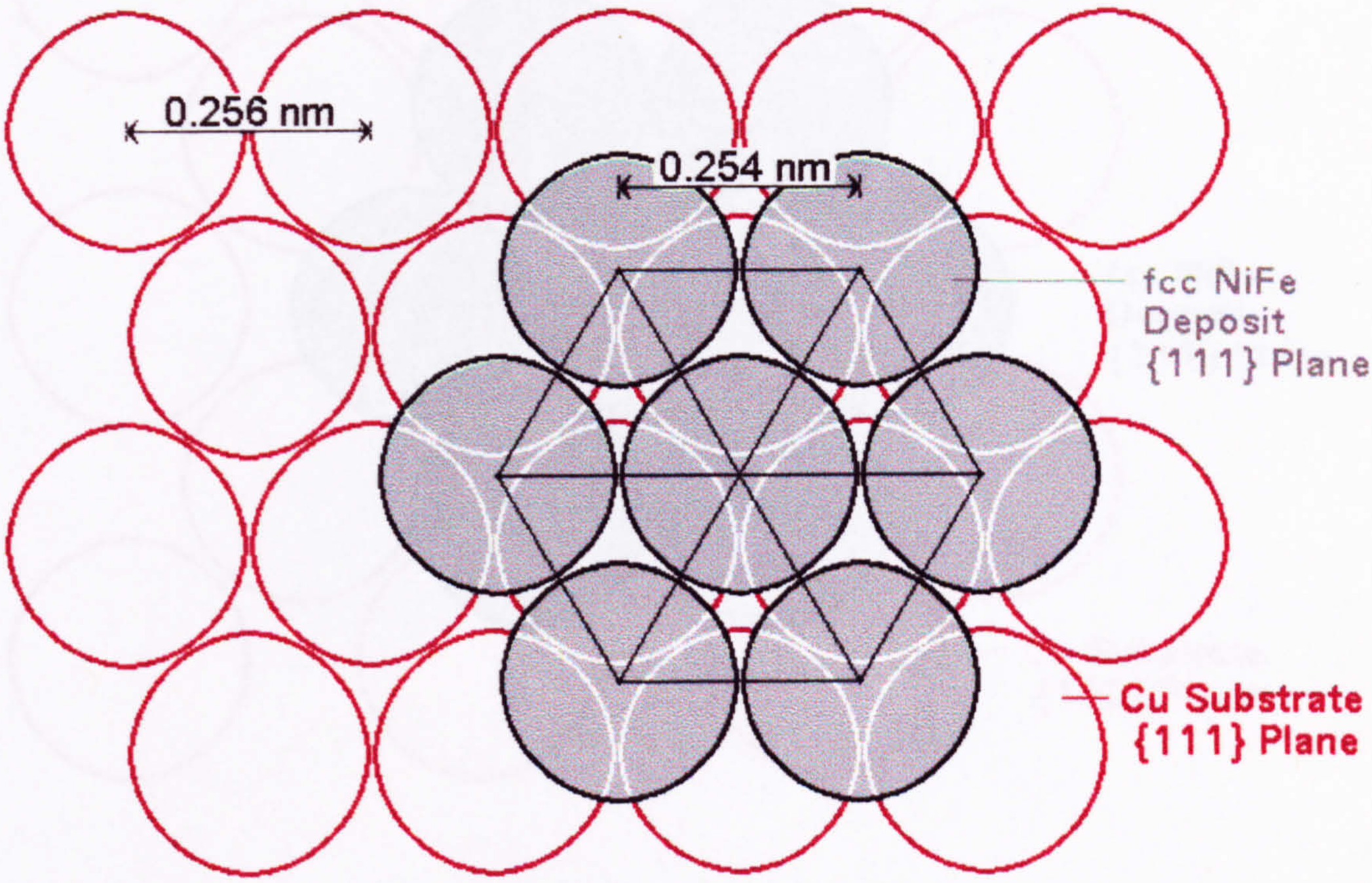

Fig. 5-3: Model of Atoms in {111} Orientated fcc Nickel-Iron Deposit Nucleated onto {111} Textured Copper Substrate (Plan View).

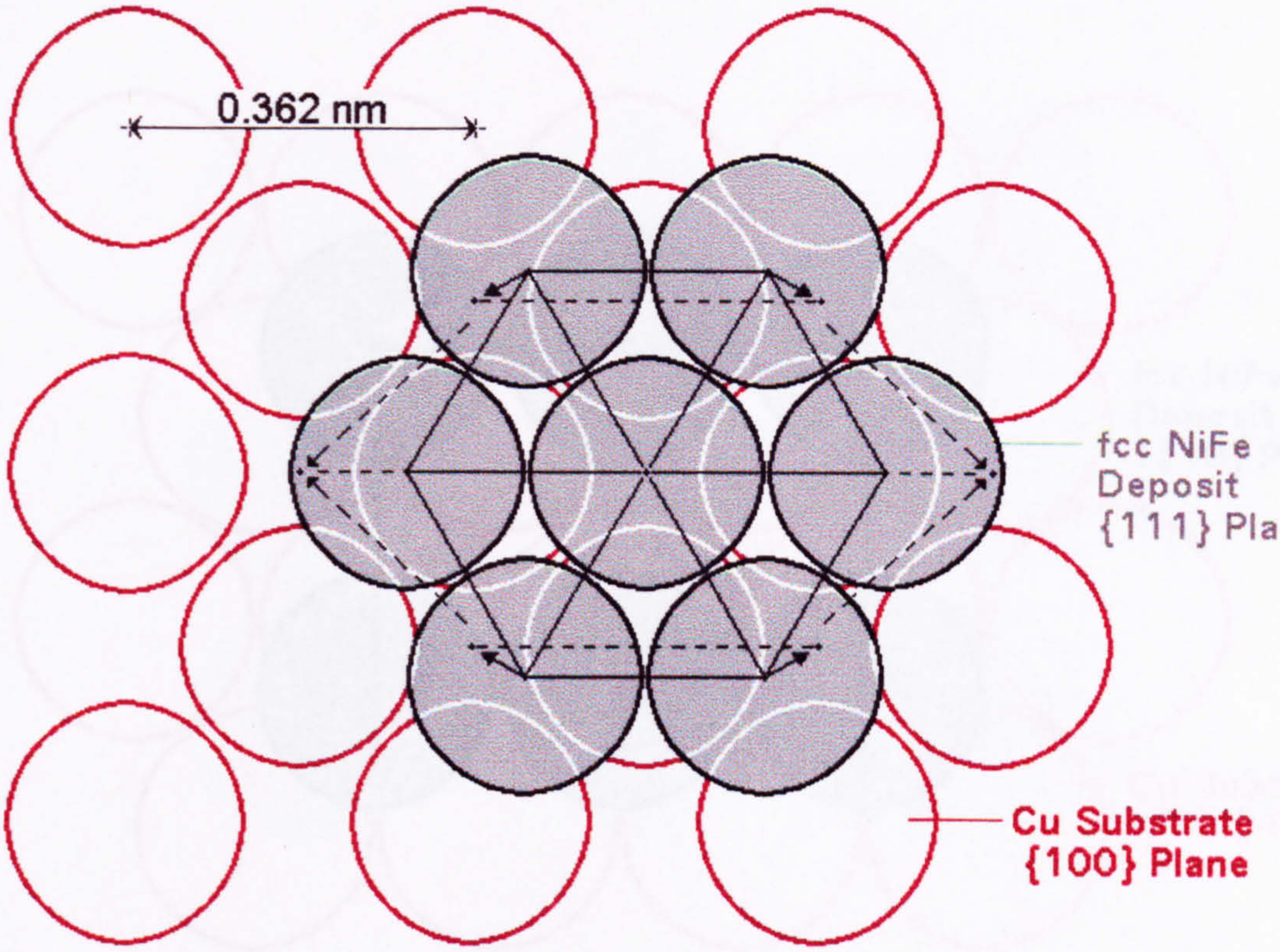

Fig. 5-4: Model of Atoms in {111} Orientated fcc Nickel-Iron Deposit Nucleated onto {100} Textured Copper Substrate (Plan View).

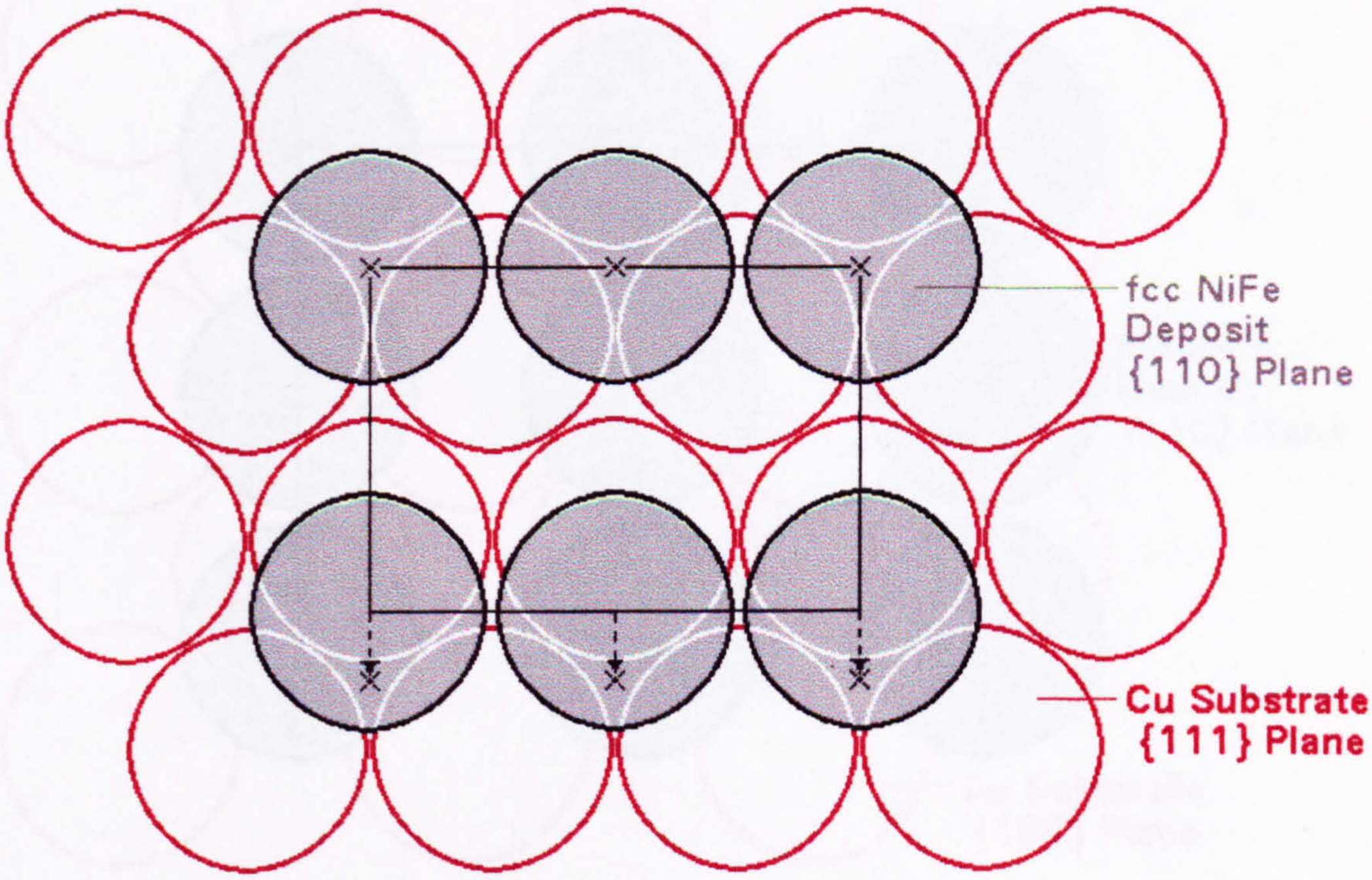

Fig. 5-5: Model of Atoms in {110} Orientated fcc Nickel-Iron Deposit Nucleated onto {111} Textured Copper Substrate (Plan View).

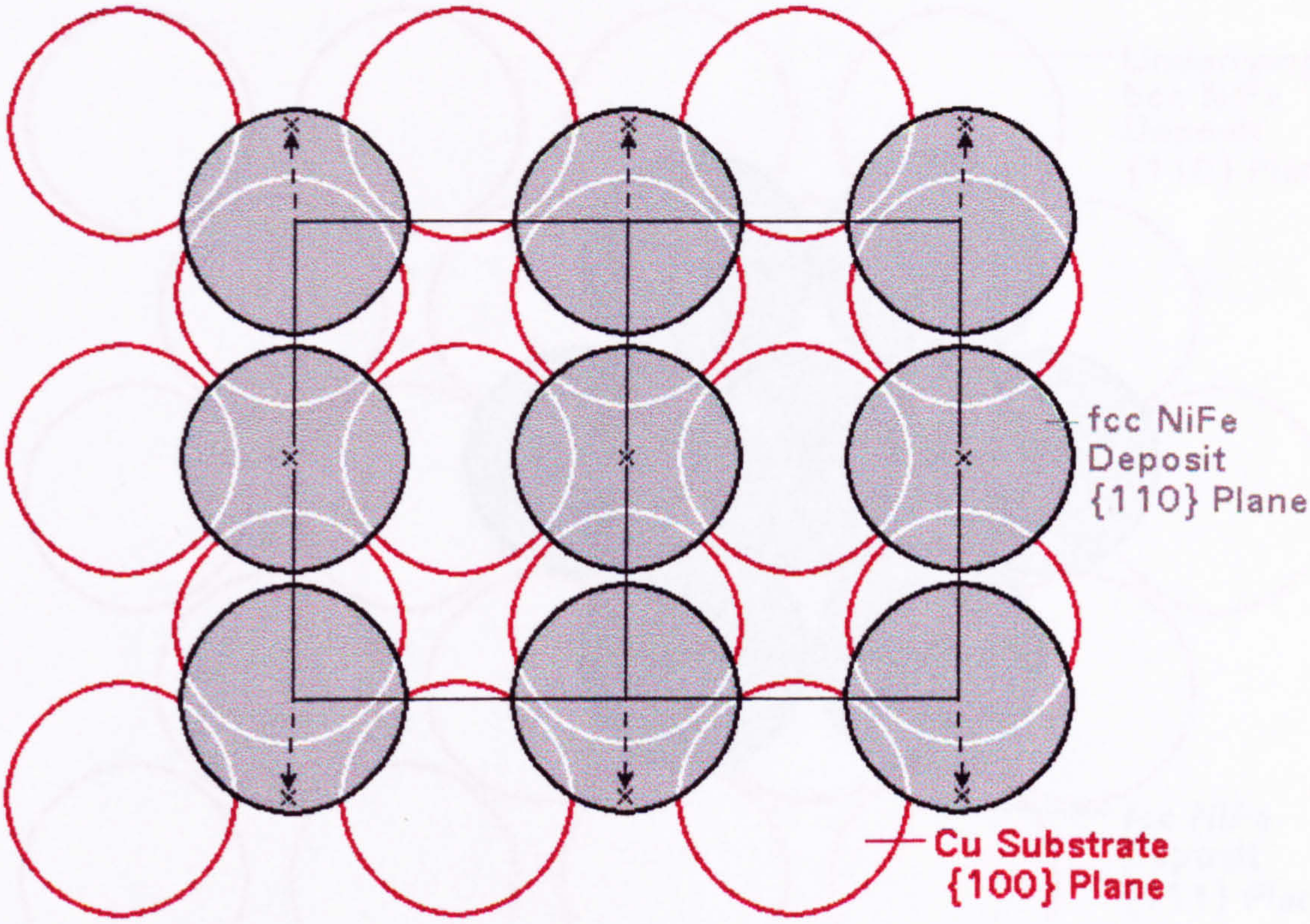

Fig. 5-6: Model of Atoms in {110} Orientated fcc Nickel-Iron Deposit Nucleated onto {100} Textured Copper Substrate (Plan View).

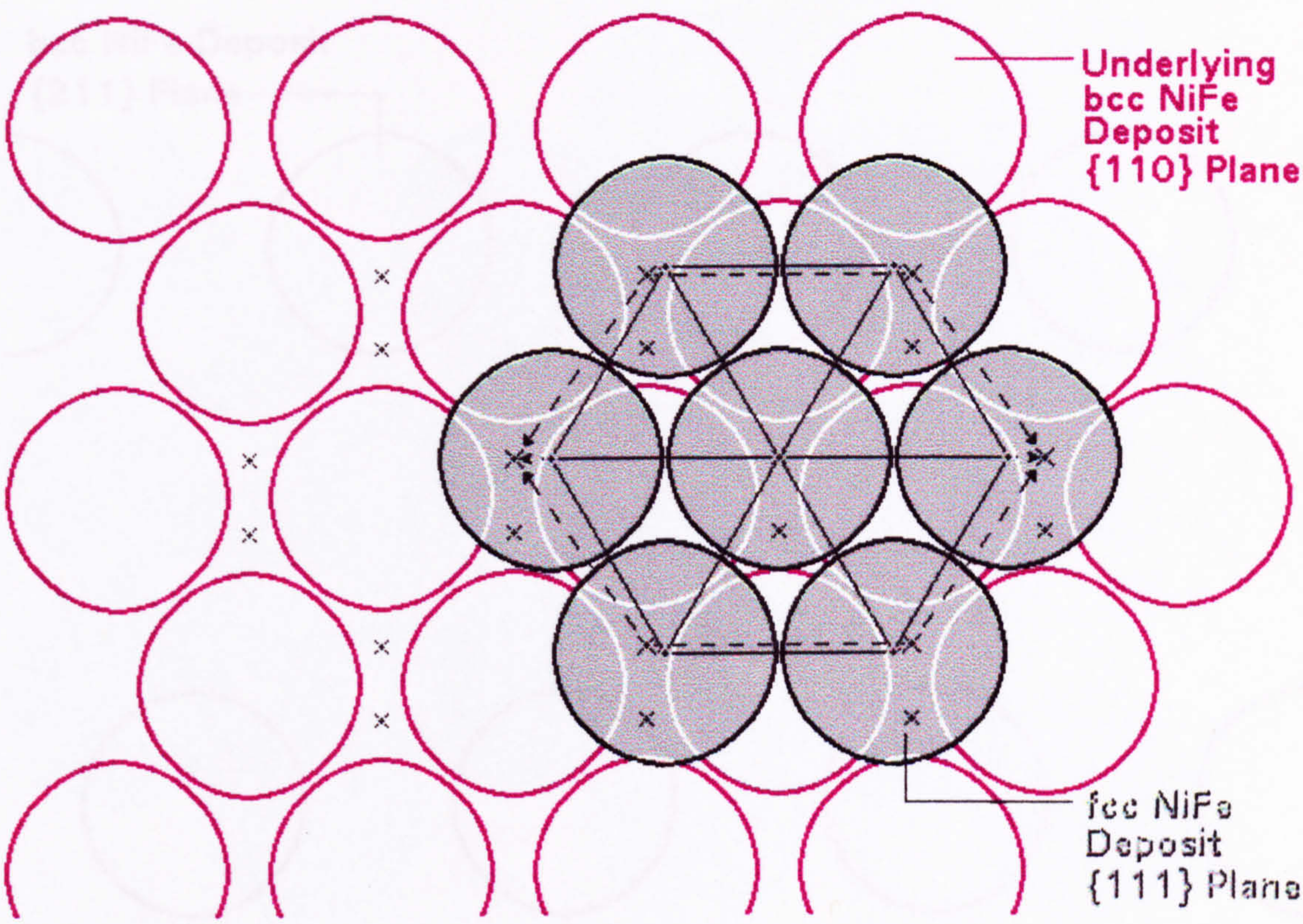

Fig. 5-7: Model of Atoms in {111} Orientated fcc Nickel-Iron Deposit Nucleated onto {110} Textured bcc Structured Nickel-Iron Electrodeposited Substrate (Plan View).

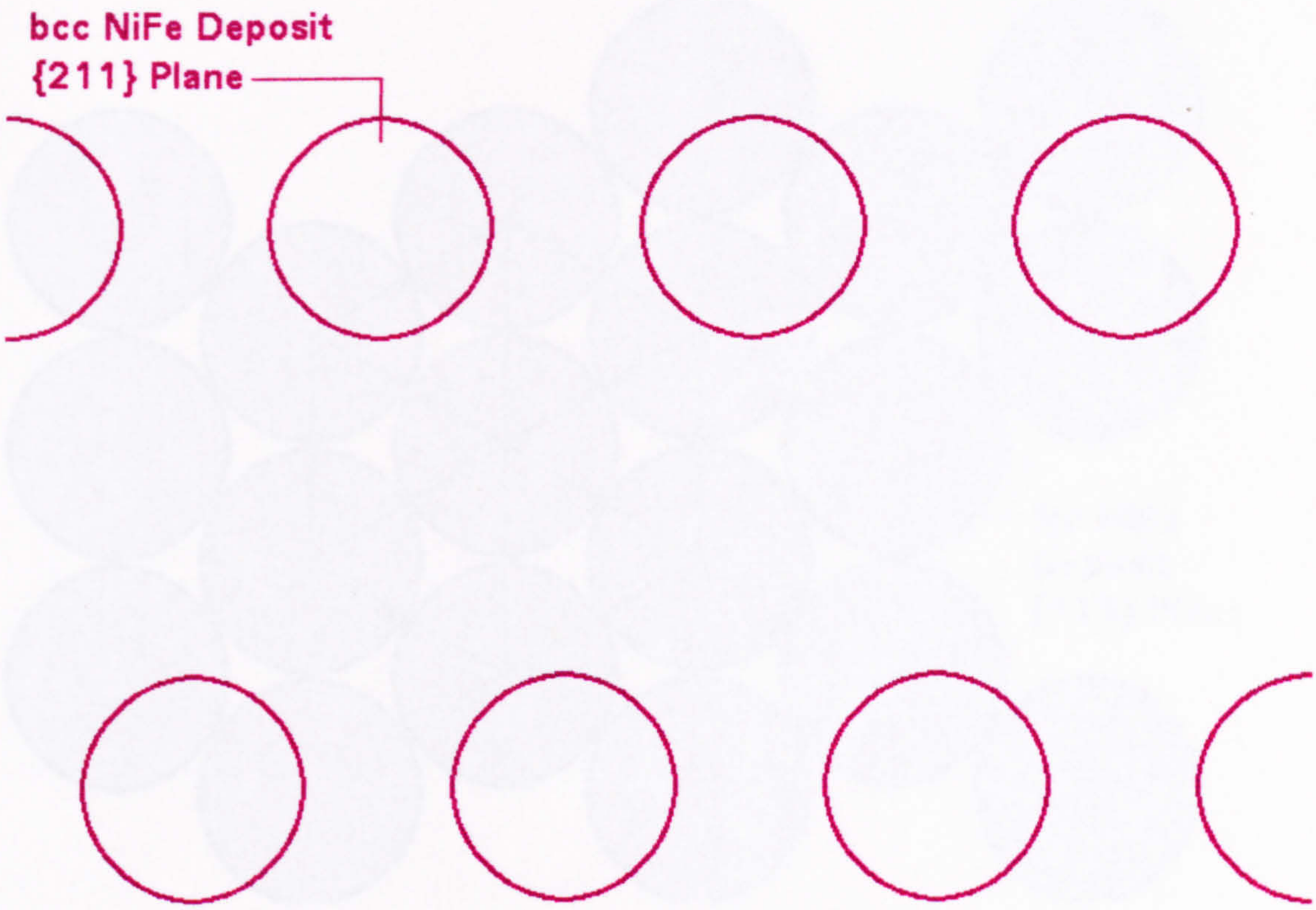

Fig. 5-8a: Model of Atoms in {211} Orientated bcc Nickel-Iron Electrodeposited Substrate (Plan View).

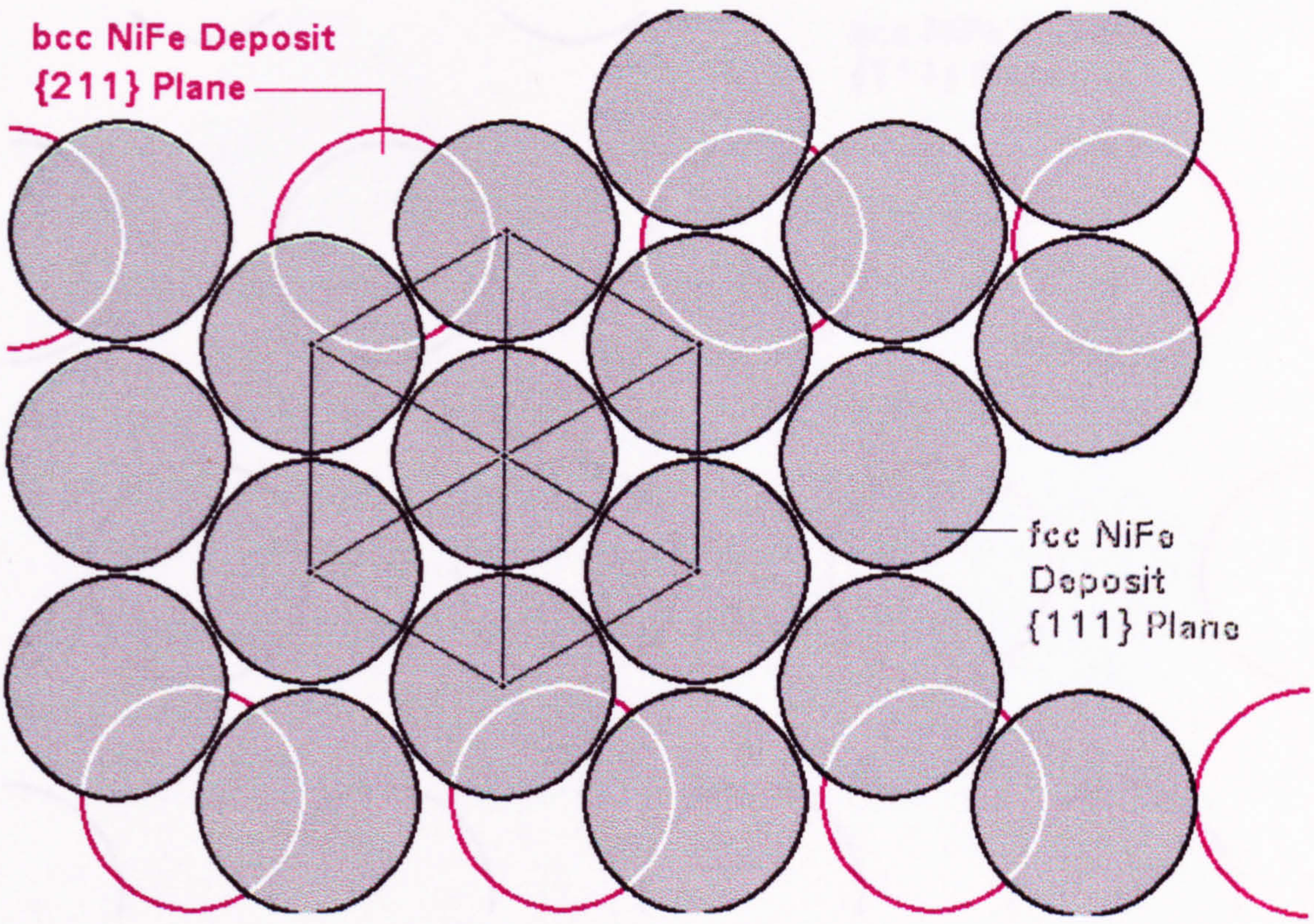

Fig. 5-8b: Model of Atoms in {111} Orientated fcc Nickel-Iron Deposit Nucleated onto {211} Textured bcc Structured Nickel-Iron Electrodeposited Substrate (Plan View).

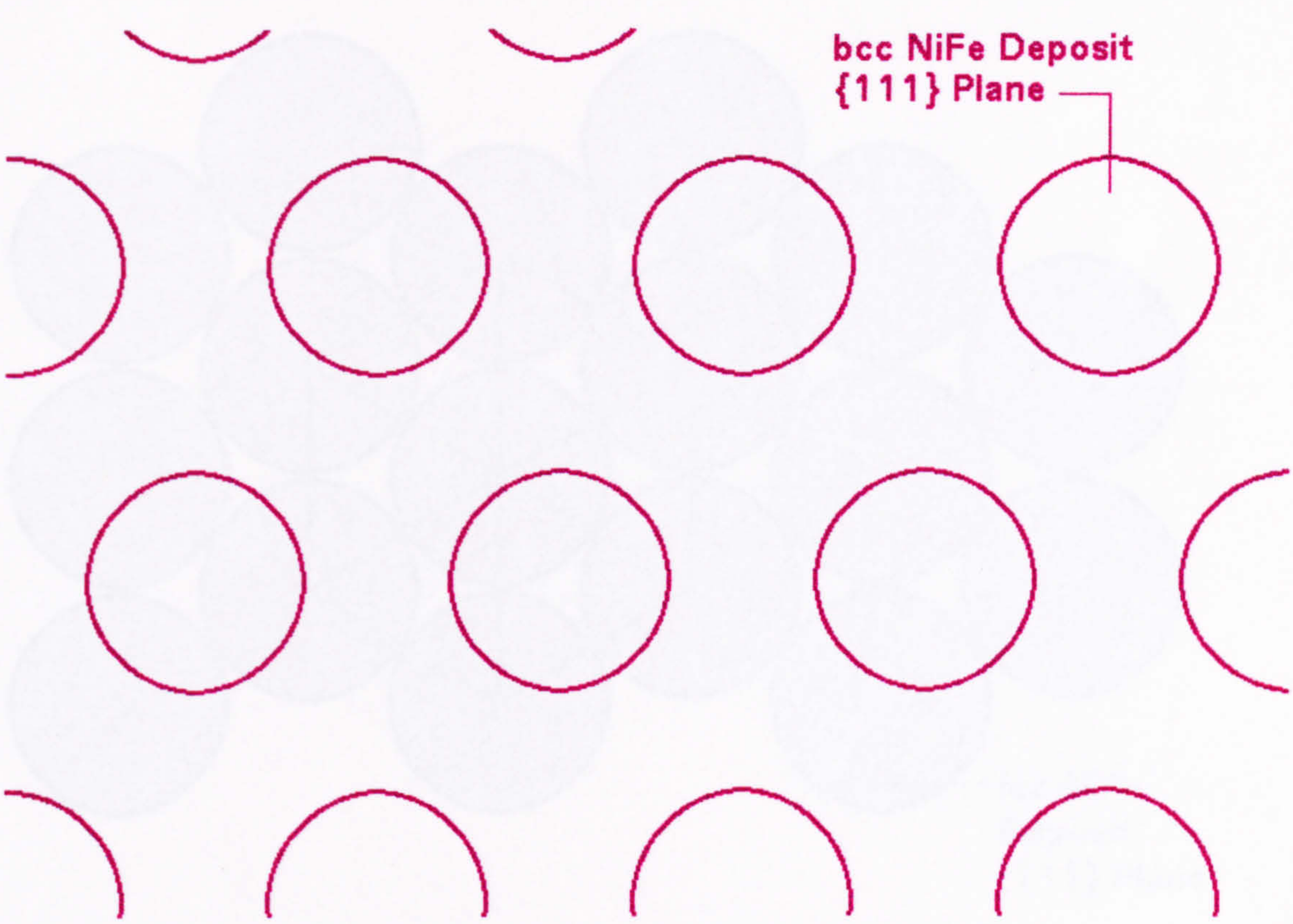

Fig. 5-9a: Model of Atoms in {111} Orientated bcc Nickel-Iron Electrodeposited Substrate (Plan View).

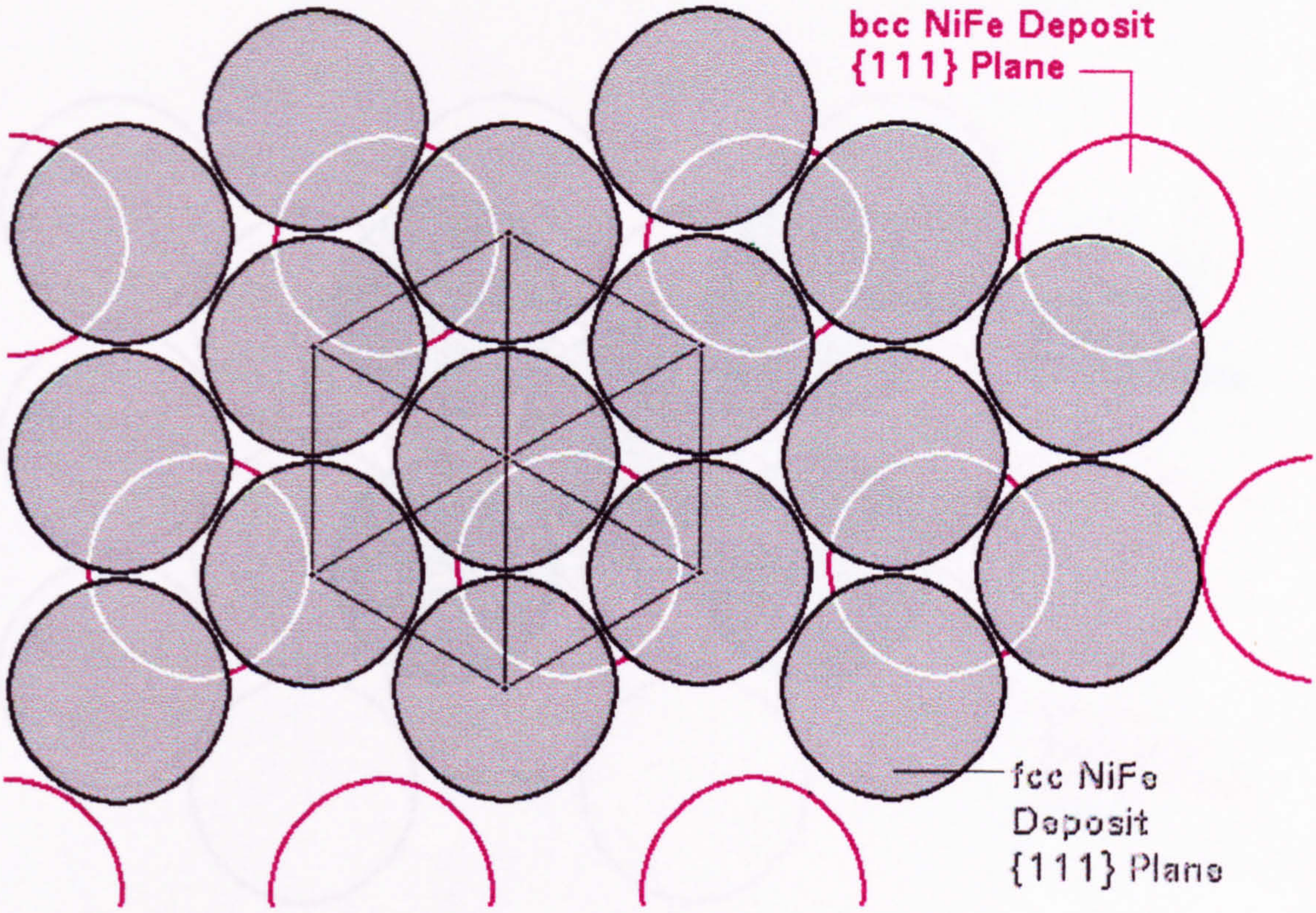

Fig. 5-9b: Model of Atoms in {111} Orientated fcc Nickel-Iron Deposit Nucleated onto {111} Textured bcc Structured Nickel-Iron Electrodeposited Substrate (Plan View).

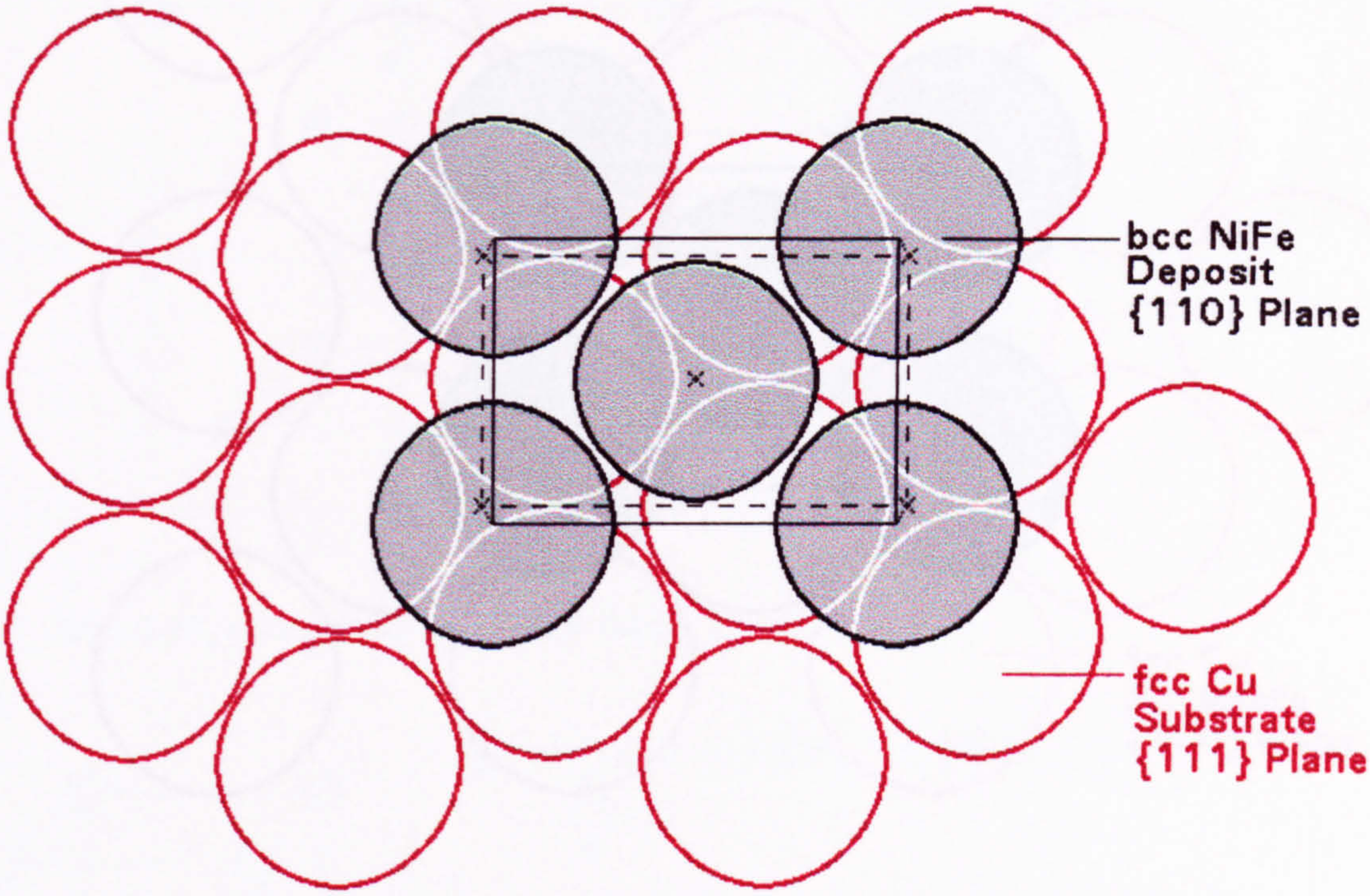

Fig. 5-10: Model of Atoms in {110} Orientated bcc Nickel-Iron Deposit Nucleated onto {111} Textured fcc Copper Substrate (Plan View).

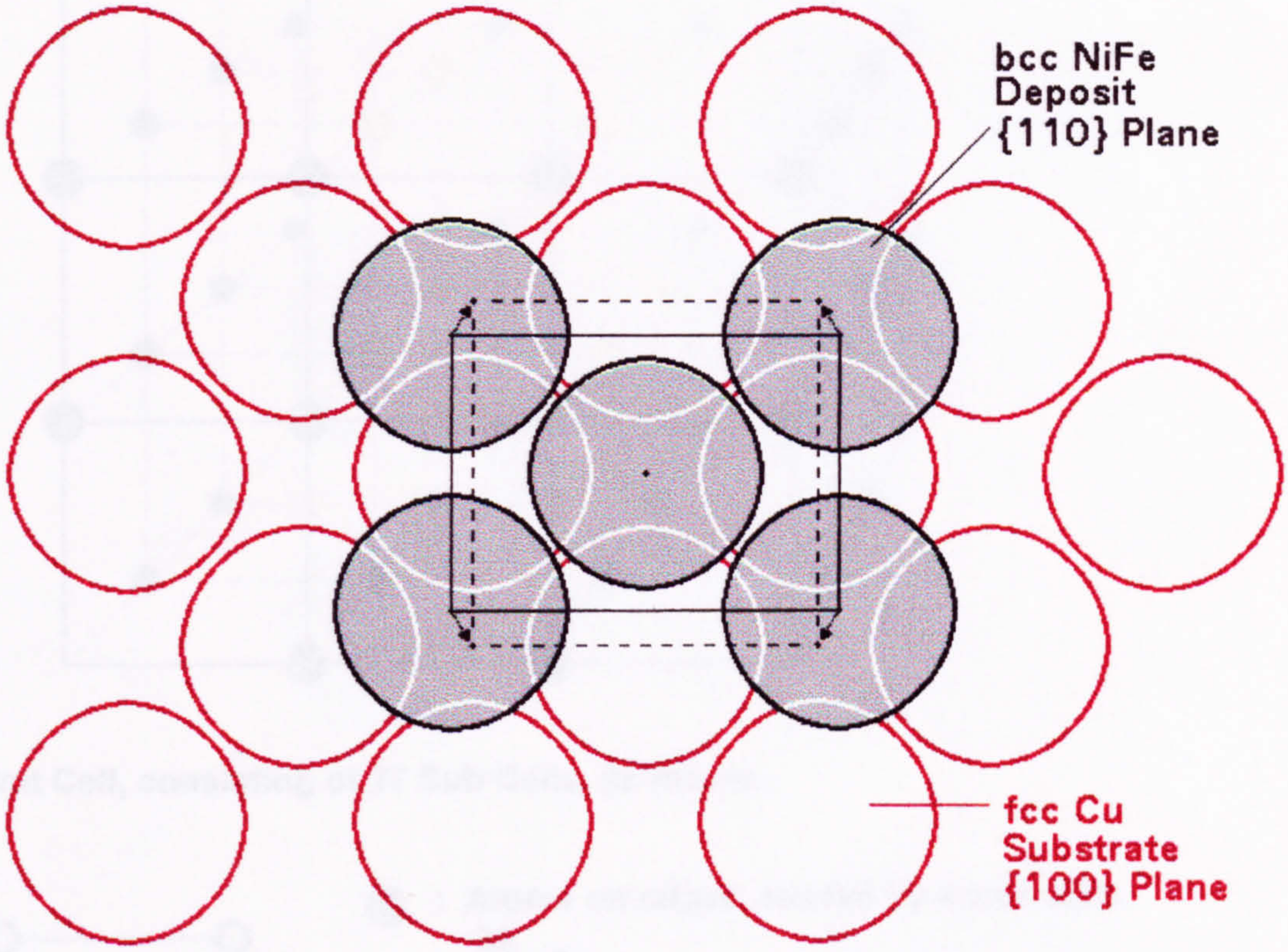

Fig. 5-11: Model of Atoms in {110} Orientated bcc Nickel-Iron Deposit Nucleated onto {100} Textured fcc Copper Substrate (Plan View).

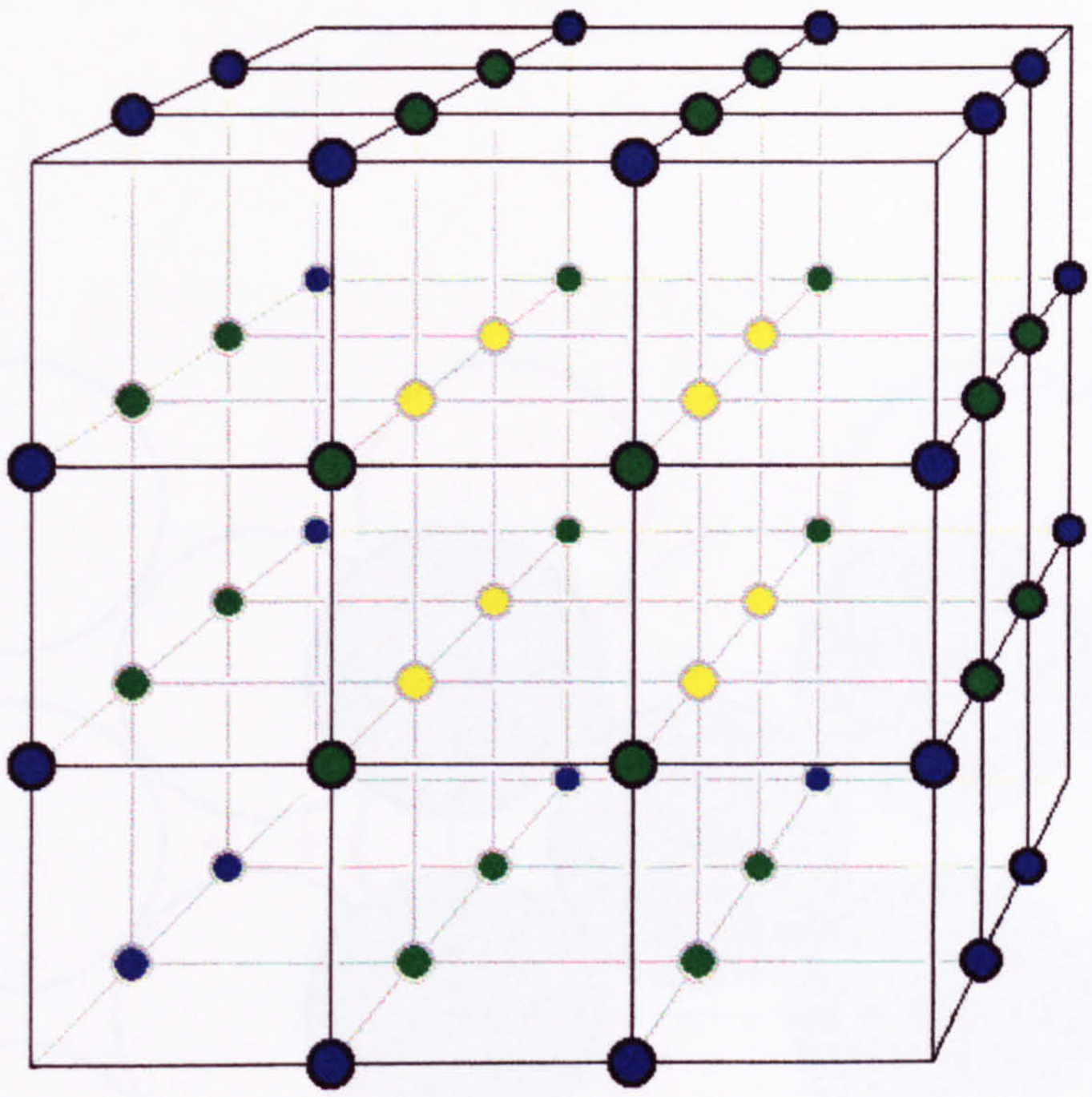

Unit Cell, consisting of 27 Sub Cells, 52 Atoms.

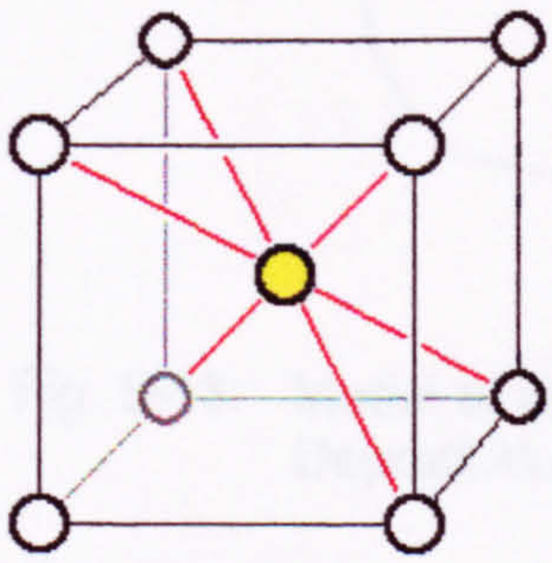

Bcc Sub Cell

- ● : **Atoms on edges, shared by 4 unit cells.**
  $\frac{24}{4} = 6$
- ● : **Atoms on face sides, shared by 2 unit cells.**
  $\frac{24}{2} = 12$
- ● : **Atoms inside the unit cell (8 atoms), and accommodated within each sub cell, except the central atom (26 atoms per unit cell), not shared.**
  $8 + 26 = 34$

Fig. 5-12: Model Depicting the Atomic Arrangement within the Ni_5Zn_{21} Unit Cell, which Consists of 27 Bcc Sub Cells, thus Working out at 52 Atoms per Unit Cell.

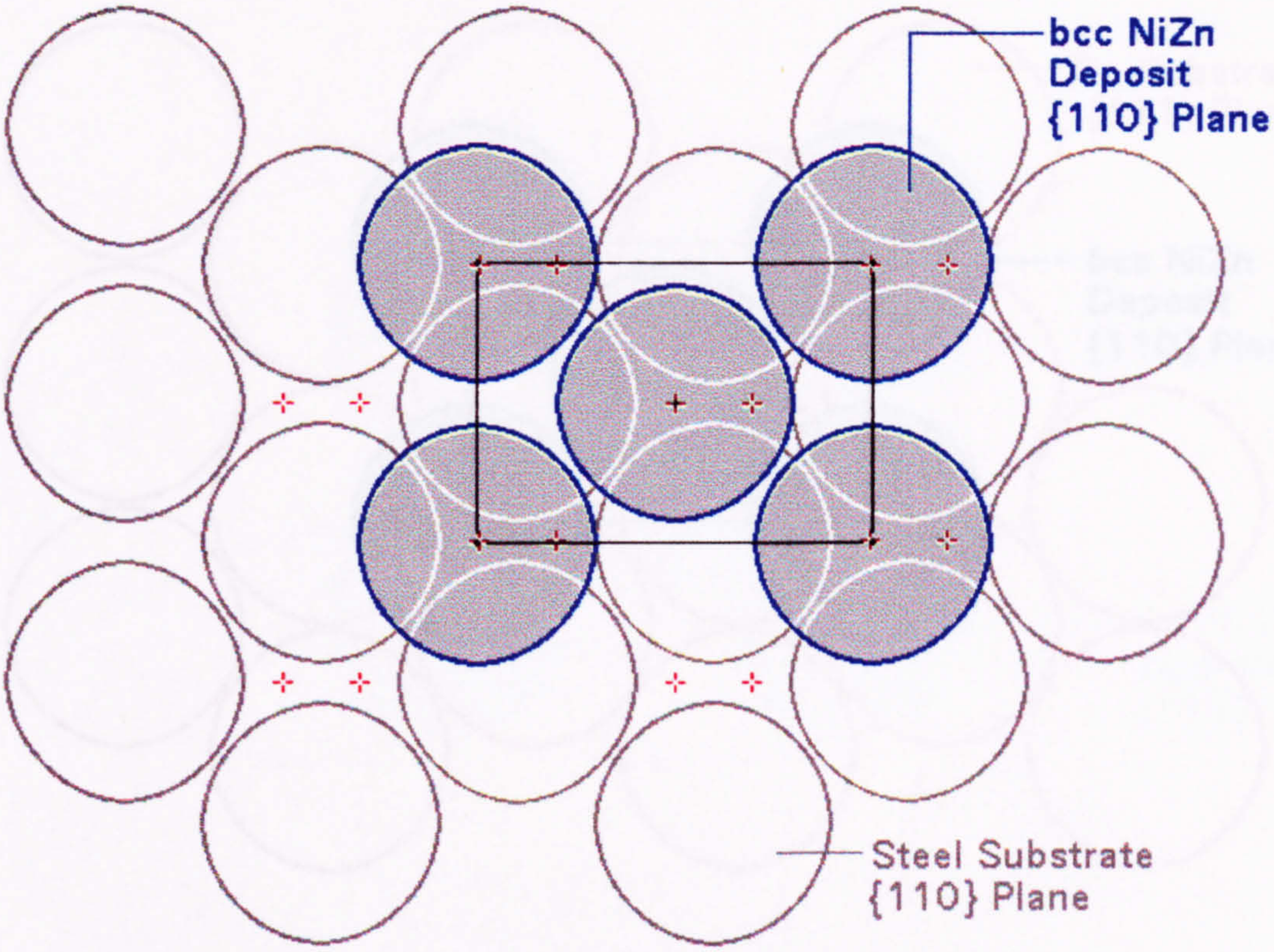

Fig. 5-13: Model of Epitaxial Growth of {110} Orientated bcc γ-Phased Nickel-Zinc Deposit Nucleated onto {110} Textured Steel Substrate (Plan View).

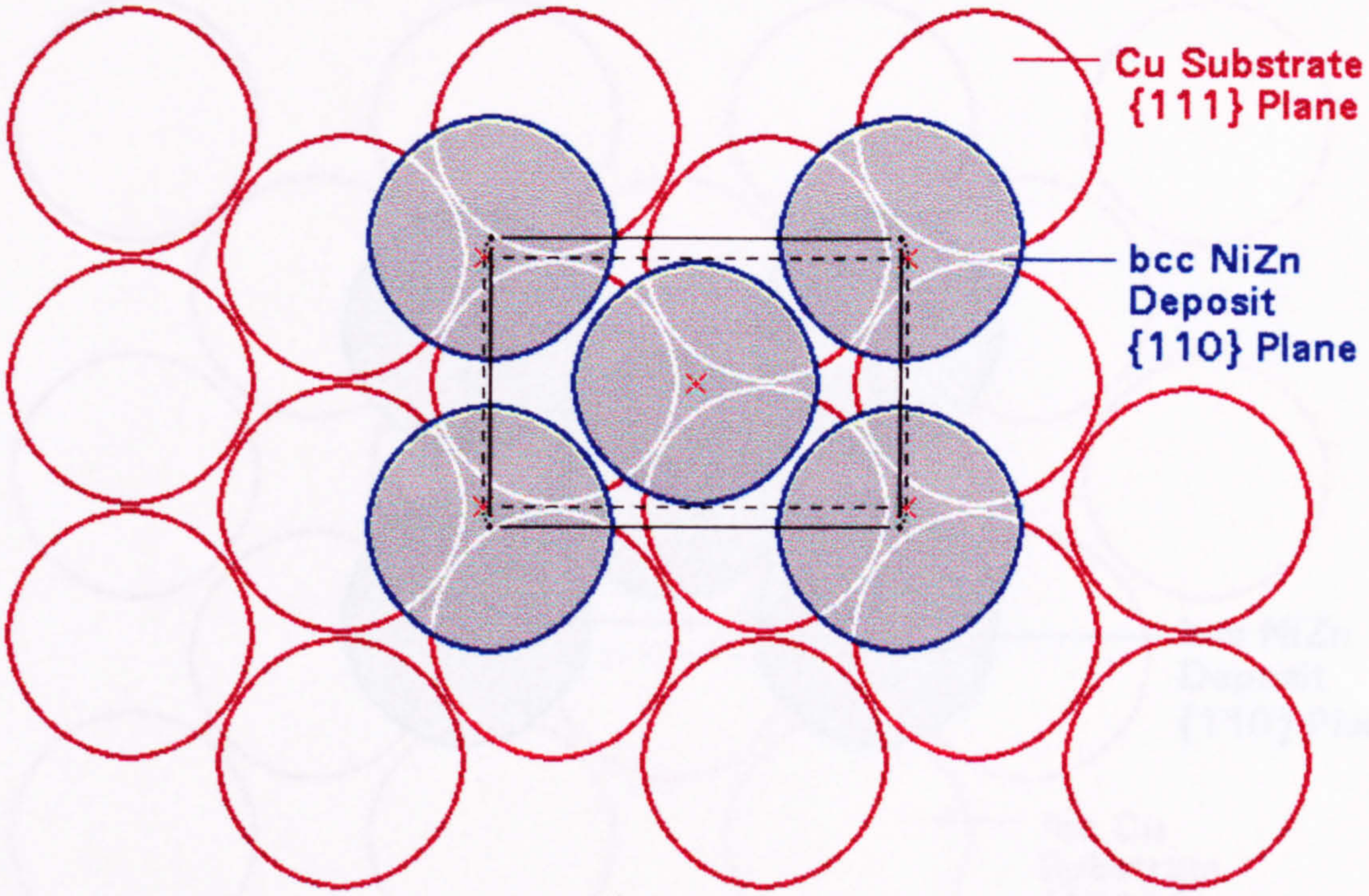

Fig. 5-14: Model of {110} Orientated bcc γ-Phased Nickel-Zinc Deposit Nucleated onto {111} Textured Copper Substrate (Plan View).

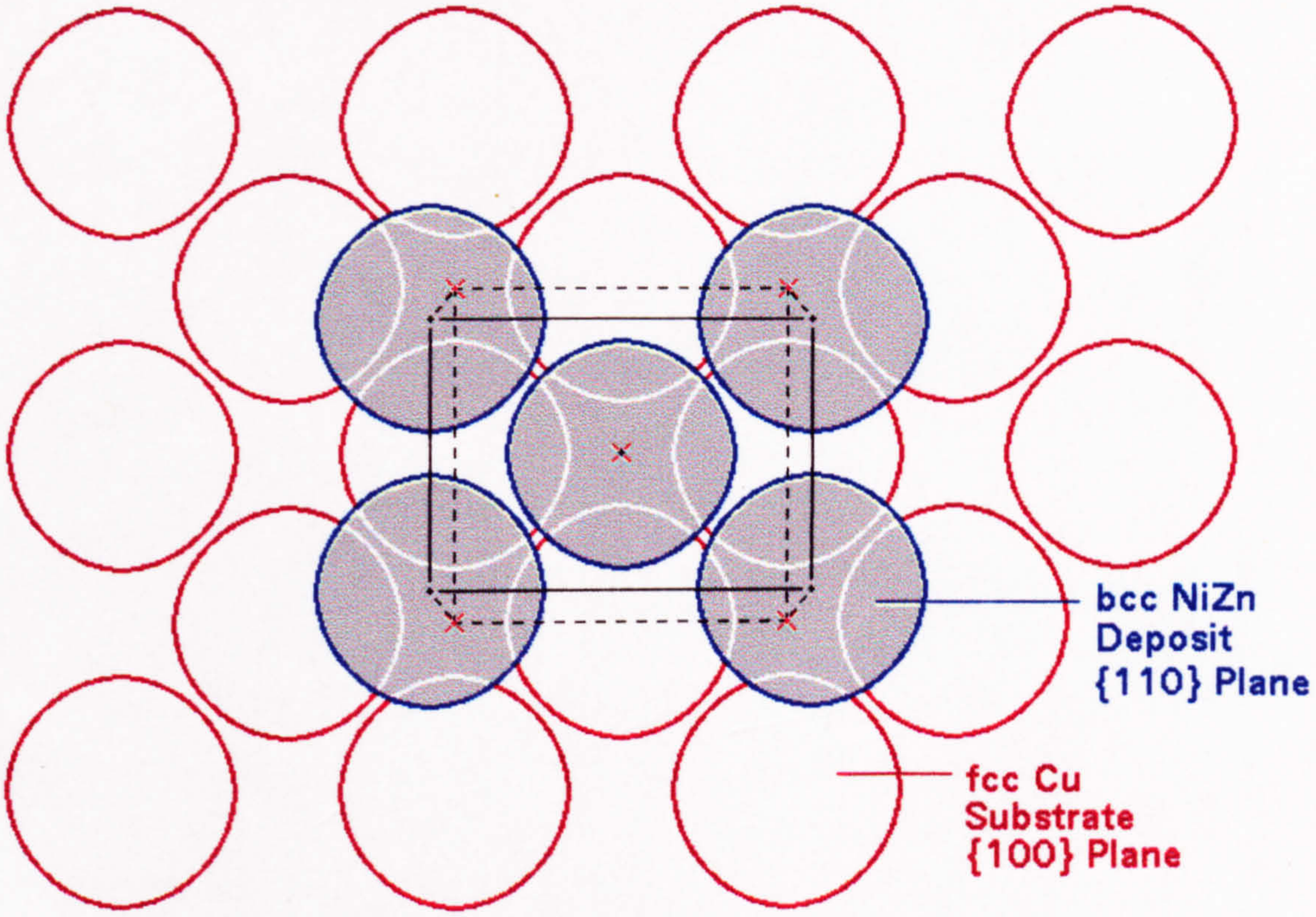

Fig. 5-15: Model of {110} Orientated bcc γ-Phased Nickel-Zinc Deposit Nucleated onto {100} Textured Copper Substrate (Plan View).